

Tailoring the Optical Properties and Morphology of Low Molecular Weight based Supramolecular Gelators

Thesis Submitted to AcSIR for the Award of the Degree of
DOCTOR OF PHILOSOPHY
In Chemical Science



(Academy of Scientific and Innovative Research)

By

ARUNAVA MAITY
(Reg. No. 10CC12A26085)

Research Supervisor
Dr. Amitava Das

CSIR-National Chemical Laboratory
Pune-411008, Maharashtra, India

February 2018

*Dedicated
To
My Beloved Parents*

DECLARATION

I hereby declare that the matter embodied in the thesis entitled "**Tailoring the Optical Properties and Morphology of Low Molecular Weight based Supramolecular Gelators**" is the result of the investigations carried out by me at Organic Chemistry Division of CSIR-National Chemical Laboratory, Pune, under the supervision of Dr. Amitava Das and the same has not been submitted elsewhere for any other degree.

In keeping with the general practice of reporting scientific observations, due acknowledgment has been made wherever the work described is based on the findings of other investigators.

Pune
February 2018



Arunava Maity


CERTIFICATE

This is to certify that the work incorporated in this Ph.D. thesis entitled **"Tailoring the Optical Properties and Morphology of Low Molecular Weight based Supramolecular Gelators"** submitted by Mr. Arunava Maity to Academy of Scientific and Innovative Research (AcSIR) in fulfillment of the requirements for the award of the Degree of Ph.D. embodies original research work under my supervision. I further certify that this work has not been submitted to any other University or Institution in part or full for the award of any degree or diploma. Research material obtained from other sources has been duly acknowledged in the thesis. Any text, illustration, table etc., used in the thesis from other sources, have been duly cited and acknowledged.

Arunava Maity
(Student)

Pune

February 2018


Dr. Amitava Das
(Thesis Supervisor)

ACKNOWLEDGEMENT

My most sincere and heartfelt thanks go to my Ph.D. supervisor, Dr. Amitava Das. I thank him for introducing me to the wonders of scientific research. I thank him for his persistent, encouragement, inspiration and support during every stage of my research work. I appreciate the confidence he had in me which enables me to grow as an independent researcher.

I would like to express my sincere gratitude to Dr. Santhosh Babu Sukumaran for fruitful discussions on research problems, appreciative comments, and continuous guidance whenever I approached which helped me to explore various aspects of the chemistry.

I would like to thank my previous and current DAC committee members Dr. Akkattu T. Biju, Dr. Rahul Banerjee, Dr. J. Nithyanandhan and Dr. Chinnakonda S. Gopinath for their continued encouragement and constructive suggestions.

I wish to express my word of thanks to Dr. P. K. Ghosh (Former Director, CSMCRI, Bhavnagar), Dr. Sourav Pal (Former Director, NCL-Pune), Dr. Ashwini K. Nangia (Director, NCL), Dr. Parimal Paul (Discipline Coordinator, CSMCRI), Dr. Pradeep Kumar Tripathi (Former Head, Organic chemistry Division, NCL-Pune), Dr. Subhash P. Chavan, Head, Organic Chemistry Division, for providing me opportunity and all necessary facilities to carry out my research work.

My sincere thanks to Dr. Sakya Sen, Dr. Arup Kumar Rath, Dr. Santosh B. Mhaske, Dr. Sreekumar Kurungot, Dr. Vijayanti Kumar, Dr. Janardan Kundu, Dr. Moneesha Fernandes, Dr. R. A. Joshi, Dr. Sayam Sengupta, Dr. B. L. V. Prasad, Dr. A. K. Siddhanta, Dr. R. I. Kureshi and Dr. Adimurthy and all other scientists of NCL and CSMCRI for their motivation, constant encouragement and support.

I am grateful to CSIR, New Delhi for fellowship support. I thank all the non-teaching staff of CSIR NCL and CRIR-CSMCRI for their assistance on various occasions. I wish to thank all my friendly and cooperative labmates Prasenjit da, Amal da, Priyadip da, Sukdeb da, Tanmay da, Upendar Reddy, Vadde Ramu, Hridesh, Monalisa, Firoj, Praveen anna, Sovan da, Shilpi di, Suman da, Ajoy da, Sunil, Anil, Koushik, Sanjukta and Ananta for creating a cheerful and enjoyable working atmosphere in the lab. They were extremely supportive as well as helpful during my tenure. I thank my M.Sc. project student Bappan for his support.

I thank my IISER Pune friends Raj, Shyamapada, Debanjan, Rahi, Sanjit for their help and support in various aspects during my tenure. Especial thanks go to Raj and Shyamapada. Without the frequent brainstorming tea breaks from the 'hectic' research work and 'relaxing' weekly parties with you people, it would never possible for me to finish.

My Ph.D. tenure has been pleasant with the association of all the research scholars at CSIR NCL and CSIR CSMCRI. I am thankful to Kanak da, Shyam da, Krishanu da, Manna da

(Arpan), Achintya da, Pravat da, Saikat da, Susanta da, Anjan da, Himadri da, Aryya da, Chini da (Mrinmoy), Tamas da, Arijit da, Sanjeev da, Chandan da, Subhadip da, Soumen da, Saibal da, Pati da, Joyashish da, Partha da, Debdeep da, Anik da, sandip da, Subha di, Munmun di, Tanaya di, Manjur, Anup, Shanti, Siba, Abhijit, Debranjana, Tapas, Tamal, Subharasis, Subrata, Sudip, Sutanu, Bipul, Jaganath, Supravat, Dibyendu, Milan, Jaswanta, Mrinal, Abul Kalam, Krishna, Anupam, Manoj, Indradweep, Somsubhra, Bikash, Arjun, Saibal, Pranab, Mahitosh, Pronoy, Sandipan, Anirban, Goudappa, Vivek, Virat for their support and to make my journey joyful and memorable.

My heartfelt thanks to my school teachers, college and university professors for their guidance and encouragement. I also thank my all school, college and MSc friends.

Finally, I would like to pay high regards to my parents and my family members for their sincere encouragement and inspiration throughout my research work and lifting me uphill this phase of life. I owe everything to them. Dedicating this thesis to them is a minor recognition for their invaluable support and encouragement.

Still, many names are missing whose contribution and help is worth mentioning, I promise I will start with them in my next thesis!!!

Arunava Maity

CONTENTS

ACKNOWLEDGEMENT	Page iii
PREFACE	xii

CHAPTER 1

An Overview of Supramolecular Gels: Tuneable Optical Properties, Morphology and Opportunities 1-49

1.1. A Brief Introduction of Supramolecular Chemistry	2
1.2. Concept Behind the Gel State	2
1.2.1. Supramolecular Gels	4
1.2.2. Polymeric Supramolecular Gels	4
1.2.3. Low Molecular Weight Supramolecular Gels (LMWSGs)	4
1.3. Mechanistic Consideration of Supramolecular Gel Formation	5
1.4. Structural Requirements for Supramolecular Gelators	6
1.5. Characterization of Supramolecular Gel	8
1.5.1. Inverted Vial Method	8
1.5.2. Gel Morphology	8
1.5.3. Viscoelastic Properties of Gel	9
1.5.4. Organization of Gelator Molecules in the Gel Fiber	9
1.6. LMW based Supramolecular Gelators with Tenable/Controllable Optical Properties	10
1.6.1. Solvent Structure Assisted Fluorescence Modulations of LMWSGs	10
1.6.2. Aggregation-Induced Enhanced Emission (AIEE) Process for Modulating the Luminescence Property of Supramolecular Gels	12
1.6.3. Supramolecular Gelators with Excited-State Intramolecular Proton Transfer (ESIPT) Features	14
1.6.4. Tuneable Luminescence Through Excited State Energy Transfer Within the Supramolecular Gel Matrix	17
1.6.5. White-Light Emitting Gels through Energy Transfer Process	19

1.6.5.1. Single Component-based White-Light Emitting Supramolecular Gelator	22
1.6.6. Basic Concept Related to Supramolecular Chirality	23
1.6.6.1. Characterization of Supramolecular Chirality	24
1.6.6.2. Random Supramolecular Chirality from C ₃ -Symmetric Achiral Gelators and Chiality Induction	26
1.7. Tuning Soft Nanostructures in Self-Assembled Supramolecular Gels	28
1.7.1. Morphological Diversity in Supramolecular Gels	29
1.7.2. Factors to Control the Morphology of the Supramolecular Gels	29
1.7.2.1. The Effect of Molecular Structures on Morphology	30
1.7.2.2. Solvent Polarity-Controlled Diverse Morphologies	31
1.7.2.3. Metal-Ligand Coordination Directed Morphological Transition	32
1.7.2.4. Ultrasound Directed Morphological Diversity	34
1.7.2.5. Effect of Temperature and Ageing Time	35
1.8. Dendritic Gelators	36
1.9. Opportunities of Supramolecular Gels	38
1.10. References	43

CHAPTER 2

Tuning of Multiple Luminescence Outputs and WhiteLight Emission from a Single Gelator Molecule through an ESIPT Coupled AIEE Process

50-72

2.1. Introduction	51
2.2. Experimental Section	52
2.2.1. Materials and Methods	52
2.2.2. General Description of the Different Experimental Techniques	53
2.2.2.1. UV-Vis and Fluorescence Study	53
2.2.2.2. General Procedure for Gelation Study of 1	54
2.2.2.3. Scanning Electron Microscopy (SEM)	54
2.2.2.4. Transmission Electron Microscopy (TEM)	54

2.2.2.5. Current (<i>I</i>) - voltage (<i>V</i>) Measurements	54
2.2.2.6. Rheology	54
2.2.3. Synthesis and Characterization	55
2.2.3.1. Synthetic Scheme	55
2.2.3.2. Synthesis of 3a and 3b	55
2.2.3.3. Synthesis and Characterization of 4	56
2.2.3.4. Synthesis of 5	56
2.2.3.5. Synthesis and Characterization of Compound 1 and 2	56
2.3. Results and Discussions	57
2.4. Conclusion	70
2.5. References	71

CHAPTER 3

Water Induced Morphological Transformation of a Poly(aryl ether) Dendron Amphiphile: Helical Fibers to Nanorods, as Light-Harvesting Antenna Systems 73-94

3.1. Introduction	74
3.2. Experimental Section	76
3.2.1. Materials	76
3.2.2. Instruments	76
3.2.3. Synthesis and Characterization	77
3.2.3.1. Synthesis of Poly(aryl ether) Dendron Amphiphile 1(D)	77
3.2.3.2. Synthetic Scheme for BODIPY based Acceptor Molecules A-1 and A-2	77
3.2.3.3. Synthesis and Characterization of A-1	78
3.2.3.4. Synthesis and Characterization of A-2	78
3.3. Results and Discussions	78
3.4. Conclusions	91
3.5. Referencess	92

CHAPTER 4

Counteranion Driven Homochiral Assembly of a Cationic C₃-Symmetric Gelator through Ion-Pair Assisted Hydrogen Bond **96-118**

4.1. Introduction	97
4.2. Experiment Section	98
4.2.1. Materials and Methods	98
4.2.2. Synthesis and Characterization	99
4.2.2.1. Synthesis of Tris(4-pyridinecarboxaldehyde)triaminoguanidinium chloride (L.Cl ⁻)	99
4.2.2.2. Synthetic Scheme of Counteranion Exchanged Ligands L.(+)-MS* ⁻ and L.(-)-MS* ⁻	100
4.2.2.3. Synthesis and Characterization of L.(-)-MS* ⁻	100
4.2.2.4. Synthesis and Characterization of L.(+)-MS* ⁻	101
4.2.3. General Description of Different Experimental Techniques	101
4.2.3.1. Gelation Test	101
4.2.3.2. UV-Vis and Circular Dichroism (CD) Spectroscopy	101
4.2.3.3. Scanning Electron Microscopy (SEM)	101
4.2.3.4. Crystallization Procedure	102
4.2.3.5. Details of the Single Crystal X-ray Diffraction Studies	102
4.2.3.5.1 Crystallographic Refinement Details	102
4.3. Results and Discussions	104
4.4. Conclusions	116
4.5. References	117

CHAPTER 5

Fiber to Nanosphere Morphology Transformation and Gel-to-Sol Phase Transition Triggered by “halfcrown/two carbonyl” – Ca²⁺ Metal Ion Interactions of a Low Molecular Weight Gelator (LMWG) **119-142**

5.1. Introduction	119
5.2. Experimental Section	122

5.2.1. Materials and Methods	122
5.2.2. Instruments	123
5.2.3. Synthesis of Gelator (L)	123
5.2.4. Computational Methods	124
5.2.5. General Description of Different Experimental Techniques	125
5.2.5.1. Gelation Test	125
5.2.5.2. Scanning Electron Microscopy (SEM)	125
5.2.5.3. Transmission Electron Microscopy (TEM)	125
5.2.5.4. Rheology	125
5.2.5.5. UV-vis and Fluorescence Studies	126
5.2.5.6. Fourier Transform Infrared (FT-IR) Study	126
5.3. Results and Discussions	126
5.4. Conclusions	138
5.5. References	140
<i>Summary: Conclusion of all Chapters and Future Directives</i>	143-144
A. Conclusion of the Thesis	143
B. Possible Direction of Future Work	144
<i>Appendix: Characterization Details of the Newly Synthesized Compounds</i>	145-156
<i>List of Publications</i>	157-158
<i>Selected Presentations</i>	159

ABBREVIATIONS

3D	Three dimensional
SEM	Scanning electron microscopy
TEM	Transmission electron microscopy
AFM	Atomic force microscopy
STM	Scanning tunneling microscopy
AIE	Aggregation induced emission
AIEE	Aggregation induced enhanced emission
ESIPT	Excited state intramolecular proton transfer
CGC	Critical gelation concentration
CT	Charge transfer
ET	Energy transfer
EET	Electronic energy transfer
DCC	Dicyclohexylcarbodiimide
HOBt	Hydroxybenzotriazole
DMF	Dimethyl formamide
DMSO	Dimethyl sulfoxide
MeOH	Methanol
H ₂ O	Water
ACN	Acetonitrile
MCH	Methylcyclohexane
THF	Tetrahydrofuran
CDCl ₃	Deuterated chloroform
DMSO-d ₆	Deuterated dimethyl sulfoxide
RB	Round bottom flux
NDI	Naphthalene diimide
TPE	Tetraphenylethene
DSC	Differential scanning calorimetry

FT-IR	Fourier transform-Infrared spectroscopy
TCSPC	Time correlated single photon counting
UV-Vis	Ultraviolet-visible spectroscopy
CD	Circular dichroism
TCOSY	Total Correlation Spectroscopy
PXRD	Powder X-ray diffraction
B-H plot	Benesi-Hildebrand plot
ESI	Electron spray ionization
NMR	Nuclear magnetic resonance
SAXS	Small angle X-ray scattering
SANS	Small angle neutron scattering
LMWG	Low molecular weight gelators
TICT	Twisted intramolecular Charge Transfer
OLED	Organic light-emitting diode
RT	Room temperature
IPH-bond	Ion-pair assisted hydrogen bond
DAD	Donor acceptor donor
ADA	Acceptor donor acceptor
OPVs	Oligo(p-phenylvinylene)s

PREFACE

Molecular self-assembly is an important offshoot of supramolecular chemistry, which originated as a laboratory curiosity among the chemists, and over the decades it has matured as an interdisciplinary research area. Researchers from various disciplines, namely, chemistry, physics, biology, material science have contributed to the growth of this discipline beyond the stage of its infancy. Among the various class of molecular self-assemblies, supramolecular gels obtained from low molecular weight-based species (gelators) are relatively new and important soft materials, which exhibit striking properties with respect to self-assembly phenomena and leading to diverse supramolecular architectures through various non-covalent interactions for immobilizing the solvents within their matrix. There are many important fundamental issues related to these gels, such as the design of the gelator, synergism of various non-covalent interactions between gelators, gelator-solvents, study their self-assembly mechanism and so on. Another interesting aspect is the ability of gels to respond to external stimuli in order to get tunable optical properties and various morphological nanostructures. The onus lies on the researchers in exploiting such tunable changes in developing multifunctional materials.

Discussions in the dissertation are limited to design and synthesis of low molecular-weight based supramolecular gelators (LMWG) with purposefully chosen different chromogenic functional groups and studies their self-aggregation behavior. Issues that are crucial in tuning/controlling their optical properties, phase transitions and morphology changes of such self-assembled gelators with the changes in the solvent compositions, structural modification, or in response to external stimuli in molecular level are being discussed.

The thesis is comprised of five chapters. Chapter 1 provides an introduction of supramolecular gel and the important methods of characterization, classification, and examples of some of the significant works carried out by different research groups regarding functional low molecular weight based gel systems. Attention has been paid to discuss various chromophore derived gelators with controllable/tuneable optical properties, morphology in response to applying different external stimuli, which is relevant to the objective of the present study. In addition, an overview of the wide variety of opportunities of the supramolecular gel systems presented in this chapter.

Chapter 2 describes the design and synthesis of a poly(aryl ether) dendron based amphiphilic gelator molecule, which has been found to emit white-light in solution, by simply changing its solvent compositions. In this work, we have thoroughly studied the solvent dependent aggregation behavior of the gelator. With the help of spectroscopic

study, we demonstrated that an ESIPT coupled AIEE process is the reason behind its tuneable luminescence color over a wide energy range “blue-green-white-yellow” (adopted from *Chem. Commun.*, 2015, **51**, 2130).

Chapter 3 describes the morphological transformation (from helical fiber to nanorod) behavior of the same poly(aryl ether) dendron based amphiphilic gelator molecule (which is studied in Chapter 2) with varying the water fraction in its THF solution. The work mainly deals with a mechanistic aspect of morphology transformation, which has unambiguously explored through different microscopic and spectroscopic techniques as well as with the help of self-assembly model. In addition, the poly(aryl ether)dendron amphiphile has been exploited as a light-harvesting antenna chromophore for two newly designed BODIPY based acceptor molecules (adopted from *Nanoscale.*, 2018, **10**, 1464).

Chapter 4 contains the discussion about a synthesized achiral C_3 -symmetric cationic gelator molecule, which simultaneously self-assembled into the right (*P*) and left (*M*) handed helical rope-like structure, and successful demonstration the role of its counteranion in inducing chirality and switching into a preferred helicity. This work introduces a general methodology to control and bias chirality in ionic achiral assemblies and also stabilize the chiral assembly in (MeOH/H₂O; 1:1 v/v) polar media (adapted from *J. Am. Chem. Soc.*, 2016, **138**, 11113).

Chapter 5 describes the fiber to nanosphere morphology transformation along with gel-to-sol phase transition of a low molecular weight gelator in response to external stimuli (metal ion). In this work, we have introduced a low molecular weight gelator with an unusual metal binding motif termed as “*half-crown/two carbonyl*”, which is coordinated with metal ions (Ca²⁺) and transform its morphology form fiber to nanosphere upon gel-to-sol phase transition. By different analytical as well as the computational study we confirmed the interactions between the metal ion and “*half-crown/two carbonyl*” binding motif and established the morphological transformation mechanism of the corresponding gelators molecule.

At the end, the portion “Summary”, will provide the conclusion of the overall work presented in this thesis along with suggestions for the future direction.

Arunava Maity

CHAPTER 1

An Overview of Supramolecular Gels: Tuneable Optical Properties, Morphology and Opportunities

1.1. A Brief Introduction of Supramolecular Chemistry

In nature, large and complex biological systems such as the lipid bilayers, the DNA double helix, the collagen triple helix and the tertiary and quaternary structures of proteins are formed by the distinct supramolecular organization of natural building blocks with the help of numerous noncovalent interactions. This unrivalled complexity and elegance of natural assemblies through molecular recognition and the desire to understand, mimic the structure, and functions of such architectures were the inspiration to chemists to the development of supramolecular chemistry. It is generally defined as the “chemistry beyond the molecule” and deals with the design and synthesis of novel supramolecular architectures via spontaneous self-assembly of molecules, governed by various noncovalent interactions between or within molecules.¹ Professor. Jean-Marie Lehn introduced the term supramolecular chemistry and its concept in 1978. According to him, supramolecular chemistry may be divided into two broad and partially overlapping areas as supermolecules and supramolecular assemblies. Supermolecules are well-defined, discrete oligomolecular species formed by the intermolecular association of a few components based on the principles of molecular recognition. Supramolecular assemblies are polynuclear entities that result from the spontaneous self-assembly of a large undefined number of components into a specific phase having more or less well-defined microscopic organization and macroscopic characteristics depending upon its nature, as in the case of membranes, vesicles, micelles etc.

Started only as a laboratory curiosity nearly 40 years ago, supramolecular chemistry has emerged into one of the most fascinating and active fields of research of modern chemistry. The roots of the supramolecular chemistry lie on molecular recognition and host-guest interaction. However, the modern supramolecular chemistry stretches from molecular recognition in natural and artificial complexes to the design of functional supramolecular materials for applications in biology, medicine and material science. Therefore, supramolecular chemistry is an interdisciplinary area of research and plays a crucial role in the development of the emerging area of nanoscience and nanotechnology.

1.2. Concept Behind the Gel State

In general, gels are soft materials which do not flow and capable to sustain its own weight. In spite of the fact that gels are common in nature and frequently encountered in our everyday life and in the industry, there is no precise definition of the gel. This ambiguity was first indicated by Jordan-Lloyd; who in 1926 stated that “the

colloidal condition, the gel, is one which is easier to recognize than to define".² Since that time, scientific understanding about gels has made major improvements and nowadays scientists from various backgrounds are working on diverse types of gels. However, it remains difficult to make a consistent definition as to what composes a gel. Recently, Flory included structural criteria, such as the formation of an infinite entangled network, or a three dimensional (3D) structure in exhibiting properties such as coherence and connectedness, in the definition of a gel.³ A more recent definition offered by Murphy states gel as a viscoelastic solid, which, in a rheological test, exhibits a plateau in the real part of the complex modulus extending over an appreciable window of frequencies.⁴ Later on, both of these definitions were accepted and modified by Almdal *et. al.* who stated that a gel is a soft material exhibiting solid or solid-like character, which composed of two or more components, one of which is a liquid, present in substantial quantity.⁵ The most recent definition of the gel was given by Keller; gels are fluid-containing self-sustainable dispersed systems where the nonfluidic connecting elements, such as polymer chains or large molecular assemblies are responsible for the continuity to give the retention of shape.⁶ A 3D network structure is important in imparting the mechanical strength and the networks get connected at the junctions, i.e. crosslinking points in polymer gels or contact area in molecular gels. Depending upon nature of the interaction at the cross-link points there are two kinds of gels (Figure 1.1); a) chemical gel (covalent bonding at crosslink junctions) and b) physical or supramolecular gel (supramolecular bonding at crosslink junctions). In this chapter, we will mainly focus on various aspects of supramolecular gels.

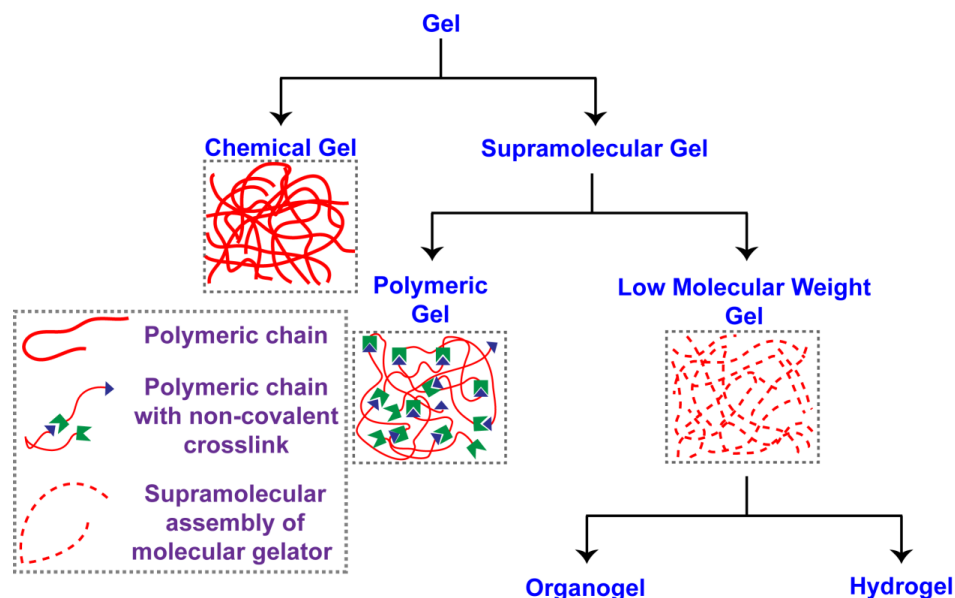


Figure 1.1. Classification of gels based on nature of gelator.

1.2.1. Supramolecular Gels

Since chemical gels are interconnected via non-dynamic covalent bonds, they are mechanically stable and can be considered permanent on an experimental timescale. The same qualities that make these chemical gels so suitable for some applications (stability, chemical inertness) also make them less suitable for others, specifically if these materials need to be further processed or recycled. Hence, the utility of chemical gels for an application like encapsulation and controlled release or stimuli-responsive “smart materials” is limited. On the contrary, supramolecular gels are stimuli responsive tuneable form of a soft matter. Reversible nature of supramolecular interactions in gel networks greatly facilitates their processing and recyclability. There exist a wide range of external stimuli which can dramatically affect the physical properties of the resulting gels. Such stimuli include temperature variation, mechanical agitation, oxidation, change of pH value, the addition of specific chemical compounds as well as light irradiation. Hence, the environmental responsiveness makes the supramolecular gels smart media for immobilizing guest molecules (drugs, proteins, etc.) and their controlled release.

1.2.2. Polymeric Supramolecular Gels

The formation of gels from macromolecules (e.g. polyacrylate, polymethacrylate *etc.*) using physical interaction rather than the strong covalent bond in their cross-link position is typically known as a polymeric supramolecular gel. Polymeric supramolecular gels not only retain the mechanical characteristics of chemical gels,⁷ but also de-crosslinks under the incidence of certain external stimuli,⁸⁻¹² which significantly promotes the utility of supramolecular gels.

1.2.3. Low Molecular Weight Supramolecular Gels (LMWSGs)

In contrast to macromolecular based gels, the low molecular weight gels (LMWGs) are composed of small molecules with molar mass of ≤ 3000 .¹³ Usually these small molecules are self-assembled into gel through certain non-covalent interactions like H-bonding, π - π stacking, electrostatic interactions, metal ion coordination, solvophobic forces (hydrophobic forces for gels in water) and van der Waals interactions, which drive the one-dimensional growth of these molecules to produce nanoscale or microscale structures in the form of fibers, strands and tapes *etc.* Hence in the strictest sense, they are supramolecular in nature and termed as LMWSGs.

As the low molecular weight gelators are basically small molecules; they allow us to probe how molecular structure of the gelator controls the nano-scale assemblies

they form and how this in turn controls the properties of the gel formed. Again, as they are held together by non-covalent interactions they tend to be more responsive (or “smart”) than their chemical gel counterparts and more readily synthesizable. This ease of synthesis and ability to better characterize a small molecule than a polymer should mean that it is easier to incorporate functionality into the gelator, and to monitor how changes in structure to the gelator molecule control gel properties, leading to more tuneable materials.¹⁴ In this dissertation, few examples of the low molecular weight based supramolecular gels have been discussed. Two most important factors, namely, synthetic methodologies for incorporating desired structure/morphology directing functionality(ies) in the molecular structure of the building blocks of **LMWSGs** as well as the stimuli responsiveness shall be the subject of further review in this chapter. To develop a better insight, it is important to discuss about the mechanism as well as the factors that govern gel formation, common functional groups that usually help to design new low molecular weight gelators, their essential characterization procedures/techniques. Further how introduction of certain functionality(ies) could influence the eventual morphology of the supramolecular aggregates will be discussed along with the changes in optical responses/properties of certain **LMWSGs** in response to certain external stimuli.

1.3. Mechanistic Consideration of Supramolecular Gel Formation

Supramolecular gelation is a multistep event (Figure 1.2)¹⁵. However, the general mechanism of supramolecular gelation contains three key stages: (1) The supramolecular interactions such as hydrogen bonding and π - π stacking, which enable molecular fragment to form supramolecular polymer (referred to as fibrils); (2) Subsequent self-assembly of fibrils to form nanoscale bundle, which are known as fibres; (3) Eventually such fibres tangle and interact with one another to form self-supporting, solid like network where the solvent was trapped to result in a macroscopic gel.

Supramolecular gel can be prepared either by mixing gelator into a good solvent (highly soluble) and followed by addition of a bad solvent (poorly soluble) or by heating and cooling the gelator in a solvent. Sonication can also be used for gelation, instead of heating. Gel formation is strongly depended on two factors: gelator concentration and temperature. Raise in gelator concentration enhances the degree of self-assembly, whereas a rise in temperature disfavors the self-assembly. There are two key characteristics physical parameters of gel used to quantify the gelation property: minimum gelator concentration (CGC) and gel-sol transition temperature (T_g).

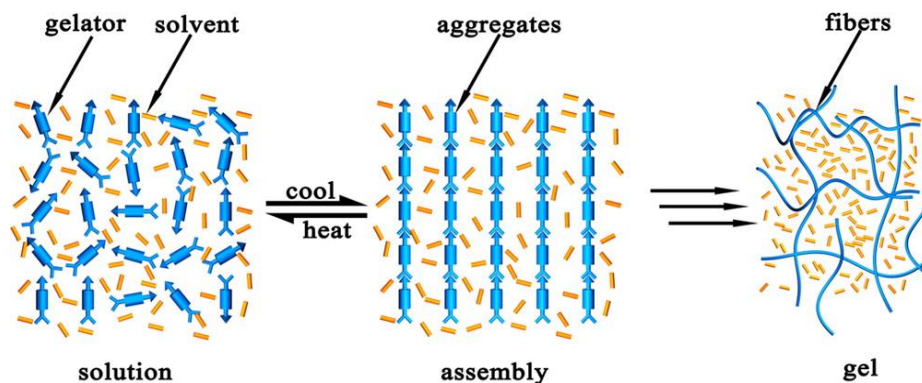


Figure 1.2. Schematic representation of the supramolecular gelation process of low molecular weight gelators [reproduced with permission from the American Chemical Society (ref. 15)].

A close look at the wide range of gelator molecules and the properties as well as the morphology of the **LMWSGs** reveals that supramolecular gelator molecules need to satisfy the following criteria. (a) Gelator molecule must be partially soluble in the solvent, where it gels. The complete miscibility of solute molecules will hinder the solute-solute interactions and gelation will not be possible. Similarly, poor solubility will lead to precipitation. (b) The option for multiple supramolecular interactions between the monomer units. Generally, hydrogen bonding and π - π stacking are the main driving forces for gelation in organogel (gels formed in organic solvents). In addition to these forces, hydrophobic interaction also plays a key role in hydrogel (gel formed in aqueous medium) formation. (c) The supramolecular interaction must be directional, leading to assembly of anisotropic nanoscale fibres.

1.4. Structural Requirements for Supramolecular Gelators

Even though the chemical structure of many of the gelators appears rather simple, it is quite hard to envisage the structural requirements for molecules to show gelation process. However, the information gained from a variety of different types of gelators helped in rationalizing the general structural requirements of molecular gelators. In the majority of the cases, the presence of functional groups such as hydroxyl, amide, urea and carboxylic acid that are capable of forming H-bonded assemblies has been proved to be essential for gelation. The directionality, specificity along with the rigidity imparted by the multiple H-bonding interactions help spatial arrangement of functional chromophores in achieving efficient gelation. For example, the complexation between ditopic N,N'-disubstituted melamine type DAD (D: hydrogen(H)-bond Donor and A: H-bond Acceptor) module and barbiturate or

cyanurate type ADA modules as well as the complementary interactions of acid-pyridine derivatives have also been widely used for gelation (Chart 1a). Molecules with structural motifs such as amino acids, peptides, cholesterol, sugar, cyclohexylamine, chiral/achiral aliphatic/oligoethylene chains (Chart 1b), etc. have been found to facilitate gelation of a variety of solvents.

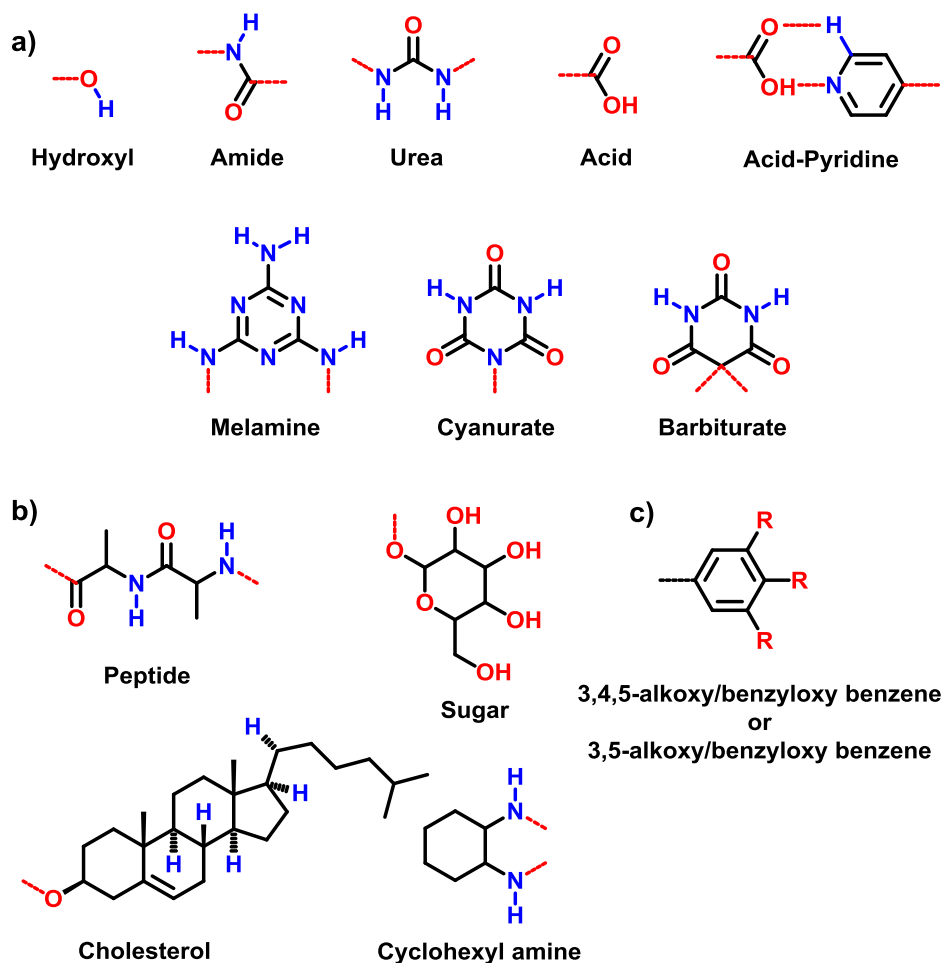


Chart 1.1. Structural requirements for the design of gelators.

Presence of an aromatic core that favours π - π stacking is another requirement for the design of organogelators. Molecules that facilitate dipole-dipole and donor-acceptor interactions can also lead to the gelation of solvents. Another important structural requirement for molecules to favour gelation is the presence of hydrocarbon chains with optimum chain length or an appropriately substituted aryl ether functional group. For example, functionalization of molecules with 3,4,5- or 3,5-alkoxy substituted benzene (Chart 1c and 1d) moieties helps to induce gelation. The presence of alkoxy chains maintains the subtle balance between solubility and precipitation of the gelator

molecules in a given solvent. The presence of hydrocarbon chains also facilitates Van der Waals interaction of gelator molecules. However, the benzyloxy functional group increases the π - π and hydrophobic interactions. In a majority of cases, more than one such structural requirement is essential for the design of gelator molecules, even though there are exceptions.

1.5. Characterization of Supramolecular Gel

Many techniques have been developed to characterize gel systems. These techniques provide information about intra as well as intermolecular interactions which leads to gelation, morphology of the gel, viscoelastic properties and molecular packing of the gelators in its gel state.

1.5.1. Inverted Vial Method

Inverted vial method is the simplest method to confirm gelation by direct visualization. In this method, the weighed amount of gelator is taken in a vial with the required amount of solvent. The vial is then closed properly and carefully heated to the optimum temperature so as to melt its content completely. The vial is then allowed to cool or sonicate for sufficient time before inverting it. The absence of flow of the evolved semisolid mass after inversion the vial indicates the formation of gel.¹⁶ The minimum concentration of the gelator required to generate the gel is known as the critical gel concentration (CGC).

1.5.2. Gel Morphology

There are several methods for determining the morphology of gel systems. These methodologies include direct imaging techniques such as scanning electron microscopy (SEM) and transmission electron microscopy (TEM). In these techniques, a gel patch is dried, and often, stained with the heavy element to enhance the image contrast. The sample is then placed under ultra-high vacuum and imaged with an electron beam. While analysis of SEM images provides the surface morphology of the gel. More insightful morphology information such as hollow nature of the gel fiber, wall thickness *etc.* can be obtained from the analysis of TEM images. Atomic force microscope (AFM) can give information about the thickness as well the height of the gel fibers. An indirect method used to determine the morphology is based on scattering techniques such as small angle X-ray scattering (SAXS) or small angle neutron scattering (SANS) in which sample is hit by X-ray or neutron radiation.^{17,18} The particle in the beam is scattered depending on the size and shape of fibers and mathematical treatment of the scattering

intensity as a function of angle and size provide the information regarding morphology of the gel fiber.¹⁹

1.5.3. Viscoelastic Properties of Gel

Rheology offers a very convenient and relatively easy way to measure the viscoelastic properties of gels. These properties are measured by rheometer, in which the sample is placed and subjected to shear. Viscoelastic properties of the compound are determined in terms of viscoelastic storage moduli (G') and loss moduli (G'').²⁰⁻²² The numerical values for both G' and G'' are obtained from the oscillatory rheology experiment. G' represents the amount of energy that can be stored in the sample, which indicates the elasticity of the sample. G'' symbolizes the tendency of the material to flow. For ideal solid, $G'' = 0$ and for Newtonian liquids $G' = 0$. For viscoelastic materials like gels, G' is greater than G'' , which suggests the dominant elastic behaviour of the system.

Gels behave either as a viscoelastic solid or viscoelastic liquid, which depends on whether the molecular network is static or highly dynamic. Two types of rheological measurement are often performed on gels: (i) Determination of mechanical stress resistance and ii) Dynamic moduli measurement. The dynamic moduli mainly depend on frequency (time scale) of the measurement. The observed frequency dependence gives insightful information about the relaxation and lifetime of the bonds between gelator molecules.²⁰⁻²² For example, if the bonding is static, relatively low frequency-dependence is expected and $G' \gg G''$ in all frequencies. This is often observed in static gels structure.²³ If the bonding is dynamic, $G' < G''$ at lower frequencies and $G' > G''$ at higher frequencies. This is often observed in wormlike micelles.²⁴

1.5.4. Organization of Gelator Molecules in the Gel Fiber

Understanding the organization of molecules in the gel phase is most relevant in the characterization study of gels. The organization of molecule provides direct information on different intermolecular interactions present in the gel fiber and how it contributes to gelation properties. 2D NMR spectroscopy and single crystal X-ray diffraction are normally utilized to determine the organization of the supramolecules. However, 2D NMR spectroscopy is limited in its use for gel, since gel fiber in the solid state generally do not provide clear signals.²⁵ The single crystal X-ray can be performed only on crystal of sufficient size and it is not easy to generate single crystals from gel phase. Only very few instances have been known where the crystal structure of gelators is completely resolved.²⁶ Therefore, powder X-ray diffraction (PXRD) technique is used, which provides the information regarding the organization of the gelators.²⁷ The

information about the organization of the molecule in the gel fiber is also obtained indirectly by FT-IR spectroscopy. The chemical environment of each functional group in the gelator is probed from the position of the vibrational peak in the FT-IR spectra.²⁸

1.6. LMW based Supramolecular Gelators with Tenable/Controllable Optical Properties

The optical property of any material is defined as its interaction with electromagnetic radiation in the visible. Manifestation of the optical properties of LMWSGs range from absorbance and reflection to fluorescence, molecular or macroscopic chirality, non-linear optical properties *etc.*²⁹ These properties strictly depend on the supramolecular arrangement of the molecular building blocks in the bulk systems. The non-covalent interactions associated with the chromophoric gelators as well as the relative nature of the particular chromophoric moieties influence these properties, and therefore a wide range of effects can be observed for the chromophores under the influence of supramolecular gelation. Among the various kinds of optical properties, here we will illustrate the tuneable absorbance and fluorescence colour, and the supramolecular chirality of few low molecular weight based gelators composed of various chromophoric functional units with the changes of solvent structure/polarity or on applying the external stimuli. In addition, we will look into the few photophysical process of chromophoric functional groups containing LMWSGs.

1.6.1. Solvent Structure Assisted Fluorescence Modulations of LMWSGs

Nature of solvent structure could play an excellent role in alteration of molecular organization mode of self-assemblies. For example, aromatic solvents (e.g. benzene, toluene, *o*-xylene, mesitylene *etc.*) usually prefer to interact with the aromatic functional groups of the assemblies. In contrast, aliphatic solvents (e.g. *n*-decane, hexadecane, *n*-octane) prefer to interact mainly with the alkyl regions of the assemblies. Hence the molecular organisation of the self-assemblies is strongly influenced by the nature of the solvent molecules or the other dopant having comparable concentration. Presence of appropriate fluorophore or chromogenic molecule in such self-assembled structures would result in the modulated optical properties either through altered degree of molecular rigidity or through some photoinduced process that is/are influenced by the aggregated state.

This fundamental concept was recently utilised by Das *et al.* to modulate the luminescent color of C_3 -symmetric donor-acceptor molecules containing 1,3,4-oxadiazole and bithiophene moieties in the central core functionalized with octyl (**1A**) and dodecyl (**1B**) substituted phenyl acetylene units at the periphery (Figure 1.3a).³⁰

Compound **1B** formed gels in both aliphatic and aromatic solvents. The gelation of **1B** in aliphatic solvent *n*-decane shows red color emission with maxima at 610 nm and in aromatic solvent toluene, it shows green emission with a significant blue shift of emission maxima at 500 nm.

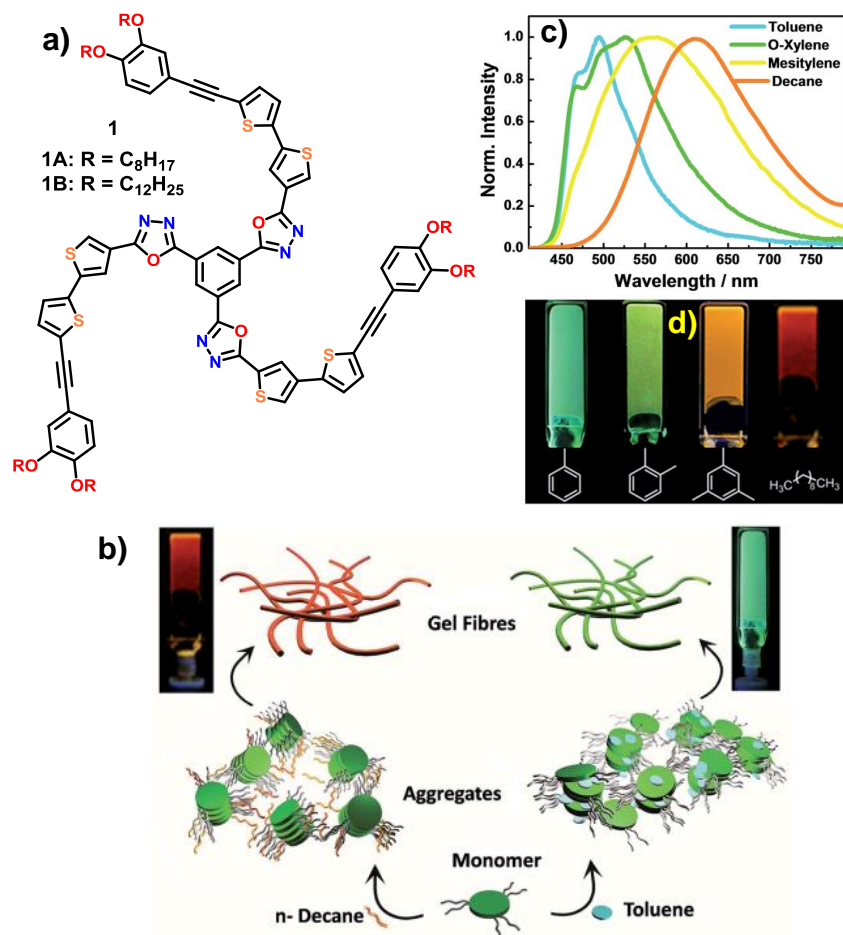


Figure 1.3. (a) Molecular structure of the gelators; (b) Schematic representation of the aggregate formation of **1B** in *n*-decane and toluene; (c, d) Emission spectrum of **1B** in the gel state in different solvents ($\lambda_{\text{ex}} = 400$ nm; 1 mm cuvette) and photograph of **1B** in various gels under 365 nm UV illumination respectively [reproduced with permission from the Royal Society of Chemistry (ref. 30)].

As an explanation, they show a schematic presentation of the molecular organization mode of the gelator **1B** (Figure 1.3b). In aliphatic *n*-decane solvent, the solvent molecules interact largely with the alkyl regions of **1B**, which probably helps to happen to have π - π interaction between of the central 1,3,4- oxadiazole and bithiophene based aromatic moieties of the neighbouring molecules and resulting in strong excitonic coupling between the neighbouring molecules leading to excimer type

emission in the red region (Figure 1.3b). In aromatic toluene solvent, the solvent molecules interact mainly with the central chromophoric aromatic part of **1B** resulting in reduced π -stacking between the molecules in the aggregate leading to monomer type green emission (Figure 1.3b). Luminescence color modulation was proved by recording the luminescence spectra of **1B** in its solution as well as gel state and by direct visualization by capturing the photograph of the prepared gel in different solvent (Figure 1.3c and 1.3d)

A similar concept was utilized by Banerjee *et al.* through a delicately designed gelator **2** containing naphthalene diimide (NDI) as π -conjugated chromophoric moiety, an amino acid residue as well as a long alkyl chain to favour the H-bonding and Vander walls interaction (Figure 1.4a).³¹ The gelator showed a remarkable “turn on” luminescence response in toluene due to the *J*-type molecular aggregation (Figure 1.4c and 1.4e), however in *n*-octane the gelator attain an *H*-type molecular aggregation and showed a “turn off” luminescence property (Figure 1.4b and 1.4d).

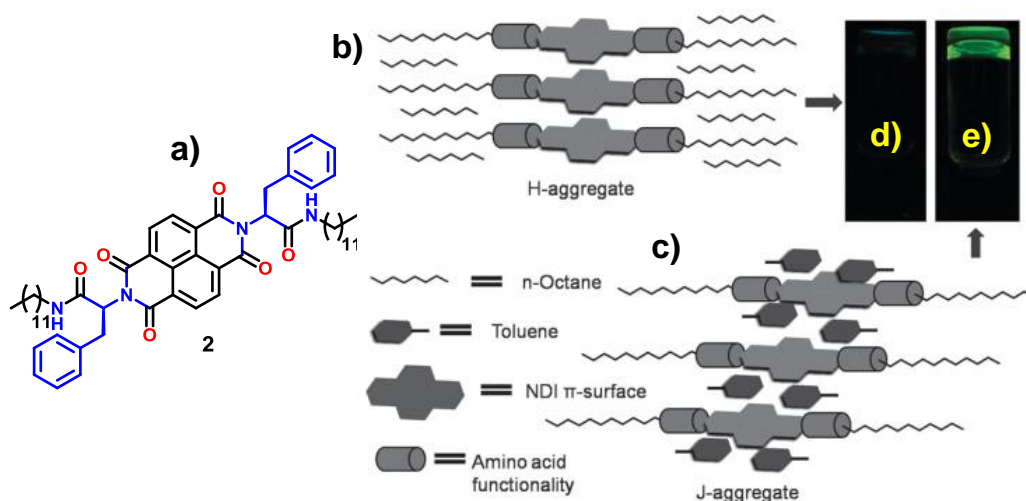


Figure 1.4. (a) Chemical structure of gelator **2**; (b, c) *H* and *J*-type molecular aggregation mode of gelator **2** in *n*-octane and toluene respectively. (d, e) shows the photographs of fluorescence turn off and the turn on behavior of *n*-octane and toluene gel of **2** [reproduced with permission from the Royal Society of Chemistry (ref. 31)].

1.6.2. Aggregation-Induced Enhanced Emission (AIEE) Process for Modulating the Luminescence Property of Supramolecular Gels

Certain molecules having poor or negligible emission quantum yield in their monomeric form in solution may show strong emission in their gel state due to AIEE phenomenon.³²⁻³⁴ Several factors could contribute to this enhanced emission in the

aggregated state, including the presence of a forbidden band in *H*-aggregates, *J*-aggregate formation, planarization, and restriction of conformational flexibility.

As an example, the gelation of trifluoromethyl-based cyanostilbene derivative **3** (Figure 1.5a) showed a considerable enhancement in fluorescence intensity.³³ The fibrous aggregates of **3** are strongly fluorescent due to the enhanced emission in the aggregate state (Figure 1.5e). The gelation of **3** is attributed to the cooperative effect of the π - π stacking interactions of the rigid rod-like aromatic segments and the supplementary intermolecular interactions induced by the four CF₃ units. In gel state, gelator molecules (**3**) are likely to show drastically enhanced fluorescence emission when compared to those of isolated state due to intramolecular planarization and restricted excimer formation. This can be visualized from the photograph of the gel under UV illumination (Figure 1.5b and 1.5c) and fluorescence microscopy images (Figure 1.5e).

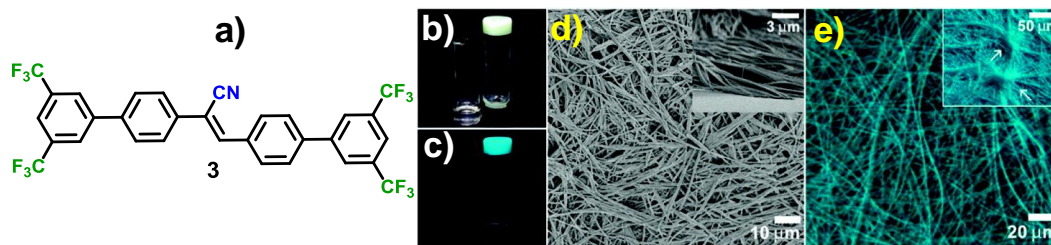


Figure 1.5. (a) Chemical structure of gelator **3**; Gel and solution state photographs in DCE of **3** (b) under day light and (c) under UV light (365 nm); (d, e) SEM and fluorescence microscope images of DCE gel of **3** respectively [reproduced with permission from the American Chemical Society (ref. 33)].

Recently, Tang and co-workers developed AIEE active gelator **4** (Figure 1.6a), by functionalizing tetraphenylethene (TPE) moiety with a stigmasterol group.³⁴ The gelator **4** in its monomeric form is highly flexible in nature due to the presence of central TPE unit and the peripheral long alkyl chain. The luminogen **4** is an excellent gelator and undergo a facile self-assembly process to form an organogel by gentle heating and subsequent cooling of its methanol solution to room temperature. The formed organogels show much stronger emission than their isolated species in solution, displaying a typical phenomenon of AIEE (Figure 1.6b and 1.6c). The self-assembly of molecules of gelator **4** into a 3D organogel should largely rigidify their molecular conformations and restrict the intramolecular rotation of the peripheral phenyl rings. This blocks the nonradiative relaxation channel of deactivation of the excited states and populates excitons that undergo radiative decay, thus making the organogel of **4** highly emissive upon photoexcitation.

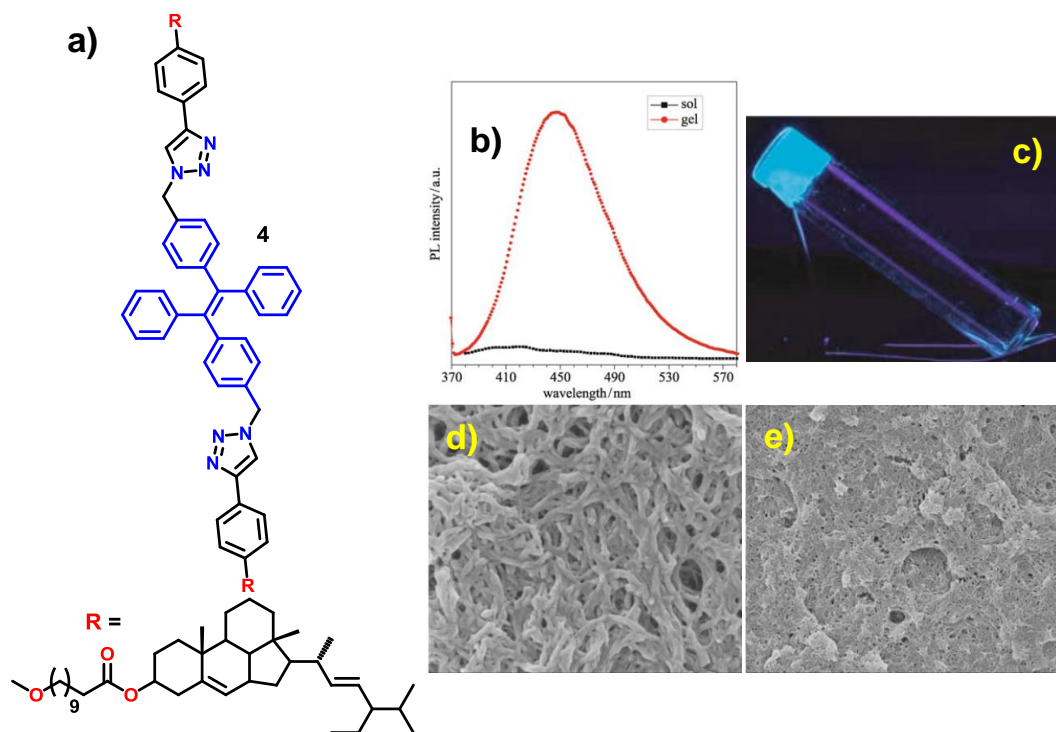


Figure 1.6. (a) Molecular structure of TPE based gelator **4**; (b) PL spectra of hot methanol solution (0.5 wt%) and organogel of **4**; (c) Fluorescent image of organogel of **4** formed in methanol (0.5 wt%) taken under UV irradiation (365 nm); (d, e) SEM images of organogel of **4** [reproduced with permission from the Springer (ref. 34)].

1.6.3. Supramolecular Gelators with Excited-State Intramolecular Proton Transfer (ESIPT) Features

2-(2'-Hydroxyphenyl)benzoxazole (HPB) chromophoric group has been extensively studied because of its reversible excited-state intramolecular proton transfer (ESIPT) feature, which endows it with tuneable emission intensity and color. Recently, Lee and co-workers developed two organogelators **5** and **6** using HPB core (Figure 1.7). Addition of cold toluene to the hot DMF solution of **5** resulted a stable gel (0.5 %, DMF-toluene, 1:9 v/v).³⁵ Emission quantum yield for the gelator **5** in its DMF solution ($\Phi_F = 1.4$ %) is reported to be poor, however, a substantial enhancement in Φ_F value to 34.7 % is observed in its organogel form. In the process of gelation, the HPB units of the molecules of **5** are aggregated. This constrains the free rotation of the benzoxazole ring and favours the ESIPT process from the hydroxyl proton to the nitrogen atom. This helps in converting the molecule from an enol tautomer to a keto form (Scheme 1.1) with a better structural planarity that favours a more efficient π -stacking interaction and gel formation. Additionally, H-bond forming ability of the urea moiety along with the Van der Waals forces between the octyl chains contribute favourably to gel formation.³⁵

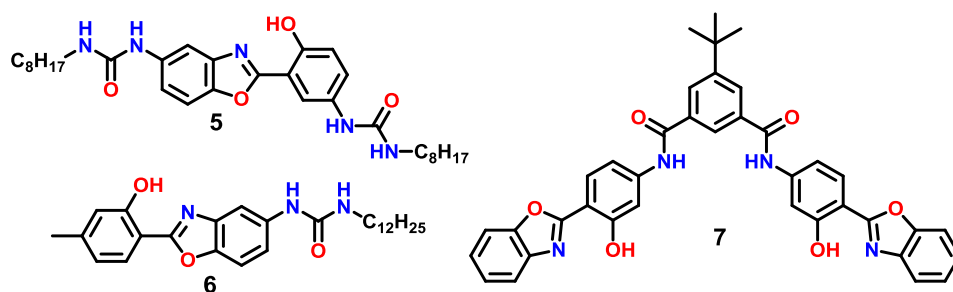
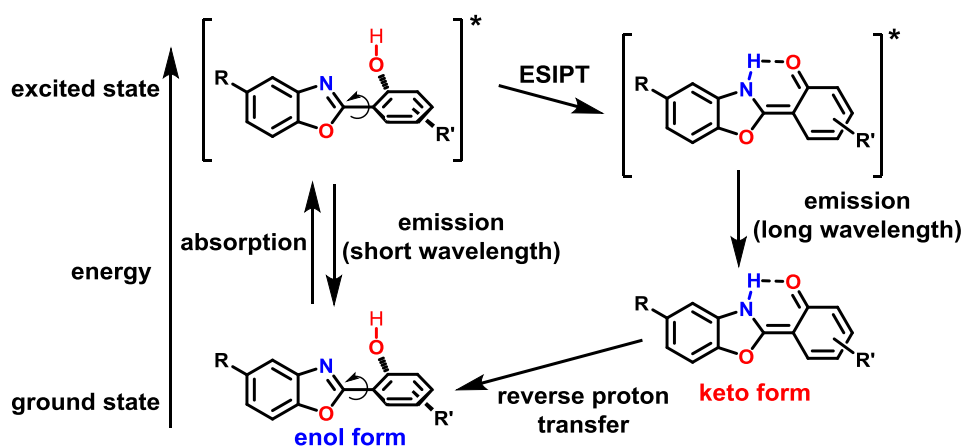


Figure 1.7. Molecular structures of organogelators consisting of ESIPT active 2-(2'-hydroxyphenyl)benzoxazole (HPB) unit.



Scheme 1.1. Proposed mechanism for the ESIPT process of HPB units.

Similarly, the gelator **6** also exhibits ESIPT characteristic due to the presence of the HPB core.³⁶ It possesses thermally reversible gelation ability (Figure 1.8). The gel of **6** exhibits dramatically enhanced fluorescence with respect to its solution state. The predominant formation of a planar keto tautomer attributes to the higher emission quantum yield with longer emission wavelength (Figure 1.8).³⁶

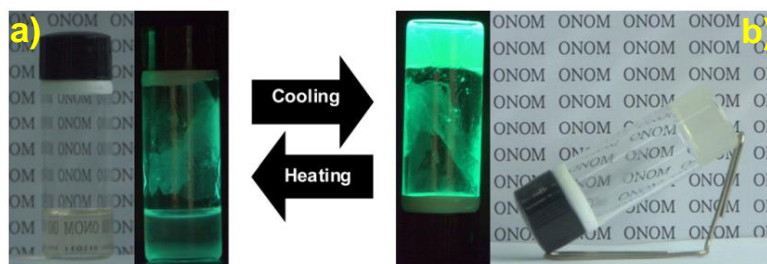


Figure 1.8. Photographs demonstrating the sol-gel process of gelator **6** in CCl_4 [1% (w/v)] using the heating-cooling method and weak and strong luminescence characteristic in solution (a) and gel state (b) [reproduced with permission from the Royal Society of Chemistry (ref. 36)].

Yang and co-workers³⁷ prepared a HPB-based gelator **7** without alkyl chains (Figure 1.7) and found that it can form a uniform, stable and thermoreversible organogels in the THF-cyclohexane mixture (Figure 1.9). In this case, it is considered that the formation of H-bonds between *J*-aggregated dimers of **7** through $\text{N}\cdots\pi$ and $\text{O}\cdots\pi$ stacking interactions of the oxazole rings have driven the self-assembly of the molecules efficiently. Similar to other HPB-based ESIPT gelators **5** and **6**, **7** is weakly fluorescent in the solution state but emit intense sky blue light in the gel state. The ESIPT phenomenon, *J*-aggregate formation and restriction of the TICT process are speculated to be responsible for the efficient emission in the gel state.³⁷

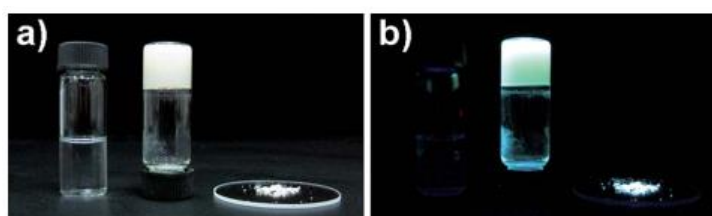


Figure 1.9. Photographs of gelator **7** in THF solution and gel (0.67 wt% in THF/cyclohexane mixture 2:3 v/v) state and solid powder states taken under (a) normal room illumination and (b) 365 nm UV irradiation [reproduced with permission from the Royal Society of Chemistry (ref. 37)].

1.6.4. Tuneable Luminescence Through Excited State Energy Transfer Within the Supramolecular Gel Matrix

The spatial arrangement of suitable donor and acceptor chromophores is important for achieving efficient intermolecular energy transfer. Supramolecular gels resulting from donor-acceptor pair based molecules have been proved to be an efficient media to promote energy-transfer process.³⁸ It is important to identify appropriate molecular donor-acceptor systems that self-assemble to form gels, in which the excited state properties of the donor and the acceptor could be exploited to control the photophysical properties of the gel matrix. With this objective, a variety of chromophores, both functional organic dyes as well as π -conjugated fluorophores, modified with functional groups that interact through noncovalent forces have been reported.³⁸

A class of supramolecular gelators that exhibit efficient energy transfer in the gel phase is oligo(*p*-phenylenevinylene)s (OPVs). So far several OPVs with different end functional groups and lateral side chains were synthesized and shown to form organogels with tunable emission colors.³⁹ Ajayaghosh *et al.* showed an excellent example of an organic supramolecular light-harvesting system comprising an OPV based gelator **8** as the donor and a π -conjugated molecular wire (PYPV) **9** as the acceptor exhibits efficient energy transfer in the organogel matrix (Figure 1.10a).⁴⁰ The broad absorption band observed for the cyclohexane solution of the acceptor **9** (6.12×10^{-6} M) overlaps well with the emission of the self-assembled donor OPV gelator **8**; which makes them suitable molecular pair for energy transfer process. The feasibility of energy transfer has been studied in the gel state of **8** by encapsulation of small quantities of **9** (0 - 1.53 %) within the self-assembled structure of the donor **8** in cyclohexane (1.12 mM). Efficient energy transfer at low mol % of the acceptor (<1.6 mol %) due to the fast exciton migration ($K_{EM} = 1.28 \times 10^{10} \text{ s}^{-1}$) of the singlet exciton within the gel medium was observed (Figure 1.10b). The fluorescence decay profile of **8** gel in cyclohexane exhibited a fast biexponential ($\tau_1 = 1.62 \text{ ns}$ (49%) and $\tau_2 = 4.43 \text{ ns}$ (51 %)) decay. In the presence of 1.53 mol % of **9**, decay profile with time constants of $\tau_1 = 0.72 \text{ ns}$ (56 %) and $\tau_2 = 2.22 \text{ ns}$ (44 %) (Figure 1.10c) is observed. This progressive shortening of the lifetime of **8** in the presence of **9** confirms the nonradiative energy transfer from donor **8** to acceptor **9**. A schematic model of this energy transfer process and donor-acceptor supramolecular interaction through noncovalent interaction has been presented in Figure 1.10d).⁴⁰

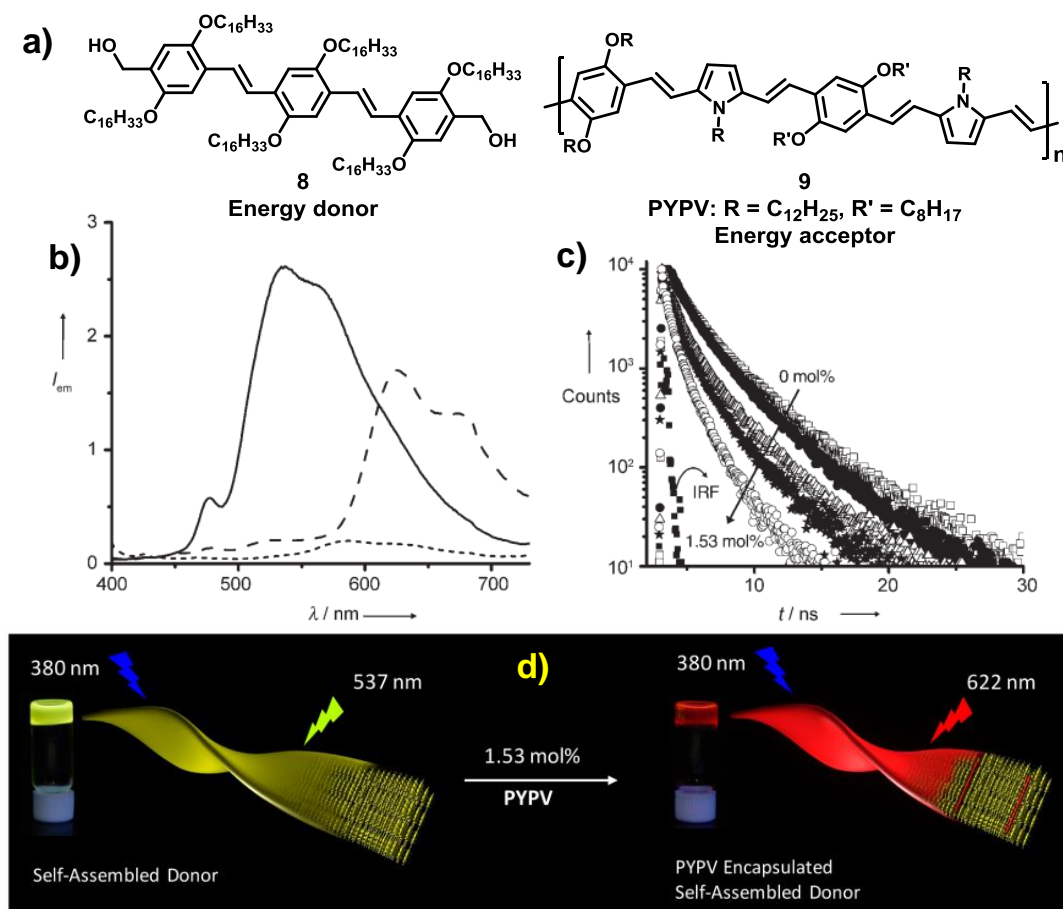


Figure 1.10. (a) Molecular structure of OPV donor gelator **8** and PYPV acceptor **9**; (b) Fluorescence spectrum of the cyclohexane gel of **8** ($c = 4 \times 10^{-4}$ M, $l = 1$ mm) in the absence (—) and in the presence (---) of **9** (1.53 mol %) and **9** alone (···) ($\lambda_{ex} = 380$ nm); (c) Fluorescence decay profiles of the **8**-cyclohexane gel at various concentrations of PYPV (0–1.53 mol %), monitored at 537 nm, IRF = instrument response function; (d) Schematic representation of the energy transfer process in **9**-encapsulated within the self-assembled tapes of the gelator **8** [reprinted with permission from (ref 40). Copyright 2007 WILEY-VCH].

In 2008, Shu and coworkers⁴¹ designed hemicyanine dye based red emitting gelator **10**, and two different C-4 substituted 1,8-naphthalimide based green and blue emitting gelators **11** and **12** (Figure 1.11a). By mixing the three gelators in appropriate proportion, they could achieve six different luminescence color (Figure 1.11b). The intermolecular energy transfer between these gelators played a crucial role in providing the tuneable color by a single excitation wavelength of 365 nm in the mixed gels.

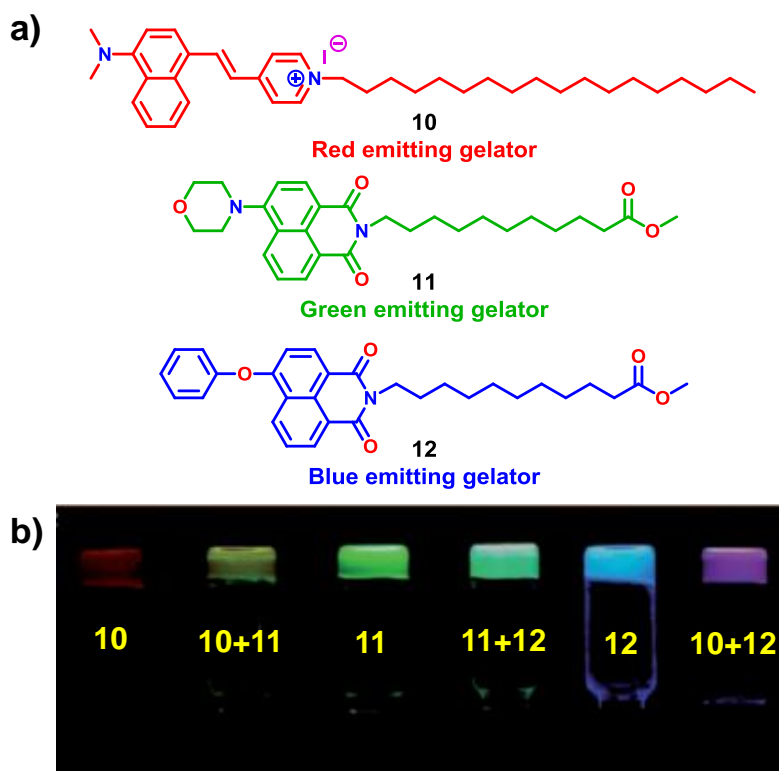


Figure 1.11. (a) Chemical structure of the gelators **10**, **11** and **12**; (b) Photographs of the individual and the mixed gels of gelators **10**, **11**, and **12**, which emit six different colors upon illumination with a single wavelength (365 nm) [reproduced with permission from the Royal Society of Chemistry (ref. 41)].

1.6.5. White-Light Emitting Gels through Energy Transfer Process

White-light-emitting organic materials have attracted much attention due to their potential applications in display and lighting devices.⁴² In general white-light is considered as the optimized composition of three complementary colors i.e. red (R), green (G) and blue (B) (RGB), or at least two complementary colors blue and orange which cover the visible wavelength region (400-700 nm).⁴² Different types of materials used for white-light-emission including π -conjugated polymers, metal complexes and low molecular weight organic gelators.⁴³ One of the strategies behind the white-light emission is to relay on series of energy transfer in suitable donor-acceptor assemblies. In 2009, Schenning *et al.* presented one of the first examples of designed white-light emission from multi-component organogels (Figure 1.12a).⁴⁴ The photoluminescence spectra of the compounds **13-16** show gradual bathochromic shift as a result of gradual changes in donor-acceptor interactions. Additionally, compound **13** and **16** can form fibrils in methylcyclohexane (MCH) solutions resulting in blue and red emitting

organogels, respectively. Mixing small amounts of **14** (green), **15** (yellow) and **16** (red) into a gel of **13** (molar ratio 1/3/4/5 = 4.5 : 0.7 : 0.2 : 0.1) resulted in partial energy transfer from the blue-emitting donor to the embedded energy acceptors upon excitation of **13**. The fluorescence lifetime of **13** in the MCH gel revealed a bi-exponential decay with lifetimes of $\tau = 0.93$ (94.5 %) and 1.81 ns (5.5 %), whereas for the white-light emitting gel, a shorter decay times were observed with $\tau = 0.28$ (95.4 %) and 1.10 ns (5.6 %), respectively. This decrease in the fluorescence lifetime of **13** showed that the emission is quenched by approximately a factor of three in the mixed gel, which indicates energy transfer process is operating.

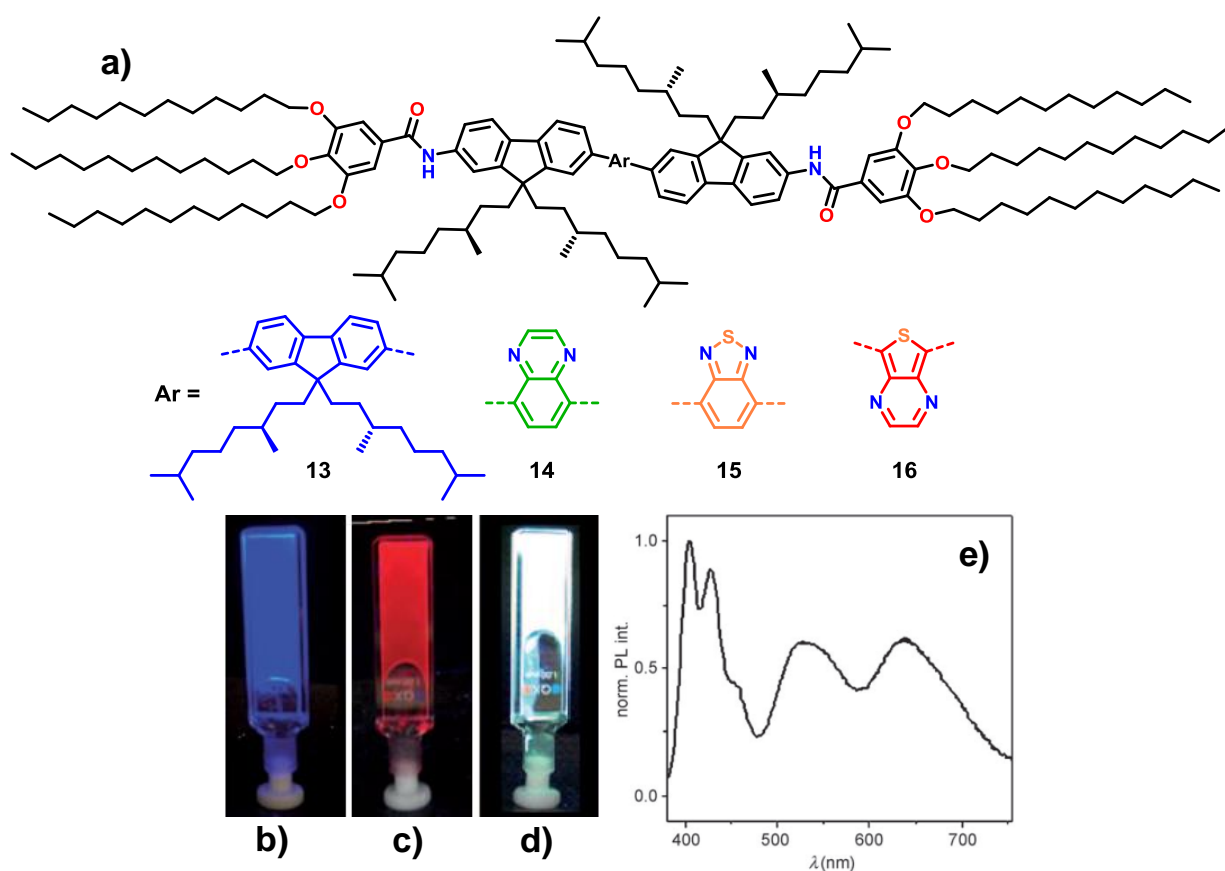


Figure 1.12. (a) Chemical structure of the compounds **13-16**; Photograph of gel (b, c) formed from **13** (blue) and **16** (red) in MCH medium respectively and (d) the coassembled white-light emitting gel mixture under UV illumination ($\lambda_{\text{ex}} = 365$ nm; molar ratio **13/14/15/16** = 4.5 : 0.7 : 0.2 : 0.1); (e) Photoluminescence spectrum of the corresponding white-light emitting gel [reprinted with permission from (ref 44). Copyright 2009 WILEY-VCH].

Recently, Guerzo and co-workers demonstrated the selfassembly of a blue-emitting anthracene chromophore based light-harvesting organogelator **17** and specifically designed highly fluorescent tetracenes (**18-19**) to yield nanofibers with tunable emissive properties.⁴⁵ The authors also showed that upon optimizing relative concentrations of the blue and red components (**18** and **19**), white-light emission can be observed from the organogels of **17** with quantum yields as high as ~26 % in DMSO medium (Figure 1.13c). Such an emission results from electronic energy transfer (EET) from the blue emissive matrix of **17** to the green and red emissive (**18** and **19**, respectively) guest molecules. Interestingly, as shown in Figure 1.13c, such energy transfer processes are only possible in the gel state and not in the solution state. The nanofibres formed during the gelation process were seen to be individual white-light emissive and the higher energy blue emission was found to be polarised.

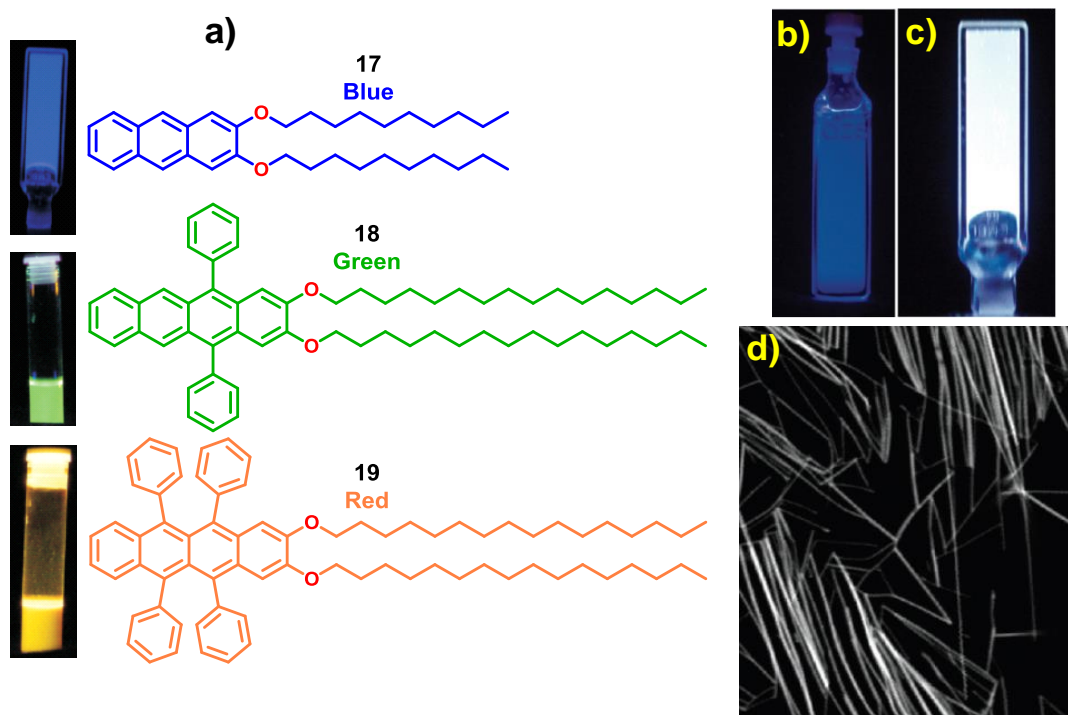


Figure 1.13. (a) Chemical structure of the compounds **17-19** and photographs of a 2 mM **17** gel (blue emitting) in DMSO, 10 μ M solutions of **18** and **19** in THF under UV light (365 nm); Pictures of cuvettes with 2.0 mM **17** with 0.012 eq of **18** and **19** under UV light, (d) THF solution and (e) white-light emitting DMSO organogel; (f) Fluorescence confocal microscopy images of the white-light emitting gel [reproduced with permission from the American Chemical Society (ref. 45a)].

1.6.5.1. Single Component-based White-Light Emitting Supramolecular Gelator

From the example of the previous section, it is realized that for white-light emission the essential criteria is the combination of different emitters (red/blue/green or blue/orange) and the efficiency of energy transfer process among them.⁴⁴⁻⁴⁵ In comparison to the multi-component based white-light emitting system, single ingredient entity of direct white-light emission is more appreciated to simplify the preparation of lighting devices and their fabrication cost.⁴⁶ Therefore, the search for new luminogens that can directly generate white-light is important and urgent. However, it is extremely difficult for single organic dyes to emit either three (blue, green and red) or two (blue and yellow) luminescence colors covering the entire visible spectral window (400-700 nm), for white-light emission. Although significant progress has been made for developing single component based organic white-light emitters in recent past. In most of these cases, the generation of white-light is limited in solution states, and few of them are capable of emitting white-light in solid state.⁴⁷

It was observed that organic fluorescent nanostructures demonstrate optical behaviour which differs significantly from that of the corresponding bulk materials. In single component systems, monomer emission features combined with their aggregate emission, can often result in broad emission profiles and in some cases, white-light. In 2012, Bhattacharya *et al.* demonstrated white-light emission from the controlled aggregation of gelator **20** composed of chromophoric phenylenedivinylene bis-N-alkyl pyridinium salts (PPV) appended with terminal aliphatic hydrocarbon chains (Figure 1.14a).^{48a} In the solution state, the disaggregated chromophores of **20** show blue emission at higher temperatures (50 °C). At lower temperatures (10 °C), the self-assembled aggregates of **20** show red-shifted orange emission (Figure 1.14b). However, at 25 °C, a dynamic equilibrium exists between the monomeric and aggregated states resulting in white color emission (Figure 1.14b). The self-assembled gel of **20** also shows the orange emission. The white-light emission only limited in the solution state, where both the monomeric and aggregated forms of **20** co-exist. The authors also demonstrated that the aggregation processes can be controlled by using external ionic electrolytes (e.g. NaBr), and could tune the multiple luminescence color along with white emission.^{48b}

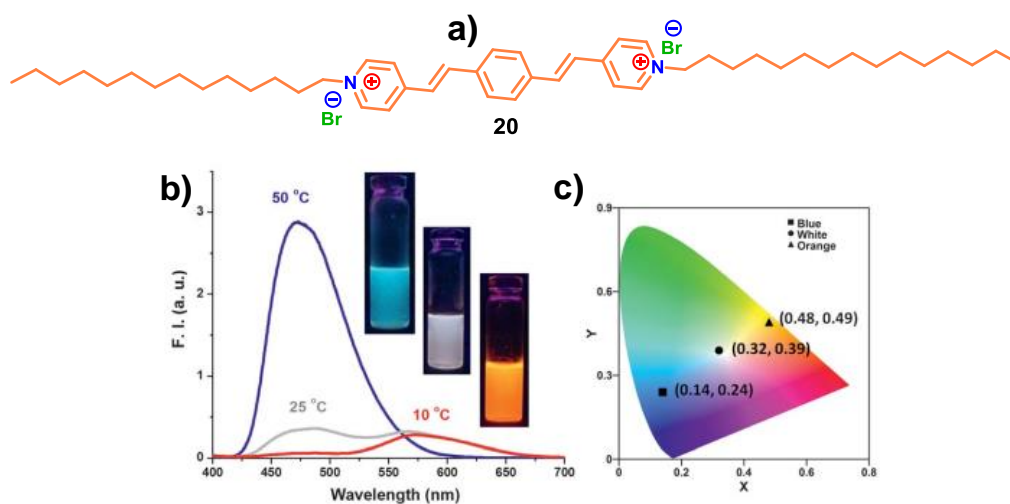


Figure 1.14. (a) The molecular formula of gelator **20**; (b) variable temperature fluorescence spectra of **20** (2×10^{-5} M) in 35 % ethanol-water mixture (excited at 380 nm); (c) Chromaticity diagram with the corresponding color coordinates of the obtained luminescence color in this molecular system [reproduced with permission from the Royal Society of Chemistry (ref. 48a)].

1.6.6. Basic Concept Related to Supramolecular Chirality

From shaking hands to putting on one's shoes, hair whorls on our heads to seed pod of bauhinia variegata or the climbing tree in the garden, artificial sweetener in soft drinks to spiral of a snail or even galaxies, in every level one common term which went unnoticed is chirality.⁴⁹ If we look at the components of our daily usages materials, such as watches, cars even medicinal drugs, nearly all of them are chiral. In short, chirality is a common and compulsory topic in different scientific disciplines ranging from chemistry, physics, biology, pharmacology, materials and nanoscience.⁵⁰ The concept of molecular chirality has long been recognized and provided guidance in the design of drugs and functional molecules, while chirality at a supramolecular level is currently attracting great attention due to rapid developments in supramolecular chemistry and molecular self-assembly.

Generally, the Supramolecular chirality is known as the asymmetric arrangement of molecules through different noncovalent interaction(s). Helical arrangement of the supramolecules usually creates an anisotropic molecular environment and show optical activity; hence mostly the supramolecular chirality identified by the helical molecular arrangement. In supramolecular chirality, it is not the obligatory condition that monomer has to be chiral.^{49d} Even achiral molecule could also show helicity and optical activity. So basically supramolecular chirality depends on how the monomers are

getting arranged in their self-assembled aggregate state and break the symmetry. Depends on the helical rotation, supramolecular chirality commonly refers to *P*/*M* helicity. Viewing from either end of a molecule or supermolecule downward along the helical axis, the system has *P* helicity if the rotation is clockwise and *M* helicity if the rotation is anticlockwise (Figure 1.15).

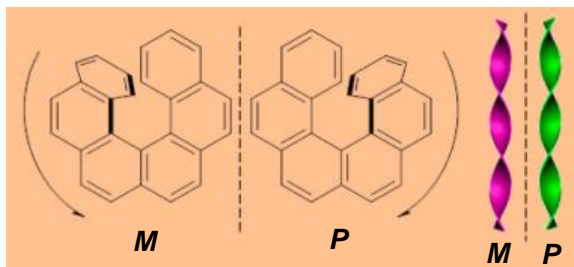


Figure 1.15. Naming conventions of supramolecular chiral molecules and arrangement [reproduced with permission from the American Chemical Society (ref. 49d)].

1.6.6.1. Characterization of Supramolecular Chirality

An important step in the research of supramolecular chirality is the characterization of the chirality. Although there are many methods to characterize the chiral features of a supramolecular system, following two classes of characterization of supramolecular chirality are commonly applied.

(a) Morphological Observation: The morphological observation by various microscopes, one can directly observe the chiral molecules and chiral structures. With the rapid development of STM, AFM, SEM, and TEM technologies, direct observation of chiral structures has been made possible, and these techniques have significantly contributed to the rapid development of research in supramolecular chiral systems.⁵¹ Figure 1.16 shows typical chiral images obtained by these techniques and a brief comparison of the key principles, measurement methods and the obtained results among these techniques.

(b) Spectroscopy Techniques: Spectroscopy provides a powerful method for detecting the chiral characteristics of supramolecular systems. Generally, circular dichroism (CD) spectroscopy is the most widely used for characterization of chiral assembly.⁵² Circular dichroism (CD) spectroscopy is the differential absorption between left and right circularly polarized light. While exposing circularly polarized light to an achiral molecule, it absorbs both left and right-handed polarized light equally and results in net zero CD signals. Whereas, either left or right-handed circularly polarized light is absorbed by chiral molecules or chiral assembly, depending on the polarization and

give rise to positive or negative CD signal. In general, enantiomers show equal and opposite CD signal. Observation of a peak or valley in the CD spectrum is referred to as the Cotton effect, which is the characteristic change in circular dichroism in the vicinity of an absorption band of a substance. The Cotton effect is deemed positive if the circular dichroism first increases as the wavelength decreases (as first observed by Cotton) and negative if the CD decreases first. The sign of the CD is determined by the handedness of the supramolecular chiral assemblies.

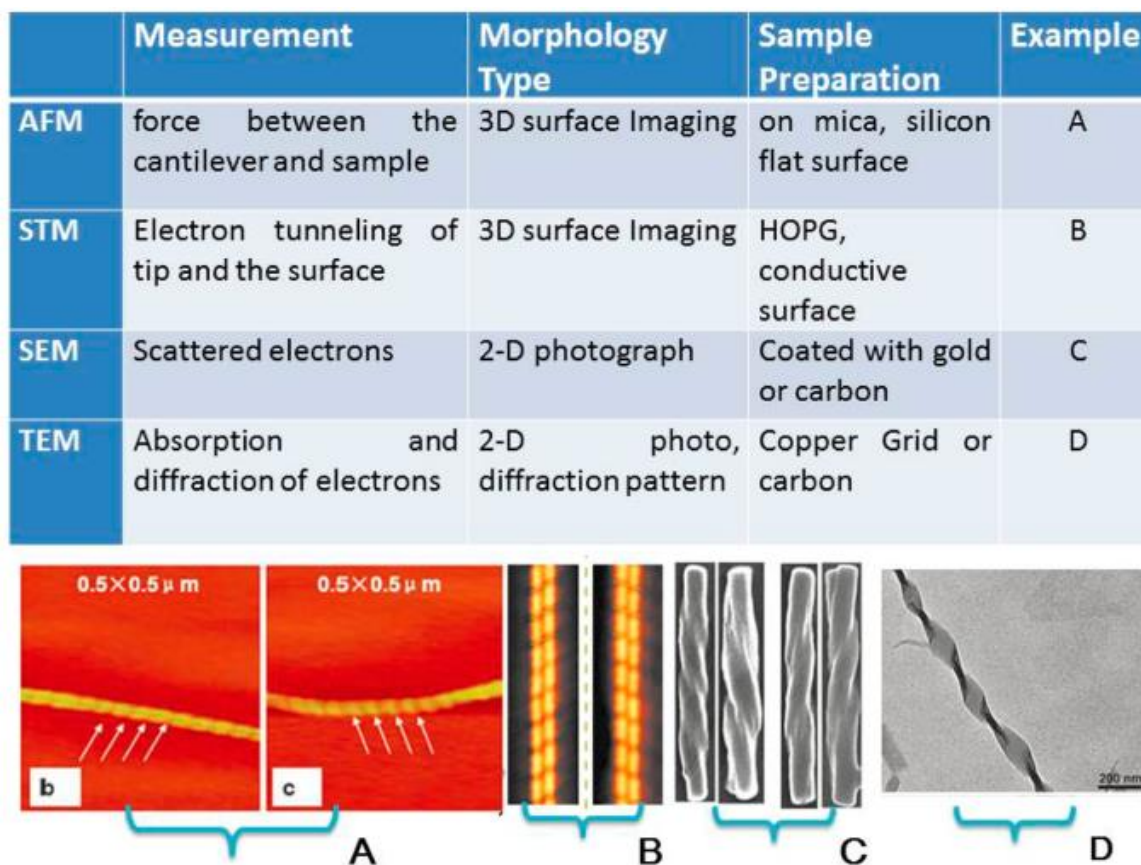


Figure 1.16. (Top) Comparison of various microscopies used to characterize the chiral architectures (ref. 49d); (Bottom) (A) AFM (ref. 51a), (B) STM (ref. 51b), (C) SEM image of Mirrorimaged nanorods self-assembled from TPPS and (1R,2R)- or (1S,2S)-1,2-diaminocyclohexane (ref. 51c), (d) TEM image of a chiral twist self-assembled from pyridine-containing L-glutamide (ref. 51d) [reproduced with permission from the American Chemical Society (ref. 49d)].

1.6.6.2. Random Supramolecular Chirality from C_3 -Symmetric Achiral Gelators and Chirality Induction

As we already discussed that, through self-assembly, not only chiral molecules but also completely achiral molecules can form chiral supramolecular assemblies. This situation results from spontaneous symmetry breaking,⁵³ which is one of the most important issues in obtaining assemblies with macroscopic chirality.⁵⁴ Due to the spontaneous symmetry breaking achiral molecules usually show random chirality, that means same molecules could assemble in either *P* helicity or *M* helicity or simultaneously both type of helicity.^{49d} However nature always prefers the homochiral structure. Hence to get a particular type of chiral structure from absolutely achiral constitute “Chirality Induction” is necessary. The term “**Chirality Induction**” generally refers to those chiral supramolecular systems where chirality is induced in an achiral molecular system as a result of asymmetric information transfer from a chiral host or vice versa. This host could be a chiral molecule, chiral pocket, cavity, chiral nanostructure or even chiral solvent. In order to produce the induced chirality, it is necessary for the achiral molecule to have a strong interaction with the chiral host through a noncovalent bond. Various kind of achiral assemblies shows the random chirality and also different types of chiral induction process was described in emerging fields of research to address the homochirality of nature.^{49d}

Recently in 2014, Liu *et al.* developed an achiral gelator of C_3 - symmetric benzene-1,3,5-tricarboxamide substituted with ethyl cinnamate (BTAC, **21**), and studied its supramolecular gelation and macroscopic chirality from the self-assembly of **21** in the DMF/H₂O mixture. Interestingly they found that upon gelation (through H-bonding and π - π staking interaction), this achiral gealtor **21** simultaneously self-assembled into unequal amounts of left- and right-handed twisted tapes. This supramolecular chirality was obtained without any chiral additives (Figure 1.17).⁵⁵ The symmetry breaking and formation of a macroscopic chirality and gelation from the assembly of this type of molecules is quite rare. The hierarchical self-assembly of an uneven number of different chiral assemblies produces the unbalanced left- and right-handed twists, as confirmed by a series of CD spectral measurements and SEM studies. Furthermore, they have implemented ester–amide exchange reactions with chiral amines to control of both the handedness of the twists and the macroscopic chirality of the gels. Depending on the structure of the chiral amines used, they could effectively produce the single handed twisted tapes (Figure 1.17).

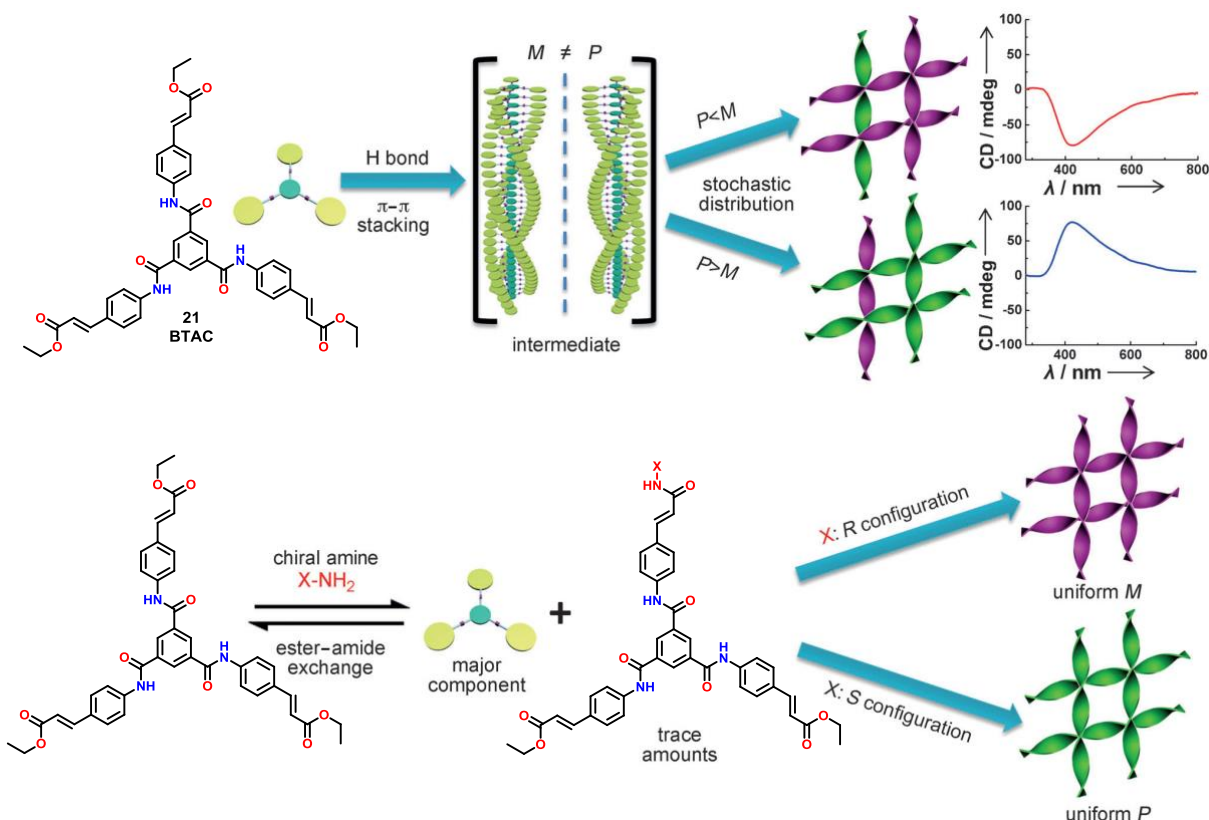


Figure 1.17. Formation of optically active supramolecular gels by the hierarchical self-assembly of achiral C_3 -symmetric BTAC (**21**) building blocks, and control of supramolecular chirality through doping with chiral amines [reprinted with permission from (ref 55). Copyright 2014 WILEY-VCH].

Very recently in 2015, the same group (Liu *et al.*) observe the spontaneous supramolecular symmetry breaking phenomenon from the organogels of an achiral C_3 -symmetric benzene-1,3,5-tricarboxylate substituted with methyl cinnamate through ester bond (BTECM, **22**). Generally for an achiral constituent, the H-bonding interactions play the most crucial role to attain supramolecular helical chiral assembly, because of its specificity and directionality. However, in this work authors showed for the 1st time that, symmetry breaking can occur in supramolecular gel system exclusively through π - π stacking. They observed that when **22** formed gels in cyclohexane, symmetry breaking occurs; i.e., optically active organogels with simultaneous left- and right-handed helical nanofibers obtained. Furthermore, using slight amount chiral solvents (R)- or (S)-terpinen-4-ol, they could successfully induce the chirality and achieve the desired handedness of the self-assembled structure. Most importantly, the handedness of supramolecular assemblies thus formed, was memorized after the removal of chiral solvents by simple drying process (Figure 1.18).

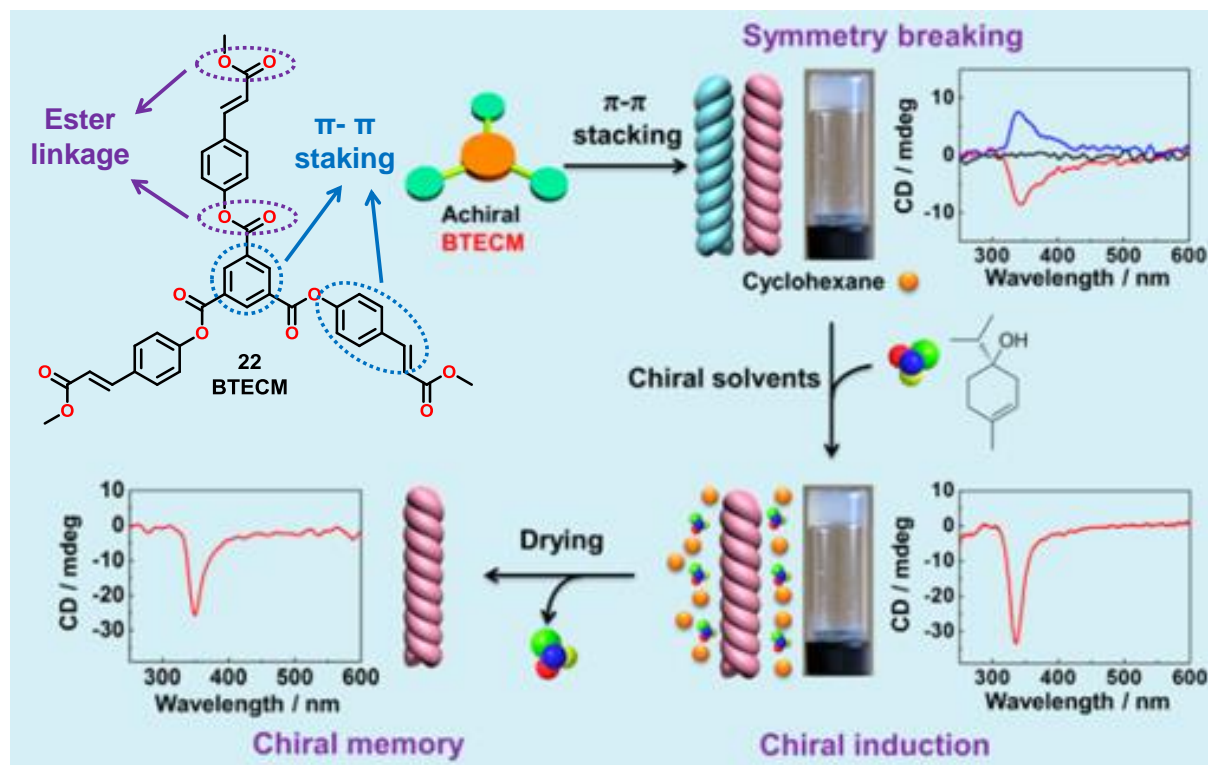


Figure 1.18. The molecular structure of the achiral C_3 -symmetric gelator **22**; and schematic illustration of symmetry breaking in cyclohexane purely through π - π stacking and supramolecular chirality memory with the “add-remove” of chiral solvents procedure [reproduced with permission from the American Chemical Society (ref. 56)].

1.7. Tuning Soft Nanostructures in Self-Assembled Supramolecular Gels

Supramolecular gels obtained from self-assembly of small organic molecules through different noncovalent interactions are known to form wide variety of entangled nanostructure to develop a 3D molecular network and immobilize the solvents.⁵⁷ Due to the weak and reversible nature of the noncovalent interactions supramolecular gel systems become a good platform for the fabrication of well-defined stimuli-responsive or smart soft materials.⁵⁸ The gelators with various self-assembled nanostructures are highly important. For example, the well-defined self-assembled nanostructures based on electroactive molecules have diverse applications such as field-effect transistors, photovoltaics, and sensors,⁵⁹ where the morphology and size of the active material play a key role in determining the electrical properties of the final device.⁶⁰ In this context, achieving control on the gel structures, size, shape and morphologies is highly desired.

1.7.1. Morphological Diversity in Supramolecular Gels

The most common morphology obtained with the gel formation is the nanofibers and fibers bundles. Besides the nanofibers, other nanostructures such as nanotapes or nanobelts, nanotubes and even nanospheres could also be obtained. If the gelator contains a chiral center, the nanobelts frequently change into nanotwists or helical nanoribbon structures and hollow tubular structures.⁶¹ For the tubes, various kinds of nanotubes with different parameters or shapes could be possible. Although the formation of the gel nanostructures is fundamentally a hierarchical self-assembly process. However, the formation of the unique nanostructures could be step by step method. Figure 1.19 illustrates the general mechanism for the formation of various types of nanostructures, which predominantly applicable to the amphiphilic gelators.

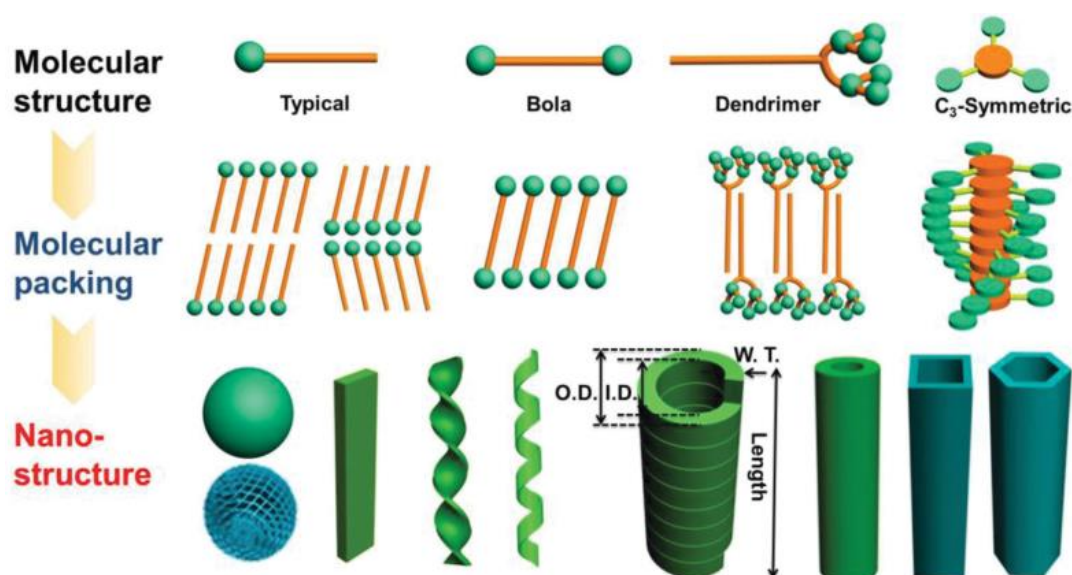


Figure 1.19. Illustration of the hierarchical self-assembly of amphiphilic gelators to diverse nanostructures [reprinted with permission from (ref 57e). Copyright 2015 WILEY-VCH].

1.7.2. Factors to Control the Morphology of the Supramolecular Gels

Many factors, such as the nature of the self-assembly motifs and the chemical structure of the building block, as well as exterior factors including solvent composition/polarity, metal-ligand coordination, temperature and ageing time, and physical stimuli such as sonication combine to form a complex ensemble from which the formation of specific nanostructures emerges.⁶²

1.7.2.1. The Effect of Molecular Structures on Morphology

The structure of gelators regulates the molecular arrangement and the morphologies of gels formed through variations in weak noncovalent interactions. Apart from the prime difference in the gelator structures, a tiny change in the molecular structures of a particular gelator may result in obvious variations in the formed architectures. For example, DMSO organogels formed by three isomeric pyridine-containing (ortho-, meta-, and para-position) L-glutamic lipids (**23-25**),⁶³ showed different morphologies, which includes nanofibers, twisted fibers and nanotubes, depending exclusively on the substituent position in the pyridine ring (Figure 1.20). The difference in the morphologies comes from the changes in the H-bonding interactions. In the case of **23**, the intermolecular H-bond is weaker than that of **24** and **25**, so packing between the molecules of **23** is weakened, which causes to its nanofibers like assembly.

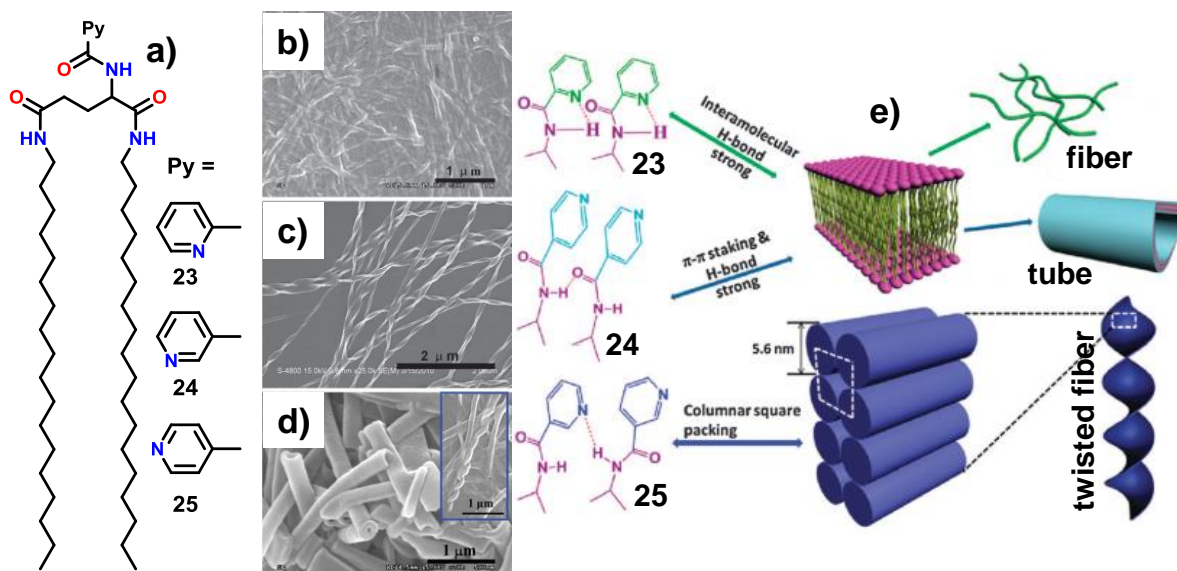


Figure 1.20. (a) Molecular structures of the gelators; (b) SEM images obtained from various DMSO gels: (b) **23**, (c) **24** and (d) **25**; (e) Illustration on the self-assembly manner of different isomeric gelators [reproduced with permission from the Royal Society of Chemistry (ref. 63)].

Organogelators containing glucose-based naphthalene derivatives with diamine linkers were reported by Fang *et al.* to self-assemble into supramolecular gels with different nanostructures from microbelts, prisms like cauliflower structures depending on the linker's length.⁶⁴ The linkers are hydrazine, ethylenediamine, 1,3-propanediamine, 1,4-butanediamine and 1,6-hexanediamine, respectively (Figure 1.21). The morphology of **26** in water exhibits microbelt structures, which is similar to that of

27 aggregates in ethanol. With the linker length increased to 3-6, cauliflower or cotton-like structures can be seen for those gelators (Figure 1.21). This result clearly confirms that structures of the gelators affect the morphologies of assemblies.

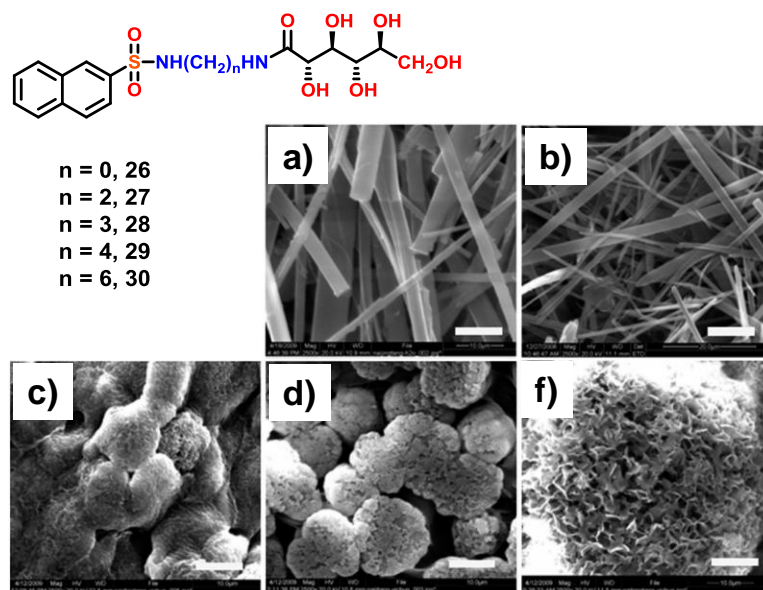


Figure 1.21. The chemical structures of the gelators **26-30** and the SEM images of **26**/water (a), **27**/ethanol (b), **28**/ethanol (c), **29**/ethanol (d), **30**/ethanol (e). Scale bar = 10 μm [reproduced with permission from the American Chemical Society (ref. 64)].

1.7.2.2. Solvent Polarity-Controlled Diverse Morphologies

In supramolecular gel system, people are mostly considering the gelator-gelator interactions, but the effect of solvent or the gelator-solvent interactions are also crucial. The solvent-gelator interaction, balance the intermolecular interactions (particularly the hydrophobic interaction between side chains) and can adjust the packing mode of gelator molecules. Selection of the solvent is a critical step toward the successful assembly of well-defined nanostructures, and hence the nanostructures of organogels could be directed by solvent selection.

Recently, Liu *et al.* observed that depending on the solvents polarity, their ability to donate (α) and accept hydrogen bonds (β), an organogelator N,N'-bisoctadecyl-2-(3-(pyridine-2-yl)-1H-pyrazol-1-yl)-L-glutamic amide (**31**) self-assembled into various nanostructures from nanofibers to nanoribbons, nanotwists, nanotubes and microtubes (Figure 1.22).⁶⁶ Not only in solution, such morphological changes can even occur for the xerogels upon treatment with solvent vapours. For example, when the xerogels displayed nanofiber structures exposed to DMF vapour for two days, nanotube

structures with “open mouths” could be obtained, while chiral twist structures formed when the xerogels were treated with chloroform vapour.

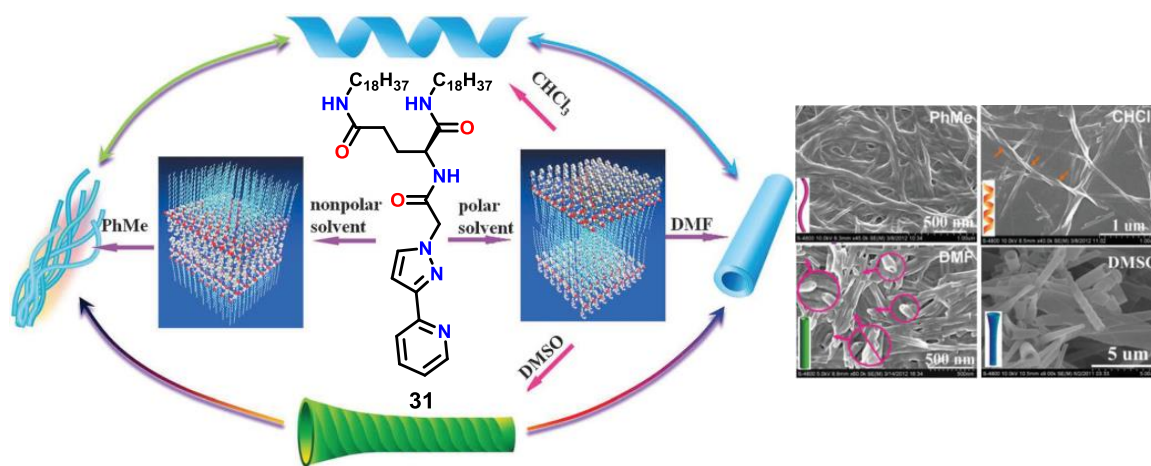


Figure 1.22. Morphology of the organogelator **31** in different solvents [reprinted with permission from (ref 66). Copyright 2013 WILEY-VCH].

Solvent compositions have also a direct effect on the gelator self-organization and hence its nanostructures. For example, Liu and coworkers designed a cationic amphiphile bearing pyridinium and long chain glutamide moiety and found that it could not immobilize any organic solvents.⁶⁷ However, with the addition of small amount of water into the organic solvents; supramolecular gelation was achieved no matter whether the organic solvents were water miscible or immiscible. Subsequently, the morphology of its assemblies also changed from nanofibers into chiral structures, such as nanotwists and nanotubes.

1.7.2.3. Metal-Ligand Coordination Directed Morphological Transition

The use of metal-ligand coordination chemistry to direct assembly of small molecules and gelation has recently become a topic of intense investigations. The reason for the growth of interest stems from the availability and the diversity of metal-ligand coordination that could readily induce or control the self-assembly process of the gel formation and thereby influences the gel properties and their self-assembled morphology.⁶⁸ In 2011, Shinkai and co-workers presented a functional low molecular-weight gelator (**32**) based on crown-appended quaterthiophene, which shows well-defined fibrillar nanostructure in alcoholic solvents. As in response to 1.0 equivalent amount of potassium (K^+) ion, the gel phase and its fibrillar morphology are maintained. Interestingly treatment with more than stoichiometry amount (< 1.0 eq of

K⁺), the fibrillar nanostructure of **32** completely vanishes upon gel-to-sol phase transition with enhanced fluorescence emission.⁶⁹ The reason behind the gel-to-sol phase transition and the morphology transformation of gelator **32**, is because of the enhanced multiple electrostatic repulsive forces among the coordinated metal ions with the gelator **32** (Figure 1.23).

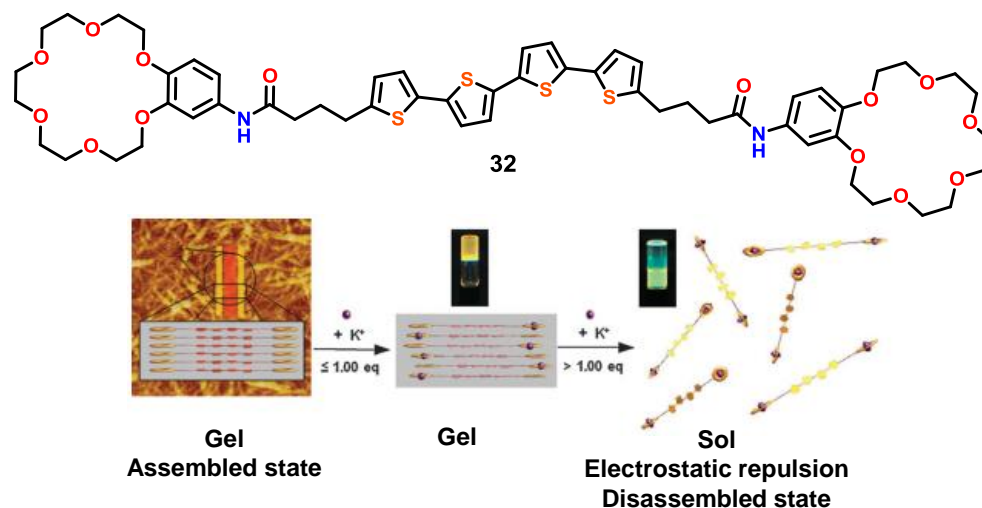


Figure 1.23. The molecular formula of gelator **32** and schematic representation of the gel-sol phase transition upon increasing concentration of K⁺ [reproduced with permission from the Royal Society of Chemistry (ref. 69)].

Recently Liu *et al.* have reported amphiphilic schiff base organogels which possessed different behaviours with various metal ions. The gel was destroyed when Zn²⁺ and Ni²⁺ were added.⁷⁰ However, the gel was maintained in presence of Cu²⁺ and Mg²⁺ and shows twisted tape and fibrillar type nanostructures with distinct luminescence properties, respectively (Figure 1.24).

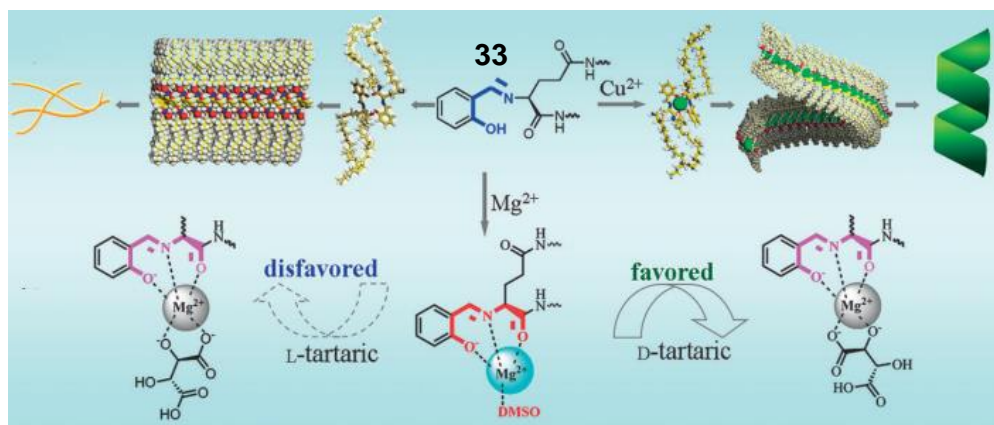


Figure 1.24. The assembly mechanism of gelator **33** in presence of different metal ions [reprinted with permission from (ref 70). Copyright 2012 WILEY-VCH].

1.7.2.4. Ultrasound Directed Morphological Diversity

The ultrasound wave is unique to gel formation and to control the supramolecular aggregation by modifying the noncovalent intermolecular interactions, such as cleaving self-locked intramolecular hydrogen bonds or π - π stacking to form interlocked gel states through intermolecular interactions. Yao *et al.* found that ultrasound resulted in a switch from intramolecular to intermolecular H-bonds. The varied molecular geometries and intermolecular interactions lead to different nanoscale morphologies from unbranched nanowires to entangled fibrous networks, which is responsible for the gelation under ultrasonic treatment.⁷¹

Ultrasound has several other effects on the supramolecular gel morphology, such as cutting, knitting, unfolding, homogenizing and even cross-linking. Sonication has also been considered as being responsible for the demetallation and reorganisation of coordinating units leading to gelation.⁷² In 2017, Dubey *et al.* showed an ultrasound-induced fluorescent metallogel based on a non-fluorescent citric acid derived ligand (**34**), LiOH and Cd(OAc)₂ in DMF.⁷³ Ultrasound is shown to promote the de-metallation and re-complexation of Cd(II) ions proceeding through the disruption and reformation of dynamic metal-ligand coordination bonds ultimately leading to gelation (Figure 1.25). The Ultrasound also proved to be responsible for the formation of uniform nanofibers, which was characterized by AFM and TEM microscopy.

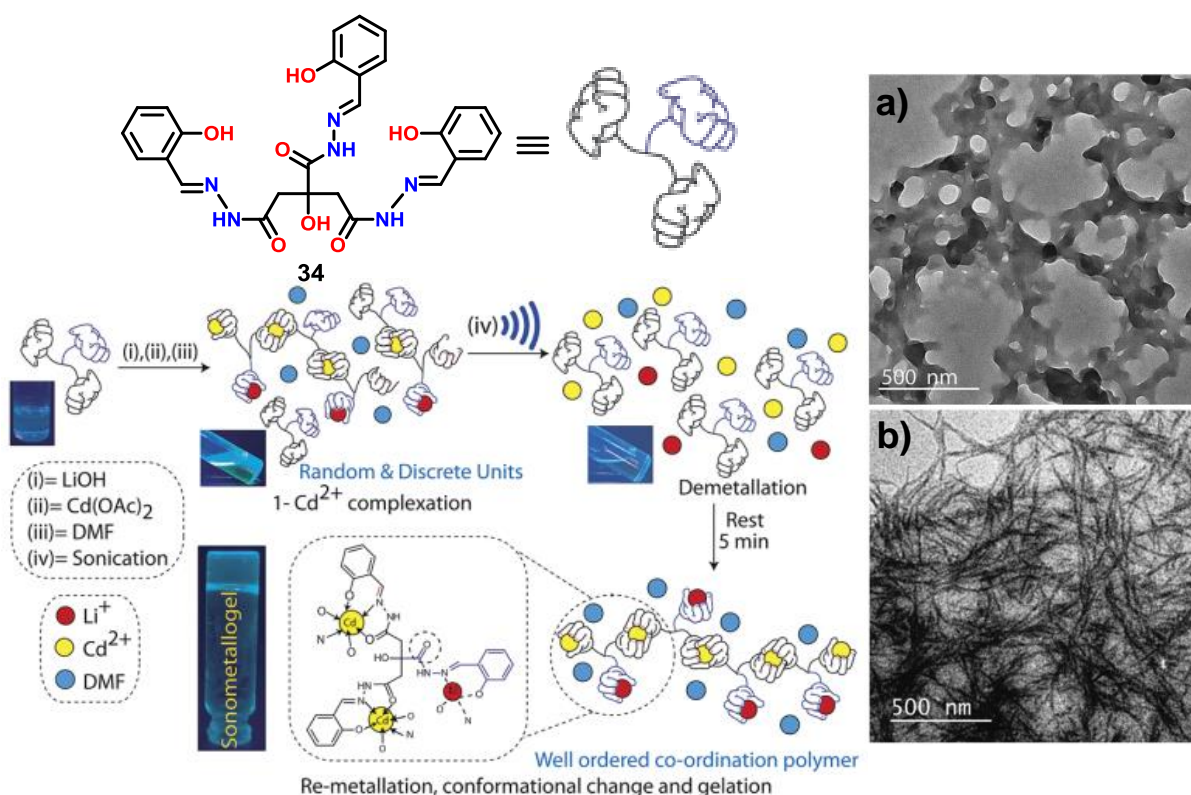


Figure 1.25. Structure of the gelator **34**, and model depiction of steps involved in sonometallogel formation; TEM images showing sonication induced morphological transformation from (a) random aggregates to (b) nanofiber [reproduced with permission from the Royal Society of Chemistry (ref. 73)].

1.7.2.5. Effect of Temperature and Ageing Time

In general for supramolecular gel formation, first, the LMMG (low molecular weight gelator) was dissolved in a certain solvent at high temperature and then cooled the hot solution to a lower temperature. The temperature at which self-assembly occurred, the time for cooling or the ageing time at the low temperature may strongly affect the assembling process and morphology.

Wan *et al.* have reported a cooling rate controlled self-assembly process for a sugar-based organogelator.⁷⁴ The fast-cooling gel was metastable while the slow-cooling gel was stable. On slow-cooling gelator formed left-handed helical ribbons, while on fast-cooling rate induced right-handed counterparts. The authors concluded that the formation of right-handed and left-handed helical ribbons was kinetically and thermodynamically favoured, respectively. In the fast-cooling process, the metastable nuclei directly grow up to right-handed ribbons, while in the slow-cooling process,

initially, the metastable nuclei evolved into stable nuclei and then further aggregated to become left-handed ribbons.

Another example of agitation-triggered organogelation was found in cholesteryl derivatives of calix[4]arene with L- or D-phenylalanine (**35**).⁷⁵ The SEM measurements revealed that structures of the gel networks are greatly affected by the ageing time. With increasing ageing time, the morphologies of the aggregates of **35** in the system changed from globules to globules and short rods, then to short rods alone, and finally to rod-based networks (Figure 1.26). There was a sharp transition between 12 min and 15 min of treatment time. After the 15 min of ageing time, the aggregates become much thinner and homogeneous. A further increase in the agitation time, however, had little effect on the morphologies of the gel networks, as characterized by the images of the gel networks obtained after 15 min of agitation, which is almost the same as those obtained after 30 min.

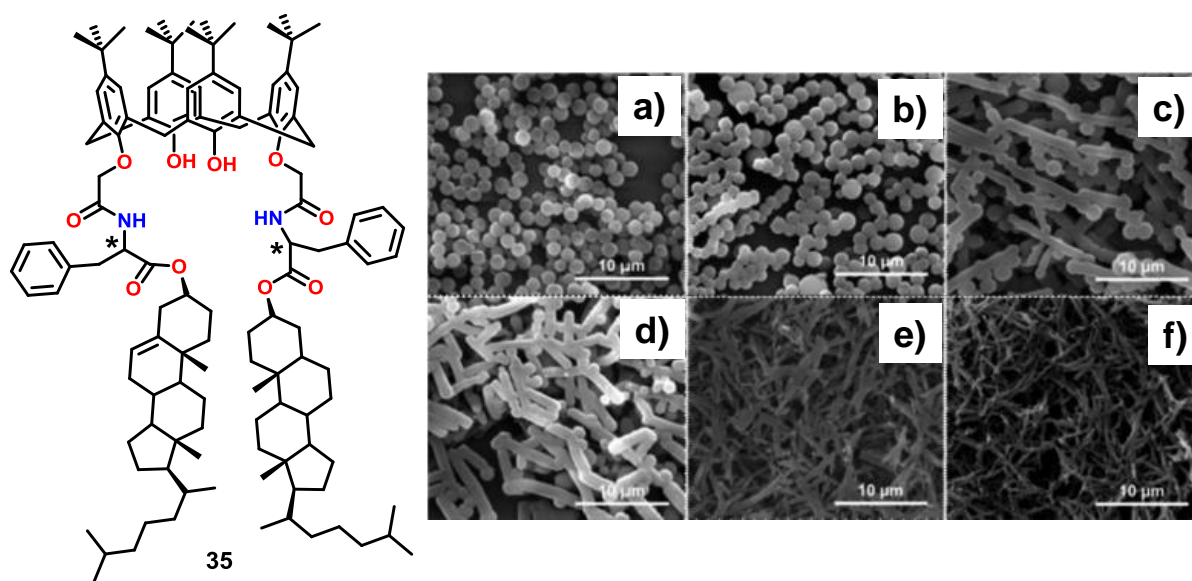


Figure 1.26. Molecular formula of the gelator **35** and its SEM images of the isopropanol gel ageing for different times, 3 min (a), 6 min (b), 9 min (c), 12 min (d), 15 min (e), and 30 min (f) [reproduced with permission from the Royal Society of Chemistry (ref. 75)].

1.8. Dendritic Gelators

Dendron or dendrimer are highly branched macromolecules with a unique shape and multiple functional properties.⁷⁶⁻⁷⁹ They have been identified as potential building blocks for the construction of organized functional materials.

Poly(aryl ether) dendron is one of the reliable class of building blocks for construction of various supramolecular systems. Several literature reports are available for modification of poly(aryl ether) backbone, either at the core or at the periphery, which produces self-assembly and gel formation.⁸⁰ Percec and his co-workers have extensively explored the self-assembly of poly(aryl ether) dendron under thermotropic condition in solution phase. Fan and co-workers reported the gelation of poly(aryl ether) dendron without conventional gelation motif, where the existence of multiple aromatic groups provided an opportunity for design of dendritic organic gelators. Fan and co-workers also reported the organo gelator based on peripherally functionalized poly(benzyl ether) dendron by dimethylisophthalate.⁸⁰ In the case of poly(aryl ether) dendrons, the dendrimer generation, peripheral functional groups, substitution at the focal point, and configuration of the dendron play key role in self-assembly and gel formation. Detailed investigation shows that apart from π - π interactions, non-classical hydrogen bonding interaction and C-H- π interactions also play a vital role in the formation of fibrillar morphology. Interestingly, many poly(aryl ether) based gel shows multistimuli responsive and self-healing nature.⁸¹ Liu *et al.* reported the photo responsive supramolecular gels obtained from azobenzene functionalised poly(aryl ether) dendron derivative (Figure 1.27).^{81b} The photo isomerisation of azobenzene group was responsible for the reversible sol-gel transformation triggered by UV-visible light irradiation (Figure 1.27).

Amino acids are one of the important classes of biomaterials, which can also be introduced into the dendritic structure to form functional supramolecular gel.⁸² The H-bonding interaction between amide groups enhances the gelation propensity. Smith and co-workers reported the dendritic amino acid-based gelator with peripheral modification with aliphatic long chain. Systematic mechanistic studies provided an insight into the effect of solvent, generation of dendron, the ratio of two components, the chirality of amino acids and spacer length during the two-component gelation. Less polar and non-H-bonding solvents were found to be efficient for gelation. The dendron showed special dendritic effect, as the second-generation derivatives formed efficient gel than first and third generation. Interestingly, sol-gel transition temperature for the pure enantiomers was always higher than the racemic mixture. Similarly, the morphology of pure enantiomers and racemic mixtures differed dramatically. The results indicated that the spacer length also has prominent effect in thermal stability and morphology of gel.⁸³

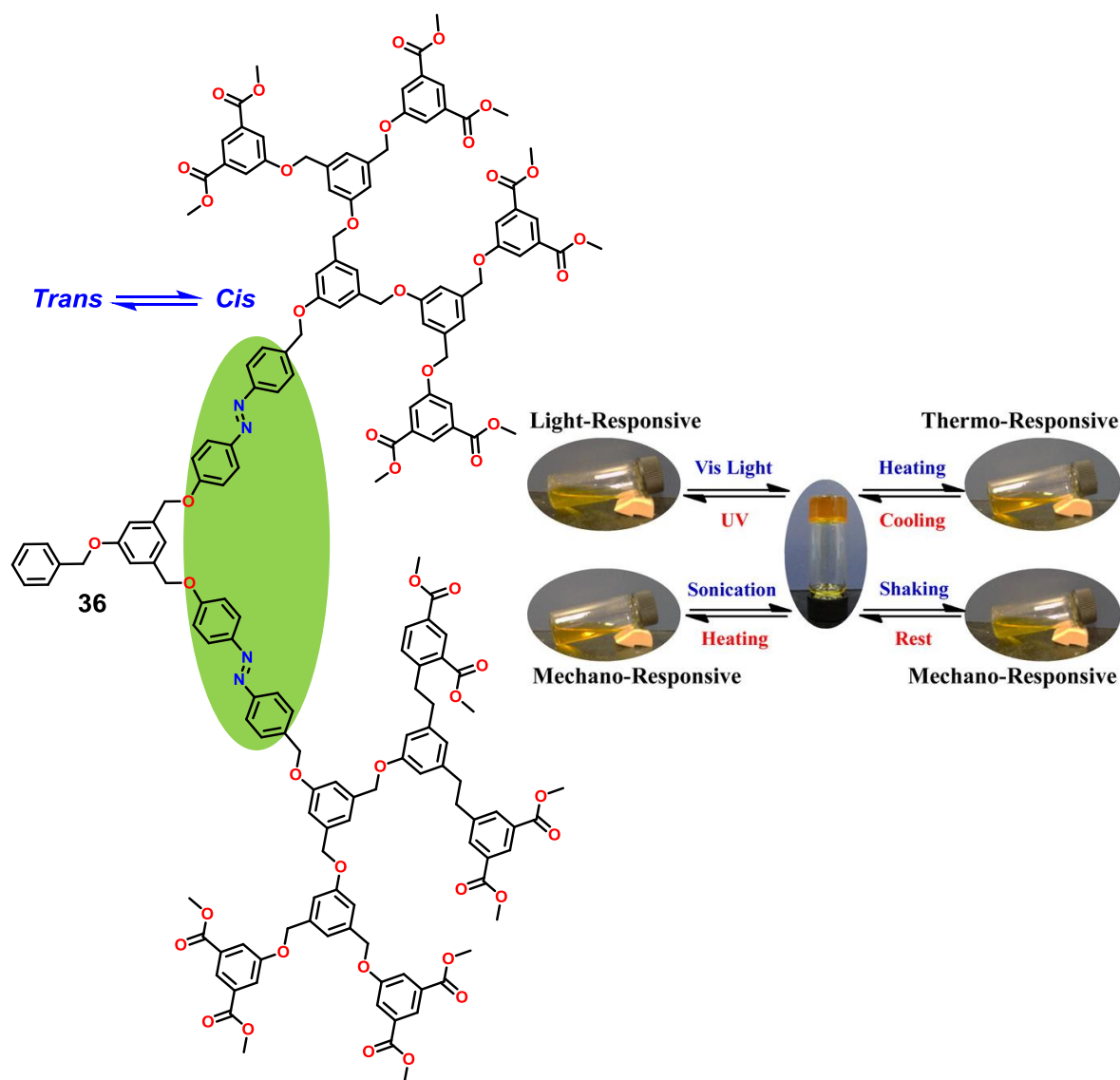


Figure 1.27. Multi-stimuli responsive dendritic organ gels based on azo-functionalized poly (aryl ether) Dendron gelator **36** [reproduced with permission from the American Chemical Society (ref. 81b)].

1.9. Opportunities of Supramolecular Gels

Recent advancement shows that the applications of supramolecular gels span over a range of research areas starting from industries (food, cosmetics and lubricants *etc.*) to biomedical, molecular electronics, chemical and biological sensors, nanoscience and nanotechnology. Several novel supramolecular gels were synthesized for high-tech applications such as light emitting device (luminescent gelators), drug carrier, tissue engineering, explosive sensors, *etc.*⁸⁴

Biom mineralisation is one of the key biological processes where inorganic components grow with a specific shape. The protein, lipid structure and larger macromolecular framework provided the ideal atmosphere for nucleation and growth to achieve specific shape, size and strength.⁸⁵ The template from small organic gelator offers the controlled nucleation and growth, which offers novel nanofabrication process towards the organized synthetic material. Shinkai and co-workers reported the hollow fibrillar silica using cholesterol based gelator. Where tetraethylorthosilane (TEOS) polymerized inside cholesterol based gel template.⁸⁶ Calcination removed organic materials and produced hollow silica fibre. Further, they have reported the effect of chirality, where chiral gel produced specific handed helical silica fibre.

With the incorporation of spectroscopically active or a receptor unit as part of the gelator molecule, the supramolecular gels become sensitive to various external stimuli. This makes them suitable for applications such as sensing and actuating. The ready reversibility of gelation of supramolecular gel can be exploited, for example, to release cells from gels on demand in a manner that does not lead to cell death. Ready gel formation by a simple trigger can also be used to allow easy and efficient gel loading.⁸⁴

Supramolecular gel could be used as an adsorbent to remediate unwanted pollutants from the environment, which include immobilization of oil spills, removal of dyes, extraction of heavy metals or toxic anions, and the detection or removal of chemical weapons. For example, Sureshan *et al.*^{87b} have developed a novel sorbent by impregnating cellulose pulp with a sugar-derived oleogelator, 1,2:5,6-di-O-cyclohexylidene-mannitol (Gelator **37**). With the help of H-bonding, the gelator molecules mask the surface-exposed hydroxyl groups of cellulose fibrils, and make the cellulose fibers temporarily hydrophobic (Figure 1.28). Due to the hydrophobicity, the cellulose based porous sorbent absorbs oil from oil-water mixture through capillary action and then release the phase selective gelator (**37**) uniformly into the oil phase. The released gelator transforms the oil into floating solid mass through gelation which was easily collected out from the water. Later on, the oil was quantitatively recovered from the gel by vacuum distillation (Figure 1.28). This is a unique example in the current literature, where the gelator was used at room temperature, without sonication and without using any carrier solvent of gelator for phase selective gelation of oil from the oil-water mixture.

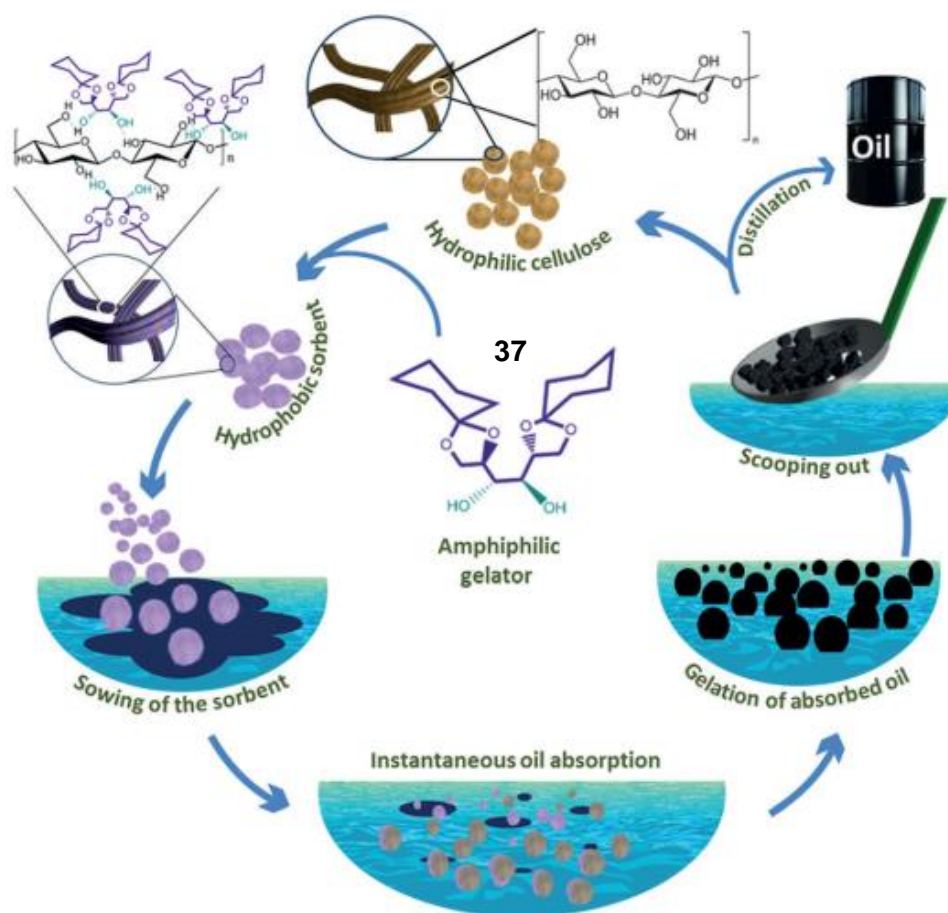


Figure 1.28. Schematic proposal for the eco-friendly marine oil-spill recovery using a simple sugar-based gelator (**37**) [reprinted with permission from (ref 87b). Copyright 2017 WILEY-VCH].

Furthermore, Sureshan et al. utilized the same 1,2:5,6-di-O-cyclohexylidene-mannitol (Gelator **37**) used for the development of “soft optical devices” (such as lenses and prisms) which further broadening the span of supramolecular gel applications.⁸⁸ They used very low concentration of this gelator to make series of gels from hydrocarbon-based solvents such as paraffin oil and pump oil. The most interesting aspect of this gelator system was its propensity to form organogels with remarkable strength, high elasticity, and self-healing properties. The strength and elasticity of the organogels were displayed by molding the gels in numerous self-supporting shapes (Figure 1.29c,d). The self-healing property was demonstrated by fusing several blocks of gel to develop a self-supporting continuous bar (Figure 1.29e). Apart from the extraordinary mechanical properties of the organogels of gelator **37**, it also exhibits high transmittance in the visible region with glass-like refractive indices ($n \approx 1.5$) due to its transparent appearance. These gels display a unique combination of properties which

was exploited to conceptually develop soft optical devices such as flexible lenses and prisms which showed potential in their ability to magnify objects and refract white light, respectively (Figure 1.29f-h). It has been hypothesized by the author that, the soft nature and self-healing properties of such gels may render the devices shatter- and scratch-free. Overall self-healing properties, scratch resistance, and glass-like refractive index make these systems highly attractive for eye protection and even for intraocular lenses.

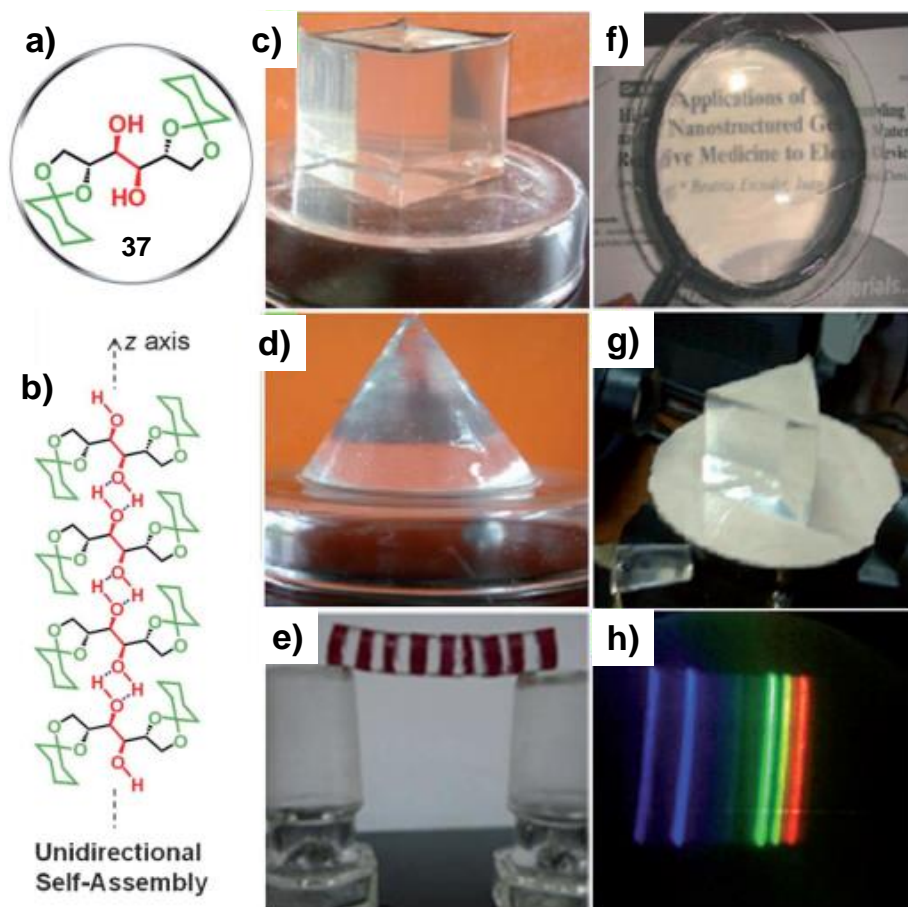
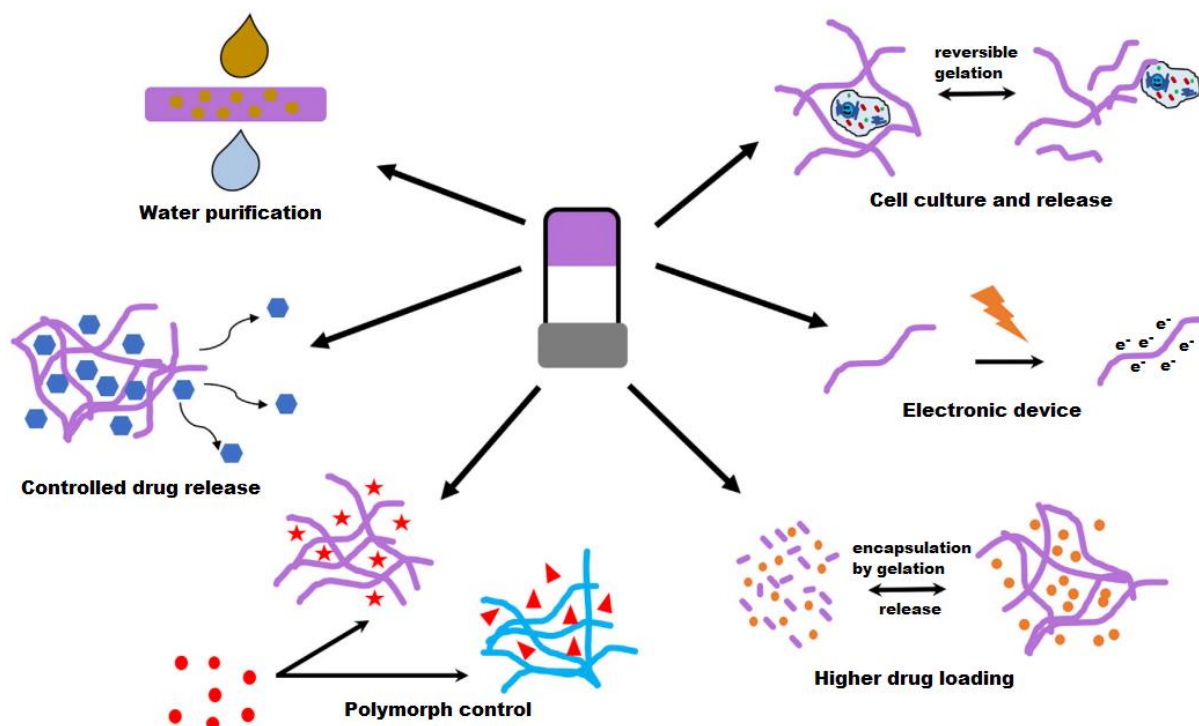


Figure 1.29. a) The molecular structure of the gelator **37**, from which organogels and optical devices were developed; b) Molecular arrangement of **37** in an organic solvent; c,d) A self-standing cube and cone shape made from pump oil gel; e) A self-supporting gel cylinder made by fusing 17 different pump oil gel discs. The alternate discs were doped with perylenetetracarboxylic anhydride for better visualization; f) A planoconvex lens made from paraffin oil gel; g,h) A prism made from paraffin oil gel and the diffraction pattern observed after refraction of white light [reprinted with permission from (ref 88a). Copyright 2017 WILEY-VCH].



Scheme 1.2. Opportunities of supramolecular gels: Schematic presentation showing some the potential uses of supramolecular gelators, including cell culture and differentiation with non-harmful release from the gelled material, photoresponsive semiconducting gel fibers, high loading of a drug particle with a targeted release, slow and controlled drug release upon addition of a stimulus, water purification by the removal of unwanted pollutants, and the control of polymorph by changing the gel network [reprinted from (ref 84c)].

In the current literature, there are plenty of examples available regarding different aspects of applications of supramolecular gels, which could not be possible to discuss separately. However, for a quick look at opportunities of supramolecular gels in the above we have presented a schematic; which cover almost all exciting features of supramolecular gels and their basic concept of working functions (Scheme 1.2).

1.10. References

1. (a) J.-M. Lehn, *Supramolecular Chemistry*; VCH: Weinheim, Germany, 1995; (b) H.-J. Schneider, A. Yatsimirsky, *Principles and Methods in Supramolecular Chemistry*; Wiley: Chichester, 2000; (c) J. W. Steed, J. L. Atwood, *Supramolecular Chemistry*; Wiley: Chichester, 2000.
2. D. J. Lloyd, In *Colloid Chemistry*., Alexander, J., Ed. Chemical Catalogue Company: New York, 1926; Vol. 1.
3. (a) P. J. Flory, Molecular Size Distribution in Three Dimensional Polymers. I. Gelation. *J. Am. Chem. Soc.*, 1941, **63**, 3083; (b) P. J. Flory, Constitution of Three-dimensional Polymers and the Theory of Gelation. *J. Phy. Chem.*, 1942, **46**, 132; (c) W. H. Stockmayer, Theory of Molecular Size Distribution and Gel Formation in Branched Polymers II. General Cross Linking. *J. Chem. Phy.*, 1944, **12**, 125.
4. Burchard, W. R.-M., S. B., Burchard, W. R.-M., B., Ed. Elsevier: London, 1990.
5. Almdal K, D. J., Hvidt S, and Kramer O., 1993, **1**, 5.
6. A. Keller, Introductory lecture. Aspects of polymer gels. *Faraday Discussions* 1995, **101**, 1.
7. Q. Wang and M. Y. J. L. Mynar, E. Lee, M. Lee, K. Okuro, K. Kinbara, T. Aida, *Nature*, 2010, **463**, 339.
8. S. Dong, B. Zheng, D. Xu, X. Yan, M. Zhang and F. Huang, *Adv. Mater.*, 2012, **24**, 3191.
9. (a) B. L. Feringa, *Molecular Switches*; Wiley-VCH Verlag GmbH: Weinheim, Germany, 2001; (b) M. Irie, Diarylethenes for Memories and Switches. *Chem. Rev.* 2000, **100**, 1685.
10. A. Hashidzume, F. Ito, I. Tomatsu, A. Harada, *Macromol. Rapid Commun.* 2005, **26**, 1151.
11. Y. Takashima, T. Nakayama, M. Miyauchi, Y. Kawaguchi, H. Yamaguchi, A. Harada, *Chem. Lett.* 2004, **33**, 890.
12. I. Tomatsu, A. Hashidzume, A. Harada, *Macromol. Rapid Commun.* 2006, **27**, 238.
13. N. M. Sangeetha and U. Maitra, *Chem. Soc. Rev.*, 2005, **34**, 821.
14. (a) J. H. van Esch, *Langmuir*., 2009, **25**, 8392; (b) M. de Loos, B. L. Feringa and J. H. van Esch, *Eur. J. Org. Chem.*, 2005, 3615; (c) P. Dastidar, *Chem. Soc. Rev.*, 2008, **37**, 2699.
15. S. S. Babu, V. K. Praveen and A. Ajayaghosh, *Chem. Rev.*, 2014, **114**, 1973.
16. K. Murata, M. Aoki, T. Suzuki, T. Harada, H. Kawabata, T. Komori, F. Ohseto, K. Ueda and S. Shinkai, *J. Am. Chem. Soc.*, 1994, **116**, 6664.
17. L. A. Feigin and D. I. Svergun, *Structure analysis by small-angle XRay and neutron scattering*. Plenum Press, New York. ISBN, 1987.

18. J. S. Higgins and H. C. Benoit Polymers and Neutron Scattering, Clarendon Press, Oxford, 1994.
19. P. Terech, F. Volino and R. Ramasseul, *J. Phys. France.*, 1985, **46**, 895.
20. P. Sollich, *Phys. Rev. E.*, 1998, **58**, 738.
21. M.-O. M. Piepenbrock, G. O. Lloyd, N. Clarke and J. W. Steed, *Chem. Rev.*, 2010, **110**, 1960.
22. G. Yu, X. Yan, C. Han and F. Huang, *Chem. Soc. Rev.*, 2013, **42**, 6697.
23. J. Brinksma, B.L. Feringa, R. M. Kellogg, R. Vreeker and J. Van Esch, *Langmuir.*, 2000, **16**, 9249.
24. S. R. Raghavan and E. W. Kaler, *Langmuir.*, 2001, **17**, 300.
25. D. C. Duncan and D. G. Whitten, *Langmuir.*, 2000, **16**, 6445.
26. D. K. Kumar, D. A. Jose, A. Das and P. Dastidar, *Chem. Commun.*, 2005, 4059.
27. D. J. Abdallah and R. G. Weiss, *J. Braz. Chem. Soc.*, 2000, **11**, 209.
28. A. Baral, S. Basak, K. Basu, A. Dehsorkhi, I. W. Hamley and A. Banerjee, *Soft Matter.*, 2015, **11**, 4944.
29. D. B. Amabilino, D. K. Smith and J. W. Steed, *Chem. Soc. Rev.*, 2017, **46**, 2404.
30. D. D. Prabhu, A. P. Sivadas and S. Das, *J. Mater. Chem. C*, 2014, **2**, 7039.
31. S. Basak, N. Nandi, A. Baral and A. Banerjee, *Chem. Commun.*, 2015, **51**, 780.
32. (a) Y. Hong, J. W. Y. Lam, B. Z. Tang, *Chem. Commun.*, 2009, 4332; (b) Z. Zhao, J. W. Y. Lamb and B. Z. Tang, *Soft Matter.*, 2013, **9**, 4564; (c) S. S. Babu, K. K. Kartha and A. Ajayaghosh, *J. Phys. Chem. Lett.*, 2010, **1**, 3413.
33. B. -K. An, D. -S. Lee, J. -S. Lee, Y. -S. Park, H. -S. Song and S. Y. Park, *J. Am. Chem. Soc.*, 2004, **126**, 10232.
34. Y. Liu, J. W. Y. Lam, F. Mahtab, R. T. K. Kwok and B. Z. Tang, *Front. Chem. China.*, 2010, **5**, 325.
35. T. H. Kim, M. S. Choi, B.-H. Sohn, S.-Y. Park, W. S. Lyoo and T. S. Lee, *Chem. Commun.*, 2008, 2364.
36. T. H. Kim, D. G. Kim, M. Lee and T. S. Lee, *Tetrahedron.*, 2010, **66**, 1667.
37. Y. Qian, S. Li, Q. Wang, X. Sheng, S. Wu, S. Wang, J. Li and G. Yang, *Soft Matter.*, 2012, **8**, 757.
38. (a) A. Ajayaghosh, V. K. Praveen and C. Vijayakumar, *Chem. Soc. Rev.*, 2008, **37**, 109; (b) P. Terech, R. G. Weiss, *Chem. Rev.*, 1997, **97**, 3133; (c) A. Dawn, T. Shiraki, S. Haraguchi, S.-I. Tamaru, S. Shinkai, *Chem. Asian J.*, 2011, **6**, 266.
39. (a) V. K. Praveen, S. J. George, R. Varghese, C. Vijayakumar and A. Ajayaghosh, *J. Am. Chem. Soc.*, 2006, **128**, 7542; (b) A. Ajayaghosh, S. J. George and V. K. Praveen, *Angew. Chem. Int. Ed.*, 2003, **42**, 332; (c) A. Ajayaghosh, C. Vijayakumar, V. K. Praveen, S. S. Babu and R. Varghese, *J. Am. Chem. Soc.*, 2006, **128**, 7174.

40. A. Ajayaghosh, V. K. Praveen, C. Vijayakumar and S. J. George, *Angew. Chem. Int. Ed.*, 2007, **46**, 6260.
41. T. Shu, J. Wu, M. Lu, L. Chen, T. Yi, F. Li and C. Huang, *J. Mater. Chem.*, 2008, **18**, 886.
42. (a) J. Kido, M. Kimura and K. Nagai, *Science.*, 1995, **267**, 1332; (b) Y. Sun, N. C. Giebink, H. Kanno, B. Ma, M. E. Thompson and S. R. Forrest, *Nature.*, 2006, **440**, 908; (c) B. W. D'Andrade, S. R. Forrest, *Adv. Mater.*, 2004, **16**, 1585; (d) K. T. Kamtekar, A. P. Monkman, M. R. Bryce, *Adv. Mater.*, 2010, **22**, 572; (e) M. C. Gather, A. Köhnen, K. Meerholz, *Adv. Mater.*, 2011, **23**, 233.
43. (a) J. Liu, X. Guo, L. Bu, Z. Xie, Y. Cheng, Y. Geng, L. Wang, X. Jing and F. Wang, *Adv. Funct. Mater.*, 2007, **17**, 1917; (b) P. Coppo, M. Duati, V. N. Kozhevnikov, J. W. Hofstraat and L. D. Cola, *Angew. Chem. Int. Ed.*, 2005, **44**, 1806; (c) Y. S. Zhao, H. Fu, F. Hu, A. Peng, W. Yang and J. Yao, *Adv. Mater.*, 2008, **20**, 79; (d) S. Mukherjee, P. Thilagar, *Dyes and Pigments.*, 2014, **110**, 2; (e) V. K. Praveen, C. Ranjith and N. Armaroli, *Angew. Chem. Int. Ed.*, 2014, **53**, 365; (f) K. V. Rao, K. K. R. Datta, M. Eswaramoorthy and S. J. George, *Adv. Mater.*, 2013, **25**, 1713; (g) C. Vijayakumar, V. K. Praveen and A. Ajayaghosh, *Adv. Mater.*, 2009, **21**, 2059; (h) P. Bairi, B. Roy, P. Chakraborty and A. K. Nandi, *ACS Appl. Mater. Interfaces.*, 2013, **5**, 5478.
44. R. Abbel, R. van der Weegen, W. Pisula, M. Surin, P. Leclre, R. Lazzaroni, E. W. Meijer and A. P. H. J. Schenning, *Chem. Eur. J.*, 2009, **15**, 9737.
45. (a) C. Giansante, G. Raffy, C. Schäfer, H. Rahma, M. -T. Kao, A. G. L. Olive and A. D. Guerzo, *J. Am. Chem. Soc.*, 2011, **133**, 316; (b) C. Giansante, C. Schäfer, G. Raffy and A. D. Guerzo, *J. Phys. Chem. C.*, 2012, **116**, 21706.
46. (a) H. J. Bolink, F. De Angelis, E. Baranoff, C. Klein, S. Fantacci, E. Coronado, M. Sessolo, K. Kalyanasundaram, M. Grätzel and Md. K. Nazeeruddin, *Chem. Commun.*, 2009, 4672; (b) G. Zhou, Q. Wang, X. Wang, C.-L. Ho, W.-Y. Wong, D. Ma, L. Wang and Z. Lin, *J. Mater. Chem.*, 2010, **20**, 7472.
47. (a) P. Nandhikonda and M. D. Heagy, *Chem. Commun.*, 2010, **46**, 8002; (b) Y. Yang, M. Lowry, C. M. Schowalter, S. O. Fakayode, J. O. Escobedo, X. Xu, H. Zhang, T. J. Jensen, F. R. Fronczek, I. M. Warner and R. M. Strongin, *J. Am. Chem. Soc.*, 2006, **128**, 1408; (c) Y. I. Park, O. Postupna, A. Zhugayevych, H. Shin, Y. S. Park, B. Kim, H. J. Yen, P. Cheruku, J. S. Martinez, J. W. Park, S. Tretiak and H. L. Wang, *Chem. Sci.*, 2015, **6**, 789; (d) M. R. Molla and S. Ghosh, *Chem. Eur. J.*, 2012, **18**, 1290; (e) S. Park, J. E. Kwon, S. H. Kim, J. Seo, K. Chung, S. -Y. Park, D. -J. Jang, B. M. Medina, J. Gierschner and S. Y. Park, *J. Am. Chem. Soc.*, 2009, **131**, 14043; (f) K. -C. Tang, M. -J. Chang, T. -Y. Lin, H. -A. Pan, T. -C. Fang, K. -Y.

- Chen, W. -Y. Hung, Y. -H. Hsu and P. -T. Chou, *J. Am. Chem. Soc.*, 2011, **133**, 17738; (g) Y. Liu, M. Nishiura, Y. Wang and Z. Hou, *J. Am. Chem. Soc.*, 2006, **128**, 5592; (h) Q. -Y. Yang and J. -M. Lehn, *Angew. Chem. Int. Ed.*, 2014, **53**, 4572; (i) X. -H. Jin, C. Chen, C. -X. Ren, L. -X. Cai and J. Zhang, *Chem. Commun.*, 2014, 50, 15878.
48. (a) S. K. Samanta and S. Bhattacharya, *J. Mater. Chem.*, 2012, **22**, 25277; (b) S. Bhattacharya and S. K. Samanta, *Chem. Eur. J.*, 2012, **18**, 16632.
49. (a) R. A. Hegstrom and D. K. Kondepudi, *Sci. Am.*, 1990, **262**, 108; (b) Y. Wang, J. Xu, Y. Wang and H. Chen, *Chem. Soc. Rev.*, 2013, **42**, 2930; (c) B. L. Feringa, R. A. van Delde, *Angew. Chem. Int. Ed.*, 1999, **38**, 3418; (d) M. Liu, L. Zhang and T. Wang, *Chem. Rev.*, 2015, **115**, 7304.
50. C. Bai and M. Liu, *Angew. Chem., Int. Ed.*, 2013, **52**, 2678.
51. (a) J. Jiang, T. Wang and M. Liu, *Chem. Commun.*, 2010, **46**, 7178; (b) J. Weckesser, A. D. Vita, J. V. Barth, C. Cai and K. Kern, *Phys. Rev. Lett.*, 2001, **87**, 096101; (c) Y. Rong, P. Chen and M. Liu, *Chem. Commun.*, 2013, **49**, 10498; (d) P. Duan, X. Zhu and M. Liu, *Chem. Commun.*, 2011, **47**, 5569.
52. (a) L. Brunsveld, A. P. H. J. Schenning, M. A. C. Broeren, H. M. Janssen, J. A. J. M. Vekemans and E. W. Meijer, *Chem. Lett.*, 2000, 292; (b) P. Jonkheijm, P. V. D. Schoot, A. P. H. J. Schenning and E. W. Meijer, *Science.*, 2006, **313**, 80; (c) D. K. Smith, *Chem. Soc. Rev.*, 2009, **38**, 684; (d) Y. Nagata, T. Nishikawa, and M. Suginome, *ACS Macro Lett.*, 2016, **5**, 519; (e) A. Desmarchelier, X. Caumes, M. Raynal, A. Vidal-Ferran, P. W. N. M. v. Leeuwenll and L. Bouteiller, *J. Am. Chem. Soc.*, 2016, 138, 4908.
53. L. Pérez-García and D. B. Amabilino, *Chem. Soc. Rev.*, 2007, **36**, 941.
54. T. Yamaguchi, T. Kimura, H. Matsuda, T. Aida, *Angew. Chem., Int. Ed.*, 2004, **43**, 6350.
55. Z. Shen, T. Wang and M. Liu, *Angew. Chem. Int. Ed.*, 2014, **53**, 13424.
56. Z. Shen, Y. Jiang, T. Wang and M. Liu, *J. Am. Chem. Soc.*, 2015, **137**, 16109.
57. (a) L. E. Buerkle and S. J. Rowan, *Chem. Soc. Rev.*, 2012, **41**, 6089; (b) A.Y. Y. Tam and V.W. W. Yam, *Chem. Soc. Rev.*, 2013, **42**, 1540; (c) L. C. Palmer and S. I. Stupp, *Acc. Chem. Res.*, 2008, **41**, 1674; (d) M. George and R. G. Weiss, *Acc. Chem. Res.*, 2006, **39**, 489; (e) L. Zhang, X. Wang, T. Wang and M. Liu, *small.*, 2015, **11**, 1025.
58. (a) M. O. Piepenbrock, G. O. Lloyd, N. Clarke and J. W. Steed, *Chem. Rev.*, 2010, **110**, 1960; (b) W. Edwards, C. A. Lagadec and D. K. Smith, *Soft Matter.*, 2011, **7**, 110; (c) M. L. Muro-Small, J. Chen and A. J. McNeil, *Langmuir.*, 2011, **27**, 13248.
59. (a) Y. Che, X. Yang, G. Liu, C. Yu, H. Ji, J. Zuo, J. Zhao and L. Zang, *J. Am. Chem. Soc.*, 2010, **132**, 5743; (b) X. Yang, G. Zhang, D. Zhang and D. Zhu, *Langmuir.*,

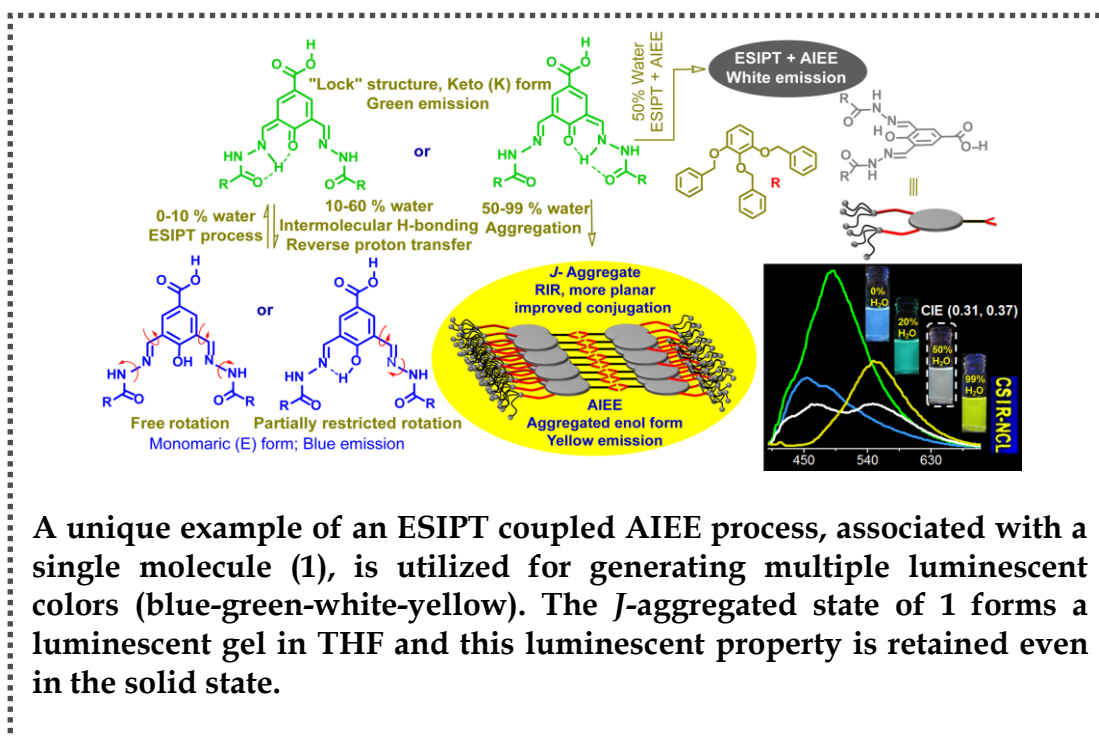
- 2010, **26**, 11720; (c) P. Xue, Q. Xu, P. Gong, C. Qian, A. Ren, Y. Zhang and R. Lu, *Chem. Commun.*, 2013, **49**, 5838.
60. (a) K. Sakakibara, P. Chithra, B. Das, T. Mori, M. Akada, J. Labuta, T. Tsuruoka, S. Maji, S. Furumi, L. K. Shrestha, J. P. Hill, S. Acharya, K. Ariga and A. Ajayaghosh, *J. Am. Chem. Soc.*, 2014, **136**, 8548; (b) T. Akutagawa, K. Kakiuchi, T. Hasegawa, S. Noro, T. Nakamura, H. Hasegawa, S. Mashiko and J. Becher, *Angew. Chem. Int. Ed.*, 2005, **117**, 7449.
61. (a) X. Zhu, Y. Li, P. Duan and M. Liu, *Chem. Eur. J.*, 2010, **16**, 8034; (b) Q. Jin, L. Zhang, X. Zhu, P. Duan and M. Liu, *Chem. Eur. J.*, 2012, **18**, 4916; (c) Q. Jin, L. Zhang and M. Liu, *Chem. Eur. J.*, 2013, **19**, 9234; (d) S. R. N. H. Y. Lee, J. Hong and J. Am. Chem. Soc., 2007, **129**, 1040.
62. (a) G. Cravotto and P. Cintas, *Chem. Soc. Rev.*, 2009, **38**, 2684; (b) N. Yan, G. He, H. Zhang, L. Ding and Y. Fang, *Langmuir.*, 2010, **26**, 5909.
63. P. Duan, X. Zhu and M. Liu, *Chem. Commun.*, 2011, **47**, 5569.
64. N. Yan, G. He, H. Zhang, L. Ding and Y. Fang, *Langmuir.*, 2010, **26**, 5909.
65. Y. Jeong, K. Hanabusa, H. Masunaga, I. Akiba, K. Miyoshi, S. Sakurai and K. Sakurai, *Langmuir.*, 2005, **21**, 586.
66. Q. Jin, L. Zhang and M. Liu, *Chem. Eur. J.*, 2013, **19**, 9234.
67. C. Liu, Q. Jin, K. Lv, L. Zhang and M. Liu, *Chem. Commun.*, 2014, **50**, 3702.
68. A. Y. -Y. Tam and V. W. -W. Yam, *Chem. Soc. Rev.*, 2013, **42**, 1540.
69. A. A. Sobczuk, S. -I. Tamarua and S. Shinkai, *Chem. Commun.*, 2011, **47**, 3093.
70. Q. Jin, L. Zhang, X. Zhu, P. Duan and M. Liu, *Chem. Eur. J.*, 2012, **18**, 4916.
71. Y. Wang, C. Zhan, H. Fu, X. Li, X. Sheng, Y. Zhao, D. Xiao, Y. Ma, J. S. Ma and J. Yao, *Langmuir.*, 2008, **24**, 7635.
72. S. Zhang, S. Yang, J. Lan, Y. Tang, Y. Xue and J. You, *J. Am. Chem. Soc.*, 2009, **131**, 1689.
73. V. K. Pandey, M. K. Dixit, S. Manneville, C. Bucherc and M. Dubey, *J. Mater. Chem. A.*, 2017, **5**, 6211.
74. J. Cui, A. Liu, Y. Guan, J. Zheng, Z. Shen and X. Wan, *Langmuir.*, 2010, **26**, 3615.
75. X. Cai, Y. Wu, L. Wang, N. Yan, J. Liu, X. Fang and Y. Fang, *Soft Matter.*, 2013, **9**, 5807.
76. (a) G. R. Newkome, C. N. Moorefield, F. Vögtle, *Dendritic Molecules: Concepts Syntheses, and Applications*, Wiley-VCH, Weinheim, 1996; (b) G. R. Newkome, C. N. Moorefield, F. Vögtle, *Dendrimers and Dendrons: Concepts Syntheses, and Perspectives*; Wiley-VCH, Weinheim, 2001; (c) F. Vögtle, G. Richardt, N. Werner, *Dendrimer Chemistry: Concepts, Synthesis Properties, Applications*, Wiley-VCH: Weinheim, 2009.

77. E. Buhleier, W. Wehner and F. Vögtle, *Synthesis.*, 1978, 155.
78. (a) U. Boas, and P. M. H. Heegaard, *Chem. Soc. Rev.*, 2004, **33**, 43; Q. Chen, Y. Feng, D. Zhang, G. Zhang, Q. Fan, S. Sun and D. Zhu, *Adv. Funct. Mater.*, 2010, **20**, 36.
79. (a) B. M. Rosen, C. J. Wilson, D. A. Wilson, M. Peterca, M. R. Imam and V. Percec, *Chem. Rev.*, 2009, **109**, 6275; (b) L. M. Bronstein and Z. B. Shifrina, *Chem. Rev.*, 2011, **111**, 5301.
80. (a) Y. Feng, Z. -X. Liu, H. Chen, Z. -C. Yan, Y. -M. He, C. -Y. Liu and Q. -H. Fan, *Chem. Eur. J.*, 2014, **20**, 7069; (b) Y. Feng, Y. -M. He and Q. -H. Fan, *Chem. Asian J.*, 2014, **9**, 1724.
81. (a) Y. Feng, H. Chen, Z. -X. Liu, Y. -M. He and Q. -H. Fan, *Chem. Eur. J.*, 2016, **22**, 4980; (b) Z. -X. Liu, Y. Feng, Z. -C. Yan, Y. -M. He, C. -Y. Liu and Q. -H. Fan, *Chem. Mater.*, 2012, **24**, 3751.
82. (a) J. C. Stendahl, L. Lia, R. C. Claussen and S. I. Stupp, *Biomaterials.*, 2004, **25**, 5847; (b) M. Suzuki, and K. Hanabusa, *Chem. Soc. Rev.*, 2009, **28**, 967; (c) J. E. Marine, S. Song, X. Liang, and J. G. Rudick, *Biomacromolecules.*, 2016, **17**, 336; (d) V. Percec, A. E. Dulcey, V. S. K. Balagurusamy, Y. Miura, J. Smidrkal, M. Peterca, S. Nummelin, U. Edlund, S. D. Hudson, P. A. Heiney, H. Duan, S. N. Magonov, and S. A. Vinogradov, *Nature.*, 2004, **430**, 764; (e) A. R. Hirst and D. K. Smith, *Top. Curr. Chem.*, 2012, **256**, 237.
83. (a) J. G. Hardy, A. R. Hirst, D. K. Smith, C. Brennan and I. Ashworth, *Chem. Commun.*, 2005, 385; (b) J. G. Hardy, A. R. Hirst and D. K. Smith, *Soft Matter.*, 2012, **8**, 3399; (c) A. R. Hirst and D. K. Smith, *Org. Biomol. Chem.*, 2004, **2**, 2965; (d) A. R. Hirst, D. K. Smith, M. C. Feiters, H. P. M. Geurts and A. C. Wright, *J. Am. Chem. Soc.*, 2003, **125**, 9010; (e) A. R. Hirst, D. K. Smith and J. P. Harrington, *Chem. Eur. J.*, 2005, **11**, 6552.
84. (a) B. O. Okesola, V. M. P. Vieira, D. J. Cornwell, N. K. Whitelaw and D. K. Smith, *Soft Matter.*, 2015, **11**, 4768; (b) A. R. Hirst, B. Escuder, J. F. Miravet and D. K. Smith, *Angew. Chem. Int. Ed.*, 2008, **47**, 8002; (c) E. R. Draper and D. J. Adams, *Chem.*, 2017, **3**, 390; (d) S. S. Babu, S. Prasanthkumar and A. Ajayaghosh, *Angew. Chem. Int. Ed.*, 2012, **51**, 1766; (e) A. Dawn, T. Shiraki, S. Haraguchi, S. -I. Tamaru and S. Shinkai, *Chem. Asian J.*, 2011, **6**, 266; (f) W. J. Frith, *Philos. Trans. A Math. Phys. Eng. Sci.*, 2016, **374**, 20150138; (g) E. V. Alakpa, V. Jayawarna, A. Lampel, K. V. Burgess, C. C. West, S. C.J. Bakker, S. Roy, N. Javid, S. Fleming, D. A. Lamprou et al., *Chem.*, 2016, **1**, 298; (h) S. Ghosh, V. K. Praveen and A. Ajayaghosh, *Annu. Rev. Mater. Res.*, 2016, **46**, 235; (i) K. J. Skilling, F. Citossi, T. D. Bradshaw, M. Ashford, B. Kellam and M. Marlow, *Soft Matter.*, 2014, **10**, 237; (j)

- M. D. S. Maset, V. J. Nebot, J. F. Miravet and B. Escuder, *Chem. Soc. Rev.*, 2013, **42**, 7086; (k) S. Uzan, D. Barış, M. Çolak, H. Aydın and H. Hoşgören, *Tetrahedron.*, 2016, **72**, 7517; (l) N. M. Sangeetha and U. Maitra, *Chem. Soc. Rev.*, 2005, **34**, 821; (m) S. S. Babu, V. K. Praveen and A. Ajayaghosh, *Chem. Rev.*, 2014, **114**, 1973.
85. (a) L. Bozec, and M. A. Horton, *J. Mater. Sci. Mater. Med.*, 2006, **17**, 1043; (b) S. Weiner and L. Addadi, *J. Mater. Chem.*, 1997, **7**, 689; (c) S. I. Stupp and P. V. Braun, *Science.*, 1997, **277**, 1242.
86. (a) Y. Ono, K. Nakashima, M. Sano, Y. Kanekiyo, K. Inoue, S. Shinkai, M. Sano and J. Hojo, *Chem. Commun.*, 1998, 1477; (b) J. H. Jung, S.-H. Lee, J. S. Yoo, K. Yoshida, T. Shimizu and S. Shinkai, *Chem. Eur. J.*, 2003, **9**, 5307; (c) J. H. Jung, Y. Ono and S. Shinkai, *Angew. Chem. Int. Ed.*, 2000, **15**, 1931.
87. (a) B. O. Okesola and D. K. Smith, *Chem. Soc. Rev.*, 2016, **45**, 4226; (b) A. Prathap and K. M. Sureshan, *Angew. Chem. Int. Ed.*, 2017, **56**, 9405.
88. (a) A. Vidyasagar, K. Handore and K. M. Sureshan, *Angew. Chem. Int. Ed.*, 2011, **50**, 8021; (b) G. John, S. R. Jadhav, V. M. Menon and V. T. John, *Angew. Chem. Int. Ed.*, 2012, **51**, 1760.

CHAPTER 2

Tuning of Multiple Luminescence Outputs and White-Light Emission from a Single Gelator Molecule through an ESIPT Coupled AIEE Process



A unique example of an ESIPT coupled AIEE process, associated with a single molecule (1), is utilized for generating multiple luminescent colors (blue-green-white-yellow). The *J*-aggregated state of 1 forms a luminescent gel in THF and this luminescent property is retained even in the solid state.

Publication:
Chem. Commun., 2015, 51, 2130.

2.1. Introduction

Luminescent functional soft materials derived from supramolecular self-organization of small organic molecules or achieved from various π -conjugated macromolecules have attracted considerable attention due to their potential applications in color tuneable displays,¹ optoelectronic devices,² chemical sensors³ and many related research fields.⁴ Soft materials with tuneable luminescence responses are considerably important for developing multiple color emitting devices. Such color tuneable responses are generally achieved by appropriate modulation of energies of the frontier orbitals through systematic structural modification of a luminophore or in the presence of an appropriate external stimulus,^{5a-d} as well as through mixing of several discrete compounds with different luminescence outputs.^{5e} However, examples of such response from a single molecule without applying these condition are seldom reported. Further, an ideal white-light emitter demands simultaneous emission of three primary RGB (red, green and blue) colors or at least two complementary colors with a nearly similar distribution of intensities covering the entire visible wavelength range from 400 to 700 nm.^{6a} Due to the technological relevance there has been a significant surge in interest in this area in the recent past. Förster resonance energy transfer (FRET) between donor and acceptor components has been used to achieve white-light emitting organic assemblies in gels,^{6a,b} solution,^{5d,6c} nanoparticles,^{6d,e} nanofibers,^{6f} and in the solid state.^{6g} But the use of multiple components for generating white-light emission is argued as a relatively complicated process.

Processes like excited state intramolecular proton transfer (ESIPT),^{7a,b} and aggregation induced emission (AIE) or aggregation induced emission enhancement (AIEE)^{7c,d} for organic molecules have been utilized for generating tuneable luminescence responses and in some instances white-light emission. The ESIPT process generally results in an excited keto tautomer (K^*) with abnormal emission properties and large Stokes shift relative to that observed for the normal excited enol form (E^*).^{7a} Dual emission (E^*/K^*) is also expected over the wide wavelength range if the proton transfer is not quantitative and this has been utilized for generating white-light emission.⁸ However, such reports are scanty in the contemporary literature.

Tang and his co-workers were first to report that a certain class of luminophores exhibited AIE in their aggregated state.^{7c} The aggregation process helped such molecules to pack efficiently through a π - π stack interaction, which eventually blocked the non-radiative deactivation pathway through restricted intramolecular rotations (RIR). This accounted for an improved luminescence response in the aggregated state and was also utilized for developing certain luminescent gels.⁹ A few AIE or AIEE

responsive single molecules could also exhibit multiple color emission either due to different conformation and/or packing modes in the aggregated state or due to a change in the degree of aggregation.¹⁰ In some instances, these resulted in white-light emission.^{5c,d,11} Few recent reports discuss ESIPT active molecules with AIEE properties.¹² However, to the best of our knowledge, there is no report that has discussed the ESIPT coupled AIEE process for a single molecule for developing tuneable multiple luminescence colors at room temperature.

In this chapter, we have reported such a phenomenon using a newly synthesized poly(aryl ether) dendron based gelator molecule (compound **1**, Figure 2.1). Its luminescence color was found to change from blue-green-white and then eventually to yellow with a gradual increase of water percentage in its THF solution. Interestingly, **1** showed an intense yellow color emission in gel, powder and in thin film states. Compound **1** with a flexible and freely rotatable acylhydrazone spacer and a free -OH group participated in intramolecular six-membered hydrogen-bond (H-bond) with the N_{imine} atom. To investigate the specific role of the ESIPT process in the luminescence responses, model compound **2** was also synthesized (Figure 2.1).

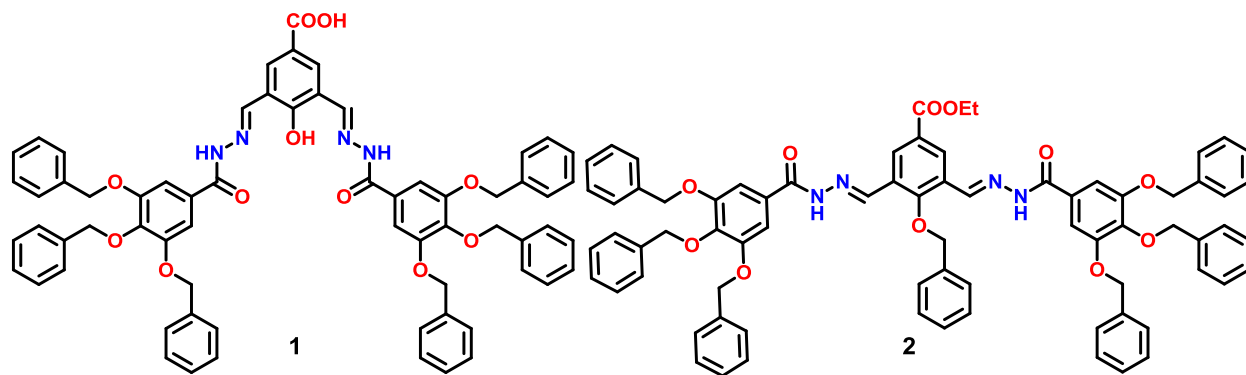


Figure 2.1. Structure of the synthesized molecules used in the present study.

2.2. Experimental Section

2.2.1. Materials and Methods

Unless otherwise stated, all reagents used for the synthesis of compound **1** and **2** (Figure 2.1) were purchased from commercial suppliers and used as such without further purification. Organic solvents were purified according to the standard procedure.¹³ HPLC grade solvents were used for recording spectrometric data. FTIR spectra were recorded as KBr pellets in a cell fitted with a KBr window, using a Perkin-

Elmer Spectra GX 2000 spectrometer. ^1H and ^{13}C NMR spectra have been recorded on a Bruker 200/400/500 MHz FT NMR (Model: Avance-DPX 200/500) and all spectra were calibrated against TMS. Mass spectrometric data were acquired by an electron spray ionization (ESI) technique on a Q-tof-micro quadrupole mass spectrometer (Micro mass). High-resolution mass spectra were recorded on JEOL JM AX 505 HA mass spectrometer. Thermo-gravimetric analyses (TGA) were carried out on a TG50 analyzer (Mettler-Toledo) or a SDT Q600 TG-DTA analyzer under N_2 atmosphere at a heating rate of $10\text{ }^\circ\text{C min}^{-1}$ within a temperature range of 20-480 $^\circ\text{C}$. UV-Vis spectra were recorded using a PerkinElmer Lambda- 950 UV-Vis spectrometer equipped with a peltier system for variable temperature experiments, while fluorescence, as well as fluorescence excitation spectra, were recorded using Qunata Master 400, PTI spectrofluorometer. FESEM images were obtained using Nova Nano SEM 450 and QuantaTM Scanning Electron Microscope. TEM images were recorded using a FEI Tecnai G2 F20 X-TWIN TEM at an accelerating voltage of 200 kV. Rheological measurements were carried out on a Rheoplus MCR302 (Anton paar) rheometer with parallel plate geometry and obtained data were processed with start rheometer software. The gap distance between the plates was fixed at 0.5 mm. X-ray powder diffraction (XRPD) of air-dried THF gel of **1** were recorded on a Phillips PANalytical diffractometer for Cu K_α radiation ($\lambda = 1.5406\text{ \AA}$).

2.2.2. General Description of the Different Experimental Techniques

2.2.2.1. UV-Vis and Fluorescence Study

For recording the Uv-Vis and fluoresce spectra, initially, 1.0 nM stock solutions of both the compounds (**1** and **2**; Figure 2.1) were made in THF. An aliquot (0.5 mL) was taken from the stock solution and was added with an appropriate amount of THF and water (H_2O) to adjust the desired solvent composition and final concentration (10 μM). Each solution was allowed to equilibrate at room temperature for 1h before spectral measurements. For variable-temperature experiments, THF/Water (3:7) mixed solvent solution of **1** in was used. The solution was heated from lowest to the highest temperature and allowed to equilibrate for 15 min at the desired temperature before each measurement. All luminescence measurements were recorded using, $\lambda_{\text{ex}} = 365\text{ nm}$ and 306 nm for compound **1** and **2** respectively with an emission slit width of 2 nm. Fluorescence excitation spectra were recorded using the same solution used for fluorescence studies.

2.2.2.2. General Procedure for Gelation Study of **1**

Due to the limited solubility of **1** in common organic solvent, gelation property of **1** was checked with three solvents, namely DMF, DMSO and THF. Compound **1** was highly soluble in DMF and DMSO and resulted in the solution. Whereas in case of THF, a weighted amount **1** was dissolved in THF (1.0 mL) by heating in closed vials. The clear solution was left to cool down to the room temperature without any disturbance. The gel formation was confirmed by the failure of the soft mass to flow by inverting the glass vial.

2.2.2.3. Scanning Electron Microscopy (SEM)

100 μ M concentrated solutions of **1** in THF as well as in the different composition of THF/water solvent mixture were drop-casted (10 μ L) on a silicon wafer and allowed to air dry for 6-7 hrs in a dust-free place and then under desiccator for overnight. Before taking images the dried samples were coated with gold vapour.

2.2.2.4. Transmission Electron Microscopy (TEM)

TEM samples were prepared drop-casting 5 μ L of the 100 μ M concentrated THF solution of **1** onto carbon-coated copper grids (200 mesh). TEM images were obtained after drying the sample in vacuum for 24 hours.

2.2.2.5. Current (*I*) - voltage (*V*) Measurements

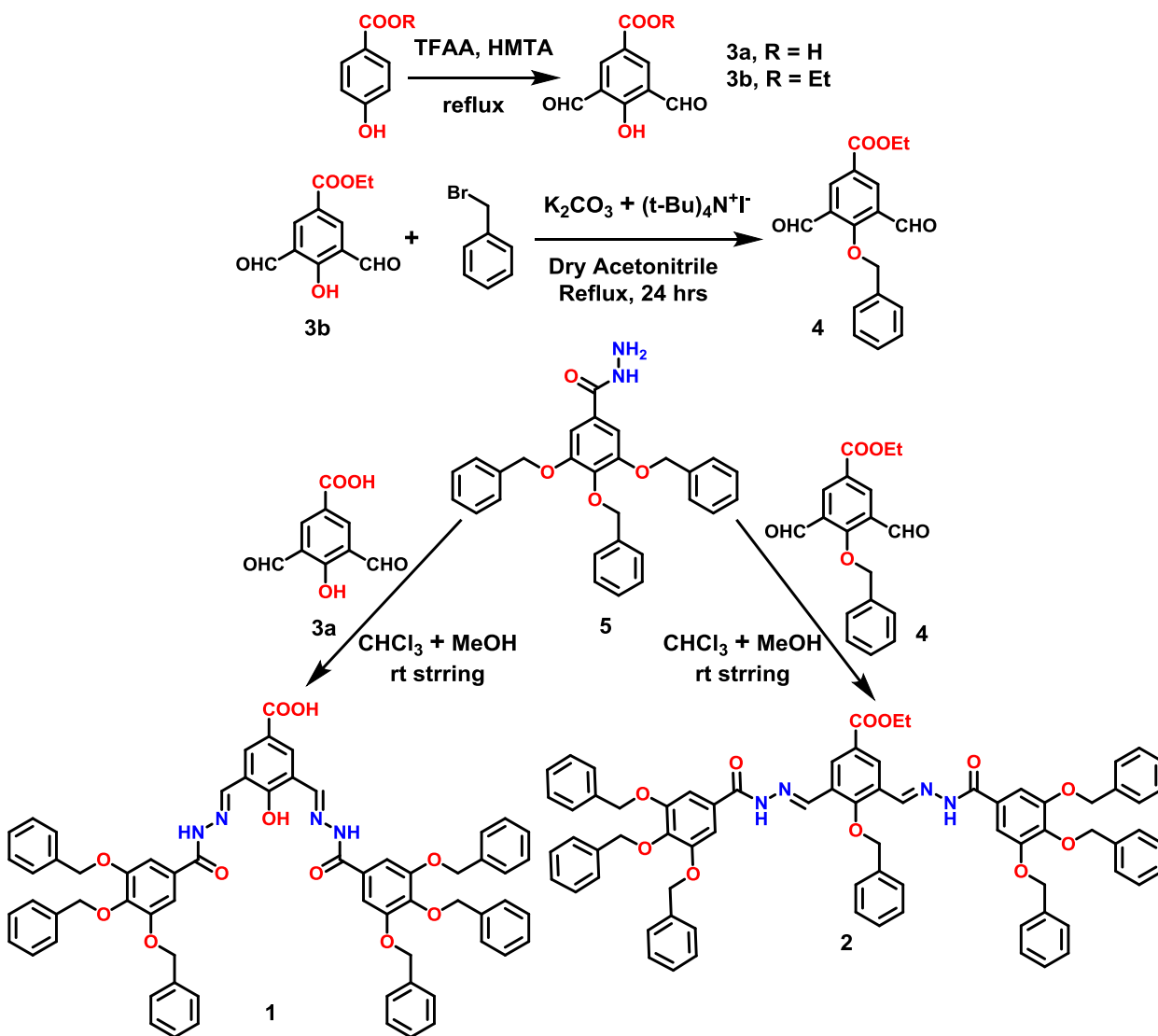
The gel solution of **1** (10.0 mg/mL of THF) was drop-casted on indium tin oxide (ITO) coated glass surfaces and dried for 24 hrs at room temperature. *IV* characteristic profile of this sample was measured in a two-probe electrode using a KEITHLEY 4200-SCS programmable electrometer instrument.

2.2.2.6. Rheology

A freshly prepared THF gel (1.0 wt %) of the compound **1** was carefully scooped out and placed on the parallel plate of the rheometer very quickly to minimize solvent evaporation. Dynamic strain sweep tests were carried out to increase the amplitude of oscillation from 0.1 % up to 100 % apparent strain shear (with a frequency $\omega = 10$ rad/s) at 25 °C. Frequency sweep experiment was performed from 0.1 to 100 rad/s at constant strain (γ) of 1 % at 25 °C.

2.2.3. Synthesis and Characterization

2.2.3.1. Synthetic Scheme



Scheme 2.1. Methodologies that were adopted for the synthesis of compound **1** and **2**, and their intermediates **3a**, **3b**, **4** and **5**.

2.2.3.2. Synthesis of **3a** and **3b**

3a and **3b** were synthesized following the previously reported procedure.¹⁴

2.2.3.3. Synthesis and Characterization of 4

In a 100 mL two neck round bottom flask (RB) 3,5-bisformyl-4-hydroxyethyl benzoate (**3b**)¹⁴ (200.0 mg, 0.9 mM), commercially available benzyl bromide (169.5 mg, 0.99 mM) and anhydrous K₂CO₃ were mixed in 20~25 mL of dry acetonitrile (ACN). Followed by a pinch of tetrabutylammonium iodide (t-Bu)₄N⁺I⁻ was added and was reflux for 24 hrs under N₂ atmosphere. The reaction mixture was cooled to room temperature, and then the solvent was removed under reduced pressure using a rotary evaporator. The oily residue was taken in 80 mL of CHCl₃, and washed with distilled water (3 X 30 mL). Organic layer dried over anhydrous Na₂SO₄. Finally, solvent was evaporated to get the crude product as colourless oil. It was purified by column chromatography using silica gel as the stationary phase and 25 % ethyl acetate in hexane as eluent to obtain pure product (**4**) as white solid. Yield = 35 %, ¹H NMR (200 MHz, CDCl₃, TMS): δ (ppm) = 10.23 (2H, s, -CHO), 8.72 (2H, s, ArH), 7.41-7.36 (3H, m, ArH), 7.32-7.29 (2H, m, ArH), 5.24 (2H, s, -CH₂), 4.47-4.36 (2H, q, -CH₂ ester), 1.44-1.37 (3H, t, -CH₃ ester); ¹³C NMR (100 MHz, CDCl₃, TMS): δ (ppm) = 187.82, 165.81, 164.35, 138.35, 134.02, 130.57, 129.56, 129.06, 128.98, 127.52, 81.71, 61.84, 59.51, 14.72; HRMS (ESI): m/z calculated for C₁₈H₁₆O₅Na [M + Na]⁺ = 335.0890, found 335.0884.

2.2.3.4. Synthesis of 5

Compound **5** was synthesized by exactly following the previously reported procedure by Prasad *et al.*¹⁵

2.2.3.5. Synthesis and Characterization of Compound 1 and 2

Synthetic procedure of both compounds was followed according to the reported procedure with slight modification.¹⁵ A solution of compound **3a** (136.2 mg, 0.7 mM) or **4** (219.1 mg, 0.7 mM) in methanol was added dropwise to a CHCl₃ solution of compound **5** (638.0 mg, 1.4 mM). The reaction mixture was stirred at room temperature for ~9-10 hrs. The resulting precipitate [for compound **1** (yellow) and for compound **2** (colourless)] was filtered off using G4-gooch crucible. Further, the precipitates were washed with (1:1) CHCl₃/MeOH mixture for several times, dried under desiccator to obtain the pure products.

Compound **1**: Yield = 90 %, ¹H NMR (500 MHz, DMSO-d₆, TMS): δ (ppm) = 13.30 (1H, s, -COOH), 12.18 (2H, s, -NH), 8.82 (2H, s, -CH=N), 8.34 (2H, s, ArH), 7.51-7.49 (8H, d, *J* = 7 Hz, ArH), 7.45-7.40 (12H, m, ArH), 7.37-7.36 (8H, m, ArH), 7.28-7.27 (6H, m, ArH), 5.22 (8H, s, ArCH₂O), 5.04 (4H, s, ArCH₂O); ¹³C NMR (100 MHz, DMSO-d₆, TMS): δ (ppm) = 166.37, 162.27, 159.82, 152.08, 145.15, 140.30, 137.30, 136.67, 130.84, 128.39,

128.11, 128.01, 127.91, 127.82, 127.65, 122.18, 120.23, 106.95, 74.22, 70.44; **HRMS (ESI)**: m/z calculated for $C_{65}H_{55}O_{11}N_4$ $[M + H]^+ = 1067.3862$, found 1067.3861.

Compound **2**: Yield = 84 %, **1H NMR** (400 MHz, DMSO- d_6 , TMS): δ (ppm) = 11.94 (2H, s, -NH), 8.75 (2H, s, -CH=N), 8.57 (2H, s, ArH), 7.56-7.54 (2H, m, ArH), 7.50-7.48 (6H, m, ArCH₂O), 7.43- 7.34 (26H, m, ArH), 7.29-7.27 (5H, m, ArH), 5.22 (8H, s, ArCH₂O), 5.04 (6H, s, ArCH₂O), 4.42-4.41 (2H, board, -CH₂ ester), 1.37 (3H, board, -CH₃ ester); **^{13}C NMR** (125 MHz, DMSO- d_6 , TMS): δ (ppm) = 164.77, 162.80, 159.11, 152.07, 141.57, 140.25, 137.31, 136.71, 135.29, 129.20, 128.92, 128.58, 128.41, 128.34, 128.15, 128.05, 127.94, 127.87, 127.56, 126.56, 107.05, 78.44, 74.25, 70.48, 61.22, 14.22; **HRMS (ESI)**: m/z calculated for $C_{74}H_{65}O_{11}N_4$ $[M + H]^+ = 1185.4644$, found 1185.4647.

2.3. Results and Discussions

The methodology adopted for the synthesis of the compound **1** and **2** is shown in Scheme 2.1. Analytical, as well as spectroscopic data, confirmed the purity of both the synthesized compounds. All studies were performed using double distilled water and HPLC grade THF solvent medium unless mentioned otherwise.

The absorption spectrum (Figure. 2. 2a; black line) of **1** (10 μ M) in pure THF showed a band maxima at 306 nm ($\epsilon = 4.69 \times 10^4 \text{ M}^{-1} \text{ cm}^{-1}$) and 355 ($\epsilon = 1.7 \times 10^4 \text{ M}^{-1} \text{ cm}^{-1}$) nm with two shoulders at 320 and 372 nm. Upon gradual addition of water into its THF solution, intensities of all absorption bands were found to decrease due to the formation of molecular aggregates. Eventually, in THF-water (1:9; v/v) solution a distinct red shift of 10 and 12 nm was observed for the absorption band at 355 and 372 nm, respectively (Figure 2.2a and 2.2b). Such bathochromic shifts for the absorption bands were anticipated for *J*-type aggregation.^{5b,11b} To determine the stability of the aggregated structures of **1**, we have performed the variable-temperature Uv-Vis study of the (3:7; v/v) THF-water solution of **1** (10 μ M). With increasing the solution temperature from 10-70 °C, the absorption spectra pattern remained almost invariant (Figure 2.2c). This result confirmed the high thermal stability of the *J*-aggregated structure of **1**. Again the result of the thermogravimetric analysis (TGA) confirmed that **1** was stable up to 280 °C (Figure 2.2d).

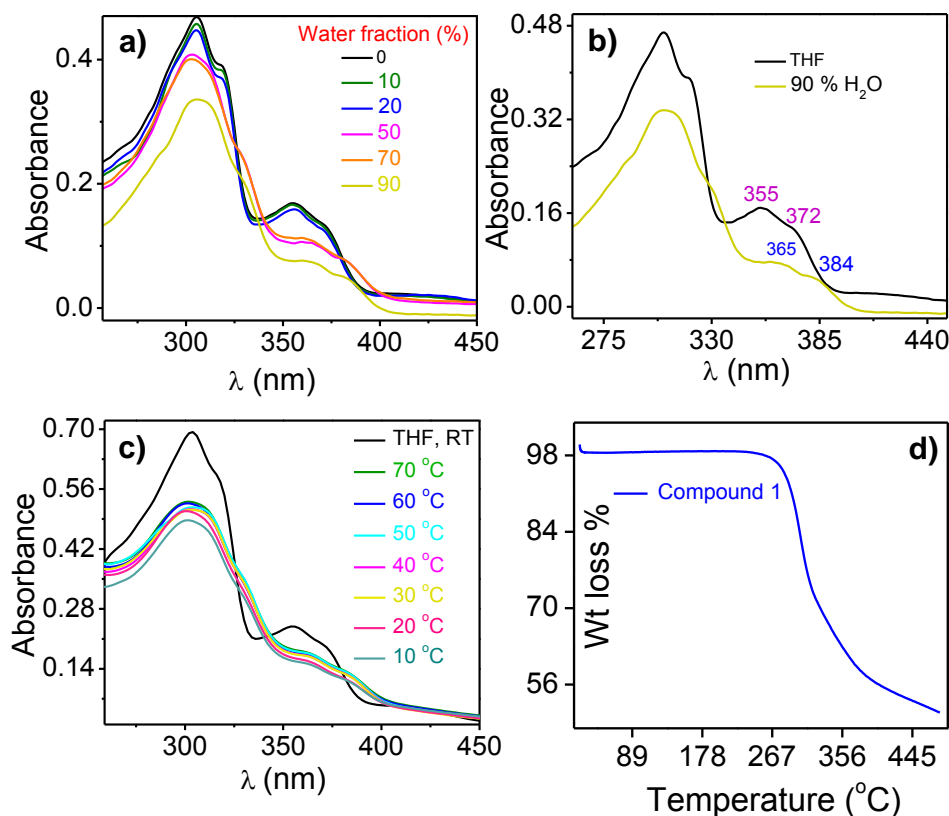


Figure 2.2. (a, b) UV-Vis spectra of **1** (10 μ M) in THF and THF– water mixed solvent medium; (c) Variable-temperature UV-Vis spectra of **1** (10 μ M) in THF-water (3:7; v/v). Temperature varied from 10–70 $^{\circ}\text{C}$; (d) Weight-loss profile for pure solid sample of **1** obtained using thermogravimetric analysis (TGA).

The steady state luminescence spectra of **1** were studied carefully to understand the effect of the ESIPT coupled AIEE process that could be operational. Luminescence spectra of **1** were recorded with a gradual increase of water percentage (from 0–90 %) into its THF solution keeping the 10 μ M of constant concentration (Figure 2.3). A broad emission band with two maxima at 454 and 487 nm ($\lambda_{\text{ex}} = 365$ nm) was observed in THF solution. In THF-water (9:1; v/v) solution, an appreciable increase in emission intensity was observed at 487 nm. Bleaching of this emission band was observed with small associated blue shifts (Figure 2.3) on further increase in water content, while a subsequent new emission band appeared at 551 nm. This new band was evident for a THF-water solvent mixture having a composition of 1 : 1 (v/v). An emission band with a maximum at 487 nm eventually disappeared for THF-water solution having water content ≥ 70 %. The band at 551 nm became more intense upon further increase in the water content (Figure 2.3). Thus, an eventual Stokes shift of 186 nm was observed.

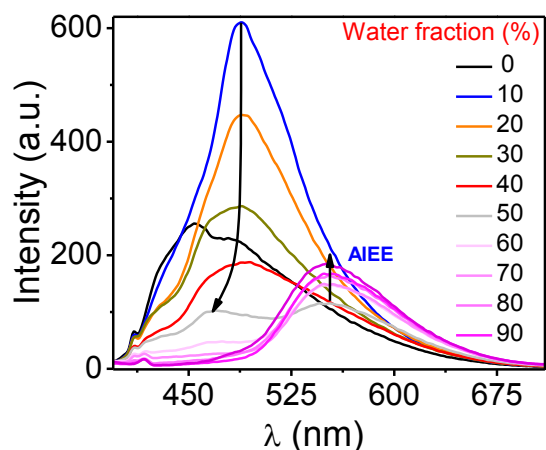
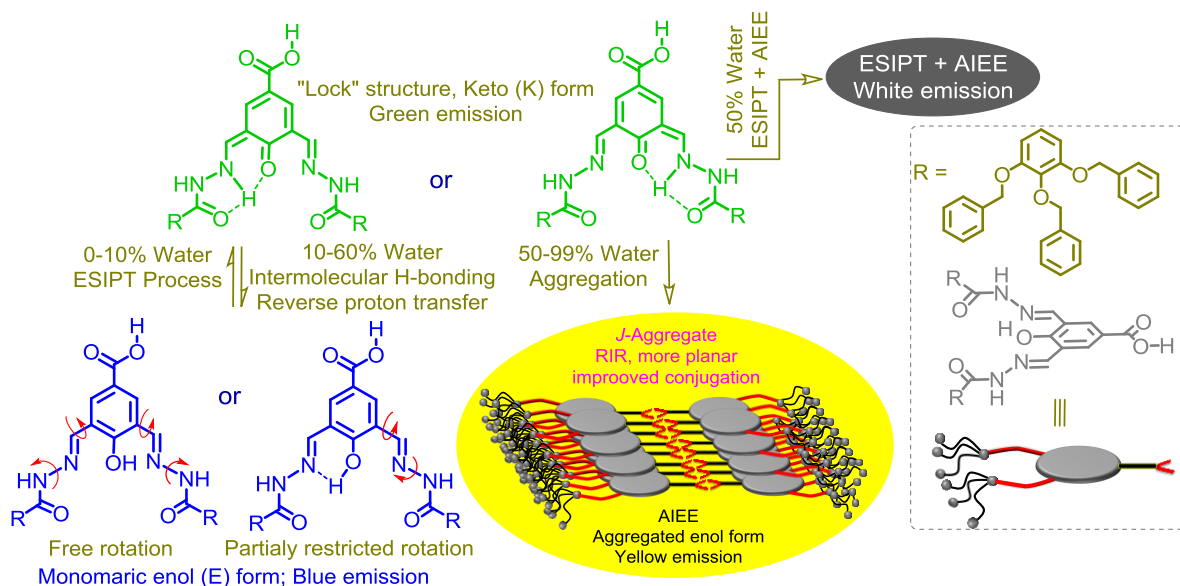


Figure 2.3. Luminescence spectra of **1** (10 mM) in THF and THF-water mixed solvent medium with various % of water. ($\lambda_{\text{ex}} = 365$ nm).

In THF solution, compound **1** could adopt various conformations due to several combinations of C-C/N-N or even C=N_{imine} bond rotations/isomerisation with a broad range of torsional angles (Scheme 2.2). Such conformational changes or isomerization are expected to favour the non-radiative deactivation of the excited state and a nominal emission quantum yield. However, the presence of bulky poly(aryl ether) dendron groups and a preformed six-membered H-bond between -OH and N_{imine} centres (Scheme 2.2) were expected to partially restrict the above referred rotations and/or isomerisation process(es), which could be accounted for the observed weak and broad emission in pure THF (Figure 2.3). Additionally, ESIPT process is known to be sensitive to media polarity. In non-polar solvent, the emission band with a large Stokes shift is generally observed, which is attributed to the emission from the excited keto form (K*) of two tautomers. In protic or polar solvent, enol (E) form gets stabilized through the formation of intermolecular hydrogen bonds with solvent molecules. This accounted for the emission band of excited enol form (E*) with a normal Stokes shift value before undergoing ESIPT.^{7a} Relative intensities of these two emission bands are expected to vary according to the media polarity and structure of the respective luminophore. For the present study, **1** could exist in E as well as in K form in THF, a solvent with moderate polarity. Thus, two emission maxima at 454 and 487 nm ($\lambda_{\text{ex}} = 365$ nm) in pure THF solution were



Scheme 2.2. Changes in the configuration of **1** from the twisted ground state to a more planar excited state, and finally *J*-aggregated rigid structure through ESIP coupled AIEE processes with the variation of the water fraction to its THF solution.

attributed to monomeric E* and K* form, respectively. Interestingly, excitation spectrum recorded for **1** using λ_{em} of 454 and 487 nm in pure THF was significantly different from its corresponding absorption spectrum (Figure 2.4a). This confirmed that the final emitting state(s) is/are different from the one that accounted for emission at 454 and 487 nm. This new emission could arise from the follow-up ESIP process. Upon addition of water to the THF solution of **1**, the media polarity was enhanced and this was expected to favour the emission from E* at 454 nm with normal Stokes shift, which was contrary to our observation (Figure 2.3). In a THF–water solvent mixture with maximum 15 % water content, the emission band at 487 nm was prominent, which was linked to the emission from K*. This unusual phenomenon could be explained if the certain planar structure for **1** was possible due to RIR. Water is a non-solvent for **1** and this would help molecules of **1** to aggregate in addition of ~10 or 15 % water to its THF solution. Such aggregation was expected to impose certain restrictions on the intramolecular torsional motions and would help molecules to attain somewhat planar structure that was favourable for the proton transfer from –OH to the N_{imine} atom upon photoexcitation.^{12b} This ESIP process was expected to fully restrict the intramolecular rotation and help molecules of **1** to attain a “lock” structure (Scheme 2.2), which accounted for the shift in the band maxima from 454 to 487 nm (Figure 2.3), an enhanced emission band of K*. As was observed in the case of pure THF, fluorescence excitation spectra (λ_{em} = 487 nm) of a solution having 10 % water also yielded similar

results (Figure 2.4b). With further increase of the media polarity by gradual addition of water, intermolecular H-bonding was preferred over the intramolecular H-bonding process and thus, one would expect E-form to prevail over the K-form. Hence, for solution having increasingly higher water content (~20 to 60 %), the emission band with maxima at 487 nm was found to bleach gradually along with a distinct blue shift (Figure 2.3).

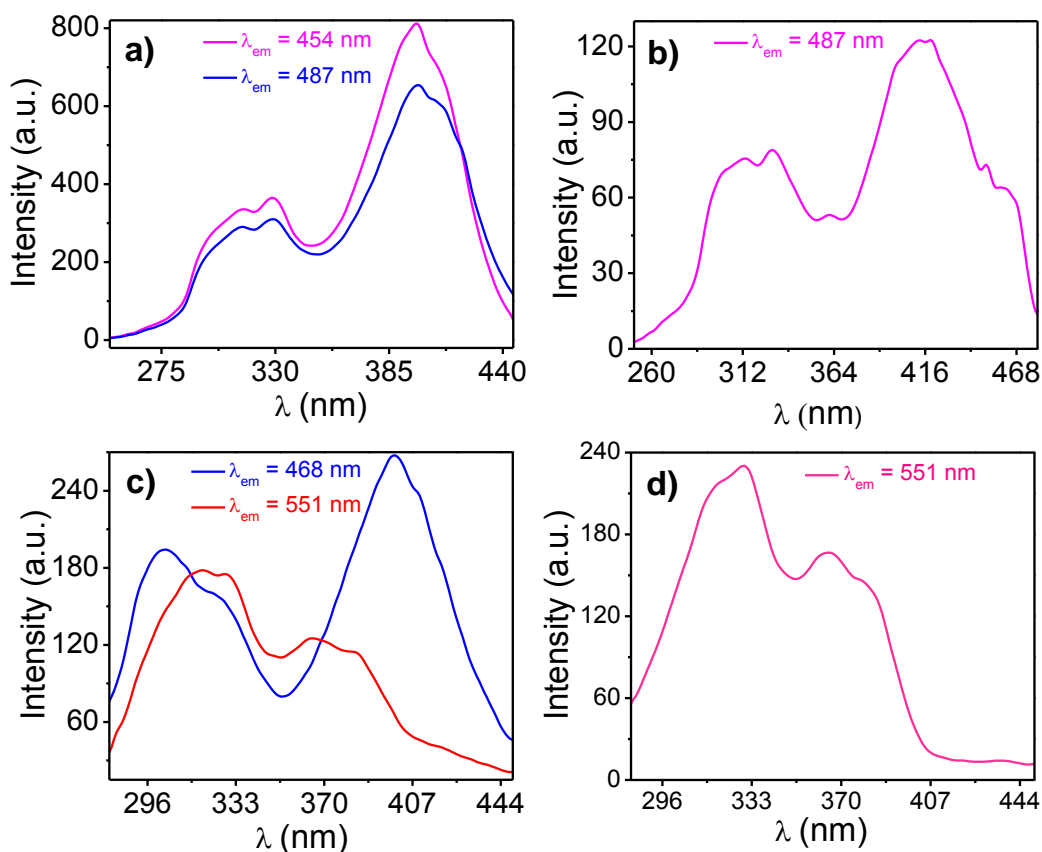


Figure 2.4. Fluorescence excitation spectra of **1** in (a) THF ($\lambda_{em} = 454$ and 487 nm); (b) THF-water (9:1; v/v) ($\lambda_{em} = 487$ nm); (c) THF-water (1:1; v/v) ($\lambda_{em} = 468$ and 551 nm); (d) THF-water (1:9; v/v) ($\lambda_{em} = 551$ nm).

This signified the transformation from K to E tautomer. For ~ 50 % water content, an additional emission band at 551 nm was observed (Figure 2.3). The degree of aggregation of **1** was expected to be more significant in the solution having higher water content. For water content ≥ 50 %, such extensive aggregation was expected to restrict all the C-C/N-N bond rotation or C=N bond isomerization and molecules of **1** would attain a more planar structure (Scheme 2.2). This should enhance molecular planarity and conjugation, which subsequently induced the red shifted emission band maxima at 551 nm with a Stokes shift of 186 nm (Figure 2.3). Thus, this emission band with a high Stokes shift value was assigned as the AIEE band of the aggregated E form

of **1**.¹¹ For solution with ~ 50 % water content, we have also recorded excitation spectra (using λ_{em} of 468 and 551 nm). The excitation spectrum observed for λ_{em} of 468 nm was different from its absorption spectrum, whereas that obtained for λ_{em} of 551 nm was identical to its absorption spectrum (Figure 2.4c). This further confirmed that the E-form of **1** was stabilized in its aggregated state in solution having water content ≥ 50 %. Results of the electronic spectral studies (Figure 2.2a) revealed *J*-type aggregation (Scheme 1). Thus, both the ESIPT and AIEE processes were operational for solution with ~ 50 % water content and accounted for a broad emission spectrum with two emission maxima at 468 and 551 nm, respectively (Figure 2.3). Upon further increase of the water fraction (~60 to 90 %), the AIEE process prevailed over the ESIPT process and a gradual growth in emission band intensity with λ_{max} at 551 nm was observed for a normal AIEE process involving E form. For solution with 90% water content the fluorescence excitation spectrum (λ_{em} of 551 nm) matched with its corresponding absorption spectrum (Figure 2.4d), which again confirmed that only the E form of **1** existed in the aggregated state. Compound **2** was used for control experiments and failed to show any such spectral changes (like compound **1**) for identical experiments (Figure 2.5). Due to the absence of free -OH proton, this molecule had no chance to form an analogous “lock” structure like **1** (Scheme 2.2) through ESIPT processes, at a relatively low water content. With higher water content (~ 70–99 %), an insignificant board emission band was observed at 481 nm (Figure 2.5b), which was attributed to an AIE effect.

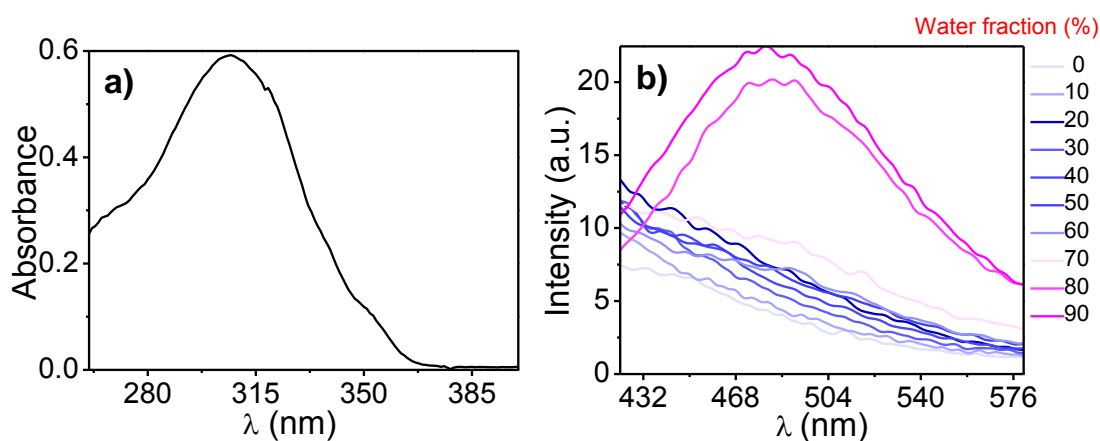


Figure 2.5. (a) Absorption spectrum of **2** in pure THF; (b) Luminescence spectra of **2** in THF and THF-water mixed solvent (Concentration used = 10 μ M; λ_{ex} = 306 nm).

To confirm that the ESIPT process was really operational, luminescence spectra of **1** (10 μ M) were recorded in solvents with different polarities and band maximum

was found to be red shifted with decrease in the solvent polarity (Figure 2.6). This corroborated our presumption that the ESIPT process was operational under appropriate conditions.

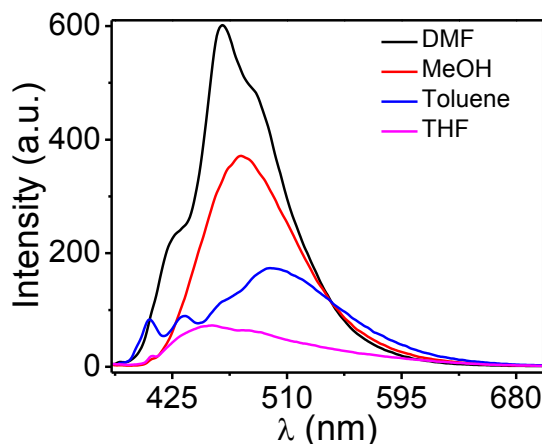


Figure 2.6. Luminescence spectrum of **1** (1 μ M) in solvent with different polarities (λ_{ex} = 365 nm).

A visually detectable luminescence color was also examined carefully upon irradiation with 365 nm UV light of the (Figure 2.7a). This was found to change from blue-green-white-yellow respectively, for **1** with the change in the THF-water ratio to 100:0, 9:1, 1:1 and 1:90 (Figure 2.7b inset). Luminescence spectra recorded for solution having 50 % water content covered the entire visible range (\sim 400–700 nm) and this accounted for white-light emission (Figure 2.7a). CIE coordinates were also calculated using luminescence data to check the purity of the white-light and this fell in the range of (0.31, 0.37), which was very close to pure white-light (0.33, 0.33). CIE coordinates for other luminescent colors are shown in Figure 2.7c.

To understand conformational changes associated with **1** for varying water content in THF-water medium, field emission scanning electron microscopic (FESEM) studies were performed (Figure 2.8). In THF and in a THF-water (9:1, v/v) mixture, entangled fibre-like aggregates were observed (Figure 2.8a and 2.8b). Nanorod shaped aggregates were obtained for a THF-water (1:1, v/v) mixture, while marine habitats like nanostructure were observed in THF-water (1: 9, v/v) medium (Figure 2.8c and 2.8d). These also supported our argument on changes in conformation and the aggregation pattern upon increase in water content in the THF-water medium.

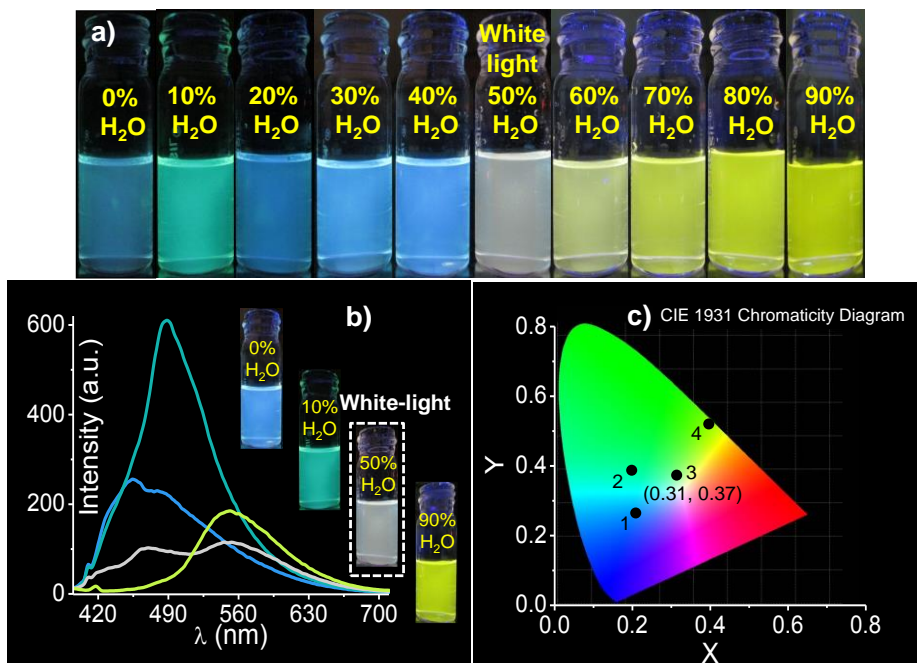


Figure 2.7. (a) Photographs of luminescence color of 10 μM solution of **1** in THF and THF-water mixed solvent under UV light (365 nm); (b) Changes in the emission spectra of **1** (10 μM) with varying water content in THF-water medium, inset: photographs showing luminescent colors upon irradiation with 365 nm light with different water contents; (c) CIE chromaticity diagram for blue (1), green (2), white (3) and yellow (4) emission, respectively.

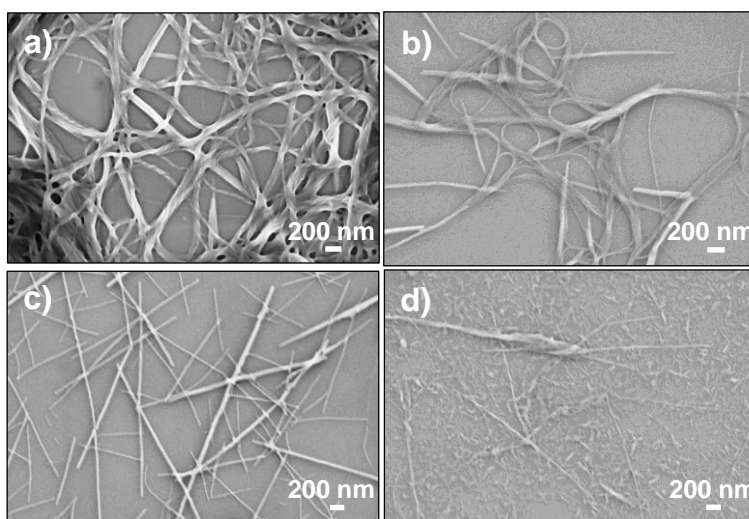


Figure 2.8. Solvent dependent FESEM images of **1** (100 μM) having (a) 0, (b) 10, (c) 50 and (d) 90 % water content in THF; (Scale bar 200 nm).

FTIR spectra were recorded for **1** and **2** as KBr pellets. For **1**, an intense and sharp band for stretching frequency of -C=N appeared at 1656 cm^{-1} , while a much weaker band at 1606 cm^{-1} was observed for **2** (Figure 2.9). This was attributed to a conformationally rigid structure of **1** and a flexible structure of **2**, where -C=N bond isomerization was possible. Additionally, respective stretching frequency of $\text{-C=O}_{\text{amide}}$ for **1** and **2** appeared at 1619 cm^{-1} and 1643 cm^{-1} , which revealed that the strength of the H-bonding in **2** was less as compared to that of **1**. All these results indicated that **1** adopted a rigid and planar structure.

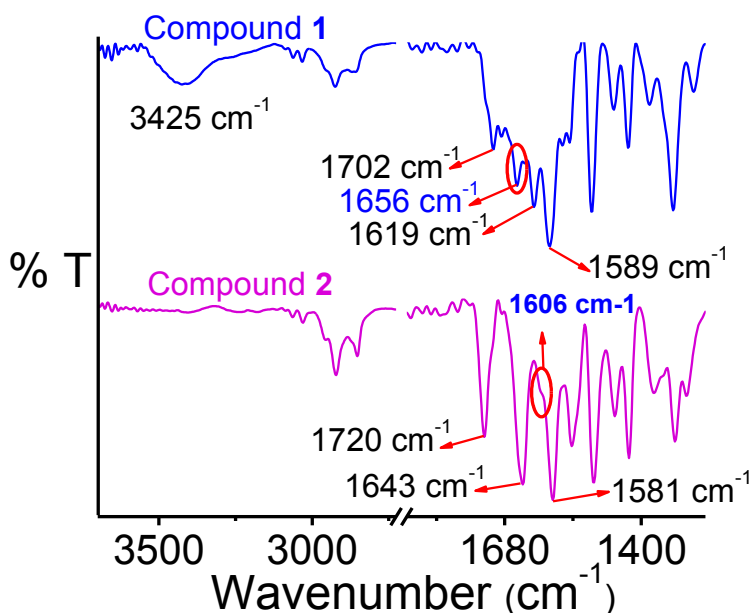


Figure 2.9. Comparisons of FT-IR spectrum of compound **1** and **2** at room temperature.

Compound **1** was sparingly soluble in THF at ambient temperature and was found to dissolve completely upon gentle heating (Figure 2.10a). A yellow color opaque gel was formed (CGC is 1.0 wt %) upon cooling to room temperature and this was confirmed by an inverted vial method (Figure 2.10b). Bright yellow fluorescence was observed from this gel, when exposed to 365 nm UV light (Figure 2.10c). However, **2** failed to give gel (Figure 2.10d-f) under identical conditions. Even after keeping the THF solution of **2** for 24 hrs, it maintain to its solution state (Figure 2.10e). This perhaps revealed the role of the pendent -COOH functionality in **1** for gel formation. Interestingly, the correspondingly THF solution of **2** showed the blue emission under illumination of 365 nm UV lamp (Figure 2.10f). This is due to the AIE property of **2**, which we have examined by recording the luminescence spectra with increasing the water fraction to its THF solution (Figure 2.5b).

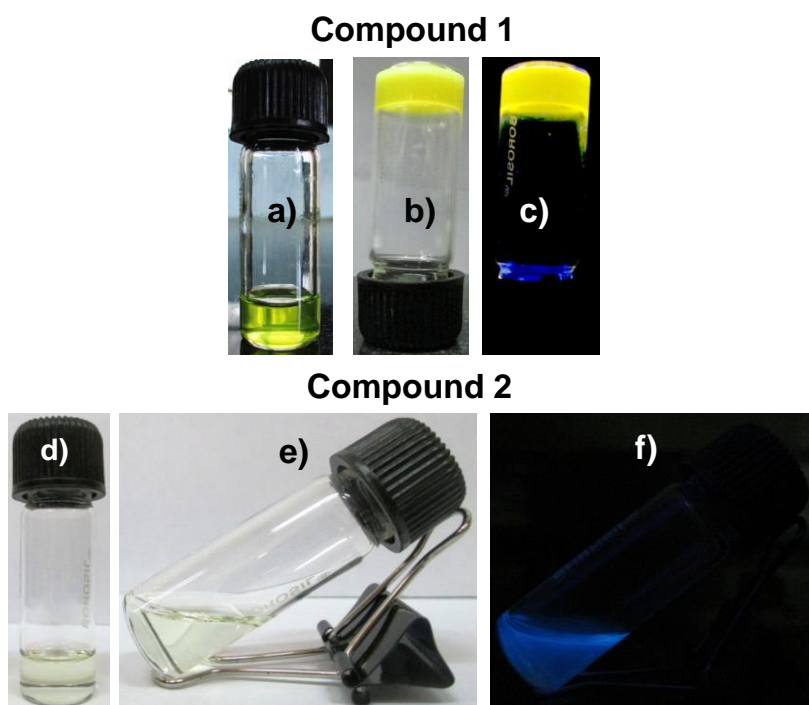


Figure 2.10. 1st row: Photographs of THF solution (10.0 mg/mL) of compound **1** (a) immediate after dissolving by heating; (b) Yellow color opaque gel after cooling the hot solution for ~30 min; (c) Bright yellow luminescence of the corresponding formed gel under illumination of 365 nm UV light. 2nd row: Photographs of THF solution of compound **2** (d) immediately after dissolving the compound (16.0 mg/mL of THF) by gentle heating; (e) after 24 hrs upon cooling to room temperature; (f) under 365 nm UV light shows blue emission. Indicating Under identical condition or even higher concentration (compare to compound **1**) compound **2** is unable to give gel.

The gel formation of the compound **1** was also confirmed by rheology experiment. A frequency-sweep experiment where the storage modulus (G') and loss modulus (G'') were measured as a function of angular frequency at 0.1% constant strain suggests that G' and G'' values are feebly dependent on frequency, inferring the formation of a stable gel of compound **1** (Figure 2.11). Further, the FESEM and TEM experiments of the gel obtained from **1** (Figure 2.10f and 2.10g) in THF show the typical nanoscale fibrous architecture with a diameter range of 50–150 nm and several micrometers of length (Figure 2.12). This morphological identity also confirmed the gel formation of the compound **1**.

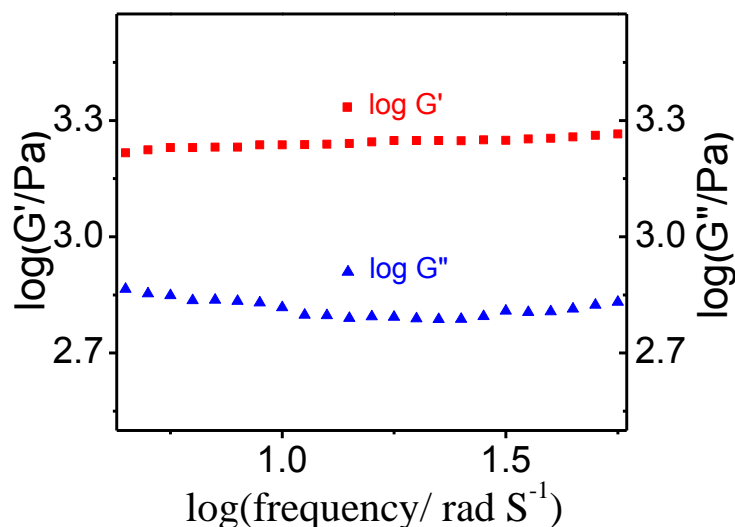


Figure 2.11. Dynamic frequency sweep measurement of storage modulus (G') and loss modulus (G'') for THF gel (1.0 wt %) of **1**.

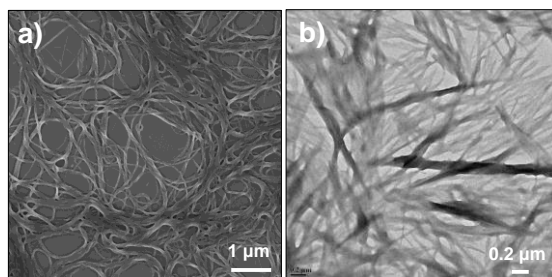


Figure 2.12. (a) FESEM and (b) TEM images showing the typical fibrillar morphology of the THF gel of compound **1**.

To gain additional insight into the modes of molecular packing in self-assembled gel state of **1**, X-ray powder diffraction (XRPD) patterns were recorded for small as well as for wide angle regions of the air-dried THF gel of **1**. In the small angle region peak at $2\theta = 3.1^\circ$ with a d spacing value of 28.5 Å (D) (Figure 2.13a) was followed by several other peaks in the wide angle region (Figure 2.13b) in a periodical order with d spacing values of 13.8 Å (D/2), 9.5 Å (D/3), 7.1 Å (D/4), 5.5 Å (D/5), 4.8 Å (D/6). These data suggested that molecules of **1** were self-assembled in a lamellar fashion in the gel state.^{9c} In the wide angle region one more peak at $2\theta = 23.9^\circ$ with d spacing value of 3.7 Å were observed. This suggested the presence of π - π staking interactions of dendrons in the gel fiber.^{4c} Collectively, from the optical study, morphological investigation and PXRD results we propose the gelation mechanism of compound **1** in the Scheme 2.3.

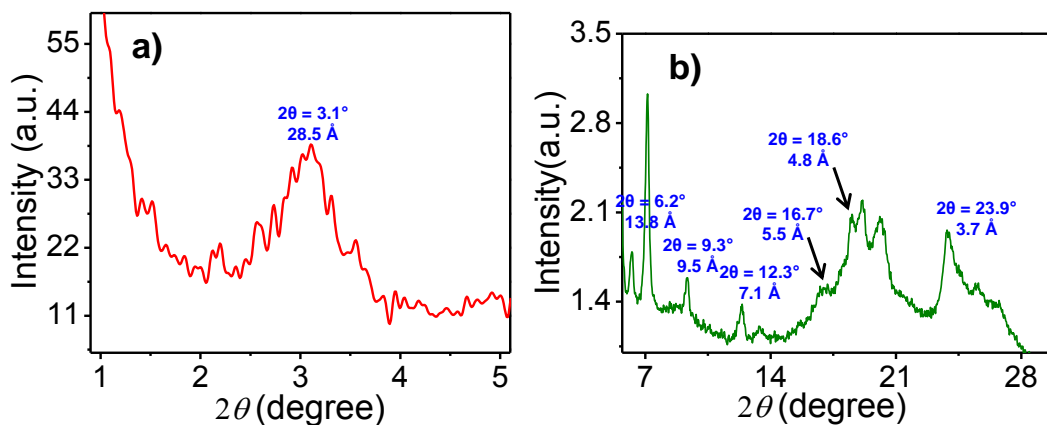
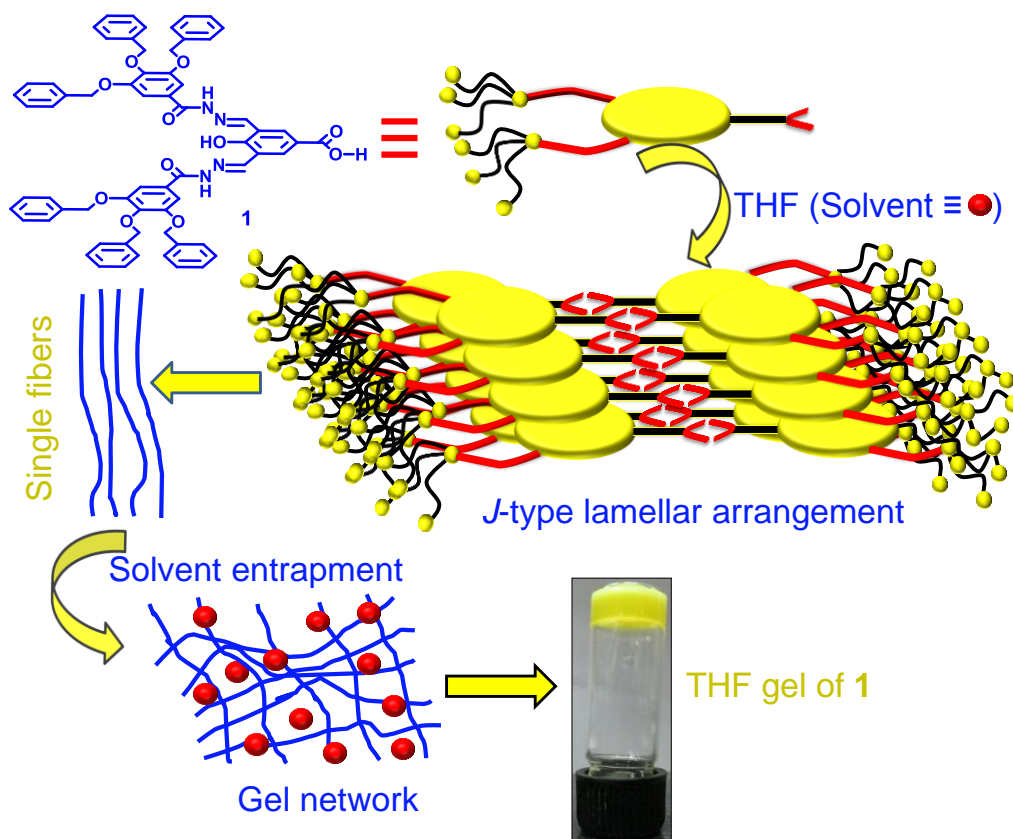


Figure 2.13. (a) Small-angle and (b) wide-angle XRPD diffraction pattern of **1** in xerogel state.



Scheme 2.3. Pictorial presentation of gelation mechanism of THF gel formation of compound **1**.

Like gel state, importantly the compound **1** showed the effective bright yellow color luminescence in its powder state (Figure 2.14a). In addition a thin film of **1** on a glass plate as well as a print “CSIR-NCL” on a silica gel plate (thickness 0.2 mm & pore size of 60 Å on aluminium plate) using THF solution of **1** were also found to be strongly emissive upon irradiation with 365 nm light (Figure 2.14b and 2.14c). Such properties have relevance for energy efficient display devices.



Figure 2.14. Solid state emitting property of compound in (a) powder and (b) film state; (c) utilization of solid state emitting property compound **1** as fluorescent ink to write our institute name. All photographs are taken under the under 365 nm UV light irradiation.

From the photophysical studies, we concluded that in the aggregated state **1** adopted a more planar π -conjugated structure (Scheme 2.2). This led us to examine the electrical conductivity of the gel obtained from **1** at room temperature by following the two-probe method with drop casting the THF solution of **1** (10 mg/mL of THF) on the surface of an ITO glass. The corresponding I - V plot was obtained (Figure 2.14). In the low voltage region (~ 2.5 to 5.5 V), a linear plot was obtained, however deviation from the linearity was observed for the higher voltage region and this indicated the semiconducting nature of compound **1**.^{9c,11b}

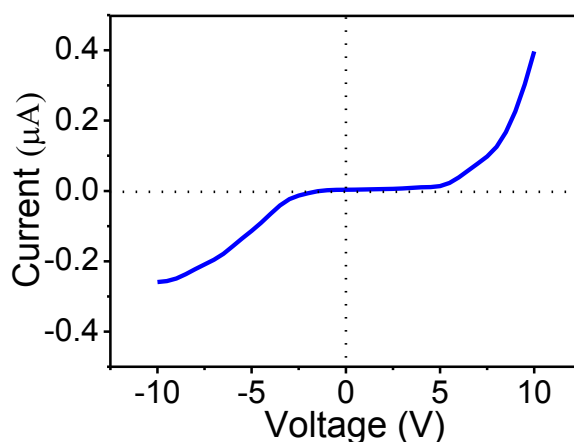


Figure 2.14. Electrical conductivity studies showing I - V characteristics of compound **1** in a two-probe electrode.

2.4. Conclusion

In summary, we have demonstrated that an ESIPT coupled AIEE process could be utilized for tuning the luminescence color of a single molecule over a wide energy range (blue-green-white-yellow). To the best of our knowledge, no such example is available in the contemporary literature. Interestingly, compound **1** exhibits bright yellow color luminescence in the gel as well as in the solid state. Photophysical studies and the XRPD pattern revealed *J*-type lamellar arrangement among molecules of **1**. Finally, the solid state emitting capabilities and the semiconducting nature of compound **1** may be exploited for organic field-effect transistors and OLED device fabrication.

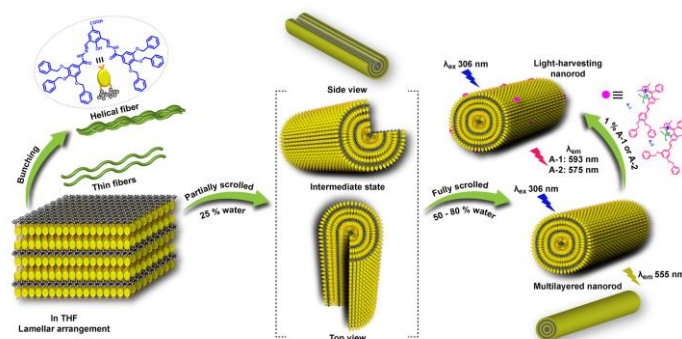
2.5. References

1. (a) Y. S. Zhao, H. Fu, F. Hu, A. D. Peng and J. Yao, *Adv. Mater.*, 2007, **19**, 3554; (b) J. E. Kwon, S. Park and S. Y. Park, *J. Am. Chem. Soc.*, 2013, **135**, 11239.
2. (a) S. S. Babu, V. K. Praveen and A. Ajayaghosh, *Chem. Rev.*, 2014, **114**, 1973 and references therein; (b) A. Vidyasagar, K. Handore and K. M. Sureshan, *Angew. Chem.*, 2011, **123**, 8171.
3. (a) M. O. M. Piepenbrock, G. O. Lloyd, N. Clarke and J. W. Steed, *Chem. Rev.*, 2010, **110**, 1960; (b) X. Zhang, S. Lee, Y. Liu, M. Lee, J. Yin, J. L. Sessler and J. Yoon, *Sci. Rep.*, 2014, **4**, 4593.
4. (a) A. Chakrabarty, S. Chatterjee and U. Maitra, *J. Mater. Chem. C.*, 2013, **1**, 2136; (b) K. Peng, I. Tomatsu and A. Kros, *Chem. Commun.*, 2010, **46**, 4094; (c) S. Basak, J. Nanda and A. Banerjee, *J. Mater. Chem.*, 2012, **22**, 11658.
5. (a) A. Ajayaghosh, V. K. Praveen, S. Srinivasan and R. Varghese, *Adv. Mater.*, 2007, **19**, 411; (b) P. Rajamalli, S. Atta, S. Maity and E. Prasad, *Chem. Commun.*, 2013, **49**, 1744; (c) S. Bhattacharya and S. K. Samanta, *Chem. – Eur. J.*, 2012, **18**, 16632; (d) A. Ajayaghosh, V. K. Praveen, C. Vijayakumar and S. J. George, *Angew. Chem., Int. Ed.*, 2007, **46**, 6260; (e) Q. Chen, D. Zhang, G. Zhang, X. Yang, Y. Feng, Q. Fan and D. Zhu, *Adv. Funct. Mater.*, 2010, **20**, 3244.
6. (a) C. Vijayakumar, V. K. Praveen and A. Ajayaghosh, *Adv. Mater.*, 2009, **21**, 2059; (b) P. Bairi, B. Roy, P. Chakraborty and A. K. Nandi, *ACS Appl. Mater. Interfaces.*, 2013, **5**, 5478; (c) C. Deng, P. Jiang, X. Shen, J. Ling and T. E. H. Esch, *Polym. Chem.*, 2014, **5**, 5109; (d) C. Vijayakumar, K. Sugiyasu and M. Takeuchi, *Chem. Sci.*, 2011, **2**, 291; (e) D. K. Maiti, S. Roy, A. Baral and A. Banerjee, *J. Mater. Chem. C.*, 2014, **2**, 6574; (f) C. Giansante, G. Raffy, C. Schäfer, H. Rahma, M. T. Kao, A. G. L. Olive and A. D. Guerzo, *J. Am. Chem. Soc.*, 2011, **133**, 316; (g) K. V. Rao, K. K. R. Datta, M. Eswaramoorthy and S. J. George, *Adv. Mater.*, 2013, **25**, 1713.
7. (a) J. E. Kwon and S. Y. Park, *Adv. Mater.*, 2011, **23**, 3615; (b) J. Zhao, S. Ji, Y. Chen, H. Guo and P. Yang, *Phys. Chem. Chem. Phys.*, 2012, **14**, 8803; (c) J. Luo, Z. Xie, J. W. Y. Lam, L. Cheng, H. Chen, C. Qiu, H. S. Kwok, X. Zhan, Y. Liu, D. Zhuc and B. Z. Tang, *Chem. Commun.*, 2001, 1740; (d) Y. Hong, J. W. Y. Lam and B. Z. Tang, *Chem. Soc. Rev.*, 2011, **40**, 5361 and references therein.
8. (a) K. C. Tang, M. J. Chang, T. Y. Lin, H. A. Pan, T. C. Fang, K. Y. Chen, W. Y. Hung, Y. H. Hsu and P. T. Chou, *J. Am. Chem. Soc.*, 2011, **133**, 17738; (b) W. Sun, S. Li, R. Hu, Y. Qian, S. Wang and G. Yang, *J. Phys. Chem. A.*, 2009, **113**, 5888; (c) K. Sakai, T. Ishikawaa and T. Akutagawa, *J. Mater. Chem. C.*, 2013, **1**, 7866.
9. (a) B. K. An, D. S. Lee, J. S. Lee, Y. S. Park, H. S. Song and S. Y. Park, *J. Am. Chem. Soc.*, 2004, **126**, 10232; (b) W. Z. Yuan, F. Mahtab, Y. Gong, Z. Q. Yu, P. Lu, Y.

- Tang, J. W. Y. Lam, C. Zhuc and B. Z. Tang, *J. Mater. Chem.*, 2012, **22**, 10472; (c) S. Basak, J. Nanda and A. Banerjee, *Chem. Commun.*, 2013, 49, 6891.
10. (a) X. Luo, J. Li, C. Li, L. Heng, Y. Q. Dong, Z. Liu, Z. Bo and B. Z. Tang, *Adv. Mater.*, 2011, **23**, 3261; (b) H. Tong, Y. Hong, Y. Dong, Y. Ren, M. Haussler, J. W. Y. Lam, K. S. Wong and B. Z. Tang, *J. Phys. Chem. B.*, 2007, **111**, 2000.
11. (a) M. R. Molla and S. Ghosh, *Chem. – Eur. J.*, 2012, **18**, 1290; (b) S. K. Samanta and S. Bhattacharya, *J. Mater. Chem.*, 2012, **22**, 25277.
12. (a) G. Li, D. Zhu, Q. Liu, L. Xue and H. Jiang, *Org. Lett.*, 2013, **15**, 924; (b) T. He, X. T. Tao, J. X. Yang, D. Guo, H. B. Xia, J. Jia and M. H. Jiang, *Chem. Commun.*, 2011, **47**, 2907; (c) Y. Qian, S. Li, G. Zhang, Q. Wang, S. Wang, H. Xu, C. Li, Y. Li and G. Yang, *J. Phys. Chem. B.*, 2007, **111**, 5861.
13. D. Perrin, W. L. F. Armarego and D. R. Perrin, *Purification of Laboratory Chemicals*, 2nd Ed., Oxford: Pergamon **1980**.
14. N. K. Lifshin, L. Albertazzi, M. Bendikov, P. S. Baran and Doron Shabat, *J. Am. Chem. Soc.*, 2012, **134**, 20412.
15. P. Rajamalli and E. Prasad, *Org. Lett.*, 2011, **13**, 3714.

CHAPTER 3

Water Induced Morphological Transformation of a Poly(aryl ether) Dendron Amphiphile: Helical Fibers to Nanorods, as Light-Harvesting Antenna Systems



Self-assembly of suitable molecular building blocks is an efficient and convenient approach to generate nanomaterials with various morphologies and functions. Moreover, understanding the nature of molecules and controlling factors of their self-assembly process is crucial in fundamental aspects of molecular self-assembly which provide insights into the design of new assemblies with functional nano-architectures. To this end, the present study reports water induced self-assembled multifaceted morphology formation and the plausible pathway of the morphology transformation of a single poly(aryl ether) dendron amphiphile **1**. In THF, **1** self-assembles into helical fibers. However, with an increase in the water fraction in its THF solution, the morphology changes to nanorods through an intermediate scroll-up pathway of exfoliated fibers. The nanorod formation and transformation of **1** are investigated using various microscopy and spectroscopy techniques, which indicate that it has highly ordered multilayered arrays of **1** molecules. Finally, these multilayered arrays of **1** nanorods are exploited for constructing a model light-harvesting system via the incorporation of small quantities of two newly designed BODIPY based molecules as energy acceptors and **1** as an antenna chromophore.

Publication:
Nanoscale, 2018, 10, 1464.

3.1. Introduction

Fabrication of functional nano- and micro-structures with dissimilar morphologies using energy and resource saving bottom-up techniques such as self-assembly has become a topic of intense investigation.¹ Quite often, it was perceived that the morphological identities of self-assemblies exclusively determine their specific applications.² Thus, tuning the morphology of self-assemblies is highly desirable, and in particular the fabrication of multiple nanostructures from a single molecular backbone is of huge significance. In this context, amphiphilic molecules having hydrophobic and hydrophilic segments are proved to be promising building blocks for switchable superstructures in response to different external forces as well as to solvent polarity.^{3,4} As one case in point, achieving the cylindrical (nanorod/nanotube) morphology by the self-assembly of organic amphiphilic molecules is highly desired because of their extremely ordered molecular arrangements with high surface area, density and hollow nanospace (of nanotubes), which is suitable for nanoelectronics, catalysis, drug delivery carriers, adsorbents, and other related applications.⁵ Despite its emerging applications, fundamental insights, such as the understanding the mechanism of cylindrical morphology formation as well as the correlation between the nature of molecules and their arrangements for attaining this particular morphology, are also crucial. There are few excellent and comprehensive reviews as well as some interesting articles by Shimizu *et al.* and a few other research groups for elucidating the mechanism of nanotube formation through a helical intermediate or by the direct scrolling of sheets.⁶ In addition, continuous stacking of the toroidal and nanoring type architecture or fusion of connecting spheres are other possible ways of nanotube formation.⁷ However, reports that could reveal the stepwise morphological transition of nanorod formation through visualization of intermediate topologies for predicting the molecular arrangements and the mechanistic pathway are scanty in the contemporary literature.⁸

The construction of new organic self-assemblies that are capable of solar light-harvesting and conversion has been the subject of intense research.⁹ In the typical light-harvesting system, energy is absorbed by a well-organized array of the donor chromophores and the excitation energy is transferred to appropriate acceptors.¹⁰ For efficient transport of the excitation energy, the light-harvesting system should have the following two factors: (1) the donor chromophore arrays should be densely packed without the self-quenching effect, and (2) self-assembled aggregates should have a relatively high donor/ acceptor ratio. These factors help in minimizing the energy loss and achieving higher efficiency in energy transfer.¹¹ In this milieu, tightly packed rod-shaped chromophoric assemblies are highly relevant, as such scaffolds afford the option of having a high chromophore density and a large cross-section for absorbing light with

a higher donor to acceptor molecule ratio.¹² It is worth mentioning that natural light-harvesting antennas of green photosynthetic bacteria and a filamentous anoxygenic phototroph, called “chlorosome”, also contain the photo-functional rod-shaped aggregates of supramolecules.^{12,13} Keeping this in mind (the naturally occurring architecture of chlorosome), the construction of new rod-shaped chromophoric assemblies, with light-harvesting antenna properties, is highly desired.

Harnessing the above two points, in this chapter we describe the formation of light-harvesting nanorods from a poly(aryl ether) dendron amphiphile **1** (Figure 3.1a). The poly(aryl ether) backbones are well recognized for the construction of amphiphilic and non-amphiphilic assemblies with diverse nano- and micro-structures such as vesicles, sheets, fibers, helical fibers/ porous structures with interesting optical properties.¹⁴ Furthermore, many of the poly(aryl ether) dendron based systems have been found to be useful as metal ion sensors, anion sensors and stabilizing agents for nanoparticles.¹⁵ However to the best of our knowledge, this poly(aryl ether) backbone in conjugation with any chromophoric units has not been used for the construction of light-harvesting nanorods. In the previous chapter, we have utilized the same **1** molecules for solvent-induced abrupt luminescence color change over a wide energy range (blue-green-white-yellow). Here we have explored further the detailed self-assembly behavior of **1**.

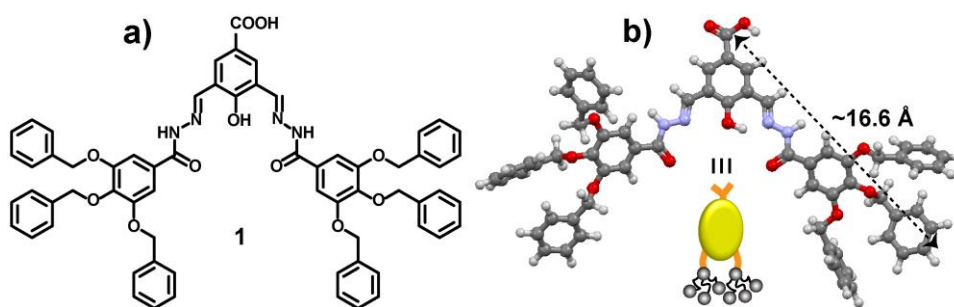


Figure 3.1. (a) Molecular structure; (b) Energy optimized structure and schematic presentation of the poly(aryl ether) dendron amphiphile **1**.

The present study deals with the mechanistic aspects of the solvent-induced helical fiber to nanorod architecture transformation from **1**. Self-assembly of **1** in THF leads to the formation of helical fibers. Upon gradual addition of water into the THF solution of **1**, aggregates having a nanorod shaped morphology through an intermediate scrolled-up pathway were obtained. The impact of various noncovalent interactions on the morphological translation (helical fiber to nanorod) including the intermediate morphology formed of **1** and alteration in its molecular assembly pattern

during changes in the water percentage to its THF solution is investigated by using microscopy and spectroscopy techniques. Finally, these constructed nanorods of **1** were doped with two newly designed BODIPY acceptor (**A-1** and **A-2**; Scheme 3.1 and Figure 3.6a) molecules and their light-harvesting properties were studied.

3.2. Experimental Section

3.2.1. Materials

Unless otherwise stated, all reagents and organic solvents used for synthesis were purchased from commercial suppliers and used as such without further purification. Fresh double distilled water was used throughout the experiment. HPLC grade solvent was used for recording spectrometry data.

3.2.2. Instruments

^1H and ^{13}C NMR spectra for the synthesized compounds were recorded on a Bruker 400/500 MHz FT NMR (Model: AvanceDPX 400/500).

High-resolution mass spectra (HRMS) were recorded on a JEOL JM AX 505 HA mass spectrometer.

FESEM images were obtained using a Nova Nano SEM 450 and a QuantaTM Scanning Electron Microscope. Initially, 20 μM concentrated solutions of **1** were prepared in THF and THF/water mixed solvent content 25, 50 and 80 % of water. These prepared sample solutions were drop-cast on a silicon wafer and allowed to air dry for 5 hours in a dust free place. Finally, they were dried in a desiccator overnight. Before taking FESEM images, the samples were coated with gold vapour.

TEM images were recorded using an FEI Tecnai G2 F20 X-TWIN TEM at an accelerating voltage of 200 kV. The same procedure (as for FESEM experiments) was followed to prepare sample solutions of **1**, which were drop-cast on carbon-coated copper grids (200 mesh) and initially allowed to air dry for 5 hours in a dust-free place followed by keeping in a desiccator overnight. The dried samples were used for taking TEM images without staining.

The Fourier transform infrared (FT-IR) spectra of the airdried mass of **1** obtained from THF and THF/water mixed solvent with 80 % water content were recorded on a Bruker Optics ALPHA-E spectrometer with a universal Zn-Se ATR (attenuated total reflection) accessory.

The powder X-ray diffraction (PXRD) patterns of the airdried mass of **1** were recorded on a Phillips PANalytical diffractometer with Cu K_{α} radiation ($\lambda = 1.5406 \text{ \AA}$).

The UV/Vis absorption spectra were recorded with a PerkinElmer Lambda 950 UV/Vis spectrophotometer, while all emission spectra were recorded using a PTI Quanta Master™ steady state spectrofluorometer. Fluorescence lifetimes were measured by time correlated single photon counting (TCSPC), using a spectrofluorometer (Horiba Scientific) and a LED excitation source of 374 nm.

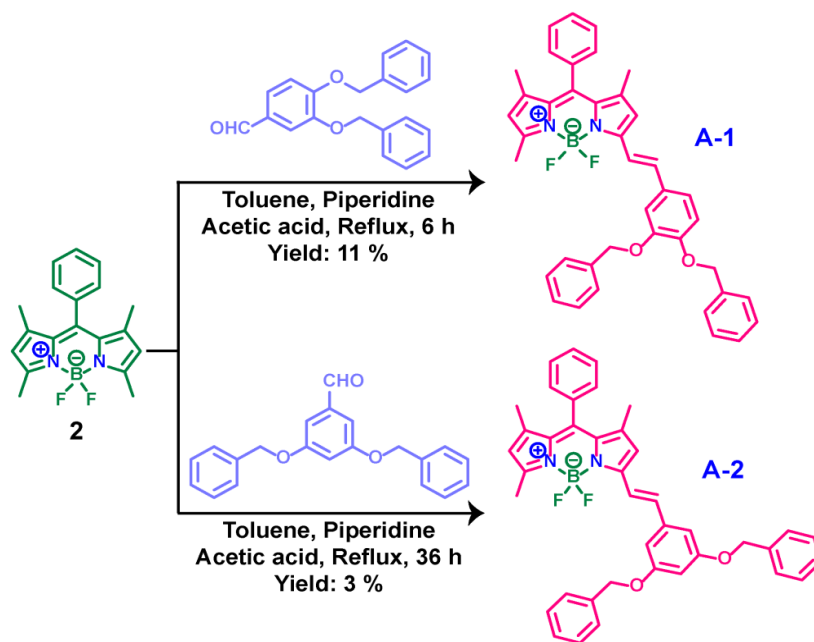
For performing these three experiments (UV-Vis, fluorescence and fluorescence lifetime) initially, we prepared stock solutions (1 mM in THF) for the three compounds **1**, **A-1** and **A-2**. Then the required amount of a stock solution sample was taken and mixed with an appropriate fraction of THF and THF/water to adjust the desired solvent compositions and concentrations (mentioned in the manuscript). The prepared sample was used for performing three consecutive (UV/Vis, fluorescence and fluorescence lifetime) experiments.

3.2.3. Synthesis and Characterization

3.2.3.1. Synthesis of Poly(aryl ether) Dendron Amphiphile 1

Details procedure of the synthesis of poly(aryl ether) dendron amphiphile **1** was discussed in the previous chapter.^{14f}

3.2.3.2. Synthetic Scheme for BODIPY based Acceptor Molecules A-1 and A-2



Scheme 3.1. Methodologies that were adopted for the synthesis of BODIPY based acceptor molecules **A-1** and **A-2**.

3.2.3.3. Synthesis and Characterization of A-1

The core BODIPY unit (compound **2**; in Scheme 3.1), which was used for the synthesis of the acceptor molecule A-1, was prepared by following our previous reports.¹⁶ This BODIPY molecule (compound **2**; 400 mg, 1.23 mM) was dissolved in 25 mL of toluene, and to this solution 3,4-dibenzyloxybenzaldehyde (470 mg, 1.47 mM), 0.9 mL piperidine and 0.6 mL glacial acetic acid were added. The resulting chemical mixture was refluxed in a Dean-Stark apparatus for 6 hrs. After that, the crude reaction mixture was evaporated under reduced pressure. The crude mass was then directly subjected to column chromatography using silica gel (100-200 mesh) as the stationary phase and 10 % ethyl acetate in hexane as the mobile phase to obtain the pure compound **A-1** as a dark brown solid. Yield = 11 %, ¹H NMR (400 MHz, CDCl₃, TMS): δ (ppm) = 7.53–7.51 (3H, d, J = 7.2), 7.49–7.47 (3H, m), 7.45–7.43 (2H, m), 7.41–7.37 (4H, m), 7.33–7.29 (4H, m), 7.22 (1H, broad), 7.13–7.08 (2H, m), 6.91–6.89 (1H, d, J = 8.4), 6.55 (1H, s), 6.00 (1H, s), 5.23 (2H, s), 5.19 (2H, s), 2.61 (3H, s), 1.41 (3H, s), 1.38 (3H, s); ¹³C NMR (100 MHz, CDCl₃, TMS): δ (ppm) = 149.99, 149.02, 140.11, 137.10, 136.99, 135.14, 129.08, 128.58, 128.22, 127.88, 127.66, 127.25, 121.92, 117.50, 114.60, 113.35, 76.71, 71.44, 71.12, 33.84, 31.95, 29.72, 29.38, 29.18, 28.97, 22.71, 14.74, 14.61, 14.36, 14.14; HRMS (ESI): m/z calculated for C₄₀H₃₅BF₂N₂O₂ [M + Na]⁺ = 647.266, found 647.265.

3.2.3.4. Synthesis and Characterization of A-2

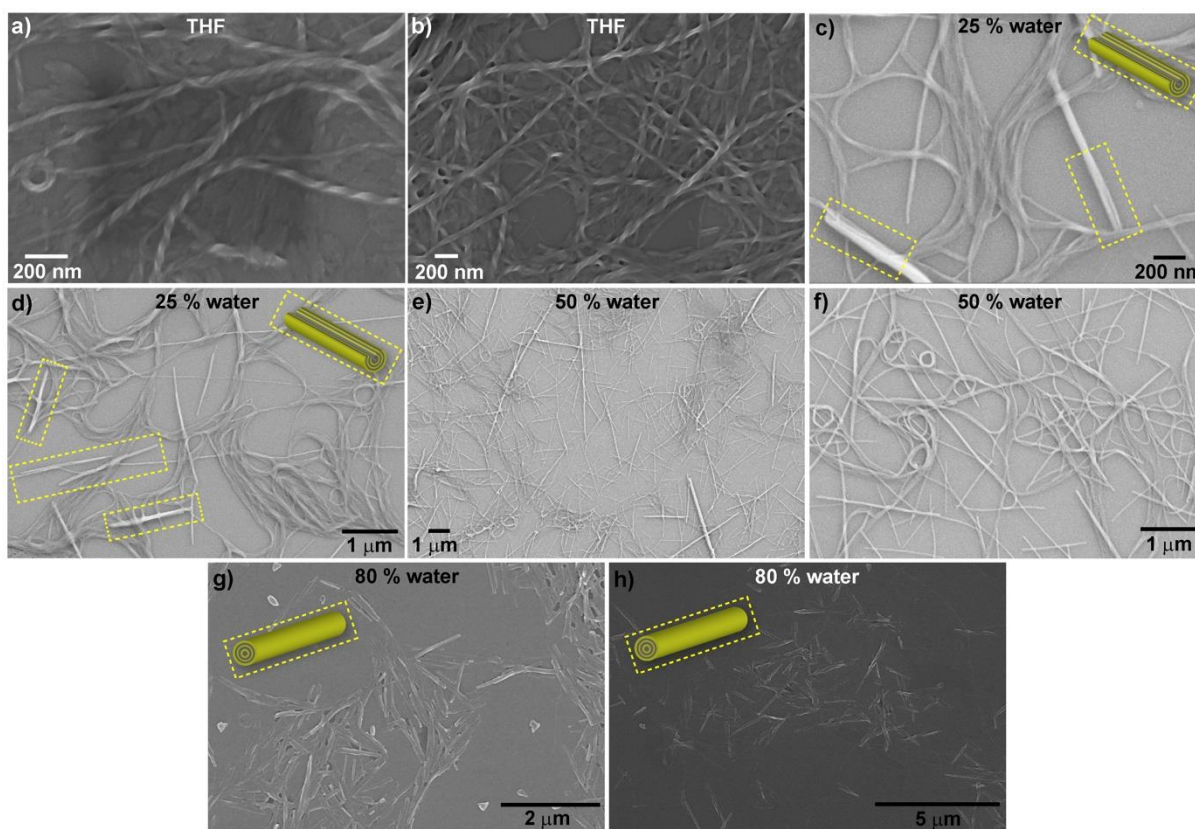
Compound **A-2** was synthesized using 3,5-dibenzyloxybenzaldehyde as a red solid by following the same procedure as that employed for the synthesis of **A-1** (Scheme 3.1). However in this case the reaction mixture was refluxed for 36 hrs (Scheme 3.1). Yield = 3 %, ¹H NMR (500 MHz, CDCl₃, TMS): δ (ppm) = 7.65–7.62 (1H, d, J = 16), 7.48–7.45 (5H, m), 7.41–7.39 (5H, broad), 7.33–7.30 (5H, broad), 7.15–7.11 (1H, d, J = 16.5), 6.84 (1H, s), 6.59–6.58 (3H, broad), 6.02 (1H, s), 5.08 (2H, s), 5.03 (2H, s), 2.61 (3H, s), 1.42 (3H, s), 1.39 (3H, s); ¹³C NMR (125 MHz, CDCl₃, TMS): δ (ppm) = 160.08, 155.90, 152.16, 143.22, 142.24, 140.61, 138.52, 138.19, 136.76, 136.69, 135.74, 135.00, 132.75, 132.01, 129.01, 128.94, 128.60, 128.11, 128.01, 127.67, 127.52, 121.51, 119.72, 117.57, 107.08, 106.60, 102.89, 101.71, 70.20, 70.11, 66.10, 29.67, 20.98, 14.76, 14.52, 14.38; HRMS (ESI): m/z calculated for C₄₀H₃₆BF₂N₂O₂ [M + H]⁺ = 625.284, found 625.283.

3.3. Results and Discussions

Initially, the morphologies of **1** in pure THF and with the addition of different fractions of water into its THF solution at a fixed concentration of 20 μ M were examined by both field emission scanning electron microscopy (FESEM) and transmission electron microscopy (TEM). The FESEM image of **1** in THF (Figure 3.2a and 3.2b) showed a

network of helical fibers composed of thin fibers of nanometer diameter and micrometer length. It is observable that each thin fiber is not exactly helical in nature. The observed helical nature of the fibers presumably occurs due to the bunching of multiple thin fibers. With the addition of 25 % water into the THF solution of **1**, instead of helical fibers a bit of exfoliated fibers was observed (Figure 3.2c and 3.2d). A careful investigation of Figure 3.2c and 3.2d reveals that, in some portion, these fibers appeared to start scrolling. The pictorial presentation of partially scrolled fibers is shown in the insets of Figure 3.2c and 3.2d. Interestingly, in the case of 50 % water content, nanorod shaped aggregates along with fibers at places were observed (Figure 3.2e and 3.2f). These nanorods are about a micrometer in length and with a diameter ranging from ~15 to 86 nm. With a further increase in the water content (80 % water) only nanorods were obtained (Figure 3.2g and 3.2h). Compared to nanorods obtained from the medium having 50 % water content, these nanorods are smaller in length (~200–900 nm).

Figure 3.2. FESEM images of amphiphile **1** (20 μM) nanostructures obtained from (a, b)



THF and THF/water mixed solvent; (c, d) 25 % water (the insets show schematic presentations of a partially scrolled fiber); (e, f) 50 % water and (g, h) 80 % water. Inset of (g and h); schematic presentations of multilayered nanorods.

In cases of THF solutions of **1** with 50 % and 80 % water content, well-defined linear rods with a comparable diameter and length (evaluated from FESEM experiments) were also observed in TEM micrographs (Figure 3.3a-f). TEM images also showed that rods obtained from the solution with a higher water content (80 %; Figure 3.3d-f) are smaller in length in comparison with rods obtained from the solution with a lower water content (50 %; Figure 3.3a-c). Both the microscopy (FESEM and TEM) experiments unambiguously confirm the nanorod shaped morphology of **1**. The energy optimized structure (evaluated using B3LYP theory) of the amphiphile **1** shows ~ 16.6 Å as the molecular length (Figure 3.1b). However, FESEM and TEM images showed the diameter of the nanorods ranges from ~ 15 to 86 nm. This suggests that the nanorods that are formed are multilayered in nature (insets of Figure 3.2g and 3.2h; Figure 3.3b and 3.3f). In addition, as shown in Figure 3.2a-h, FESEM images revealed that the helical fibers transmute into rods through an intermediate scroll-up path of exfoliated fibers (Figure 3.2c and 3.2d; insets).

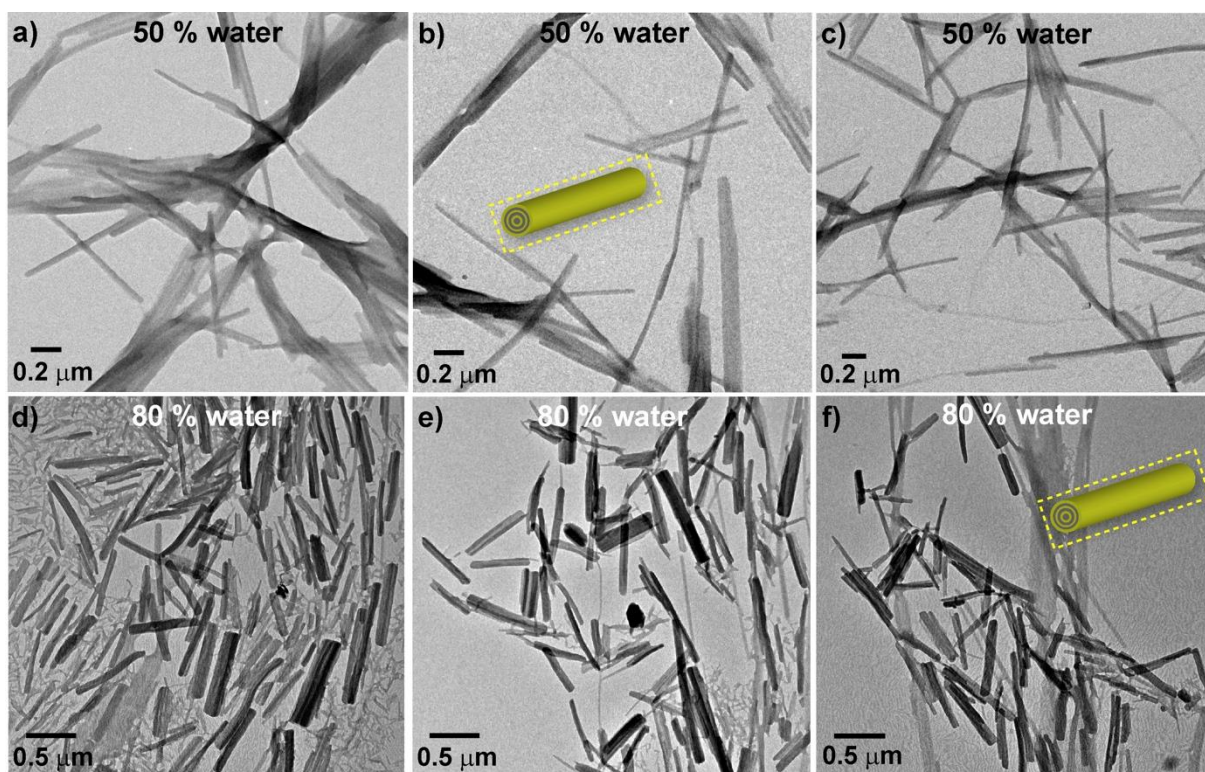


Figure 3.3. TEM images of **1** nanostructures obtained from the THF/water mixed solvent with (a-c) 50 % water and (d-f) 80 % water. Insets of (b) and (f) show the schematic presentation of multilayered nanorods.

Microscopy experiments (FESEM and TEM images) divulge that water has a definite impact on the morphological transformation (from helical fibers to nanorods) of the amphiphile **1**. This is obvious from the increase of the solvent polarity with a gradual increase in the water percentage in the THF solution of **1**, which influenced the intermolecular interactions, and molecular packing of **1** and eventually altered its morphology. Therefore we were curious to find out the existence and/or changes in intermolecular interactions and molecular packing patterns of **1** in its fibrillar and nanorod states.

In order to shed light on the above, Fourier transform infrared spectroscopy (FT-IR) and powder X-ray diffraction (PXRD) measurements were carried out with a dried solid mass of **1** obtained from THF and THF-water mixed solvent (80 % water content), respectively. Figure 3.4a shows the FT-IR spectra of **1**. Two peaks at 1689 and 1702 cm^{-1} were observed for a solid mass of **1** that was isolated from THF (Figure 3.4a; red line). Similarly, two peaks at 1691 and 1702 cm^{-1} are observed for the solid mass of **1** that was isolated from a solution containing 80 % water (Figure 3.4a; blue line).

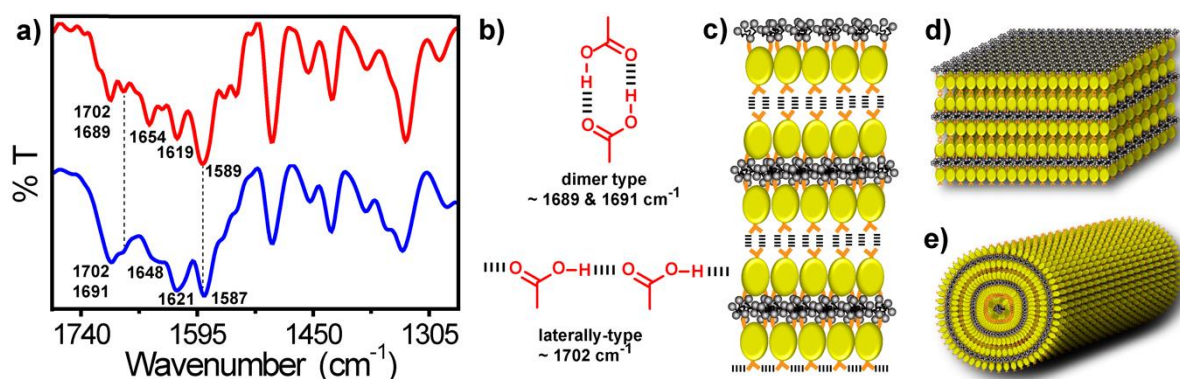


Figure 3.4. (a) FT-IR spectra of the dried mass of **1** obtained from THF (red line), and THF/water mixed solvent with 80 % water content (blue line); (b) Two different types of hydrogen-bonding modes between the COOH groups; (c) A schematic illustration of the existence of COOH in surfaces and in between the multiple layers of **1** bound through dimer and lateral type H-bonds. A schematic illustration of the arrangement of hydrophilic COOH and hydrophobic poly(aryl ether) dendron groups of **1** in (d) THF and (e) THF/water mixed solvent with 80 % water content.

According to literature reports, any assignable peaks for the C=O stretching vibration at wave numbers $\sim 1690\text{--}1750\text{ cm}^{-1}$ indicate two types of hydrogen (H) bonding modes between the COOH groups (Figure 3.4b).¹⁷ For the solid mass of **1** that was isolated from the THF solution, the peak at 1689 cm^{-1} was assigned to an acid-acid dimer type H-bond formation, whereas the peak at 1702 cm^{-1} was attributed to a lateral-

type H-bond (Figure 3.4a; red line and Figure 3.4b) formation. The solid mass of **1** that was obtained from a solution containing 80 % water was used for recording the FT-IR spectrum. This spectrum reveals that **1** molecules are associated together by utilizing both the acid-acid dimer (1691 cm^{-1}) and lateral-type (1702 cm^{-1}) H-bond (Figure 3.4a; blue line and Fig 3.4b) formation. Since two different types of H-bonding modes exist in both the self-assembled states of **1** (THF as well as 80 % water content solution), the COOH groups should exist both on the surfaces and in-between the multiple layers of **1** (Figure 3.4c). On the basis of FT-IR experiment results, we proposed the molecular arrangement of the amphiphile **1** in both the fibrillar and nanorod states (Fig 3.4d and 3.4e), where COOH groups will be situated on the surface as well as in-between its multiple layers.

For an amphiphilic molecule, the arrangement of its hydrophilic head and hydrophobic tail groups is highly sensitive to media polarity. In the midst of the apolar environment, the hydrophobic tails are usually exposed to the solvent medium with its hydrophilic heads away from the solvent molecule.⁴ Conversely, in a polar environment, the opposite molecular arrangement is found. In our present study, initially, both the hydrophobic tail (dendron part) and the hydrophilic head (carboxylic acid) groups of **1** could be exposed towards THF (Figure 3.4d), a solvent with moderate polarity. However, with the addition of water to its THF solution (increasing the solvent polarity), to keep away the hydrophobic dendron part of **1** from the contacts of water, the molecular arrangement shown in Figure 3.4d will scroll and result in the rod-shaped morphology (Figure 3.4e). In this particular molecular arrangement (Figure 3.4e), only the hydrophilic COOH groups of **1** are expected to get exposed to the solvent medium with the hydrophobic dendron groups situated at the core of the multilayered nanorods. This seems to be a highly acceptable molecular arrangement of **1** in the aqueous (80 % water content) environment.

Apart from this COOH acid dimer and lateral type H-bonding interaction peaks, we were able to assign a few other important intermolecular interaction peaks (such as $\text{-C=N}_{\text{imine}}$ (str), $\text{-C=O}_{\text{amide}}$ (str), $\text{-NH}_{\text{amide}}$ (str), etc.) in the FT-IR spectra (Figure 3.4a) of the amphiphile **1**. All the important intermolecular interaction peaks and their positions in the FT-IR spectra are summarized in Table 3.1. The intense peaks corresponding to amide ($\text{-C=O}_{\text{amide}}$ (str) and NH_{amide} (str)) vibrations (Table 3.1 and Figure 3.4a) also indicate the unambiguous signature of a network of H-bonded amides in fiber and nanorod states of **1**.

	ν (cm ⁻¹) in		assignments
	THF	80 % water	
	1702	1702	-C=O _{str} for lateral type H-bond of COOH
	1689	1691	-C=O _{str} for dimer type H-bond of COOH
	1654	1648	-C=N _{imine, str}
	1619	1621	-C=O _{amide, str}
	1589	1587	-NH _{amide, str}

Table 3.1. Frequencies and peak assignments of the FTIR bands of **1**.

Beside the FT-IR data, the modes of molecular arrangement of **1** (in fiber and nanorod states) were further recognized from the PXRD pattern of the dried mass of **1** obtained from THF and THF-water medium (80 % water content). As shown in Figure 3.5a (redline, small angle region), the diffraction peak of the dried mass of **1** (obtained from THF) is at 3.1°, followed by several other peaks in the wide angle region (Figure 3.5b; red line) in a periodical order at 6.2°, 9.3°, 12.3°, 16.6° and 18.4°. The corresponding d-spacings, calculated according to Bragg's equation, were 28.5, 14.2, 9.5, 7.2, 5.3 and 4.8 Å; the ratio of 1/2 : 1/3 : 1/4 : 1/5 and 1/6 is consistent with the lamellar arrangement of **1** molecules. Additionally, in the wide angle region, one more peak at 23.7° with

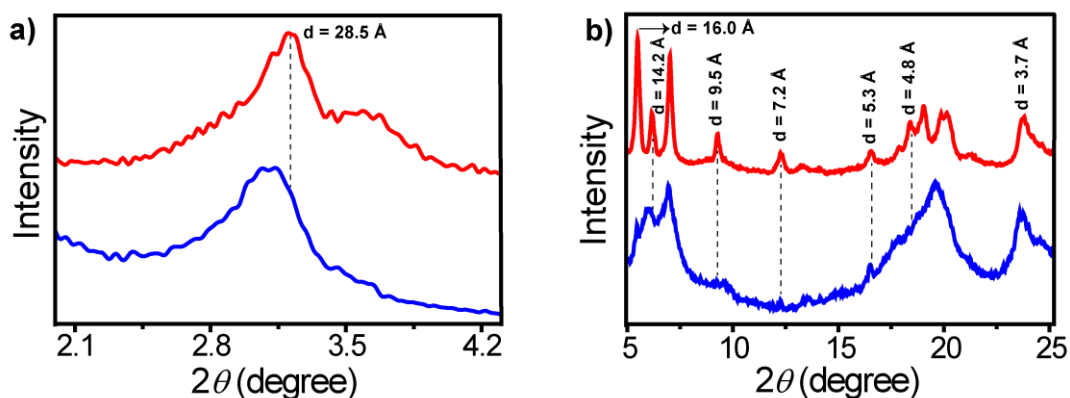
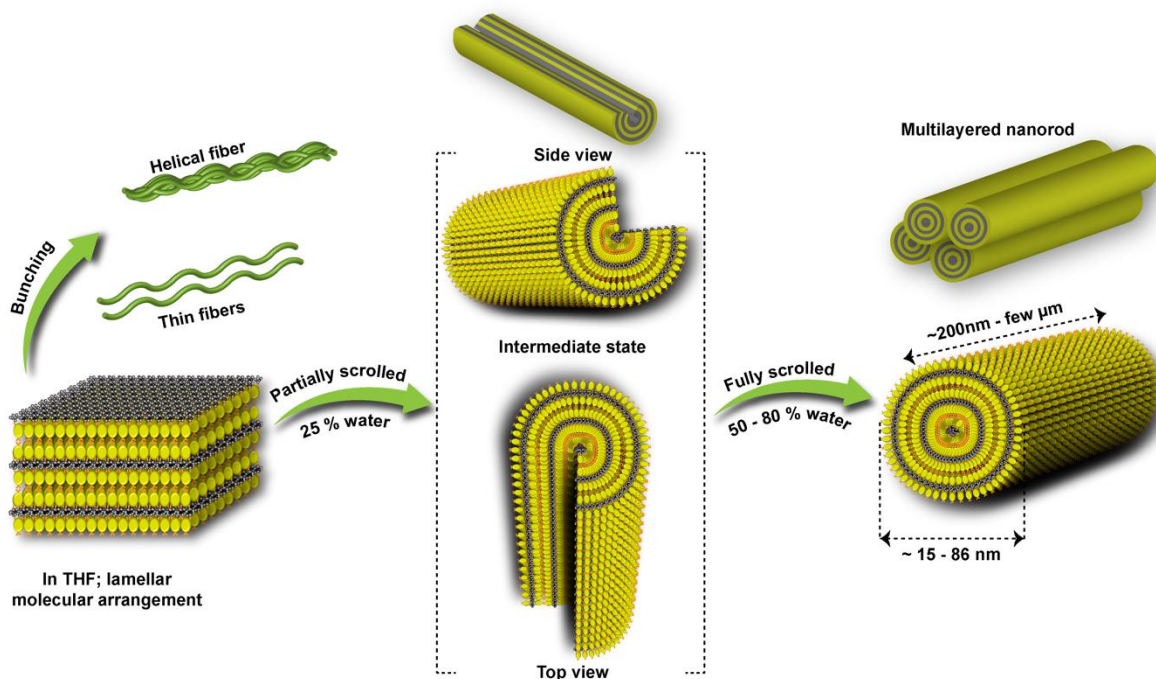


Figure 3.5. (a) and (b) The PXRD pattern in small and wide angle regions, respectively, of the dried mass of **1** obtained from THF (red line), and THF/water mixed solvent with 80 % water content (blue line).

a d-spacing value of 3.7 Å was observed (Figure 3.5b; red line), and this suggests the incidence of π - π stacking interactions among the **1** molecules. Interestingly, a strong diffraction peak corresponding to a d-spacing of 16.0 Å (at $2\theta = 5.5^\circ$) is also seen in this

PXRD curve (Figure 3.5b; red line), which is close to the calculated molecular length (~ 16.6 Å) of the amphiphile **1** (Figure 3.1b). The PXRD pattern of the dried mass of **1** obtained from the 80 % water content solution (Figure 3.5a and 3.5b; blue line) is almost identical (except for the diffraction peaks intensity) to the observed pattern of the THF dried mass of **1**. This observation also indicates that the nanorods are composed of layered arrays of **1** molecules.

Together with the above experimental facts, the water induced morphological transformation (from helical fibers to nanorods) of the amphiphile **1** can be perceived as follows (Scheme 3.2). At the beginning, in THF (a moderately polar solvent), both the hydrophobic (dendron part) and hydrophilic COOH groups of the amphiphile **1** are exposed towards the solvent molecule and attain a lamellar molecular arrangement. Such a lamellar structure is stabilized by H-bonds among COOH (Figure 3.4b, dimer and lateral type) and amide groups as well as π - π stacking interactions and the hydrophobic interactions of poly(aryl ether) dendron moieties, which preliminarily resulted in thin fibers. However, during the course of assembly formation, these thin fibers start bunching and intertwined with each other to form



Scheme 3.2. Schematic illustration of helical fiber to nanorod morphological transformation of **1** through an intermediate scroll-up pathway with a gradual increase of the water content in its THF solution.

helical fibers (Scheme 3.2). Now with the addition of water into the THF solution of **1**, the arrangement of its poly(aryl ether) dendron groups (exposed towards the solvent) becomes energetically unfavorable and unstable. To achieve the energetically more favourable molecular arrangement, as shown in Scheme 3.2, the layered arrays of **1** in fibers tend to scroll-up (from partially to scroll fully) to form nanorods. This scroll-up process will help to protect the solvophobic interactions of dendron units from water and will subsequently minimize the surface energy of **1**. Perhaps due to this minimized surface energy phenomenon, the obtained nanorods of **1** broke into pieces and became smaller in length at higher water content (Figure 3.3a-f).

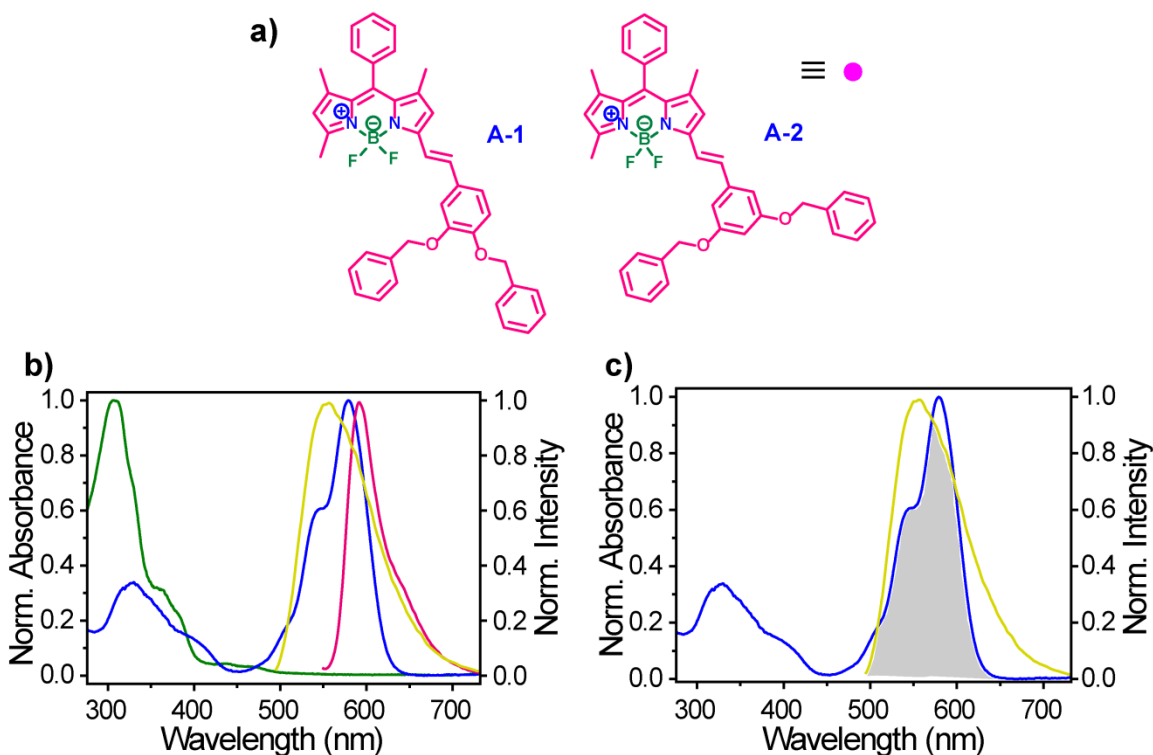


Figure 3.6. (a) Molecular structure of the BODIPY acceptor molecules **A-1** and **A-2**; (b) Absorption spectra of **1** (green line), **A-1** (blue line) and emission spectra of **1** (yellow line), **A-1** (magenta line); (c) Spectral overlap of the emission of **1** (yellow line) and absorption of **A-1** (blue line) in THF/water mixed solvent with 80 % water content (concentration used 20 μ M, for both **1** and **A-1**, λ_{ex} = 306 nm for **1** and 545 nm for **A-1**, l = 1 cm).

Such a mechanistic elucidation of the morphological transformation and nanorod formation of **1** is also expected to trigger another obvious question: what is the use of this structure? As mentioned above, the light-harvesting rod-shaped architecture is valuable to mimic the chlorosomes.¹³ Therefore, we explored the possibility of

exploiting these nanorods of **1** as a light-harvesting antenna system. To succeed in this objective, we have introduced two newly designed BODIPY based acceptor molecules (Figure 3.6a), namely **A-1** and **A-2**. The synthesis and the characterization details for both the acceptor molecules **A-1** and **A-2** (Scheme 3.1) are discussed already in the experimental section.

The THF-water mixed solvent (80 % water content) is selected here to perform the light-harvesting study. Initially, we have recorded the UV-Vis absorption and emission spectra of both **1** and **A-1** (20 μ M). **1** and **A-1** show their main absorption maxima at 306 nm and 578 nm, whereas they emit in the yellow ($\lambda_{\text{em}} = 555$ nm) and red ($\lambda_{\text{em}} = 593$ nm) regions, respectively (Figure 3.6b). It is also evident that the acceptor **A-1** has small absorption (Figure 3.6b) at the λ_{max} of the donor **1**, thus minimizing the possibility of direct excitation of **A-1**. Further, the emission spectrum of **1** and the absorption spectrum (UV-Vis) of the **A-1** molecule overlap over a long region (Figure 3.6c). Due to these optical properties, **1** and **A-1** become a good pair for the energy transfer process.

The energy transfer from **1** to **A-1** is confirmed by recording the emission spectra of **1** nanorods containing different amounts of **A-1** following excitation at 306 nm. As shown in Figure 3.7a, by increasing the concentration (0.0-1.0 mol %) of **A-1**, a decrease in the emission intensity of **1** having a λ_{em} maximum of 555 nm is observed with a simultaneous growth of a new emission band with a λ_{em} maximum of 593 nm. This is ($\lambda_{\text{em}} = 593$ nm) ascribed to the emission of **A-1** (Figure 3.7a). The emission spectra of three different solutions, a 20 μ M solution of **1**, a 20 μ M solution of **1** having its corresponding 1.0 mol % of **A-1** and a solution having only 1.0 mol % of **A-1** (following excitation at 306 nm), are shown in Figure 3.7b. The spectrum recorded for a solution having **1** and 1.0 mol % of **A-1** showed a strong emission band with a maximum at 593 nm (Figure 3.7b; red line), while the spectrum recorded for a solution having only 1.0 mol % of **A-1** showed an insignificant emission (Figure 3.7b; grey line). These observations confirm that nanorods function as a light-harvesting antenna in which the excitation energy is transferred from **1** to **A-1** acceptor molecules. With the addition of higher mol % (1.0-16.0 %) of **A-1**, the emission intensity of **1** is progressively quenched (Figure 3.7a). Interestingly, the emission intensity of **A-1** is also found to decrease gradually with a redshift of its emission maxima. This is understandable if we consider the possibility of self-aggregation of **A-1**, which is confirmed by the results of the concentration-dependent emission studies of **A-1** (Figure 3.8).

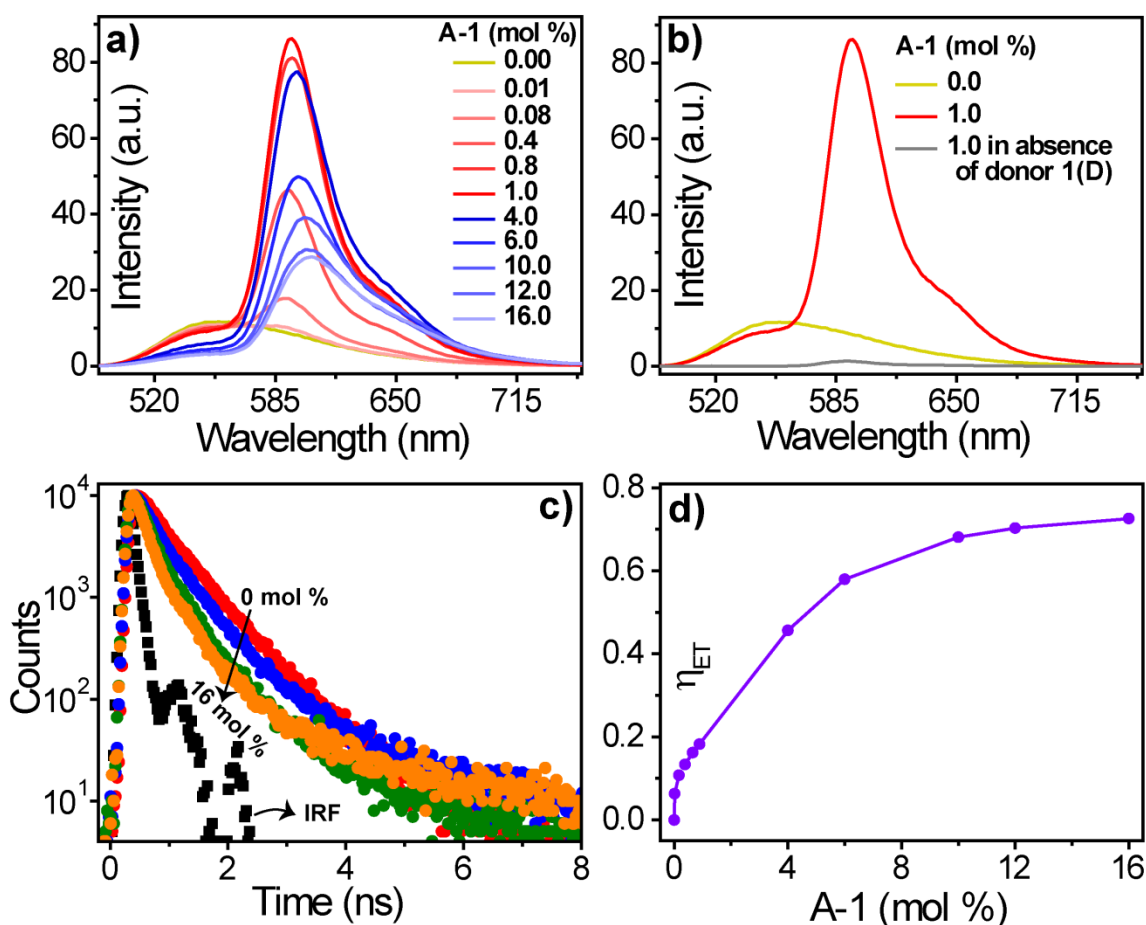


Figure 3.7. (a) Decrease of emission intensity ($\lambda_{ex} = 306$ nm) of **1** on the addition of different amounts, 0.0-16.0 mol % of **A-1**; (b) Comparison of emission spectra of 20 μ M **1**, and its corresponding 1.0 mol % solution of **A-1** in the presence (red line) and absence (grey line) of antenna molecules **1**, ($\lambda_{ex} = 306$ nm); (c) Fluorescence lifetime decay profiles ($\lambda_{ex} = 374$ nm, monitored at 555 nm) of poly(aryl ether) dendron amphiphile **1** on addition of different amounts of BODIPY acceptor **A-1** (0.0 - 16.0 mol %). IRF = instrument response function; (d) Energy transfer efficiency as a function of **A-1** concentration.

Time resolved emission studies further validated the above-described energy transfer process. Fluorescence decay profiles ($\lambda_{ex} = 374$ nm) of the **1** nanorods (monitored at 555 nm) themselves and nanorods doped with different amounts of acceptor **A-1** are shown in Figure 3.7c. With an increasing concentration of the acceptor **A-1** from 0.0-16.0 mol %, a progressively faster fluorescence decay of the **1** nanorods is observed along with the calculated decreased average lifetime (τ_{av}) from 0.49 ns to 0.17 ns (Table 3.2). These also suggest an effective energy transfer from **1** to **A-1**.

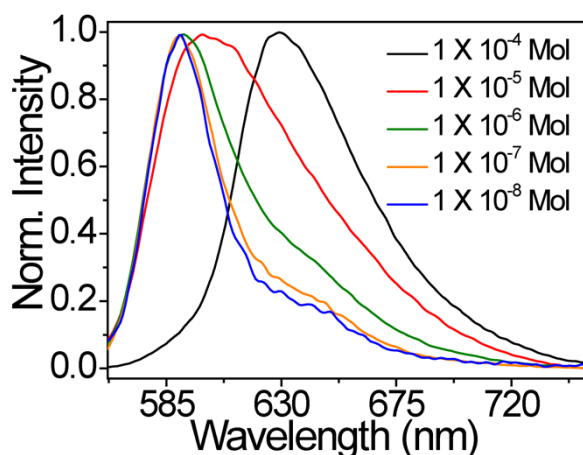


Figure 3.8. Concentration dependent emission spectra of BODIPY based acceptor molecule **A-1** in THF/water mixed solvent content 80 % water ($\lambda_{\text{ex}} = 545$ nm). With increasing the concentration of **A-1** the emission maxima shifted to longer wavelength, indicates **A-1** is self-aggregated in higher concentration range.

System	Monitoring wavelength (nm)	τ_1	τ_2	τ_3	τ_{av}
1 only	555	0.39 ns (77 %)	0.85 ns (23 %)	--	0.49 ns
1 + 1 % A-1	555	0.16 ns (53 %)	0.50 ns (45 %)	2.05 ns (2%)	0.35 ns
1 + 5 % A-1	555	0.08 ns (61 %)	0.32 ns (36 %)	1.10 ns (3%)	0.19 ns
1 + 16 % A-1	555	0.09 ns (71 %)	0.36 ns (27 %)	1.50 ns (2 %)	0.17 ns

Table 3.2. Variation of the emission lifetime of **1** with an increase of 0.0-16.0 mol % of **A-1**.

It is also interesting to investigate the energy transfer (ET) efficiency of the **1/A-1** system, as this parameter is very important to evaluate the light-harvesting ability of a model system. The ET efficiency ($\eta_{\text{ET}} = 1 - I_{\text{DA}}/I_{\text{D}}$)¹⁸ is estimated from the relative changes in emission intensities of the **1** nanorods with the increase of concentration of **A-1** from 0.0-16.0 mol % (Figure 3.7d). In the presence of 16 mol % of **A-1**, the ET efficiency reached approximately 72 % (Figure 3.7d). Furthermore, a 20 μM solution of **1**

containing 1.0 mol % of **A-1** in the THF-water mixed solvent (80 % water content) is imaged by TEM. Interestingly, it reveals only nanorods of a shape similar to those formed of **1** alone (Figure 3.9). This indicates that a small number of acceptor molecules of **A-1** have no influence on the morphology of the nanotubes of **1**.

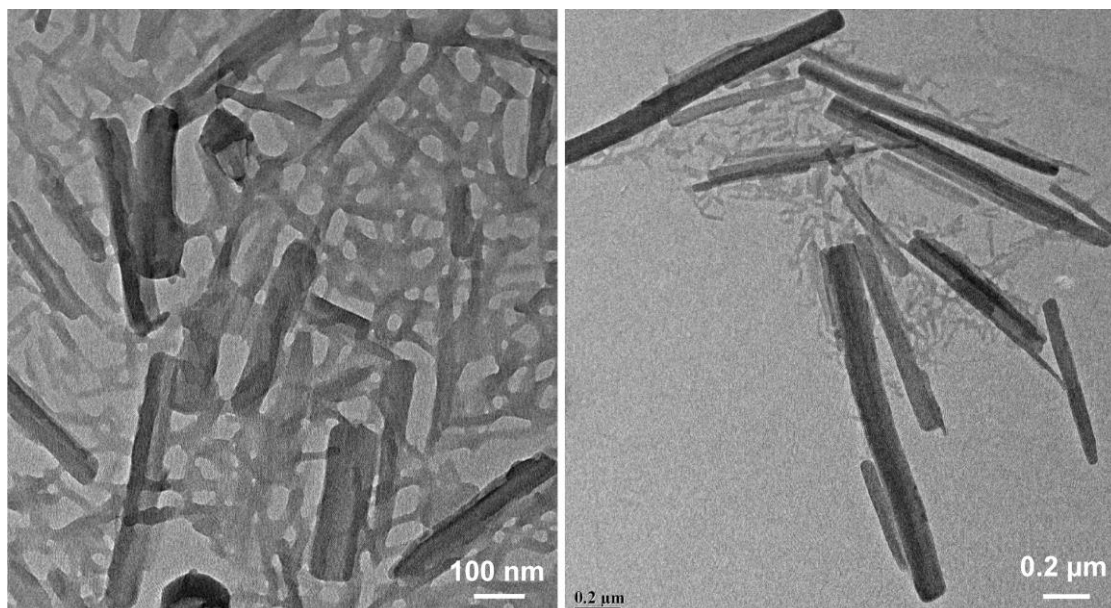


Figure 3.9. TEM images show the nanorod-shaped morphology of 20 μm solution of **1** in presence of 1.0 mol % **A-1**. Solvent used; THF/water mixed solvent (content 80 % water).

A similar kind of energy transfer process is observed for the case of the acceptor **A-2** ($\lambda_{\text{max}}(\text{abs}) = 563 \text{ nm}$ and $\lambda_{\text{max}}(\text{ems}) = 575 \text{ nm}$). All the spectroscopy studies for **A-2** are illustrated in the Figure 3.10. However, in the case of incorporation of 10.0 mol % of **A-2** to the **1** nanorods, an energy transfer efficacy of 52 % (Figure 3.10d) is achieved. Overall, the light-harvesting antenna effect of the **1** nanorods towards both the BODIPY based acceptor molecules **A-1** and **A-2** is schematically illustrated in Scheme 3.3.

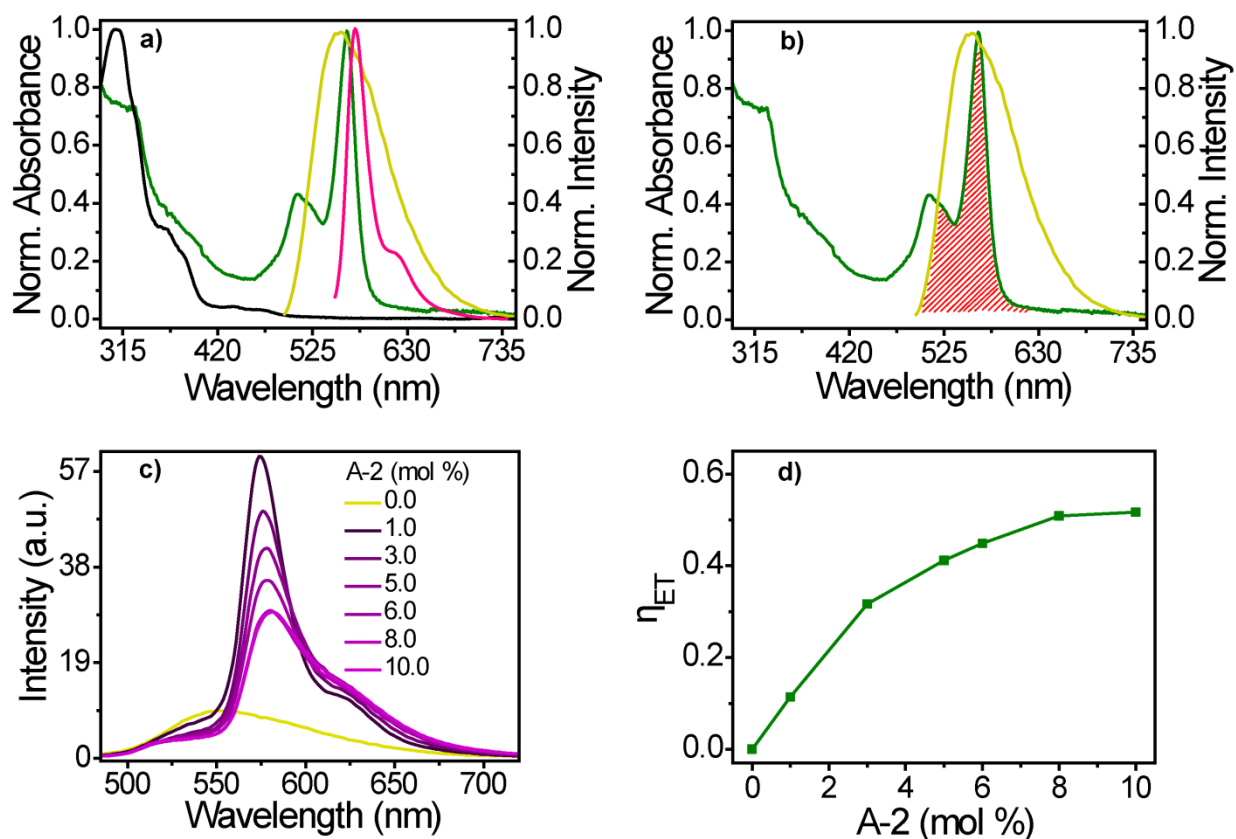
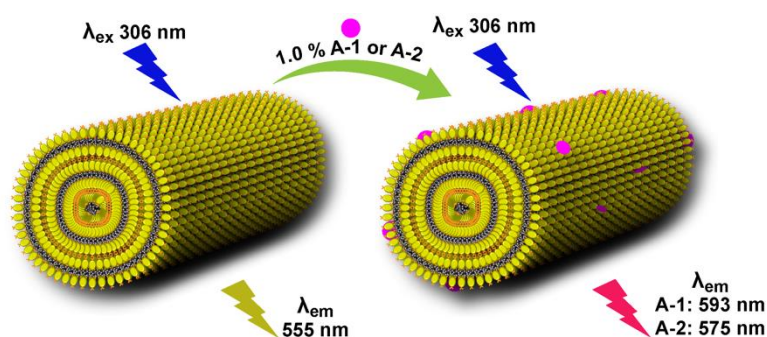


Figure 3.10. (a) Absorption spectra of **1** (black line), **A-2** (green line) and emission spectra of **1** (yellow line), **A-2** (magenta line); (b) Spectral overlap of the emission of **1** (yellow line) and absorption of **A-2** (green line) in THF/water mixed solvent content 80 % water (concentration used 20 μ M, for both **1** and **A-2**; λ_{ex} = 306 nm for **1** and 506 nm for **A-2**, l = 1 cm); (c) Emission intensity (λ_{ex} = 306 nm) of **1** on addition of different mol % of **A-2** (0.0-10.0 mol %); (d) Energy transfer efficiency as a function of **A-2** concentration.



Scheme 3.3. Schematic presentations of light-harvesting nanorods of **1**.

3.4. Conclusions

In summary, the poly(aryl ether) dendron based amphiphile **1** showed solvent polarity induced diverse self-aggregation behavior. It forms helical fibers in THF, and such helical fibers progressively transform into a rod-shaped morphology with the increasing water fraction in its THF solution. The driving force behind the morphological transformation probably originates from the hydrophobic surface energy of the bulky organic poly(aryl ether) dendron groups of **1** in the presence of water, which forces the structures to scroll to reduce their exposure to water. More importantly, the key transition states (scrolled fibers) in the formation of the nanorods were caught microscopically, which endorses our illustrated mechanistic pathway towards the structural transformation of **1** (Scheme 3.2). Moreover, these nanorods function as a light-harvesting antenna in which the excitation energy is transferred from higher ordered arrays of **1** chromophores to newly designed BODIPY based acceptor molecules (**A-1** and **A-2**, respectively). This present study not only establishes the route of forming hierarchical self-assembly through direct visualization of the intermediate topologies but also adds value to the understanding of the aggregation pattern of amphiphiles in a solvent with different polarities, which could be crucial for designing the concept of artificial structures that mimic natural systems.

3.5. References

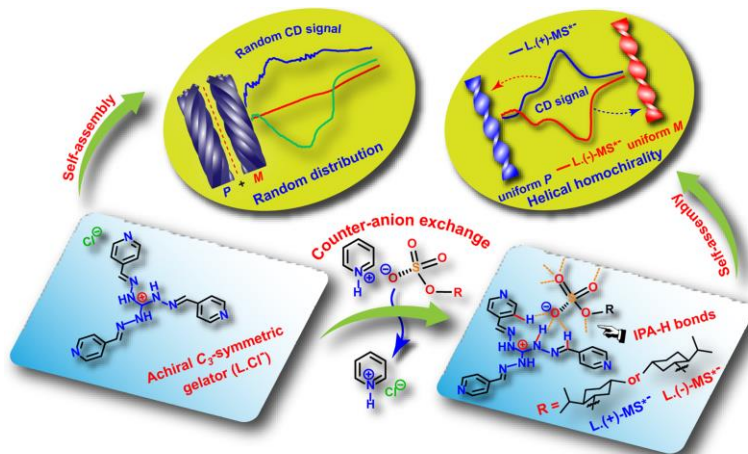
1. (a) L. C. Palmer and S. I. Stupp, *Acc. Chem. Res.*, 2008, **41**, 1674; (b) A. Ajayaghosh and V. K. Praveen, *Acc. Chem. Res.*, 2007, **40**, 644; (c) T. Aida, E. W. Meijer and S. I. Stupp, *Science*, 2012, **335**, 813; (d) G. M. Whitesides and B. Grzybowski, *Science*, 2002, **295**, 2418; (e) Y. B. Lim, K. S. Moon and M. Lee, *Chem. Soc. Rev.*, 2009, **38**, 925; (f) E. Busseron, Y. Ruff, E. Moulin and N. Giuseppone, *Nanoscale*, 2013, **5**, 7098; (g) L. Zhang, X. Wang, T. Wang and M. Liu, *Small*, 2015, **11**, 1025; (h) A. H. Gröschel and A. H. E. Müller, *Nanoscale*, 2015, **7**, 11841.
2. (a) A. T. Haedler, K. Kreger, A. Issac, B. Wittmann, M. Kivala, N. Hammer, J. Köhler, H. W. Schmidt and R. Hildner, *Nature*, 2015, **523**, 196; (b) R. Misra, R. M. Reja, L. V. Narendra, G. George, S. Raghothama and H. N. Gopi, *Chem. Commun.*, 2016, **52**, 9597; (c) J. Kumar, T. Nakashima, H. Tsumatori and T. Kawai, *J. Phys. Chem. Lett.*, 2014, **5**, 316; (d) D. Miyajima, F. Araoka, H. Takezoe, J. Kim, K. Kato, M. Takata and T. Aida, *Science*, 2012, **336**, 209; (e) K. Ishikawa, N. Kameta, M. Aoyagi, M. Asakawa and T. Shimizu, *Adv. Funct. Mater.*, 2013, **23**, 1677; (f) S. Ghosh, D. S. Philips, A. Saeki and A. Ajayaghosh, *Adv. Mater.*, 2017, **29**, 1605408.
3. (a) K. Jalani, S. Dhiman, A. Jain and S. J. George, *Chem. Sci.*, 2017, **8**, 6030; (b) J. H. Mondal, S. Ahmed, T. Ghosh and D. Das, *Soft Matter*, 2015, **11**, 4912; (c) A. Brizard, C. Aimé, T. Labrot, I. Huc, D. Berthier, F. Artzner, B. Desbat and R. Oda, *J. Am. Chem. Soc.*, 2007, **129**, 3754; (d) S. Kushwaha, A. Maity, M. Gangopadhyay, S. Ravindranathan, P. R. Rajamohanam and A. Das, *Langmuir*, 2017, **33**, 10989; (e) A. Maity, M. Gangopadhyay, A. Basu, S. Aute, S. S. Babu and A. Das, *J. Am. Chem. Soc.*, 2016, **138**, 11113; (f) D. Ke, C. Zhan, A. D. Q. Li and J. Yao, *Angew. Chem., Int. Ed.*, 2011, **50**, 3715; (g) H. Frisch, E. C. Fritz, F. Stricker, L. Schmüser, D. Spitzer, T. Weidner, B. J. Ravoo and P. Besenius, *Angew. Chem., Int. Ed.*, 2016, **55**, 7242; (h) M. Pellach, Y. Atsmon-Raz, E. Simonovsky, H. Gottlieb, G. Jacoby, R. Beck, L. Adler-Abramovich, Y. Miller and E. Gazit, *ACS Nano*, 2015, **9**, 4085; (i) G. Liu, J. Liu, C. Feng and Y. Zhao, *Chem. Sci.*, 2017, **8**, 1769; (j) P. Xing, P. Li, H. Chen, A. Hao and Y. Zhao, *ACS Nano*, 2017, **11**, 4206; (k) S. Yu, Y. Yang, T. Chen, J. Xu and L. Y. Jin, *Nanoscale*, 2017, **9**, 17975; (l) B. B. Breitenbach, I. Schmid and P. R. Wich, *Biomacromolecules*, 2017, **18**, 2839.
4. (a) Y. Huang, J. Hu, W. Kuang, Z. Wei and C. F. J. Faul, *Chem. Commun.*, 2011, **47**, 5554; (b) S. Ahmed, B. Pramanik, K. N. A. Sankar, A. Srivastava, N. Singha, P. Dowari, A. Srivastava, K. Mohanta, A. Debnath and D. Das, *Sci. Rep.*, 2017, **7**, 9485; (c) K. Lv, L. Zhang and M. Liu, *Langmuir*, 2014, **30**, 9295; (d) C. Liu, Q. Jin, K. Lv, L. Zhang and M. Liu, *Chem. Commun.*, 2014, **50**, 3702; (e) D. Mandal, S. Dinda, P. Choudhury and P. K. Das, *Langmuir*, 2016, **32**, 9780; (f) P. Mahato, S.

- Saha, S. Choudhury and A. Das, *Chem. Commun.*, 2011, **47**, 11074; (g) Q. Jin, L. Zhang and M. Liu, *Chem. – Eur. J.*, 2013, **19**, 9234.
5. (a) M. Hasegawa and M. Iyoda, *Chem. Soc. Rev.*, 2010, **39**, 2420; (b) S. I. Stupp, V. L. Bonheur, K. Walker, L. S. Li, K. E. Huggins, M. Keser and A. Amstutz, *Science*, 1997, **276**, 384; (c) L. Zang, Y. Che and J. S. Moore, *Acc. Chem. Res.*, 2008, **41**, 1596; (d) X. Wang, G. Guerin, H. Wang, Y. Wang, I. Manners and M. A. Winnik, *Science*, 2007, **644**, 644; (e) T. Komatsu, *Nanoscale*, 2012, **4**, 1910; (f) Y. Zhou and T. Shimizu, *Chem. Mater.*, 2008, **20**, 625; (g) X. Gao and H. Matsui, *Adv. Mater.*, 2005, **17**, 2037.
6. (a) T. Shimizu, M. Masuda and H. Minamikawa, *Chem. Rev.*, 2005, **105**, 1401; (b) T. Shimizu, *Bull. Chem. Soc. Jpn.*, 2008, **81**, 1554; (c) T. Shimizu, N. Kameta, W. Ding and M. Masuda, *Langmuir*, 2016, **32**, 12242; (d) N. Kameta, H. Minamikawa and M. Masuda, *Soft Matter*, 2011, **7**, 4539; (e) T. G. Barclay, K. Constantopoulos and J. Matison, *Chem. Rev.*, 2014, **114**, 10217; (f) H. Yu and R. Häner, *Chem. Commun.*, 2016, **52**, 14396; (g) S. Wang, Y. J. Zhang, Y. J. Xia and B. Song, *Nanoscale*, 2015, **7**, 17848; (h) Y. Zhang, S. Wang, Y. Liu, Y. Jin, Y. Xia and B. Song, *Nanoscale*, 2017, **9**, 1491.
7. (a) S. Yagai, M. Yamauchi, A. Kobayashi, T. Karatsu, A. Kitamura, T. Ohba and Y. Kikkawa, *J. Am. Chem. Soc.*, 2012, **134**, 18205; (b) S. Tu, S. H. Kim, J. Joseph, D. A. Modarelli and J. R. Parquette, *J. Am. Chem. Soc.*, 2011, **133**, 19125; (c) H. Shao, J. Seifert, N. C. Romano, M. Gao, J. J. Helmus, C. P. Jaroniec, D. A. Modarelli and J. R. Parquette, *Angew. Chem., Int. Ed.*, 2010, **49**, 7688; (d) D. Zhang, Y. Liu, Y. Fan, C. Yu, Y. Zheng, H. Jin, L. Fu, Y. Zhou and D. Yan, *Adv. Funct. Mater.*, 2016, **26**, 7652.
8. (a) A. Lohr and F. Würthner, *Isr. J. Chem.*, 2011, **51**, 1052; (b) J. L. Suk, J. T. Hupp and S. T. Nguyen, *J. Am. Chem. Soc.*, 2008, **130**, 9632; (c) R. Appel, J. Fuchs, S. M. Tyrrell, P. A. Korevaar, M. C. A. Stuart, I. K. Voets, M. Schönhoff and P. Besenius, *Chem. – Eur. J.*, 2015, **21**, 19257.
9. (a) N. S. Lewis and D. G. Nocera, *Proc. Natl. Acad. Sci. U. S. A.*, 2006, **103**, 15729; (b) G. D. Scholes, G. R. Fleming, A. O. Castro and R. V. Grondelle, *Nat. Chem.*, 2011, **3**, 763; (c) M. S. Dresselhaus and I. L. Thomas, *Nature*, 2001, **414**, 332.
10. (a) G. R. Fleming, G. S. Schlau-Cohen, K. Amarnath and J. Zaks, *Faraday Discuss.*, 2012, **155**, 27; (b) S. Fukuzumi and K. Ohkubo, *J. Mater. Chem.*, 2012, **22**, 4575; (c) A. Ajayaghosh, V. K. Praveen and C. Vijayakumar, *Chem. Soc. Rev.*, 2008, **37**, 109; (d) B. Jana, S. Bhattacharyya and A. Patra, *Nanoscale*, 2016, **8**, 16034; (e) Goudappagouda, V. C. Wakchaure, K. C. Ranjeesh, C. A. R. Abhai and S. S.

- Babu, *Chem. Commun.*, 2017, **53**, 7072; (f) K. V. Rao, A. Jain and S. J. George, *J. Mater. Chem. C*, 2014, **2**, 3055.
11. (a) J. J. Li, Y. Chen, J. Yu, N. Cheng and Y. Liu, *Adv. Mater.*, 2017, **29**, 1701905; (b) C. D. Bösch, S. M. Langenegger and R. Häner, *Angew. Chem., Int. Ed.*, 2016, **55**, 9961; (c) N. Kameta, K. Ishikawa, M. Masuda, M. Asakawa and T. Shimizu, *Chem. Mater.*, 2012, **24**, 209; (d) K. Ocakoglu, K. S. Joya, E. Harputlu, A. Tarnowska and D. T. Gryko, *Nanoscale*, 2014, **6**, 9625; (e) M. Suresh, A. K. Mandal, E. Suresh and A. Das, *Chem. Sci.*, 2013, **4**, 2380; (f) M. Gangopadhyay, A. Maity, A. Dey and A. Das, *J. Org. Chem.*, 2016, **81**, 8977; (g) M. Gangopadhyay, A. K. Mandal, A. Maity, S. Ravindranathan, P. R. Rajamohan and A. Das, *J. Org. Chem.*, 2016, **81**, 512.
12. (a) C. Röger, M. G. Müller, M. Lysetska, Y. Miloslavina, A. R. Holzwarth and F. Würthner, *J. Am. Chem. Soc.*, 2006, **128**, 6542; (b) C. Röger, Y. Miloslavina, D. Brunner, A. R. Holzwarth and F. Würthner, *J. Am. Chem. Soc.*, 2008, **130**, 5929; (c) S. Furumaki, F. Vacha, S. Hirata and M. Vacha, *ACS Nano*, 2014, **8**, 2176.
13. (a) S. Sengupta and F. Würthner, *Acc. Chem. Res.*, 2014, **46**, 2498; (b) S. Shoji, T. Ogawa, T. Hashishin, S. Ogasawara, H. Watanabe, H. Usami and H. Tamiaki, *Nano Lett.*, 2016, **16**, 3650; (c) A. D. Schwab, D. E. Smith, B. Bond-Watts, D. E. Johnston, J. Hone, A. T. Johnson, J. C. De Paula and W. F. Smith, *Nano Lett.*, 2004, **4**, 1261.
14. (a) P. Rajamalli and E. Prasad, *Soft Matter*, 2012, **8**, 8896; (b) P. Rajamalli, S. Atta, S. Maity and E. Prasad, *Chem. Commun.*, 2013, **49**, 1744; (c) P. Rajamalli and E. Prasad, *Langmuir*, 2013, **29**, 1609; (d) P. Malakar and E. Prasad, *Chem. – Eur. J.*, 2015, **21**, 5093; (e) W. D. Jang, D. L. Jiang and T. Aida, *J. Am. Chem. Soc.*, 2000, **122**, 3232; (f) A. Maity, F. Ali, H. Agarwalla, B. Anothumakkool and A. Das, *Chem. Commun.*, 2015, **51**, 2130; (g) V. Percec, A. E. Dulcey, M. Peterca, M. Ilies, J. Ladislav, B. M. Rosen, U. Edlund and P. A. Heiney, *Angew. Chem., Int. Ed.*, 2005, **117**, 6674; (h) V. Percec, A. E. Dulcey, M. Peterca, M. Ilies, S. Nummelin, M. J. Sienkowska and P. A. Heiney, *Proc. Natl. Acad. Sci. U. S. A.*, 2006, **103**, 2518.
15. (a) L. Xu, L. J. Chen and H. B. Yang, *Chem. Commun.*, 2014, **50**, 5156; (b) P. Rajamalli, P. Malakar, S. Atta and E. Prasad, *Chem. Commun.*, 2014, **50**, 11023; (c) L. J. Chen, G. Z. Zhao, B. Jiang, B. Sun, M. Wang, L. Xu, J. He, Z. Abliz, H. Tan, X. Li and H. B. Yang, *J. Am. Chem. Soc.*, 2014, **136**, 5993; (d) P. Rajamalli and E. Prasad, *Org. Lett.*, 2011, **13**, 3714; (e) P. Rajamalli, P. S. Sheet and E. Prasad, *Chem. Commun.*, 2013, **49**, 6758; (f) N. V. Lakshmi, D. Mandal, S. Ghosh and E. Prasad, *Chem. – Eur. J.*, 2014, **20**, 9002; (g) A. R. Hirst and D. K. Smith, *Top. Curr. Chem.*, 2005, **256**, 237; (h) Z. X. Liu, Y. Feng, Z. C. Yan, Y. M. He, C. Y. Liu and Q. H. Fan,

- Chem. Mater.*, 2012, **24**, 3751; (i) J. Liu, Y. Feng, Z. X. Liu, Z. C. Yan, Y. M. He, C. Y. Liu and Q. H. Fan, *Chem. – Asian J.*, 2013, **8**, 572.
16. (a) S. Aute, P. Maity, A. Das and H. N. Ghosh, *New J. Chem.*, 2017, **41**, 5215; (b) F. Ali, A. H. A., N. Taye, R. G. Gonnade, S. Chattopadhyay and A. Das, *Chem. Commun.*, 2015, **51**, 16932; (c) S. Saha, H. Agarwalla, H. Gupta, M. Baidya, E. Suresh, S. K. Ghosh and A. Das, *Dalton Trans.*, 2013, **42**, 15097.
17. (a) M. Kogiso, M. Aoyagi, M. Asakawa and T. Shimizu, *Soft Matter*, 2010, **6**, 4528; (b) M. Kogiso, T. Hanada, K. Yase and T. Shimizu, *Chem. Commun.*, 1998, 1791; (c) J. Dong, Y. Ozaki and K. Nakashima, *Macromolecules*, 1997, **30**, 1111; (d) L. Sun, L. J. Kepley and R. M. Crooks, *Langmuir*, 1992, **8**, 2102.
18. (a) P. K. Dutta, R. Varghese, J. Nangreave, S. Lin, H. Yan and Y. Liu, *J. Am. Chem. Soc.*, 2011, **133**, 11985; (b) H. Q. Peng, Y. Z. Chen, Y. Zhao, Q. Z. Yang, L. Z. Wu, C. H. Tung, L. P. Zhang and Q. X. Tong, *Angew. Chem., Int. Ed.*, 2012, **51**, 2088; (c) Y. Liu, S. Li, K. Li, Y. Zheng, M. Zhang, C. Cai, C. Yu, Y. Zhou and D. Yan, *Chem. Commun.*, 2016, **52**, 9394; (d) A. Ajayaghosh, C. Vijayakumar, V. K. Praveen, S. S. Babu and R. Varghese, *J. Am. Chem. Soc.*, 2006, **128**, 7174; (e) M. Gangopadhyay, A. Maity, A. Dey, P. R. Rajamohanan, S. Ravindranathan and A. Das, *Chem. – Eur. J.*, 2017, **23**, 18303.

CHAPTER 4

Counteranion Driven Homochiral Assembly of a Cationic C_3 -Symmetric Gelator through Ion-Pair Assisted Hydrogen Bond

The helical handedness in achiral selfassemblies is mostly complex due to spontaneous symmetry breaking or kinetically controlled random assembly formation. Here an attempt has been made to address this issue through chiral anion exchange. A new class of cationic achiral C_3 -symmetric gelator devoid of any conventional gelation assisting functional units is found to form both right- and left-handed helical structures. A chiral counteranion exchange-assisted approach is successfully introduced to control the chirality sign and thereby to obtain preferred homochiral assemblies. Formation of anion-assisted chiral assembly was confirmed by circular dichroism (CD) spectroscopy, microscopic images, and crystal structure. The X-ray crystal structure reveals the construction of helical assemblies with opposite handedness for (+)- and (-)-chiral anion reformed gelators. The appropriate counteranion driven ion-pair assisted hydrogen-bonding interactions are found responsible for the helical bias control in this C_3 -symmetric gelator.

Publication:
J. Am. Chem. Soc. 2016, 138, 11113.

4.1. Introduction

Self-organization of an achiral or a dynamically racemic molecular system into well-defined helical nanostructures with controllable handedness is one of the exciting topics in supramolecular chirality.¹ This area of research is particularly attractive to understand and appreciate the asymmetric induction and homochirality in nature.² It was observed that various noncovalent interactions are the major driving force to regulate the helical structures of achiral entities.^{3,4} Among various noncovalent interactions, the H-bond plays a significant role in helical self-assembly formation due to its directionality and specificity.^{3a-g} But the main drawback of H-bonded systems is that it works mostly in nonpolar organic solvents and is not stable in aqueous media due to the random and competitive H-bonding nature of water molecules. To circumvent this drawback, introduction of ionic interaction into self-assembly has been considered as an alternate strategy to strengthen the H-bonds by virtue of its strong electrostatic interaction.⁵ Moreover, ionic assemblies will generate higher order structures due to the electrostatic interaction along with different noncovalent interactions.⁶ Ionic species are known to be stable in its hydrated state, which gives a unique opportunity to study ionic assemblies in physiological conditions. Finally, for ionic components, counterions play a critical role toward its self-assembly.⁷ For instance, an appropriate choice of ion-pair could eventually lead to an ion-pair assisted H-bond (IPA-H), which possesses both ionic interaction and H-bonds, hence satisfying the strength as well as directionality.⁵

Recently, there have been many attempts to elucidate the helical assembly formation in achiral and C_3 -symmetric molecules. For example, Meijer^{8a} and Liu^{8b,c} *et al.* have shown chiral symmetry breaking phenomena of benzene-1,3,5-tricarboxamide/tricarboxylate-based achiral molecules, where self-assembly was exclusively driven by directional H-bonds between amide groups, π - π stacking of the central benzene rings, and van der Waals interaction due to peripheral hydrophobic units. In addition, various strategies such as chiral additive,^{7,8} light,^{9a,b} clockwise/counterclockwise vortex,^{9c} or spin coating direction,^{9d} rotational and magnetic force,^{9e} pH,^{9f} *etc.* are known to induce chirality in supramolecular assemblies. But for any cationic component to control the helical handedness, one of the easiest approaches is to exchange its counteranion from an achiral one to chiral one. Herein we report for the first time the formation of the chiral assembly from an ionic achiral C_3 -symmetric molecule, tris(4-pyridinecarboxaldehyde) triaminoguanidinium chloride, **L**.**Cl**⁻ (Figure 4.1). Self-assembly of **L**.**Cl**⁻ on surface leads to the formation of right (*P*)- and left (*M*)-handed helical structures. The exchange of **Cl**⁻ counteranion of **L** with

chiral pyridinium salts of (+)- or (-)-menthylsulfate (MS^{*-}) exhibited homochiral signature. The IPA-H bond between MS^{*-} and positively charged nitrogen-rich guanidinium units of **L**, which elicits the molecule to arrange in a preferred way to give the helical homochiral twist, is evident in the crystal structure. Thus, a simple strategy has been effectively utilized to bias chirality of an ionic gelator.

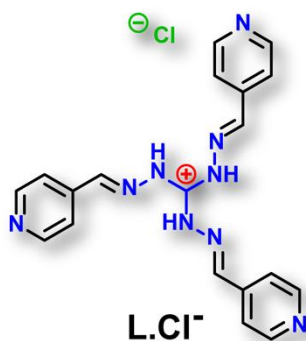


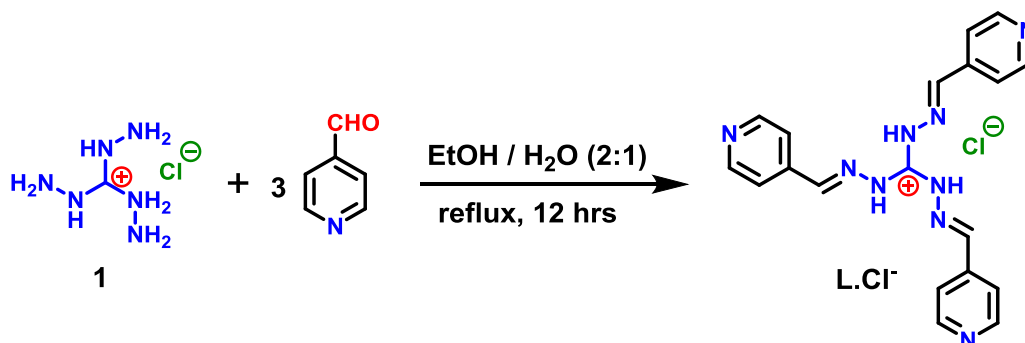
Figure 4.1. Chemical structure of the achiral C_3 -symmetric gelator used in the present study.

4.2. Experiment Section

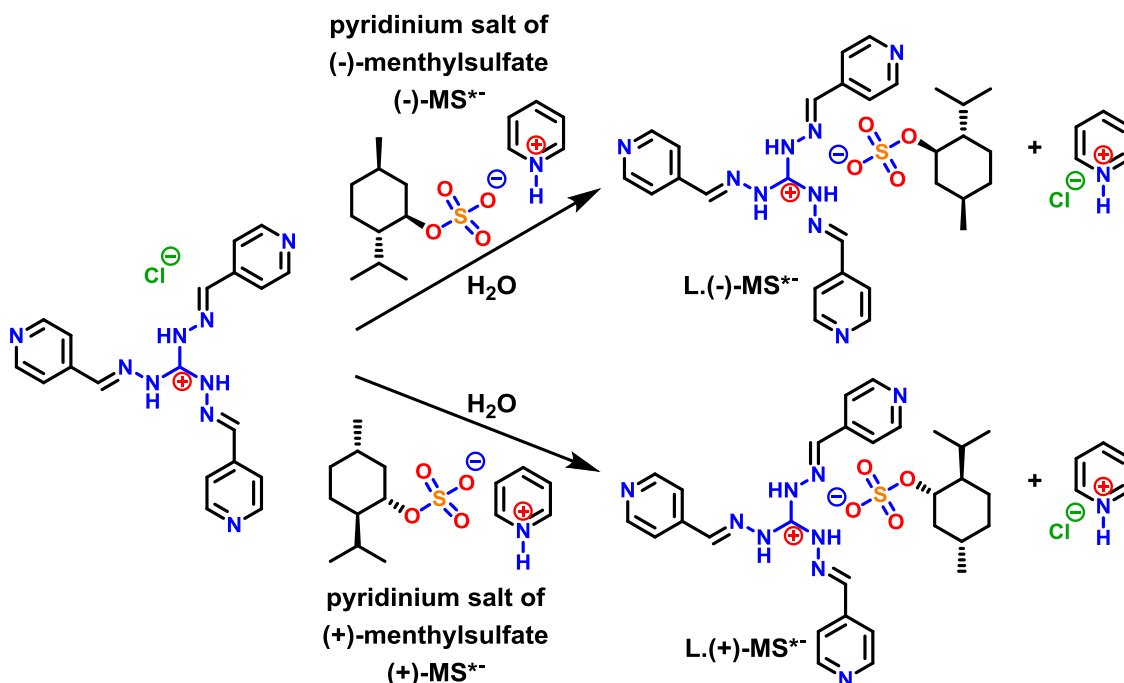
4.2.1. Materials and Methods

Unless otherwise stated, all reagents and organic solvents used for synthesis purpose were procured from commercial suppliers and used as received without any further purification. Fresh double distilled water was used throughout the experiment. HPLC grade solvents were used for recording spectrometric data. ^1H and ^{13}C NMR spectra were recorded on Bruker ^1H 400/500 MHz FT NMR (Model: Avance-DPX 400/500). Chemical shifts are reported in ppm using tetramethylsilane (TMS) as the internal standard. High-resolution mass spectra (HRMS) were recorded on JEOL JM AX 505 HA mass spectrometer. Fourier transform infrared (FT-IR) spectra were recorded on a Bruker Optics ALPHA-E spectrometer with a universal Zn-Se ATR (attenuated total reflection) accessory in the 600-4000 cm^{-1} . UV-Vis absorption spectra were measured with a Perkin Elmer Lambda 950 UV-Vis spectrophotometer equipped with a peltier system. Circular dichroism (CD) spectra were recorded on a JASCO model type J-815 spectropolarimeter.

4.2.2. Synthesis and Characterization

4.2.2.1. Synthesis of Tris(4-pyridinecarboxaldehyde)triaminoguanidinium chloride ($L.Cl^-$)Scheme 4.1. Methodology that was adapted to synthesized the $L.Cl^-$.

The central guanidinium hydrazide chloride (compound **1**; Scheme 4.1), which was used for the synthesis of the $L.Cl^-$ was 1st prepared according to previously reported procedure.¹⁰ 500 mg (4.76 mM) of this guanidinium hydrazide chloride (compound **1**)¹⁰ was taken in a 100 mL RB flask and dissolved by adding 15 mL of water. Then 4-pyridinecarboxaldehyde (1.35 mL, 14.34 mM) was mixed with ethanol (30 mL) and added dropwise to the aqueous solution of compound **1**. The resulting reaction mixture was refluxed for 12 hrs and then cooled to ambient temperature. A yellow color gelatinous precipitated was obtained within 3-4 hrs. The precipitate was filtered off, washed initially with ice-cold water (two times) and then with 10 mL of ethanol/diethyl ether (2:8) solution. Finally, the desired product ($L.Cl^-$) was collected and dried under reduced pressure. Yield: 80 %, ¹H NMR (500 MHz, DMSO-*d*₆, TMS): δ (ppm) = 8.71-8.70 (6H, d, *J* = 6 Hz), 8.58 (3H, s), 8.00-7.99 (6H, d, *J* = 6 Hz); ¹³C NMR (125 MHz, DMSO-*d*₆, TMS): δ (ppm) = 159.43, 151.03, 150.29, 150.06, 149.92, 148.39, 147.51, 147.05, 142.74, 122.15; HRMS (ESI): *m/z* calculated for C₁₉H₁₈N₉ [M-Cl]⁺ = 372.167, found 372.168.

4.2.2.2. Synthetic Scheme of Counteranion Exchanged Ligands L.(+)-MS^{*-} and L.(-)-MS^{*-}

Scheme 4.2. Methodology that was adapted to synthesized the counteranion exchanged L.(+)-MS^{*-} and L.(-)-MS^{*-} compounds.

4.2.2.3. Synthesis and Characterization of L.(-)-MS^{*-}

The intermediates [chiral pyridinium salts of (+)- or (-)-menthylsulfate (MS^{*-})], which were used for exchange the chloride (Cl⁻) counteranion of the L.Cl⁻, were synthesized following the previously reported procedure.¹¹ Next, to an aqueous solution (35 mL) of L.Cl⁻ (250 mg, 0.61 mM), an aqueous solution (2.5 mL) of pyridinium salts of (-)-menthylsulfate (MS^{*-}) (290 mg, 0.92 mMol) was added in a dropwise manner (Scheme 4.2). During the course of the addition of pyridinium salts of (-)-menthylsulfate (MS^{*-}), a yellow colour precipitate was obtained. Reaction mixture was stirred for another 5 hrs at room temperature to ensure the completion of the reaction. The precipitate was filtered off as product and this was subsequently washed thoroughly with water. The solid thus isolated was dried under desiccator for overnight to obtain the yellow color chloride (Cl⁻) counteranion exchanged ligand pure L.(-)-MS^{*-}. Yield = 95 %, ¹H NMR (500 MHz, DMSO-d₆, TMS): δ (ppm) = 8.72-8.71(6H, d, J = 6 Hz), 8.57 (3H, s), 8.02-8.01 (6H, d, J = 6 Hz), 2.26-2.24 (1H, d, J = 12 Hz), 2.09-2.06 (1H, m), 1.55-1.49 (2H, m), 1.25-1.24 (1H, broad), 1.06-1.01 (1H, m), 0.91-0.88 (1H, m), 0.81-0.76 (8H, m), 0.68-0.67 (3H, d, J = 7 Hz); ¹³C NMR (100 MHz, DMSO-d₆, TMS): δ (ppm) = 179.02, 175.16, 173.79, 169.09, 142.89, 84.89, 77.02, 52.05, 49.78, 46.58, 42.64, 33.06, 32.71,

29.07, 28.95, 21.47, 21.20, 18.81, 18.64, 18.02, 17.85, 16.41, 16.37; HRMS (ESI): m/z calculated for $C_{29}H_{36}O_4N_9S$ $[M-H]^-$ = 606.26, found 606.26.

4.2.2.4. Synthesis and Characterization of L.(+)-MS^{*-}

The title compound was prepared using [pyridinium salts of (+)-menthylsulfate (MS^{*-})]¹¹ isomer following the same procedure as that was adopted for the preparation of L.(-)-MS^{*-}. Desired compound was isolated in pure form with a ~92 % isolated yield (Scheme 4.2).

4.2.3. General Description of Different Experimental Techniques

4.2.3.1. Gelation Test

Synthesized compounds L.Cl⁻, L.(-)-MS^{*-} and L.(+)-MS^{*-} were taken in three different closed glass vial at their minimum gelation concentration and dissolved completely by heating in 1 mL of MeOH/H₂O (1:1, v/v). The clear solution was left to cool down in ambient temperature without any disturbance. A stable gel was obtained instantly from L.(-)-MS^{*-} and L.(+)-MS^{*-}, whereas it took 3-4 hours for L.Cl⁻. The gel formation was confirmed by the failure of the soft mass to flow by inverting the glass vial.

4.2.3.2. UV-Vis and Circular Dichroism (CD) Spectroscopy

L.Cl⁻ was dissolved in MeOH/H₂O (1:1, v/v) to a concentration of 15 mg/mL. Then, a 60 μ L of this resulting solution was placed on a circular quartz plate (20 mm diameter x 1 mm thick) and allowed to air dry for ~ 6-7 hrs in a dust-free place. This leads to the formation of a uniform transparent thin film. Both UV-Vis and CD spectrum was then recorded of the prepared uniform transparent thin film. For L.(-)-MS^{*-} and L.(+)-MS^{*-} same procedure was followed to prepare the film, but concentration was used 4 mg/mL in MeOH/H₂O (1:1, v/v) and recorded the UV-Vis and CD spectrum of the corresponding thin film.

4.2.3.3. Scanning Electron Microscopy (SEM)

A small portion of the freshly prepared gels of L.Cl⁻, L.(-)-MS^{*-} and L.(+)-MS^{*-} was scooped out and diluted with MeOH/H₂O (1:1, v/v). Resulting solutions are drop-casted on a silicon wafer and allowed to air dry for 5 hrs in a dust free place. Finally, it was dried under desiccator for overnight. Before taking images, samples were coated with gold vapour.

4.2.3.4. Crystallization Procedure

20 mg of **L.Cl⁻** was dissolved in 1 mL of MeOH/H₂O (1:1, v/v) inside a screw-capped vial. The solution was gently heated, then kept it in closed condition with no mechanical disturbance for allowing the crystals of **L.Cl⁻** to grow. After ~ 4-5 days high-quality rod-shaped yellow colored crystals were obtained, which was used for X-ray diffraction mediated characterization. For **L.(-)-MS⁻** and **L.(+)-MS⁻**, 15 mg of weighted corresponding compound taken in two different glass vial and dissolved with 1 mL of slight acidic MeOH (prepared by mixing 4 μ L of CH₃COOH with 1 mL MeOH). When diethyl ether vapor was allowed to diffuse slowly at 25°C into the prepared **L.(-)-MS⁻** or **L.(+)-MS⁻** solutions, X-ray quality crystals were obtained within 48 hours. These crystals are immediately used for single crystal X-ray diffraction (SC-XRD).

4.2.3.5. Details of the Single Crystal X-ray Diffraction Studies

4.2.3.5.1 Crystallographic Refinement Details

The intensity data were collected using a Bruker SMART APEXII CCD diffractometer, equipped with a fine focus 1.75 kW sealed tube CuK α radiation (λ = 1.54178 Å) at 298(2) K, with increasing ω (width of 0.3° per frame) at a scan speed of 3 s per frame. The SMART software was used for data acquisition. Data integration and reduction were undertaken with SAINT and XPREP¹² software. Multi-scan empirical absorption corrections were applied to the data using the program SADABS.¹³ Structures were solved by direct methods using SHELXL-2014 refined with full-matrix least squares on F^2 using SHELXL-2014.¹⁴ The hydrogen atoms attached to all the carbon atoms were geometrically fixed and the positional, as well as temperature factors, are refined isotropically. Structural illustrations have been drawn with Mercury for Windows.¹⁵ In all cases, non-hydrogen atoms are treated anisotropically. In other cases, the hydrogen atoms are geometrically fixed. PLATON/SQUEEZE¹⁶ was performed for complex **L.(+)-MS⁻** (**2**) and **L.(-)-MS⁻** (**3**) to remove disordered unassignable solvent molecules.

Table 4.1. Structural parameters for L.Cl⁻ (1), L.(+)-MS^{*-} (2) and L.-)-MS^{*-} (3)

Objects	L.Cl ⁻ (1)	L.(+)-MS ^{*-} (2)	L.-)-MS ^{*-} (3)
CCDC	1485416	1485417	1485418
Formula	C ₁₉ H ₃₆ Cl N ₉ O ₉	C ₃₀ H ₄₀ N ₉ O ₅ S	C ₃₀ H ₄₀ N ₉ O ₅ S
Fw	570.02	638.77	638.77
Crystal system	Monoclinic	Monoclinic	Monoclinic
Space group	P 21/c	P 21/n	P 21/n
<i>a</i> /Å	10.7037(4)	18.376(5)	18.411(4)
<i>b</i> /Å	28.6071(10)	7.384(2)	7.3949(16)
<i>c</i> /Å	9.3466(3)	26.915(7)	26.935(6)
α /deg	90.00	90.00	90.00
β /deg	104.8260(10)	104.570(17)	104.741(12)
γ /deg	90.00	90.00	90.00
<i>V</i> /Å ³	2766.66(17)	3534.5(16)	3546.4(14)
<i>Z</i>	4	4	4
<i>D_c</i> /g cm ⁻³	1.368	1.200	1.196
μ Mo K α /mm ⁻¹	1.773	1.219	1.215
<i>T</i> /K	298(2)	298(2)	298(2)
θ max.	68.37	59.75	64.57
Total no. of reflections	53881	39790	37796
Independent reflections	5082	6286	5767
Observed reflections	4595	3163	2640
Parameters refined	345	350	350
<i>R</i> ₁ , <i>I</i> > 2 σ (<i>I</i>)	0.0722	0.2114	0.1932
<i>wR</i> ₂ (all data)	0.2170	0.5381	0.5230
<i>R</i> (int)	0.0379	0.2347	0.1652
GOF (<i>F</i> ²)	1.003	1.415	1.617

Table 4.2. Hydrogen Bonding Contacts of L.Cl⁻ (1), L.(+)-MS*⁻ (2) and L.(-)-MS*⁻ (3)

Complex	D-H...A	d(H...A)/Å	d(D...A)/Å	<D-H...A/°
L.Cl⁻ (1)	O1...Cl1		3.088(2)	
	O7-H7A... Cl1	2.383	3.229(1)	173.66
	O2...Cl1	-	3.084(3)	-
	O5-H5B...Cl1	2.167	3.145()	160
	C11-H11...Cl1	2.715	3.546(1)	149
	C17-H17...Cl1	2.774	3.667(1)	160
L.(+)-MS*⁻ (2)	C5-H5...O1	2.334	3.228(1)	161
	N7-H7...O2	2.058	2.881(1)	160
	C10-H10...O2	2.460	3.384(1)	172
	C14-H14...O2	2.444	3.245(1)	144
	N1-H...O3	2.283	2.993(1)	140
	C2-H2...O3	3.208	2.481(1)	135
	C19-H19...O3	2.532	3.434(1)	163
	C10-H10...O4	2.646	3.340(1)	131
L.(-)-MS*⁻ (3)	C6-H6...O1	2.335	3.234(1)	162
	N4-H4...O2	2.306	3.031(1)	142
	C2-H2...O2	2.547	3.263(1)	132
	C10-H10...O2	2.502	3.406(1)	164
	N1-H...O3	2.017	2.839(1)	159
	C8-H8...O3	2.350	3.160(1)	145
	C16-H16...O3	2.529	3.454(1)	173
	C16-H16...O4	2.665	3.363(1)	132

4.3. Results and Discussions

The methodology adopted for the synthesis of the compound L.Cl⁻, L.(-)-MS*⁻ and L.(+)-MS*⁻ are shown in Scheme 4.1 and 4.2. Analytical, as well as spectroscopic data, confirmed the purity of these synthesized compounds. The single crystal X-ray structures for each compound also confirmed their proposed molecular structure. All studies were performed using double distilled water and HPLC grade MeOH solvent medium unless mentioned otherwise.

Although being deprived of any conventional gelation assisting functional units, gelation experiment shows that **L.Cl⁻** self-assembled to form a yellow color opaque gel in MeOH/H₂O (1:1, v/v), which was confirmed by inverted vial method (Figure 4.2a). The gel is highly thermo reversible; upon heating, it transforms to the solution and reverts to gel state after cooling to room temperature within 3-4 hrs (Figure 4.2b). Conversely, the gel is formed within 4-5 minutes upon sonication, resulting in a considerable decrease of critical gel concentration (CGC) of **L.Cl⁻** from 6.2 wt % to 3.4 wt %.

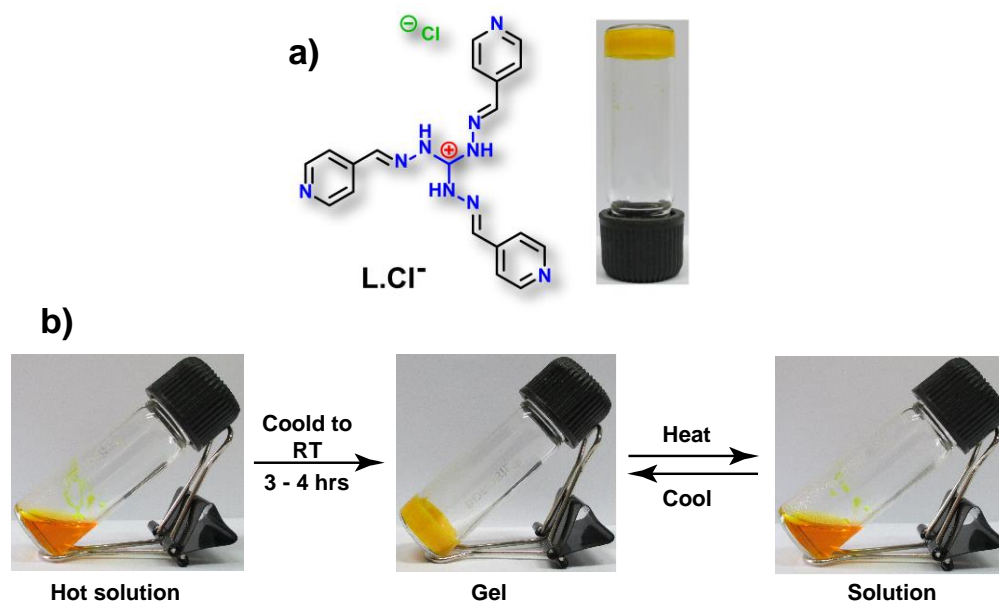


Figure 4.2. (a) Chemical structure of the gelator **L.Cl⁻** and photograph of the gel formed in MeOH/H₂O (1:1, v/v); (b) Photographs showing the thermo reversible property of the gelator **L.Cl⁻** (CGC is 6.2 wt %).

In order to have a deeper understanding of the self-assembly process, the **L.Cl⁻** gel was imaged by scanning electron microscope (SEM). **L.Cl⁻** exhibit network of helical fiber bundles or ropes composed of thin fibers of nanometer diameter and micrometer length (Figure 4.3). A careful analysis of the SEM image illustrates that, the single thin fibers are not helical in nature. However, in the course of assembly formation, fibers are bundled-up and intertwined with each other to form helical ropes with simultaneous chiral *M* and *P* twists (Figure 4.3; inset).

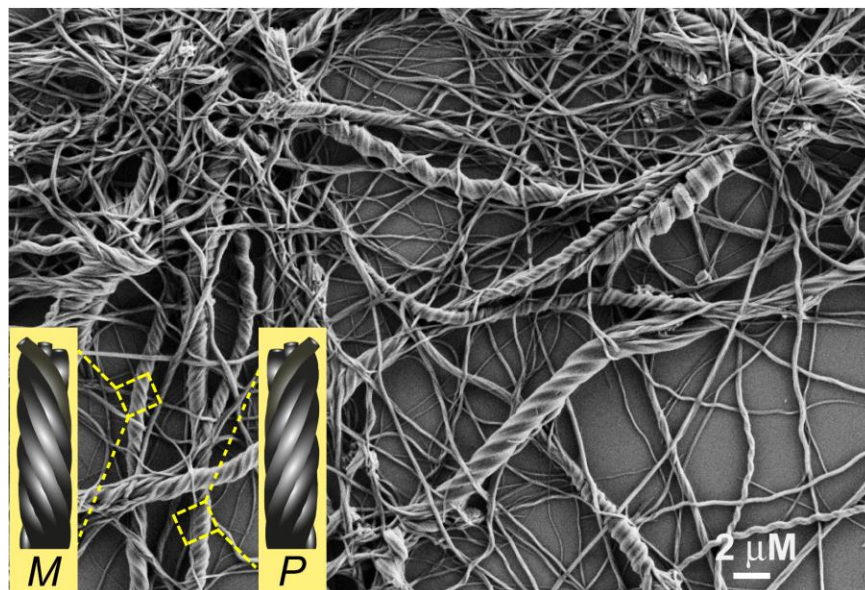


Figure 4.3. SEM image of the *P* and *M* helical ropes obtained from the self-assembled gel of **L.Cl⁻** in MeOH/H₂O (1:1, v/v); inset shows the corresponding schematic of *P* and *M* type helical ropes.

Further to confirm the origin of chirality in bundled fibers, CD spectra of **L.Cl⁻** solutions with various concentrations in MeOH/H₂O (1:1, v/v) was measured. Surprisingly, in solution state **L.Cl⁻** does not show any CD activity. This might be due to the existence of the disassembled monomeric species or optically inactive minor aggregates in dilute solution. To confirm this, we perform the variable temperature UV-Vis and CD experiment and the corresponding spectra are shown in Figure 4.4. By cooling from 70 to 5°C, no distinct UV-Vis spectral change is observed, except a slight increase in absorption intensity at 319 nm (Figure 4.4a). Moreover, characteristic aggregation features such as an isosbestic point or a shift in the absorption maximum are also missing. The slight increase in absorption intensity with decrease in the temperature could be due to the planarization of the structure of **L.Cl⁻** from its initial propeller shape.¹⁷ Hence the temperature dependent UV-Vis spectra clearly indicate that gelator **L.Cl⁻** molecule either as a monomer or as optically silent minor aggregates at lower concentration. As a result, no CD signal is identified in solution (Figure 4.4b).

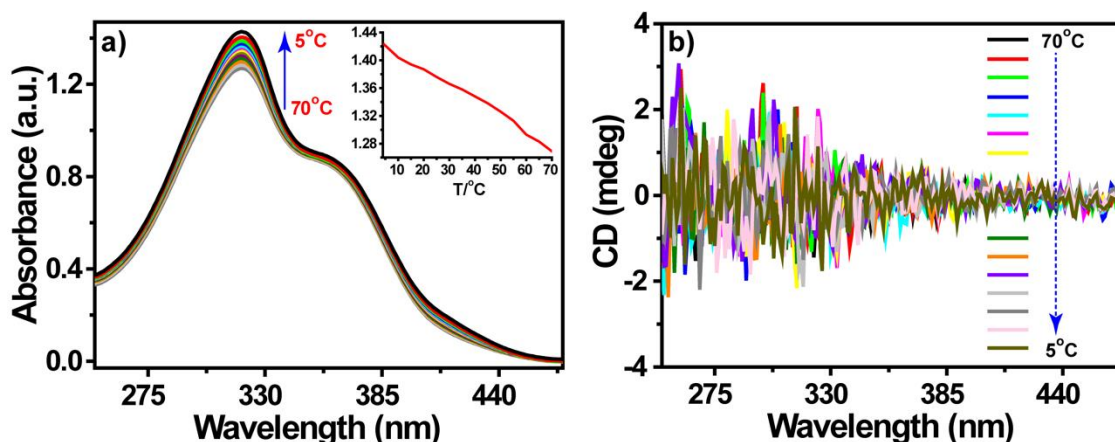


Figure 4.4. Variable temperature (a) UV-Vis and (b) CD spectra of $L.Cl^-$ (concentration used = 1.0×10^{-4} Mol in 1:1 MeOH/ H_2O , $l = 10$ mm) from 70 to 5 °C. Inset of (a) shows variation of absorbance at 319 nm with temperature.

However, the corresponding solution when drop cast on a circular quartz plate (20 mm diameter \times 1 mm thick), and prepared a transparent film and record the CD spectrum, it exhibited CD signals (Figure 4.5a). The examination of different batches of drop cast thin films prepared from same solution (15 mg/mL) showed CD signals with negative or positive cotton effects having a dominant peak at 372 nm and a shoulder peak at 464 nm (Figure 4.5a), which is well consistent with the UV-Vis absorption spectrum of the thin film (Figure 4.5b). It is also noticed that some samples are almost CD silent (Figure 4.5a; red line). This result indicates that there must be the random formation of chiral structures over the period of self-assembly process. However, the optical activity is stochastic with the appearance of negative CD signals (7 times), positive CD signals (6 times) and CD silent signals (4 times) (Figure 4.5c). Based on both microscopic and spectroscopic experiments, we conclude that even though $L.Cl^-$ is achiral in nature, during self-assembly it spontaneously form kinetically controlled aggregates with P and M helicity. When the overall distribution of M twists exceeds over the P twists or vice versa, the assembly shows CD activity. But, for a situation having comparable distribution of both P and M twists, no macroscopic optical activity is observed and hence becomes CD silent.^{8b}

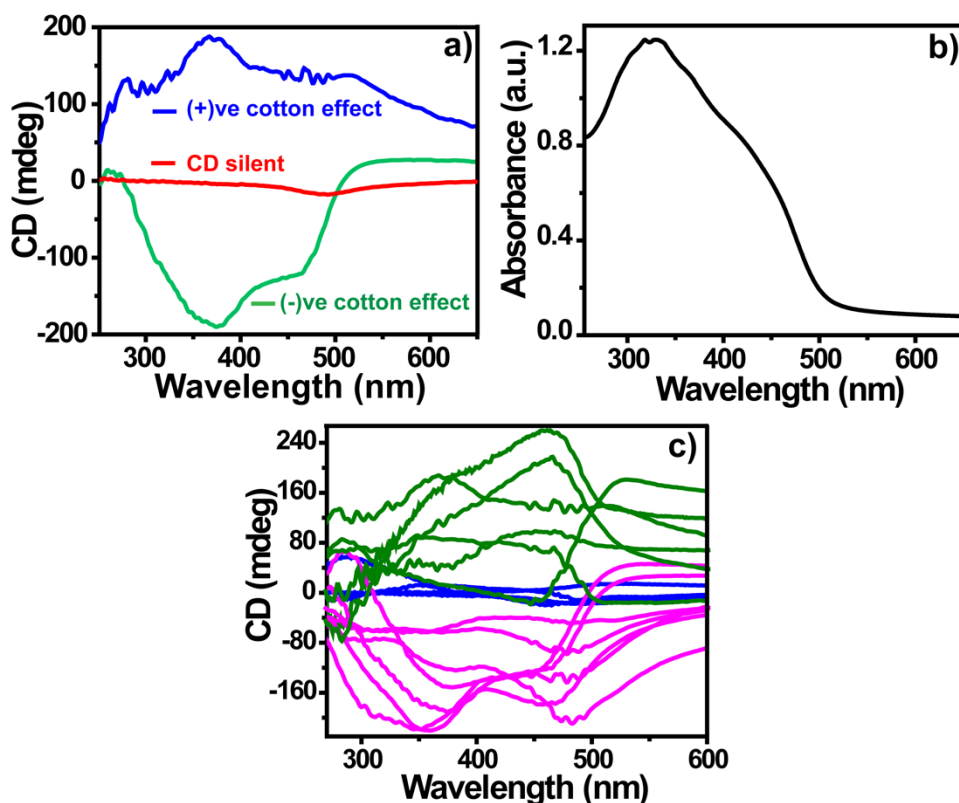


Figure 4.5. (a) CD spectra of three different thin films prepared from solutions of L.Cl^- (15 mg/mL) in MeOH/ H_2O (1:1, v/v) and (b) UV-Vis absorption spectrum of the corresponding thin films of L.Cl^- ; (c) CD spectra of 17 different batches of L.Cl^- thin films showing random cotton effect. (Concentration used to prepare film = 15 mg/mL in MeOH/ H_2O (1:1, v/v) mixture).

Since C_3 -symmetric L.Cl^- gelator shows macroscopic helical properties, it is really essential to explore its precise molecular arrangements in the aggregate state. So we crystallized L.Cl^- as a molecular assembly of $[\text{L.Cl}^- \cdot 9\text{H}_2\text{O}]$ from MeOH/ H_2O (1:1, v/v) mixture at a concentration below its CGC. Figure 4.6a and 4.6b shows that Cl^- anion is located far away from the central cationic unit. Each Cl^- ion forms four H-bonds with four water molecule (Figure 4.6b). The hydrated Cl^- ion connects the two cationic units by constructing two H-bonds with terminal pyridyl hydrogen atoms ($\text{Cl}^- \cdots \text{H-C}$; Figure 4.6b). Due to an intrinsic positive charge of guanidinium units, two consecutive molecules stack in a slipped way and formed a double propeller type arrangement (Figure 4.6b). A careful analysis of the single crystal structure showed that this double propeller-shaped dimer and the corresponding hydrated Cl^- anion forming H-bonding network with the help of solvent (water) molecule. These results in a left-handed helix-like one-dimensional (1D) arrangement (Figure 4.6c).

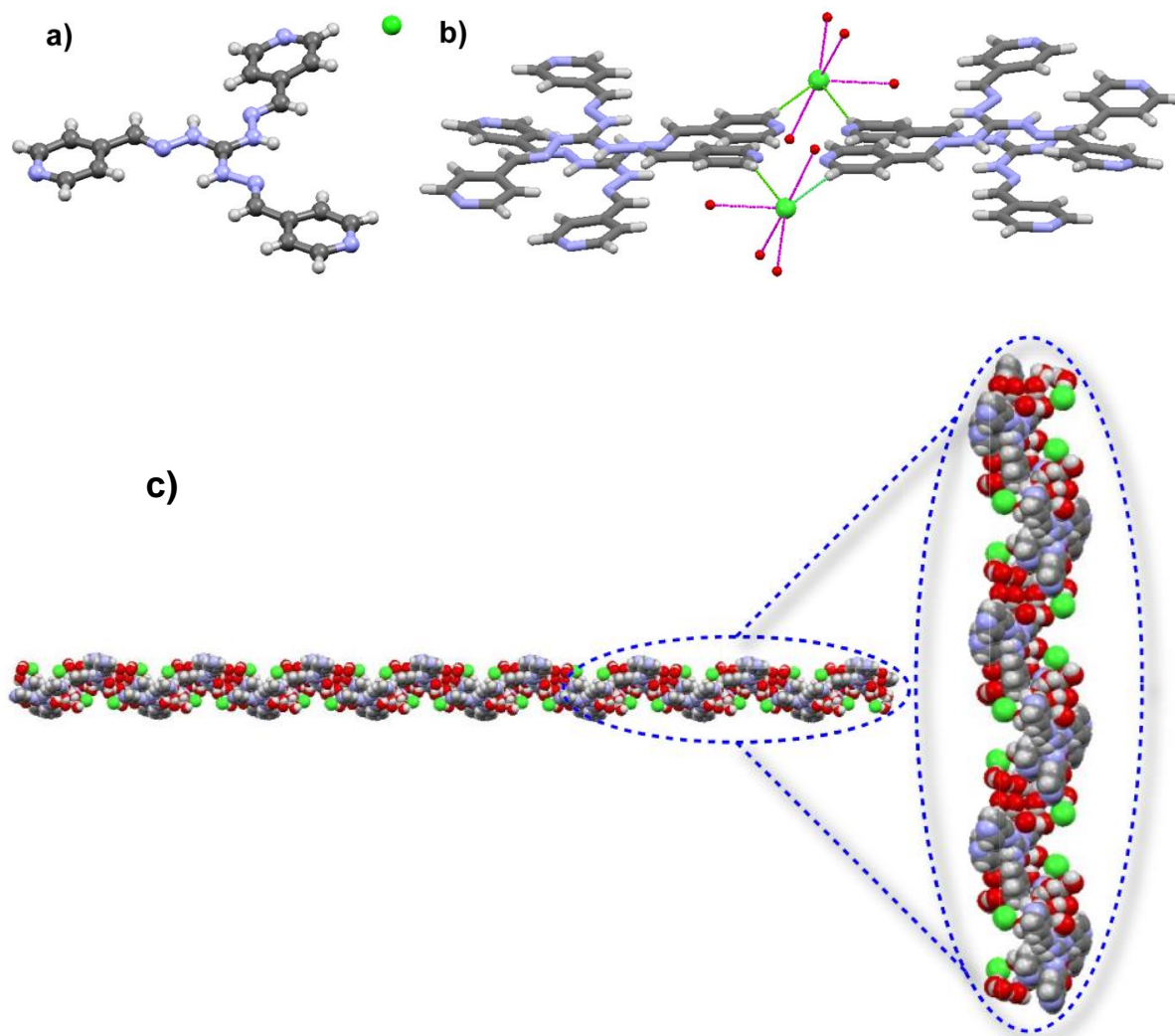


Figure 4.6. (a) Crystal structure of $L.Cl^-$ in ball and stick model, solvent molecules are omitted for clarity; (b) Packing model of $L.Cl^-$ showing the coordination of hydrated Cl^- anion with L , stabilized by multiple H-bonds; (c) 1D left-handed helical arrangements of $L.Cl^-$ in space fill model.

Achieving a helical or twisted nanostructure from an absolutely achiral molecule is a rousing issue, but without controllable handedness it is incomplete. Since the central guanidinium unit of $L.Cl^-$ is cationic, exchange of its counter anion Cl^- with an optically active one could be the simplest way to control its chirality.

In order to accomplish this, we searched for suitable anion and perceived that guanidinium units are known to strongly bind with oxoanions (e.g. phosphate, carboxylate and sulphate).⁵ However, according to *Hofmeister series* sulphate anion has maximum inclination to substitute Cl^- compared to phosphate and carboxylate. With

this rationale, we opted for chiral pyridinium salts of (+)- and (-)- MS^{*-} anion^{7b} to exchange Cl^- counter anion of **L** (Scheme 4.3). The addition of aqueous solution of MS^{*-} anions led to salting out of **L** from its aqueous solution and thus enabled us to isolate both **L**.(+)- MS^{*-} and **L**.(−)- MS^{*-} (Scheme 4.2 and 4.3). Formation of the counter anion exchanged compound **L**.(−)- MS^{*-} was confirmed by comparison of the ^1H NMR spectra (in DMSO-d_6). ^1H NMR spectra of **L**. Cl^- lacks protons in the aliphatic region whereas the pyridinium (−)- MS^{*-} ion displays aliphatic protons along with three sets of pyridinium protons (encircled peaks) in the aromatic region (Figure 4.7). However, in the final compound **L**.(−)- MS^{*-} , appearance of multiple sets of aliphatic protons (corresponds to MS^{*-} protons) and complete disappearance of pyridinium protons strongly support that the anion exchange reaction has taken place (Figure 4.7 and Scheme 4.3).

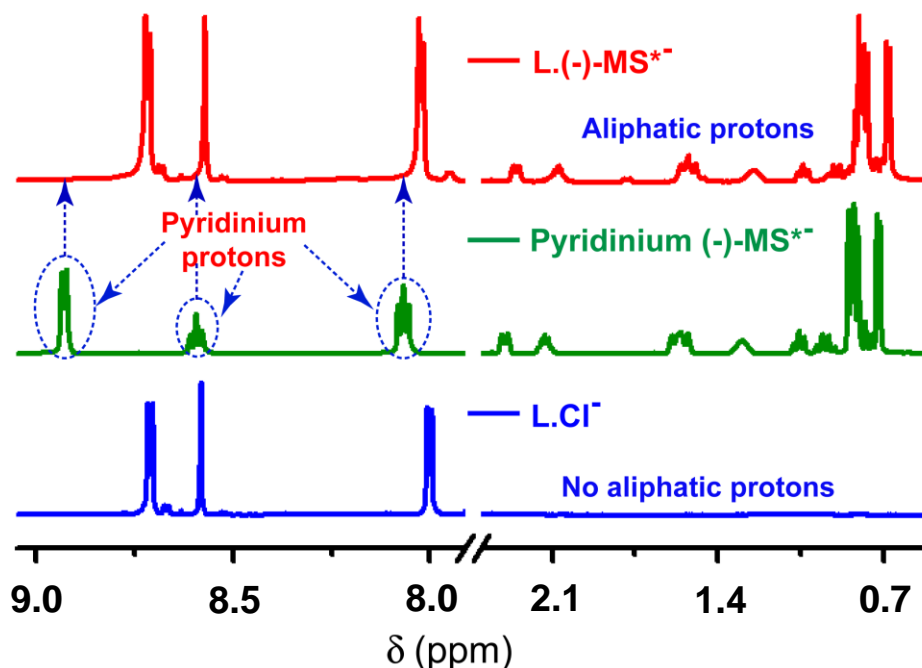
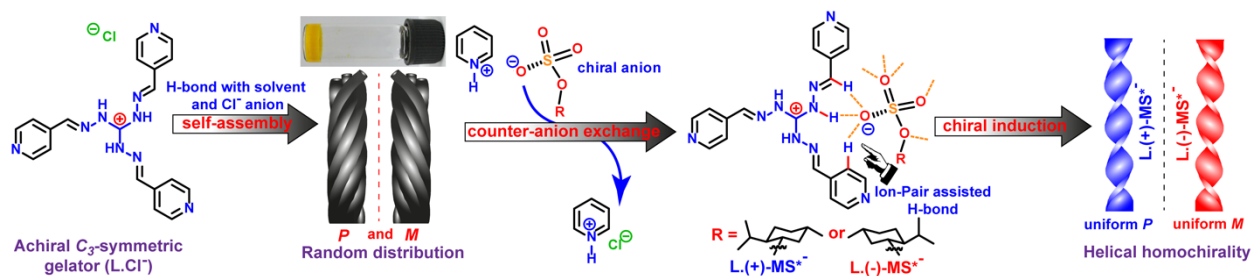


Figure 4.7. Comparison of ^1H NMR spectra (in DMSO-d_6) of **L**. Cl^- , pyridinium (−)- MS^{*-} and **L**.(−)- MS^{*-} demonstrating the successful exchange of Cl^- counteranion of **L** with chiral MS^{*-} .

Both the counter anion exchanged compounds **L**.(+)- MS^{*-} and **L**.(−)- MS^{*-} also found to form thermo reversible gels (Figure 4.8). Compared to **L**. Cl^- , CGC of these two compounds drastically decreased from 6.2 wt % to 0.7 wt % under the same solvent

composition (MeOH/H₂O; 1:1 v/v). This drastic change in CGC indicates that **MS^{*}-** counter anion plays an important role in self-assembly.



Scheme 4.3. Random formation of optically active self-assembled structures from achiral **L.Cl⁻** and control of its chirality by counter anion exchange approach.

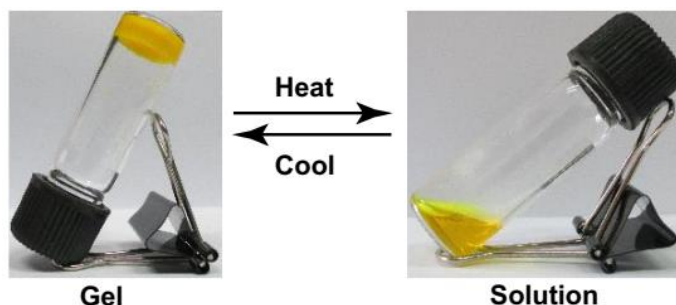


Figure 4.8. Photographs showing thermal reversibility of **L.(-)-MS^{*}-** gel prepared in MeOH/H₂O (1:1, v/v). Gel prepared from **L.(+)-MS^{*}-** is also thermo reversible. CGC for both gelators is 0.7 wt %.

Optical activity of **L.(+)-MS^{*}-** and **L.(-)-MS^{*}-** were verified by CD spectroscopy. Interestingly, **L.(+)-MS^{*}-** and **L.(-)-MS^{*}-** showed strong CD signals with positive and negative cotton effects, respectively (Figure 4.9a). The obtained CD spectrum is a mirror image of each other having two major peaks at 353 nm and 464 nm and a crossover at 330 nm (Figure 4.9a). However, corresponding UV-Vis spectra did not show any considerable difference (Figure 4.9b). Interestingly, SEM image of **L.(+)-MS^{*}-** showed helical ribbons with *P* twists (Figure 4.9c) whereas *M* twists were observed for **L.(-)-MS^{*}-** ribbons (Figure 4.9d). Hence the exchange of the achiral counteranion (**Cl⁻**) with chiral anion could efficiently control the preferred homochiral states, homochiral *P* twists for **(+)-MS^{*}-** and *M* twists for **(-)-MS^{*}-** (Scheme 4.3).

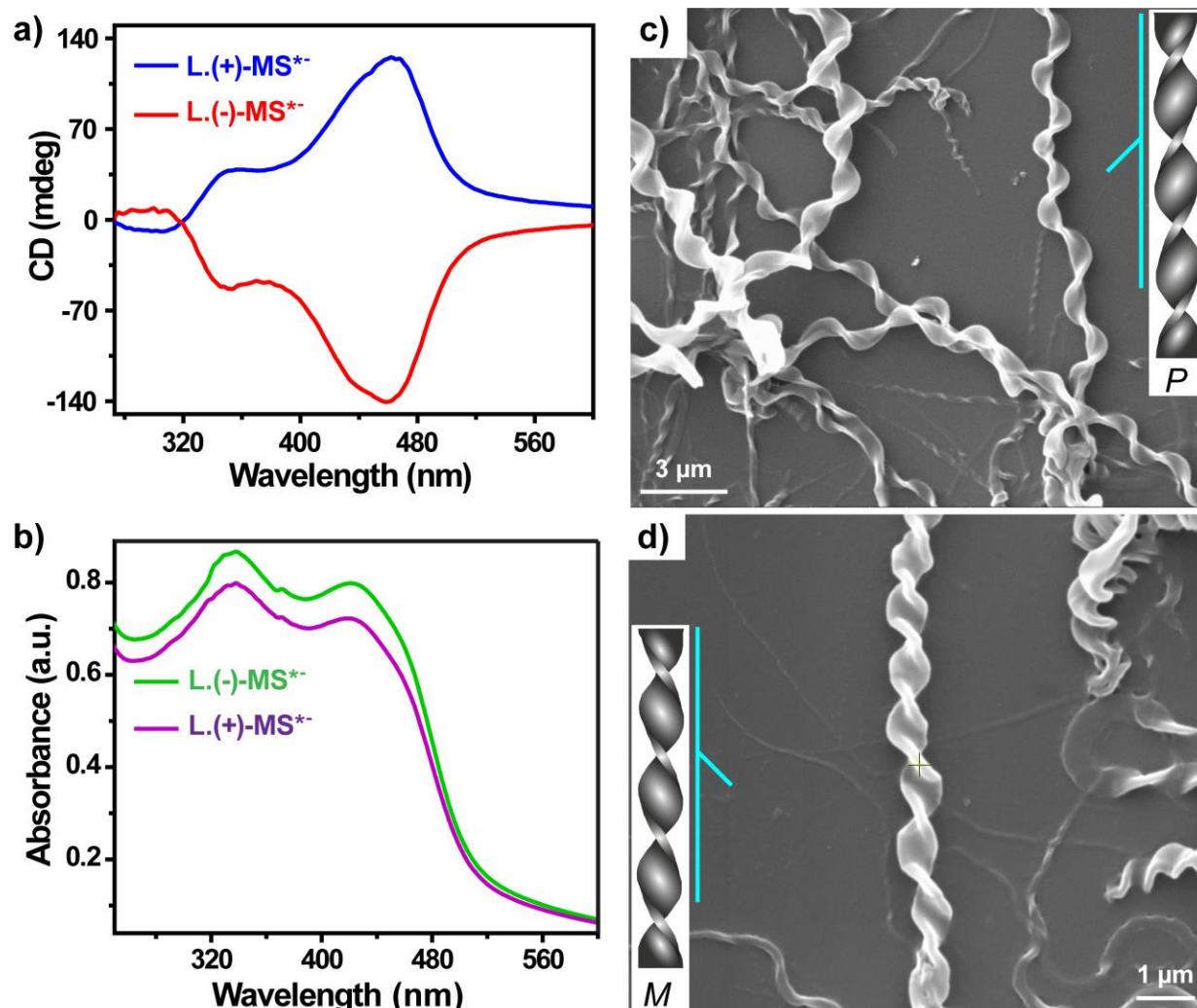


Figure 4.9. (a) CD and (b) UV-Vis spectra of L.(+)-MS*⁻ and L.-)-MS*⁻ thin films, (Concentration <CGC); SEM images of (c) right (P)- and (d) left (M)- handed twisted ribbons of L.(+)-MS*⁻ and L.-)-MS*⁻ gel (0.7 wt % in MeOH/H₂O; 1:1, v/v), respectively.

The improved gelation feature of the anion-modified gelators made crystallization from aqueous solution a tedious job. After several attempts, X-ray quality crystals were obtained by diffusion of diethyl ether into a slightly acidic methanol solution of L.(+)-MS*⁻ or L.-)-MS*⁻ (Figure 4.10). Compared to L.Cl⁻, crystal structure of L.-)-MS*⁻ displayed that the counteranion MS*⁻ is intensely oriented towards central cationic unit, because of the electrostatic interaction between oppositely charged ions (Figure 4.10a and 4.11a). This ion-pair contacts enable MS*⁻ to form eight H-bonds, two with guanidium N-H and six with different C-H of the L (Figure 4.11b; green line).

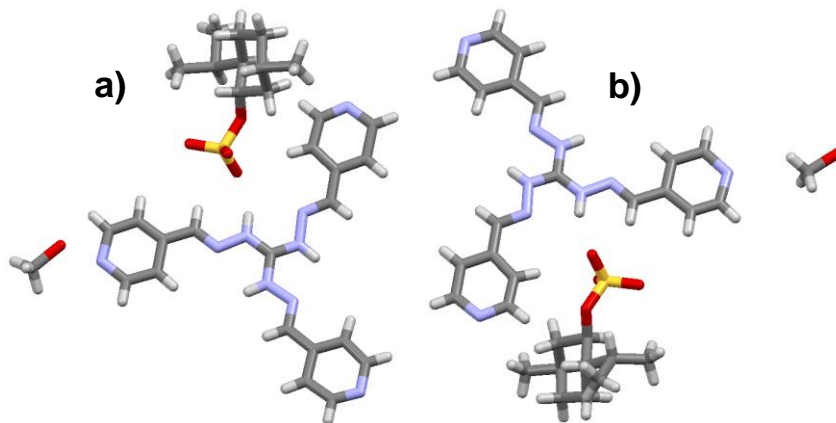


Figure 4.10. (a) and (b) crystal structure of both L.(+)-MS* and L.-)-MS* gelators respectively in capped sticks model.

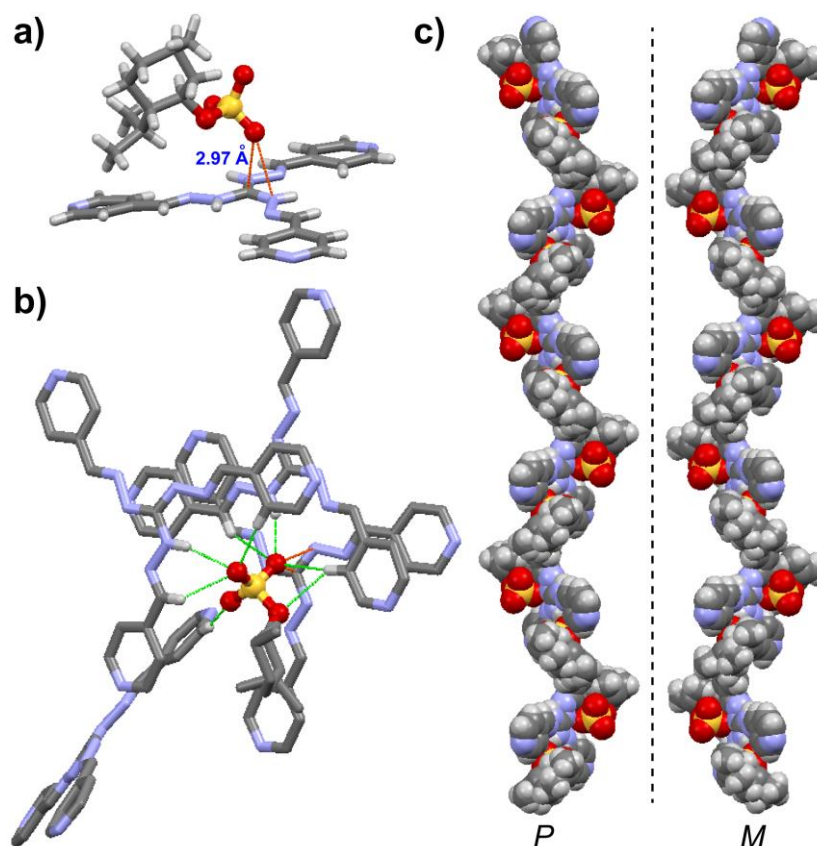


Figure 4.11. (a) Ion-pair contacts through electrostatic interaction and (b) crystal packing of L.-)-MS*, showing IPA-H bonds (solvent MeOH and non-interacting H-atoms are omitted for clarity); (c) Right (P)- and Left (M)- handed helical molecular arrangement of L.(+)-MS* and L.-)-MS* crystals, respectively in space fill model.

It was also noticed that two adjacent guanidinium units (**L**) are twisted with each other and H-bonded with **MS**^{*-} anions to result in a left-handed (*M*) helical chain (Figure 4.11c; right). However, in the case of **L**.(+)-**MS**^{*-} right-handed (*P*) helical chain was observed (Figure 4.11c; left). Most importantly, the crystallographic helical signs were exactly matched with SEM images (Figure 4.9c-d and 4.11c). Solid state structure of both **L**.(+)-**MS**^{*-} and **L**.(-)-**MS**^{*-} clearly indicate that optically active arrangement was entirely driven by IPA-H bond(s). This IPA-H bond stretches the main interactions to stabilize the assembly even in aqueous solution (MeOH/H₂O; 1:1 v/v). The UV-Vis absorption and CD spectra of **L**.Cl⁻ and **L**.(-)-**MS**^{*-}/ **L**.(+)-**MS**^{*-} showed a significant difference in shape and position of the two peaks present (Figure 4.5a-b and 4.9a-b). This could be attributed to the difference in the available intermolecular interactions and packing of molecules as visualized by the crystal structure (Figure 4.6 and 4.11 for molecular interactions; Figure 4.12, 4.13 and 4.14 for crystal packing pattern). The summary of the whole self-assembly process is given as a pictorial representation in Scheme 4.3.

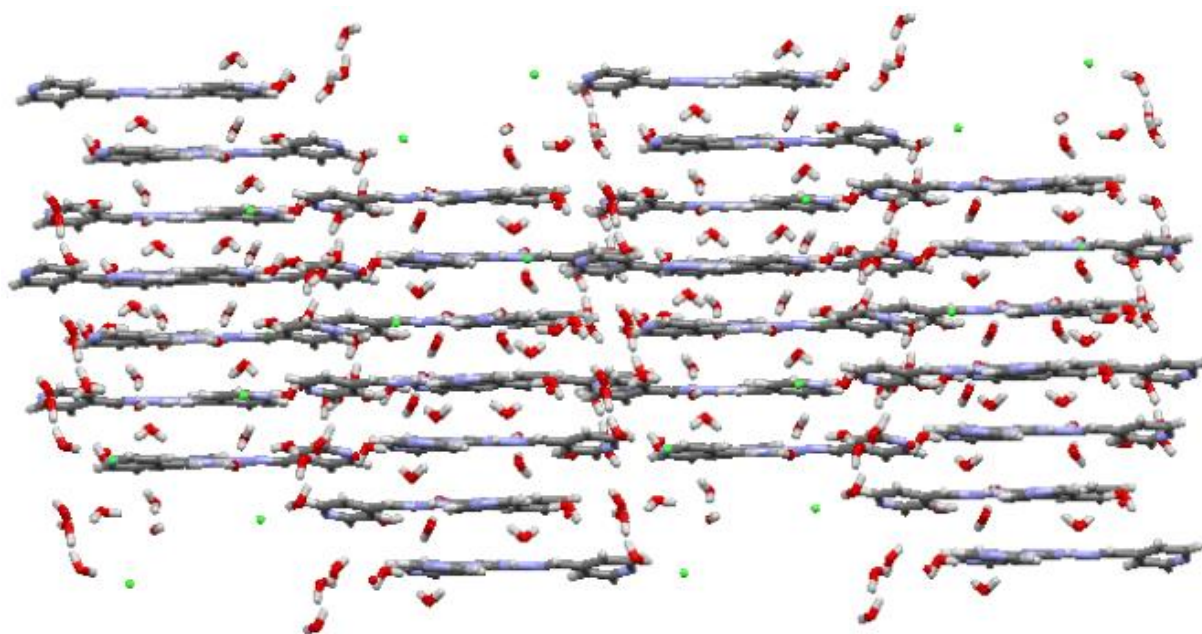


Figure 4.12. Crystal packing of **L**.Cl⁻.

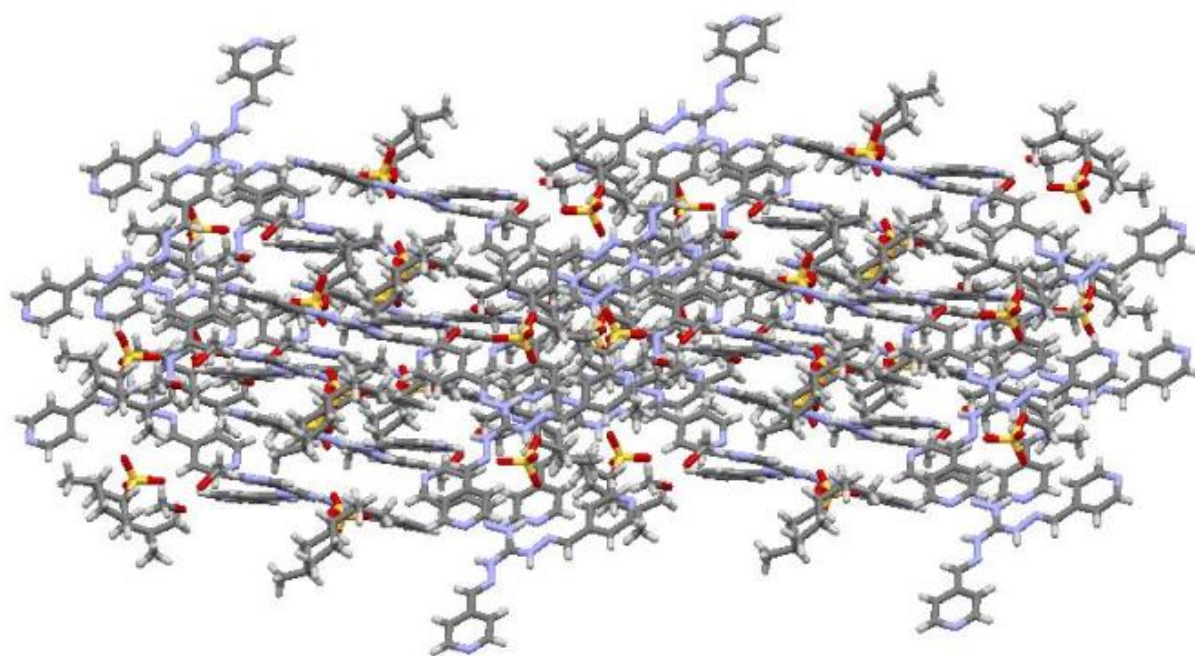


Figure 4.13. Crystal packing of L.(+)-MS*⁻.

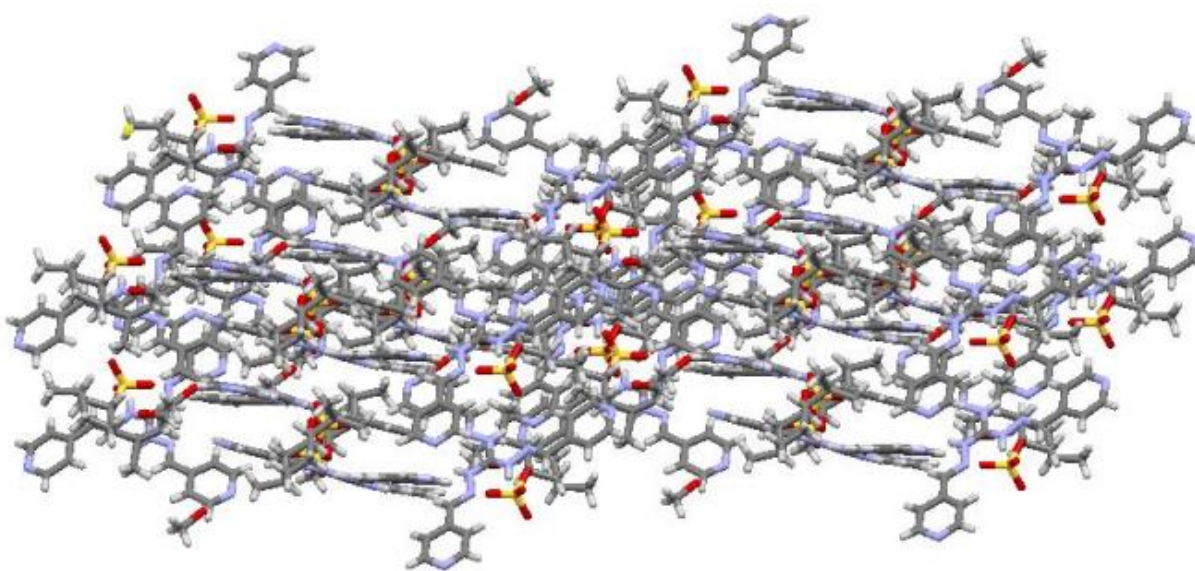


Figure 4.14. Crystal packing of L.(-)-MS*⁻.

4.4. Conclusions

In conclusion, it has been ascertained that exchange of an achiral counter anion with a chiral one can be an effective tool to bias the helical handedness of the assembly. Random formation of *P* and *M* type helical twists in the self-assembly of cationic C_3 -symmetric gelator is controlled to a preferred handedness. Our study demonstrates a radically new approach to successfully switch the handedness of random chirality to the desired homochiral assemblies. For the first time, we have utilized this simple chiral counter anion exchange methodology to induce chirality to a cationic molecule. Moreover, the solid-state structure of the assembly establishes that IPA-H bond plays a key role to form chiral helical assembly. Currently, we are exploring the possibility of other counter anions to bias the helical sense. In addition, further studies to memorize the generated chirality signs of this molecular system are underway.

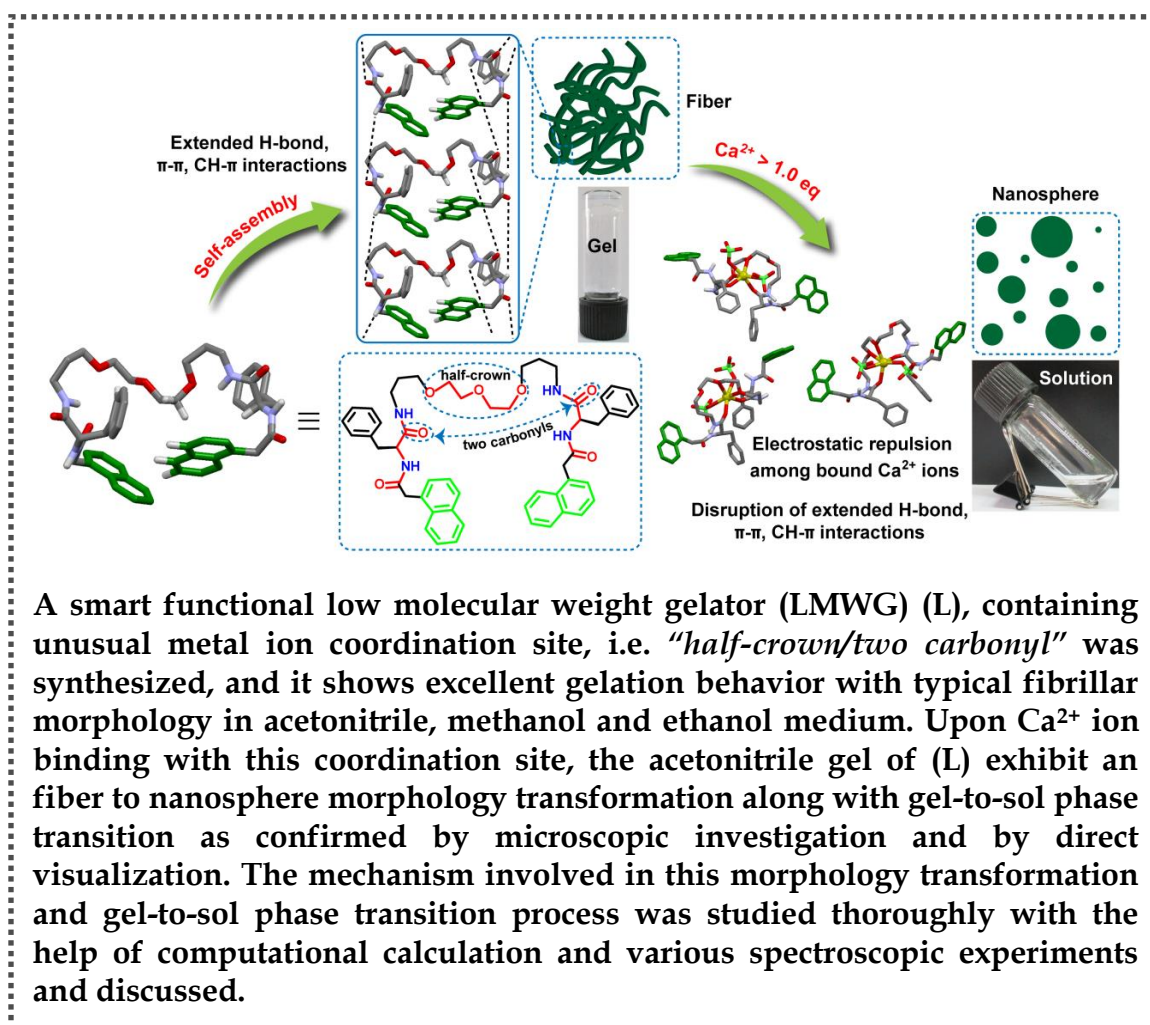
4.5. References

1. (a) M. Liu, L. Zhang, T. Wang, *Chem. Rev.*, 2015, **115**, 7304; (b) A. R. A. Palmans, E. W. Meijer, *Angew. Chem., Int. Ed.*, 2007, **46**, 8948; (c) M. A. Mateos-timoneda, M. Crego-calama, D. N. Reinhoudt, *Chem. Soc. Rev.*, 2004, **33**, 363; (d) K. Maeda, E. Yashima, *Top. Curr. Chem.*, 2006, **265**, 47; (e) A. E. Rowan, R. J. M. Nolte, *Angew. Chem., Int. Ed.*, 1998, **37**, 63.
2. (a) D. G. Blackmond, *Cold Spring Harbor Perspect. Biol.*, 2010, **2**, a002147; (b) R. A. Hegstrom, D. K. Kondepudi, *Sci. Am.*, 1990, **262**, 108.
3. (a) N. Kimizuka, T. Kwaasaki, K. Hirata, T. Kunitake, *J. Am. Chem. Soc.*, 1995, **117**, 6360; (b) N. Kimizuka, S. Fujikawa, H. Kuwahara, T. Kunitake, A. Marsh, J. M. Lehn, *J. Chem. Soc., Chem. Commun.*, 1995, **53**, 1689; (c) S. J. George, Ž. Tomović, M. M. J. Smulders, T. F. A. De Greef, P. E. L. G. Leclère, E. W. Meijer, A. P. H. J. Schenning, *Angew. Chem., Int. Ed.*, 2007, **46**, 8206; (d) M. P. Lightfoot, F. S. Mair, R. G. Pritchard, J. E. Warren, *Chem. Commun.*, 1999, 1945; (e) W. Yang, X. Chai, L. Chi, X. Liu, Y. Cao, R. Lu, Y. Jiang, X. Tang, H. Fuchs, T. Li, *Chem. -Eur. J.*, 1999, **5**, 1144; (f) X. Yan, S. Li, J. B. Pollock, T. R. Cook, J. Chen, Y. Zhang, X. Ji, Y. Yu, F. Huang, P. Stang, *J. Proc. Natl. Acad. Sci. U.S.A.*, 2013, **110**, 15585; (g) X. Ji, B. Shi, H. Wang, D. Xia, K. Jie, Z. L. Wu, F. Huang, *Adv. Mater.*, 2015, **27**, 8062.
4. (a) A. Ajayaghosh, R. Varghese, S. J. George, C. Vijayakumar, *Angew. Chem., Int. Ed.*, 2006, **45**, 1141; (b) J. Yuan, M. Liu, *J. Am. Chem. Soc.*, 2003, **125**, 5051; (c) T. Kajitani, H. Masu, S. Kohmoto, M. Yamamoto, K. Yamaguchi, K. Kishikawa, *J. Am. Chem. Soc.*, 2005, **127**, 1124; (d) S. Azeroual, J. Surprenant, T. D. Lazzara, M. Kocun, Y. Tao, L. A. Cuccia, J. M. Lehn, *Chem. Commun.*, 2012, **48**, 2292; (e) M. Kimura, T. Hatanaka, H. Nomoto, J. Takizawa, T. Fukawa, Y. Tatewaki, H. Shirai, *Chem. Mater.*, 2010, **22**, 5732; (f) U. De Rossi, S. Dähne, S. C. J. Meskers, H. P. J. M. Dekkers, *Angew. Chem., Int. Ed.*, 1996, **35**, 760.
5. (a) K. A. Schug, W. Lindner, *Chem. Rev.*, 2005, **105**, 67; (b) T. H. Hehm, C. Schmuck, *Chem. Soc. Rev.*, 2010, **39**, 3597; (c) W. Wang, J. Gu, X. Zou, W. Tong, H. Gong, *Tetrahedron Lett.*, 2015, **56**, 2684.
6. (a) K. Watanabe, H. Iida, K. Akagi, *Adv. Mater.*, 2012, **24**, 6451; (b) C. F. J. Faul, *Acc. Chem. Res.*, 2014, **47**, 3428.
7. (a) R. Oda, I. Huc, M. Schmutz, S. J. Candau, F. C. Mackintosh, *Nature.*, 1999, **399**, 566; (b) H. Yamagishi, T. Fukino, D. Hashizume, T. Mori, Y. Inoue, T. Hikima, T. Aida, *J. Am. Chem. Soc.*, 2015, **137**, 7628.
8. (a) P. J. M. Stals, P. A. Korevaar, M. A. J. Gillissen, T. F. A. D. Greef, C. F. C. Fitié, R. P. Sijbesma, A. R. A. Palmans, E. W. Meijer, *Angew. Chem., Int. Ed.*, 2012, **51**,

- 11297; (b) Z. Shen, T. Wang, M. Liu, *Angew. Chem., Int. Ed.*, 2014, **53**, 13424; (c) Z. Shen, Y. Jiang, T. Wang, M. Liu, *J. Am. Chem. Soc.*, 2015, **137**, 16109.
9. (a) W. L. Noorduin, A. A. C. Bode, M. V. D. Meijden, H. Meekes, A. F. V. Etteger, W. J. P. V. Enckevort, P. C. M. Christianen, B. Kaptein, R. M. Kellogg, T. Rasing, E. Vlieg, *Nat. Chem.*, 2009, **1**, 729; (b) A. Gopal, M. Hifsudheen, S. Furumi, M. Takeuchi, A. Ajayaghosh, *Angew. Chem., Int. Ed.*, 2012, **51**, 10505; (c) J. M. Ribó, J. Crusats, F. Sagués, J. Claret, R. Rubires, *Science.*, 2001, **292**, 2063; (d) T. Yamaguchi, T. Kimura, H. Matsuda, T. Aida, *Angew. Chem., Int. Ed.*, 2004, **43**, 6350; (e) N. Micali, H. Engelkamp, P. G. V. Rhee, P. C. M. Christianen, L. M. Scolaro, J. C. Maan, *Nat. Chem.*, 2012, **4**, 201; (f) P. G. A. Janssen, A. Ruiz-Carretero, D. González-Rodríguez, E. W. Meijer, A. P. H. J. Schenning, *Angew. Chem., Int. Ed.*, 2009, **48**, 8103.
10. Y. Zhou, Z. X. Li, S. Q. Y. Y. Zang, Zhu, H. Y. Zhang, H. W. Hou, T. C. W. Mak, *Org. Lett.*, 2012, **14**, 1214.
11. (a) A. Winkel, R. Wilhelm, *Eur. J. Org. Chem.*, 2010, 5817; (b) H. Yamagishi, T. Fukino, D. Hashizume, T. Mori, Y. Inoue, T. Hikima, T. Aida, *J. Am. Chem. Soc.*, 2015, **137**, 7628.
12. SAINT SMART and XPREP, Siemens Analytical X-ray Instruments Inc., Madison, Wisconsin, USA, 1995.
13. Sheldrick, G. M. SADABS, *software for Empirical Absorption Correction*, University of Gottingen, Institute fur Anorganische Chemieder Universitat, ammanstrasse 4, D-3400 Gottingen, Germany, 1999.
14. G. M. Sheldrick, *Acta Crystallogr., Sect. C: Struct. Chem.*, 2015, **71**, 3.
15. Mercury 2.3 Supplied with Cambridge Structural Database, CCDC, Cambridge, U.K., 2011–2012.
16. (a) P. V. D. Sluis, A. L. Spek, *Acta Crystallogr., Sect. A: Found. Crystallogr.*, 1990, **46**, 194; (b) A. L. Spek, *Acta Crystallogr., Sect. B: Struct. Sci.*, 2009, **65**, 148; (c) A. L. Spek, *Acta Crystallogr., Sect. C: Struct. Chem.*, 2015, **71**, 9.
17. M. D. Peeks, P. Neuhaus, H. L. Anderson, *Phys. Chem. Chem. Phys.*, 2016, **18**, 5264.

CHAPTER 5

Fiber to Nanosphere Morphology Transformation and Gel-to-Sol Phase Transition Triggered by "half-crown/two carbonyl" – Ca^{2+} Metal Ion Interactions of a Low Molecular Weight Gelator (LMWG)



Publication:
To be communicated

5.1. Introduction

Of the options available to produce and modulate well-defined nanostructures from suitable molecular building blocks, none is more versatile than molecular self-assembly.¹ Among the various kinds of molecular assemblies, supramolecular gels based on low molecular weight gelators (LMWGs), which prevents the free movement of huge amount of solvent fluid opposite to the gravitational force inside the entangled 3D molecular network are considered as a very useful class of components to generates distinct nanostructures and for many proposed applications in a wide range of fields.² The driving forces for gelator molecules to self-assemble into entangled nanostructures are various weak non-covalent interactions, such as intermolecular hydrogen (H) bonding, π - π stacking, solvophobic, Van der Waals, electrostatic, and charge-transfer (CT) interactions, metal-ligand coordination *etc.*³ The weak nature of these non-covalent interactions usually makes the supramolecular gels sensitive to various external stimulus (*e.g.* chemical agents, protons, oxidation or reduction reaction, temperature, light irradiation, sound, *etc.*).⁴⁻⁷ Hence the supramolecular gel system provides a good platform for modulating wide variety of self-assembled structures and functions at molecular level.^{2,8} For realizing the visual/ optical response to an external stimulus on supramolecular gels, the design of gelator molecules is also important. In fact, with a large number of gelator molecules being developed and a better insight into the understanding of their intermolecular interactions, the design of the gelator molecules has shifted from serendipity to purpose-built design. For instance, supramolecular gels which respond to light irradiation have been achieved by incorporating photo-responsive functional groups (*e.g.* azobenzene, stilbene, imine, bithienylethene and spiropyran) into the corresponding LMWGs with conventional gelation functional moieties.⁹⁻¹³

In the midst of various chemical stimuli applied to modify gel behaviour, metal ions have been the most common regulators, as because of the availability and the diversity of metal-ligand coordination that could readily induce or control the self-assembly process of the gel formations.¹⁴ Sometimes this metal-ligand coordination also can induce the entrapped solvent molecules to be released, resulting in shrinking or even a gel-to-solution (sol) phase transition, and thereby influences its self-assemble nanostructures. For example, Edwards and co-workers reported the first example about gel-to-sol disassembly through Ag^+ -alkene weak interaction as the driving forces.¹⁵ Liu et al. have reported amphiphilic Schiff base organogels which possessed different behaviors with various metal ions. The gel was destroyed when Zn^{2+} and Ni^{2+} were added. However, the gel was maintained in presence of Cu^{2+} and Mg^{2+} and shows

twisted tape and fibrillar type nanostructures with distinct luminescence properties, respectively.¹⁶ Sobczuk and co-workers displayed a gel based on crown ether appended quaterthiophene, which showed well-defined fibrillar nanostructure in alcoholic solvents, however as in response to alkali metal ion the fibrillar nanostructure completely vanishes upon gel-to-sol phase transition with enhanced fluorescence emission.¹⁷ Terech and co-workers reported a metallosupramolecular gel based on a multitopic cyclam and bis-terpyridine platform that showed a redox-responsive gel-to-sol transition and electrochromic properties.¹⁸ In addition, Deng and co-workers developed gels of cyclodextrin amine derivatives, which can quickly exhibit a response to Co^{3+} , Ni^{2+} , Cu^{2+} and Ag^+ .¹⁹ In above all cases, the gelators have been deliberately designed to have various metal-binding motifs and shown the profound effects of metal-ligand coordination on the self-assembly process, self-assembled nanostructures with number of smart properties, including luminescence, redox activity *etc.* However, to further advance towards precise control of the self-assembly process and hence towards more complex applications, novel molecular architectures are still required.

Polyoxyethylenes, are a class of highly flexible, non-cyclic crown ether type functional group, which is known to form the complexes with metal ions (mostly alkali and alkaline earth metal ions) in the same manner as the cyclic one (crown ether) with relatively lower binding constants.²⁰ These non-cyclic ether derivatives do not show a strong complexation ability compared to that of crown ethers.²¹ However, because of the flexible nature of this functional group, the conformation of its derivatives changes drastically from a linear structure to a pseudocyclic one upon the coordination with metal ions which eventually improves their low binding ability to the metal ions.^{20,21} By taking advantage of this metal ion induced structural modulation behaviour, Nakamura and co-workers have developed a series of molecules that consisted of mono- or bis(chromophores) linked with this polyoxyethylene moiety and explored their metal ion sensing property, photo-dimerization of suitable chromophore *etc.*²² Usually, in this kind of molecular system, the chromophoric moiety and the complexing part, transduced the chemical information induced by the metal ion binding event into an optical signal, such as colourimetric and/or fluorometric changes. There are also some examples present in the literature, where the polyoxyethylene unit is utilized as a spacer in the modulation of properties of various supramolecular and biologically active systems.²³ However, the gelators, which contains this non-cyclic crown ether type functional moiety, and the impact of the weak metal ion binding event with this functional moiety on the transformation of self-assemble nanostructure upon gel-to-sol phase transition has been seldom reported.

Bearing in mind to expand the scope of responsiveness of the metal ion interactions with the polyoxyethylene units, herein, we design and synthesize a non-cyclic half-crown ether like LMWG (**L**) (Figure 5.1a), in which 4,7,10-trioxa-1,13-tridecanediamine is symmetrically functionalized through amide bond formation with an amide conjugate of 1-naphthalene acetic acid and L-phenylalanine moiety²⁴ (compound **2**; Scheme 5.1). The gelator (**L**) forms a translucent, homogeneous and stable organogel, while adopting fibrillar type morphology. In response to alkaline earth metal ion (Ca^{2+}), the fibrillar morphology of (**L**) transforms to nanospheres, which is associated with instant gel-to-sol phase transitions at room temperature. The morphological transformation is confirmed by capturing the scanning electron microscopy (SEM) and transmission electron microscopy (TEM) images. The metal ion (Ca^{2+}) coordination event with the gelator (**L**) is investigated in detail with the help of computational as well as with various spectroscopic studies. The computational and the experimental results reveal that the gelator (**L**) binds with Ca^{2+} ion using its “half-crown/two carbonyl” functional motif; the central oxygen atoms of triethylene oxide linkage and its nearer two amide-carbonyl oxygen atoms (Figure 5.1b). Apart from the Ca^{2+} ion, in response to few other alkali and alkaline earth metal ions such as Li^+ , Na^+ , K^+ , Mg^{2+} , Sr^{2+} , Ba^{2+} etc. the organogel of (**L**) also exhibits a “naked eye” gel-to-sol phase transition. So overall, the impact of the metal ion binding event with the “half-crown/two carbonyl” motif on the mechanism of fiber to nanosphere morphology transformation along with gel-to-sol phase transitions of the gelator (**L**) was presented.

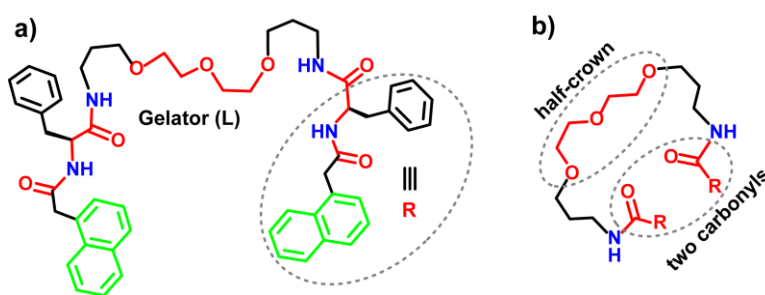


Figure 5.1. (a) The molecular structure of the Gelator (**L**); (b) Pictorial presentation of metal ion coordination site, which termed here as “half-crown/two carbonyl”.

5.2. Experimental Section

5.2.1. Materials and Methods

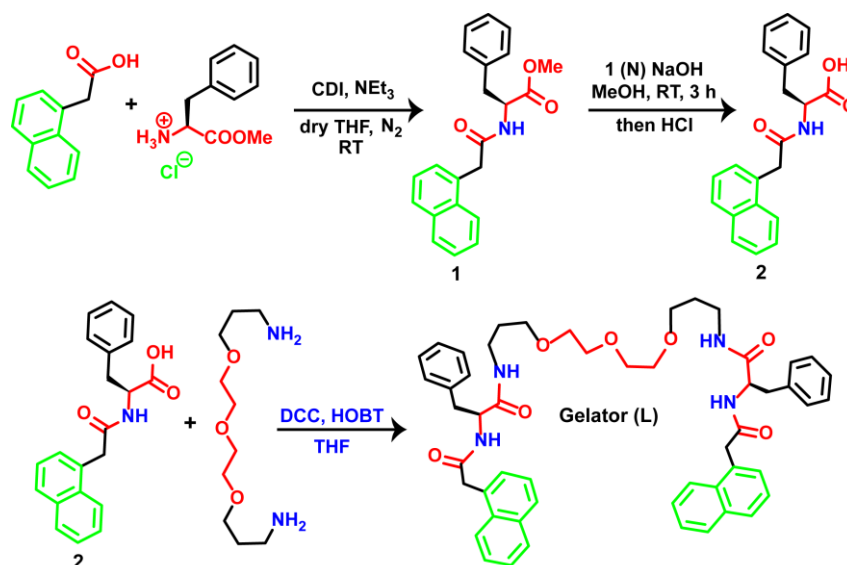
Unless otherwise stated, all reagents and organic solvents used for the synthesis of gelator (**L**) were purchased from commercial suppliers and used as such without

further purification. Solvents were dried when required according to the standard procedure.²⁵ Silica gel 100-200 mesh was used for column chromatography, to purify the synthesized gelator (**L**) and its corresponding intermediates **1** and **2** (Scheme 5.1). HPLC grade solvents were used for gelation test and for recording the spectrometric data of the gelator (**L**).

5.2.2. Instruments

¹H and ¹³C NMR spectra for the synthesized compounds were recorded on Bruker 400/500 MHz FT NMR (Model: Avance-DPX 400/500) using tetramethylsilane (TMS) as an internal standard. High-resolution mass spectra (HRMS) were recorded on JEOL JM AX 505 HA mass spectrometer. SEM images were obtained using Nova Nano SEM 450 and Quanta™ Scanning Electron Microscope. TEM images were recorded using a FEI Tecnai G2 F20 X-TWIN TEM at an accelerating voltage of 200 kV. Rheological measurements were carried out on a Rheoplus MCR302 (Anton Paar) rheometer with parallel plate geometry and obtained data were processed with start rheometer software. The gap distance between the plates was fixed at 0.5 mm. UV-Vis absorption spectra measurements were documented using Perkin Elmer Lambda 950 UV-Vis spectrometer. All emission spectra measurements were performed using PTI Quanta Master™ steady state spectrofluorometer. Fourier transform infrared (FT-IR) transmittance spectra were recorded on a FTIR-8300 (Shimadzu) spectrometer with 2 cm⁻¹ resolution at room temperature.

5.2.3. Synthesis of Gelator (**L**)



Scheme 5.1. Methodology that was adopted for the synthesis of gelator (**L**).

Initially, the amide conjugate of 1-naphthalene acetic acid and L-phenylalanine (compound **2**, Scheme 5.1), an intermediate that was used for the synthesis of gelator (**L**), was prepared by following the previously reported procedure.²⁴ This synthesized intermediate; compound **2** (1.0 mmol) was taken in 25 mL of dry tetrahydrofuran (THF) and cool to 0 °C for 10 mins under N₂ atmosphere. To this cold solution, 4,7,10-trioxa-1,13-tridecanediamine (0.5 mmol) was added. To this resulting reaction mixture, subsequently, N,N'-dicyclohexylcarbodiimide (DCC, 1.0 mmol) and 1-hydroxybenzo triazole (HOBT, 1.0 mmol) were added. The reaction mixture was stirred for about 6 hrs under an inert condition at room temperature. The progress of the reaction was monitored by TLC (eluent phase was 4 : 96; MeOH : CHCl₃). After completion of the reaction, THF was removed from the reaction mixture by vacuum and 100 ml of dichloromethane (DCM) was added to it. The DCM layer was washed subsequently with saturated NaHCO₃ (3 × 30 mL), dilute HCl (3 × 30 mL), water (3 × 30 mL) and brine solution (2 × 30 mL). Solid was then dried over anhydrous sodium sulfate. The organic layer was evaporated under reduced pressure to get crude gelator (**L**), which was purified by column chromatography using the 2 % MeOH in CHCl₃ gradient solvent system to give pure gelator (**L**) as white solid. Yield = 56 %. ¹H NMR (500 MHz, DMSO-d₆): δ (ppm) 8.43-8.42 (2H, d, *J* = 8, NH), 7.98-7.96 (2H, t, NH), 7.90-7.87 (4H, t, Nap-H), 7.78-7.76 (2H, d, *J* = 8, Nap-H), 7.49-7.46 (2H, t, Nap-H), 7.44-7.41 (2H, t, Nap-H), 7.39-7.36 (2H, t, Nap-H), 7.28-7.27 (2H, d, *J* = 7, Nap-H), 7.22-7.20 (10H, broad, Ar-H), 4.50-4.46 (2H, m, -CHCO), 3.90-3.88 (4H, broad, Nap-CH₂), 3.50-3.48 (4H, m, -C-CH₂-O), 3.43-3.42 (4H, m, -C-CH₂-O), 3.31-3.29 (4H, t, -N-CH₂-C), 3.13-3.02 (4H, m, -C-CH₂-O), 2.98-2.94 (2H, m, Ar-CH₂), 2.83-2.78 (2H, m, Ar-CH₂), 1.56-1.55 (4H, broad, -C-CH₂-C); ¹³C NMR (125 MHz, DMSO-d₆): δ (ppm) 170.79, 169.68, 137.71, 133.14, 132.56, 131.82, 129.07, 128.14, 127.9, 127.58, 126.82, 126.11, 125.75, 125.41, 125.29, 124.14, 69.63, 69.42, 67.80, 53.99, 37.93, 35.70, 29.03; HRMS (ESI): *m/z* calculated for C₅₂H₅₉N₄O₇ [M + H]⁺: 851.436, found 851.437.

5.2.4. Computational Methods

The conformational search of the gelator (**L**) and the metal ion (Ca²⁺) binding event with its "half-crown/two carbonyl" binding motif was examined with MMFF94 (Merck Molecular Force Field) force field.²⁶⁻²⁸ The conformational search was performed using the Spartan 08 program.²⁹ Further, we considered the most stable structure from the conformational analysis and optimized the selected structure with DFT B3LYP functional using the 6-31G* basis set.³⁰⁻³² Water was employed as a solvent using SMD solvent model.³³ The vibrational frequency calculations suggest that the obtained geometry is a minimum. All calculations are performed in Gaussian 09 suite of

programs.³⁴The conformation search yielded the various conformers of gelator (**L**). Similar effort with corresponding (**L**) bound to Ca²⁺-ion resulted a number of energy-optimized structures. Among all these structure, we have chosen the most stable one for (**L**) as well as for (**L**) that was bound to Ca²⁺.

5.2.5. General Description of Different Experimental Techniques

5.2.5.1. Gelation Test

A weighted amount gelator (**L**) was suspended in a series of selected organic solvents (1.0 mL) and tried to dissolve by heating in closed vial condition. The evolved hot clear solution was cooled to room temperature and then sonicated for 2-3 minutes. The system suddenly turned to semisolid like soft mass. Inverted glass vial technique was adopted to ensure the gel formation. Gelation was observed in acetonitrile and alcoholic (methanol, ethanol) solvent.

5.2.5.2. Scanning Electron Microscopy (SEM)

A small portion of the freshly prepared acetonitrile, methanol and ethanol gel obtained from the gelator (**L**) was scooped out and diluted with the respective solvents. The resulting solutions were drop-casted on a silicon wafer and allowed to air dry for 5 hours in a dust free environment. Finally, it was dried under desiccator for overnight. Before taking images, samples were coated with gold vapor. To check the effect of Ca²⁺ metal ion coordination with the gelator (**L**) on its morphology, a required amount of Ca²⁺ ion (in acetonitrile medium; 2.0 equivalents) was added to the acetonitrile gel of (**L**). Immediate after the addition of Ca²⁺, the gel turns into a solution. After 1 hour, a small portion of this subsequent solution was pipet out and diluted with acetonitrile and used for preparing the SEM sample by following the above-mentioned procedure.

5.2.5.3. Transmission Electron Microscopy (TEM)

The prepared same samples (with and without Ca²⁺ treated) which were used for (SEM analysis), were drop-casted on carbon-coated copper grids (200 mesh) and initially allowed to air dry for 6 hours in a dust-free place followed by under desiccator for overnight. The dried samples were employed for taking TEM images without staining.

5.2.5.4. Rheology

A freshly prepared acetonitrile gel (0.9 mg/mL) of (**L**) was carefully scooped out and placed on the parallel plate of the rheometer very quickly to minimize solvent

evaporation. Dynamic strain sweep tests were carried out to increase the amplitude of oscillation from 0.1% up to 100% apparent strain shear (with a frequency $\omega = 10 \text{ rad s}^{-1}$) at 25 °C. Frequency sweep experiment was performed from 0.1 to 100 rad/s at constant strain (γ) of 1 % at 25 °C.

5.2.5.5. UV-vis and Fluorescence Studies

A stock solution of (**L**) ($1.0 \times 10^{-3} \text{ M}$) was prepared in acetonitrile, and this solution was used for all electronic and fluorescence spectral studies after appropriate dilution with acetonitrile. Except for the K^+ , the perchlorate salts of each alkali and alkaline earth metal ions (Li^+ , Na^+ , K^+ , Mg^{2+} , Ca^{2+} , Sr^{2+} and Ba^{2+}) were used to prepared initially $1.0 \times 10^{-3} \text{ M}$ of stock solution in acetonitrile and used these solutions after appropriate dilution. For K^+ ion, we had used its hexafluorophosphate salt, as KClO_4 lacked the desired solubility in acetonitrile.

5.2.5.6. Fourier Transform Infrared (FT-IR) Study

2.0 mM acetonitrile solutions of (**L**) [in presence 5.0 equivalent of Ca^{2+} and in absence of Ca^{2+} metal ion] were used for FT-IR measurements. Approximately 60 microliters of freshly prepared corresponding sample solutions were loaded into a demountable cell consisting of two windows (CaF_2 , 3 mm thickness, Shenzen Laser), separated by a mylar spacer of 50 micrometers thickness, and FT-IR spectra were recorded.

5.3. Results and Discussions

The design and synthetic steps for the construction of the gelator (**L**) were shown in Scheme 5.1. We rationally introduced the central oxyethylene spacer (half-crown) and the two carbonyls units as metal ion binding scaffold, and the terminal two amide conjugate of 1-naphthalene acetic acid and L-phenylalanine moiety (compound **2**; Scheme 5.1) for self-assembly as a consequence of multiple intermolecular interactions (such as hydrogen (H) bonds, π - π stacking and CH- π interactions *etc.*) to afford better and outstanding gelation.²⁴ Desired gelator (**L**) was isolated in pure form after necessary workup. This compound was further characterized by using various analytical and spectroscopic techniques. Analytical and spectroscopic data for (**L**) confirmed the desired purity and this was used for our further studies.

First, the gelation ability of (**L**) was checked in different organic solvents (Table 5.1). Among the various solvents (Table 5.1), (**L**) was found to be sparingly soluble in acetonitrile, methanol and ethanol under ambient condition. However, it was found to dissolve completely after heating. The hot clear solution upon cooling and subsequent

sonication for 2-3 minutes, the system suddenly turned into semisolid like soft mass, which we identified as gel by the "stable-to-inversion protocol of a glass vial". The critical gelator concentration (CGC) value was determined for each solvent (Table 5.1). Figure 5.2a shows the photograph of the corresponding acetonitrile gel (CGC = 0.9 wt %) of (**L**). This was found to be translucent in appearance and remained stable for a long period of time under closed vial condition. The resulting gel was found to be highly thermo reversible; upon heating, it transformed to the solution and reverted to gel state after cooling to room temperature with little sonication (Figure 5.2b). The gelator (**L**) turn into partial gel in 1,4-dioxane and toluene, whereas it was insoluble in ethyl acetate and in hexane and was found to be soluble in each of CH₂Cl₂, CHCl₃, THF, DMF and DMSO solvents (Table 5.1).

Table 5.1. Gelation properties of **L** in different solvents.^a

Solvent	State	CGCs (wt %)
Hexane	I	-
Toluene	PG	-
Ethyl acetate	I	-
1,4-Dioxane	PG	-
DCM	S	-
CHCl ₃	S	-
Acetonitrile	G	0.9 w/v
Methanol	G	1.0 w/v
Ethanol	G	1.0 w/v
THF	S	-
DMF	S	-
DMSO	S	-

^aI = insoluble, S = solution, G = gel, PG = partial gel; gel formed by heating cooling followed by slight sonication.

In order to verify whether the identified semisolid like soft mass as gel through "stable-to-inversion protocol of a glass vial" (Figure 5.2a), is actually a gel or not? We further examined its viscoelastic behavior by rheology experiments. The viscoelastic behavior of gel is generally determined by two key parameters, elastic modulus (G' : solid-like behavior) and viscous modulus (G'' : liquid-like behavior). Figure 5.2c and 5.2d respectively showed the dynamic oscillatory stress sweep and a frequency sweep of the corresponding obtained soft mass (Figure 5.2a) of (**L**). It is evident from the

Figure 5.2c, initially G' is higher than G'' and both accomplish a linear signature. The linear viscoelastic region (Figure 5.2c) where the $G' > G''$, the solid character of this soft mass. Beyond the linear viscosity region at certain stress (25.02 Pa), G' fell lower than G'' , and the soft mass transformed into a liquid-like appearance (Figure 5.2c). Therefore, beyond the 25.02 Pa of oscillatory stress, it began to flow. The frequency sweep experiment, where the G' and G'' were measured as a function of angular frequency at 0.1 % constant strain, plot displayed that all G' values of the corresponding soft mass was much higher than that of G'' for the entire frequency range (Figure 5.2d). Both G' and G'' values were found to be weakly dependent on frequency, which signified the presence of some weak matrixes.³⁵ Higher magnitude of G' (Figure 5.2d) indicates the presence of an appreciable mechanical strength in this soft mass. Results of these thorough rheological experiments helped us to confirm that the identified semi-solid like soft mass (Figure 5.2a) possessed a certain degree of viscoelasticity and it actually was a gelatinous material.

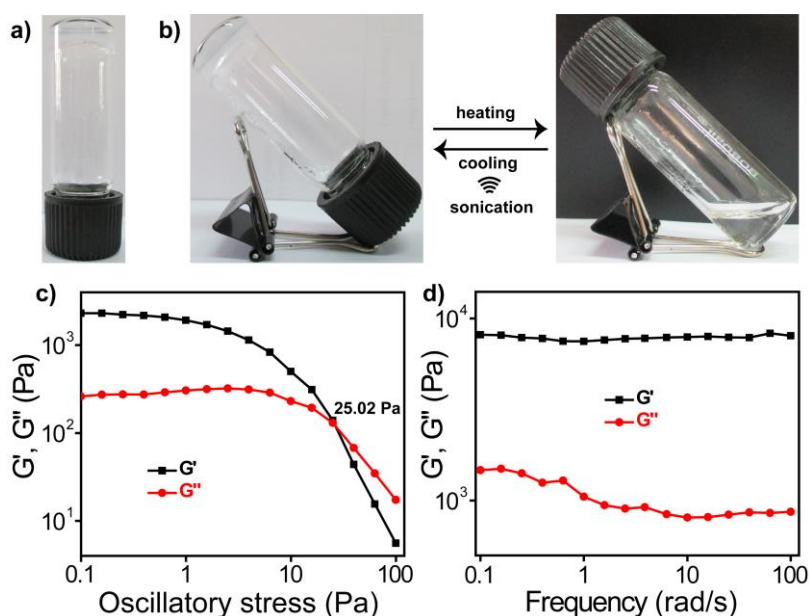


Figure 5.2. Photographs showing (a) freshly prepared translucent acetonitrile gel of (L) and (b) its temperature induced reversible gel-to-sol transition. Dynamic oscillatory stress sweep (c) and frequency sweep (d) of the acetonitrile gel of (L).

To reveal the molecular self-assembled structures at the nanoscale level of organogels of (**L**) in acetonitrile, methanol and ethanol solvent, SEM and TEM were performed. SEM image of the dilute solution of acetonitrile gel of **L** showed thin plates, which continuously connected to each other and formed flat and flexible ribbon-like network morphology (Figure 5.3a). However, SEM images of the corresponding dilute solutions obtained from methanol and ethanol gels of (**L**) showed entangled fibrous structures of high aspect ratio (Figure 5.3b and 5.3c). Although the SEM image of the acetonitrile gel of (**L**) showed a thin plate-like structure, the TEM result of the corresponding same solution sample showed well-developed fibrous network structure (Figure 5.3d). The observed fibrous network consisted of entangled thin fibrils of nanometer diameter and micrometer length (Figure 5.3d). This finding was also observed from the TEM images of methanol and ethanol gels of (**L**), respectively (Figure 5.3e and 5.3f). Results of the SEM and TEM experiments signify that the formation of the entangled fibrillar structure is a key step for gel formation of (**L**).

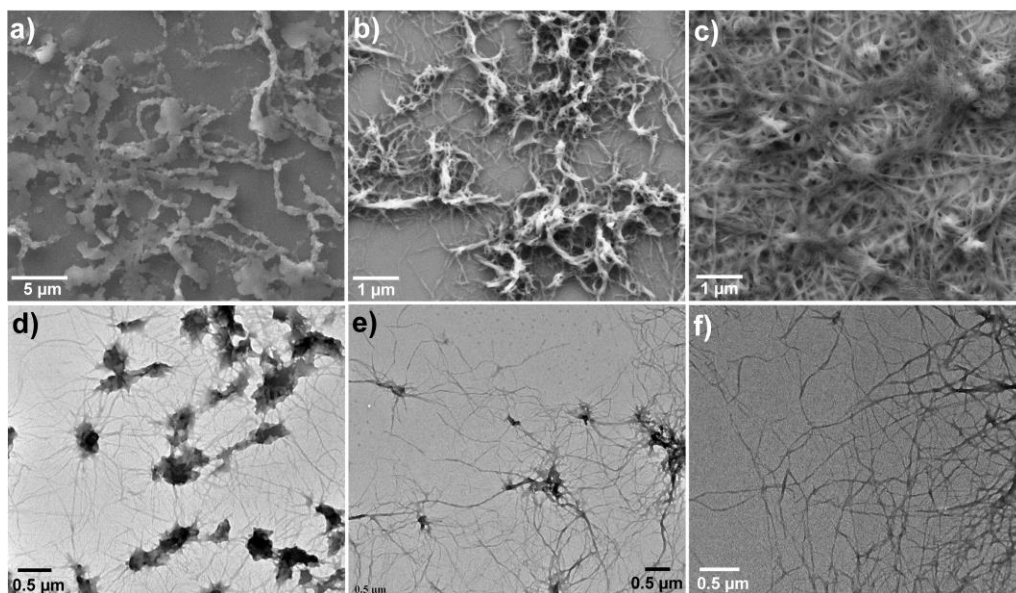


Figure 5.3. (a-c) SEM images of diluted acetonitrile, methanol and ethanol gel respectively, and (d-e) TEM images of diluted acetonitrile, methanol and ethanol gel respectively.

We expected the purpose-built gelator (**L**) to reveal the influence of metal ion on the molecular self-assembly behavior of (**L**). To examine this, we gently added the various mole equivalent of Ca^{2+} ion (as its perchlorate salt) as acetonitrile solution onto the pre-formed acetonitrile gel (0.9 wt %) of (**L**). We observed that, after immediate contact of the Ca^{2+} ion, the gel phase of (**L**) becomes unstable and starts transform into solution. Up to addition of bellow 1.0 equivalent of Ca^{2+} , the acetonitrile gel of (**L**) exists

in the partial gel state. However, with the addition of 1.0 or above the 1.0 equivalent of Ca^{2+} into the acetonitrile gel of (L), lead to the collapse of gel phase from top to bottom as the salts diffuse through the gel and transmute into a homogeneous solution. Photograph of gel-to-sol phase transition of acetonitrile gel (0.9 wt %) of (L) in response to 2.0 equivalent of Ca^{2+} ion is shown in Figure 5.4a. Stability of the acetonitrile gel of (L) was further tested with the addition of some other alkali and alkaline earth metal ions such as Li^+ , Na^+ , Mg^{2+} , Sr^{2+} , Ba^{2+} etc. (as their perchlorate salts) as well as the hexafluorophosphate salt of K^+ . In case of Li^+ , Na^+ , Mg^{2+} , Sr^{2+} , Ba^{2+} the gel phase was maintained partially till 1.0 mole equivalent of any one of these metal ion was added. With the addition of more than 1.0 equivalent of these metal ions, the gel was found to be converted to the solution as it was observed for the Ca^{2+} ion. For K^+ ion, the gel phase of (L) was maintained till 1.0 mole equivalent of K^+ was added. With the addition of more than 1.6 equivalent of K^+ , the gel phase was transformed to the homogeneous solution. These results clearly establish that this gel phase of (L) has the responsive nature to alkali and alkaline earth metal ions.

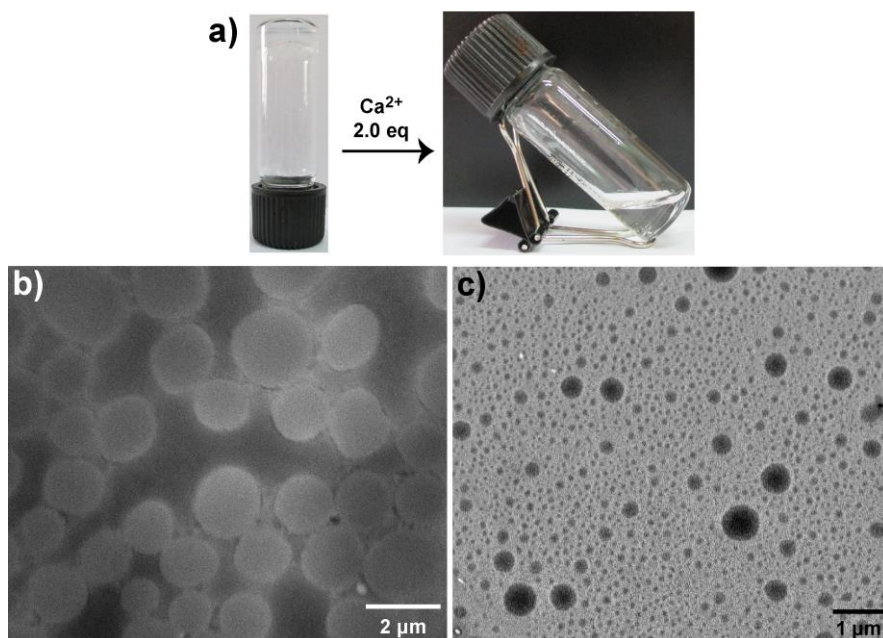


Figure 5.4. (a) Gel-to-Sol phase transition of acetonitrile gel (0.9 wt %) of (L) with the addition of 2.0 equivalents of the Ca^{2+} ion; (b and c) SEM and TEM image of the corresponding transformed sol solution (after proper dilution) respectively, show the nanosphere morphology formation with complete disappearance of the fibrillar network.

As the metal ion treatment influence the gel-to-sol phase transition, thus one might expect that self-aggregated network structure can also be affected. To examine this, SEM and TEM characterizations were performed of the dilute solution of the corresponding transformed gel-to-sol solution (Figure 5.4a) obtained after the addition of 2.0 equivalent of Ca^{2+} ion in acetonitrile gel of (**L**). Interestingly both the SEM and TEM images of the transformed sol solution of (**L**) showed a spurted nanosphere architecture (Figure 5.4b and 5.4c), with complete disappearance of their network structure (Figure 5.3a and 5.3d). This observation again confirms that the treatment of metal ion on the designed gelator (**L**) has a serious effect on its self-assembly mode which eventually triggers its morphology transformation and gel-to-sol phase transition.

After direct visualization of morphological transition from fibrillar network to nanosphere structure microscopically and naked eye detection of gel-to-sol phase transition (Figure 5.4); we are very much curious to find out the involved noncovalent interactions in gelator (**L**) and alteration of these noncovalent interactions and the specific mode of binding of Ca^{2+} in its $\text{L} \cdot \text{Ca}^{2+}$ complex. As these are the crucial factors to determine the particular molecular arrangement in self-aggregated state and established the mechanism of self-assembly process. In this milieu, the solid-state single crystal structure is the ultimate proof to establish the precise molecular arrangement and envisage the operating noncovalent interactions of any assemblies in their self-assemble state. Unfortunately after repeated trying in various solvent composition and experimental condition, we are unable to grow the single crystal of the (**L**) and its $\text{L} \cdot \text{Ca}^{2+}$ complex. As an alternative, a computational optimization study was carried out for the (**L**) and its Ca^{2+} complex $[\text{L} \cdot \text{Ca}(\text{ClO}_4)_2]$, based on density functional theory (DFT) calculations employing the hybrid B3LYP functional equipped with a 6-31G* basis set.³⁰⁻³²

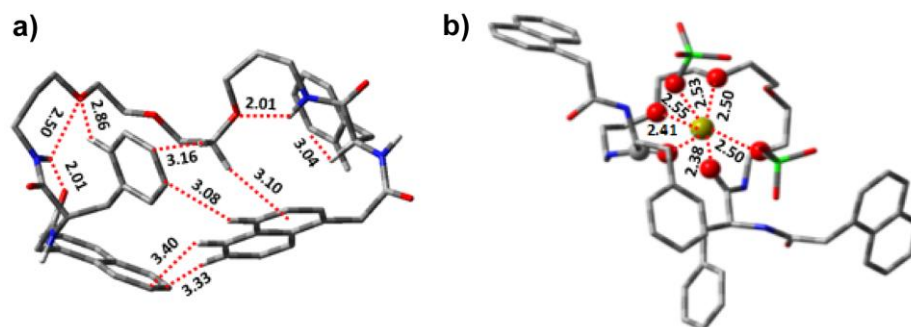


Figure 5.5. The optimized structure of gelator (**L**) and $\text{L} \cdot \text{Ca}^{2+}$ complex at B3LYP/6-31G* in aqueous phase. Non interacted H atoms are omitted for clarity. (Color code: red = oxygen; blue = nitrogen; grey = carbon; green = chlorine; olive = calcium).

The optimized structure of the metal-free gelator (**L**) showed that it attained an interesting folded structure with the assistance of several intramolecular H-bonds among the carboxyamides, aromatic H-atoms and the ethereal oxygen atoms (Figure 5.5a). A critical inspection of the Figure 5.5a reveals that the aromatic rings of the gelator (**L**) interact with each other via $\text{CH}\cdots\pi$ and $\pi\cdots\pi$ interactions. The cumulative effect of these interactions, (namely intramolecular H-bonds, $\text{CH}\cdots\pi$ and $\pi\cdots\pi$ interactions) helped the gelator (**L**) to attain this folded structure (Figure 5a). The gelator (**L**) also have free amide ($-\text{NHCO}$) functional groups (Figure 5.5a). One would expect these amide functionalities to help in the formation of the extended intermolecular H-bonds among the consecutive (**L**) molecules and eventually resulted in a fibrillar network-like structure and gel formation. The energy optimized structure of the $\text{L}\cdot\text{Ca}^{2+}$ complex having ClO_4^- counter ion is shown in Figure 5.5b. It was really interesting to note that for the energy optimized structure of metal-free gelator (**L**), the central oxyethylene moiety was poisoned in the anti-direction of its adjacent two carbonyl groups (Figure 5.5a). However, the optimized metal complex structure ($\text{L}\cdot\text{Ca}^{2+}$) showed that, both the carbonyl groups turned toward the same direction of the oxyethylene moiety (Figure 5.5b). Due to this conformation change, gelator (**L**) formed a crown ether like cavity and the Ca^{2+} ion was encapsulated within it with the help of binding to the two central amide-carbonyl oxygen and two ethereal oxygen atoms of the half-crown like triethylene oxide linkage of (**L**) (Figure 5.5b). Interestingly, two counter anions (ClO_4^-) also remained bond to the Ca^{2+} metal ion effectively and hence the $[\text{L}\cdot\text{Ca}(\text{ClO}_4)_2]$ complex accomplished a 6-coordinated quasi-octahedral type geometry with $\text{Ca}^{2+}\cdots\text{O}$ distances of 2.38-2.55 Å (Figure 5.5b). The gelator (**L**) therefore utilized its "half-crown/two carbonyl" binding motif to coordinate the Ca^{2+} metal ion (Figure 5.1b and 5.5b). Again, in comparison to the optimized structure of (**L**), the $[\text{L}\cdot\text{Ca}(\text{ClO}_4)_2]$ structure shows, upon coordination of Ca^{2+} metal ion, two naphthalene rings are positioned far away from each other and entire molecular orientation changes in such a way that all the existed non-covalent interactions (intramolecular multiple H-bonds, $\text{CH}\cdots\pi$ and $\pi\cdots\pi$ interactions *etc.*) in the metal-free gelator (**L**) completely disappears. Further, the electrostatic repulsion is also a common problem among the bound metal ions to a ligand, which usually hampered the intermolecular interactions among the consecutive molecules and results in their disassembly process.¹⁵ Perhaps, in our molecular system, the gelator (**L**) also possesses this strong charge repulsion force after the binding of Ca^{2+} ions, which profoundly affect to disrupt the inter and intramolecular H-bonds, $\text{CH}\cdots\pi$ and $\pi\cdots\pi$ interactions *etc.* and finally leads to a dissociation of the gel phase and its fibrillar network to nanosphere morphology transition

To investigate the changes in various non-covalent interactions at the molecular scale, we recorded and analyzed the FT-IR spectrum of the gelator (**L**) with and without Ca^{2+} ion in acetonitrile. The peak at 1631 cm^{-1} was attributed to the amide carbonyl stretch ($-\text{C}=\text{O}_{\text{amide, str}}$) of (**L**) in absence of metal ion (Figure 5.6; blue line). The position of this peak in the IR frequency range, as well as the weak and broad nature in appearance, collectively indicated the unambiguous signature of a network of H-bonded amides in the metal-free (**L**). On addition of Ca^{2+} , the corresponding amide carbonyl peak shifted to 1647 cm^{-1} and became sharp (Figure 5.6; green line). This shifting of peak position to higher wavenumber region and sharpening in the appearance (Figure 5.6; green line) were certainly linked to the disruption of H-bond and increase in the population of non H-bonded amide carbonyl. Thus, it was not unreasonable on our part to presume that the gel network of **L** was underpinned by intermolecular H-bond interactions among the amide ($-\text{NHCO}$) groups, and the disruption of these H-bonds on binding to Ca^{2+} ion was the primary reason for the collapse the gel phase of (**L**). This was linked to the fiber to nanosphere morphology transformation. The two peaks at 3541 cm^{-1} and 3626 cm^{-1} of (**L**) in absence of Ca^{2+} ion were assigned for the N-H stretch (N-H_{str}) (Figure 5.6; blue line). However, due to the interference of water molecule with the addition of Ca^{2+} salt, these two N-H stretches of **L** merged and appeared as a broad band at 3506 cm^{-1} (Figure 5.6; green line). The peaks at 2945 cm^{-1} and 3005 cm^{-1} of (**L**) could be attributed to the aliphatic $-\text{C-H}$ stretch ($-\text{C-H}_{\text{str}}$, Figure 5.6; blue line) and no apparent change was observed for these bands (Figure 5.6; green line). This indicated that aliphatic $-\text{C-H}$ did not participate in metal ion coordination event, which was rather anticipated.

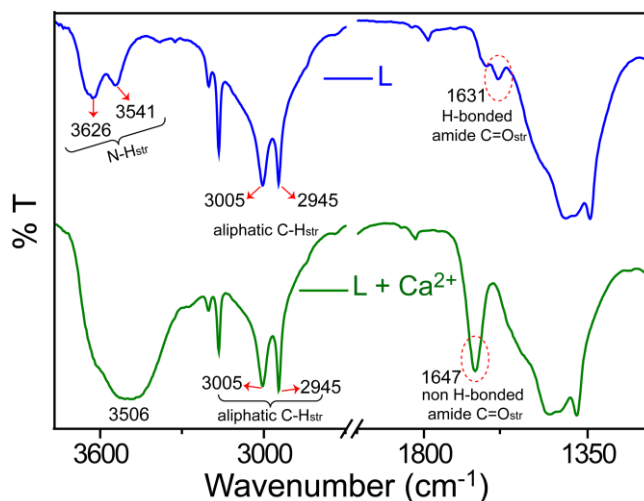


Figure 5.6. FT-IR spectra of 2.0 mM acetonitrile solution of gelator (**L**) in the presence (green line) and absence (blue line) of 5.0 equivalent of the Ca^{2+} ion.

Next In order to shed light on the coordination mode of (**L**) with the Ca^{2+} ion, we performed ^1H NMR study of (**L**) in absence and presence of a Ca^{2+} ion in DMSO-d_6 at 25°C . Due to the low solubility and high gelatinous nature of (**L**) in acetonitrile, it was not possible to investigate the ^1H NMR study in d_3 -acetonitrile. The ^1H NMR spectra of (**L**) before and after the addition of Ca^{2+} are shown in Figure 5.7 as a typical result. Assignments of the important protons were ascertained by using TOCSY NMR spectra (Figure 5.8). On complexation of (**L**) to Ca^{2+} , almost all protons were found to shift to the higher magnetic field (Figure 5.7). The central oxyethylene protons of (**L**) (protons a, b and c; Figure 5.7) showed an insignificant up-field chemical shift upon complexation. This indicates that the Ca^{2+} ion was weakly coordinated to the ethereal oxygen atom. On the other hand, the amide proton 'f' (Figure 5.7), adjacent to the central oxyethylene moiety, showed considerable up-field shift ($\Delta\delta = -0.09$ ppm) in presence of Ca^{2+} . This observation revealed that the Ca^{2+} ion is coordinating strongly with the two carbonyl oxygen atom. Another set of amide proton 'g' (Figure 5.7) also showed a significant up-field shift upon complexation of (**L**) to Ca^{2+} . The considerable shifts in the resonance of amide protons and also the oxyethelen protons signals were definitely due to the structural reorganization(s) and change(s) in the conformation of (**L**) during the binding of its central "half-crown/two carbonyl" motif toward Ca^{2+} . This was further rationalized based on the optimized structures (Figure 5.5) obtained from computational studies. Such structural reorganization and conformational change was induced by complexation of the Ca^{2+} ion and these presumably allowed certain protons to move into the shielded zone of the naphthalene moiety (Figure 5.5) and accounted for their diamagnetic shifts.^{22c}

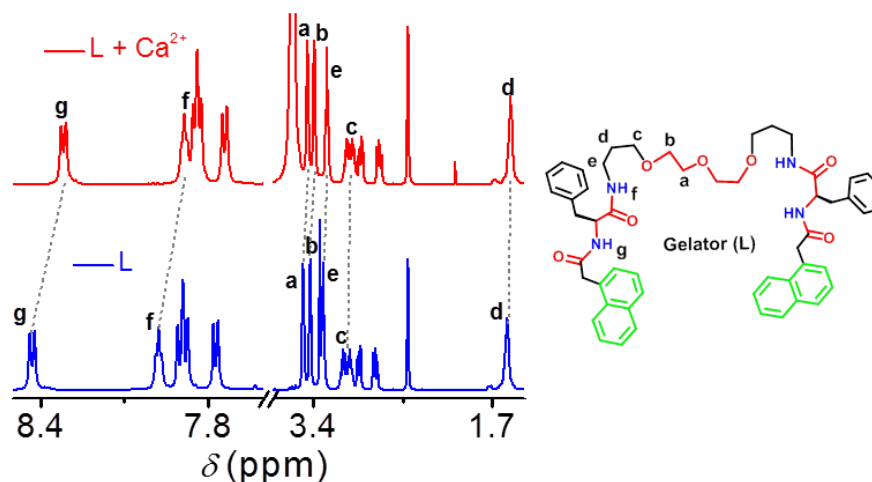


Figure 7. Partial ^1H NMR spectra (500 MHz, 25°C) in DMSO-d_6 , of gelator (**L**) (blue line; 20.0 mM) and after the addition of 5.0 equivalent of Ca^{2+} (red line).

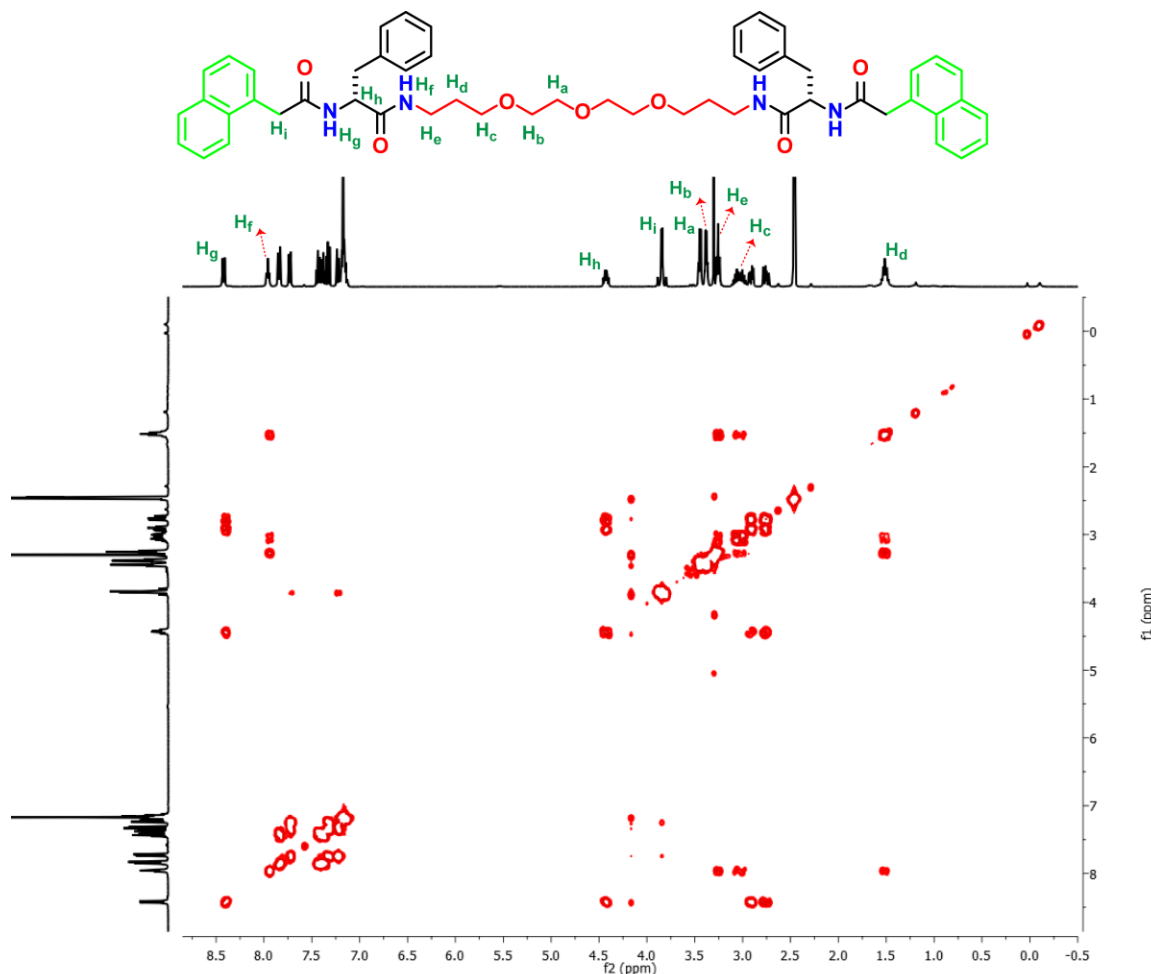


Figure 5.8. TOCSY NMR spectra (400 MHz, 25°C) of gelator (**L**) in DMSO- d_6 .

The presence of chromophoric naphthalene unit in (**L**) further enabled us to study the binding process using electronic and fluorescence spectroscopy. The UV-Vis spectrum of (**L**) was recorded in acetonitrile solution (1.0×10^{-5} M) at 25°C and this showed band maxima at 283 nm with two shoulders at 272 and 293 nm. The band at 283 nm was attributed to the π - π^* transitions of naphthalene moiety (Figure 5.9a; black line). The recorded fluorescence spectrum ($\lambda_{\text{ex}} = 283$ nm) of the same solution that was used for recording the UV-Vis absorption spectrum, showed two maxima at 328 and 337 nm (Figure 5.9b; black line). Upon addition of 20 mol equivalents of Ca^{2+} salts in acetonitrile, failed to induce any significant change in the absorption spectrum of (**L**) (Figure 5.9a; orange line). In contrast to the absorption spectrum, with the addition of 20 mol equivalent Ca^{2+} , the fluorescence intensity of the (**L**) was found to increase a little (Figure 5.9b; orange line), which was attributed to the proposed complex formation between (**L**) and Ca^{2+} .

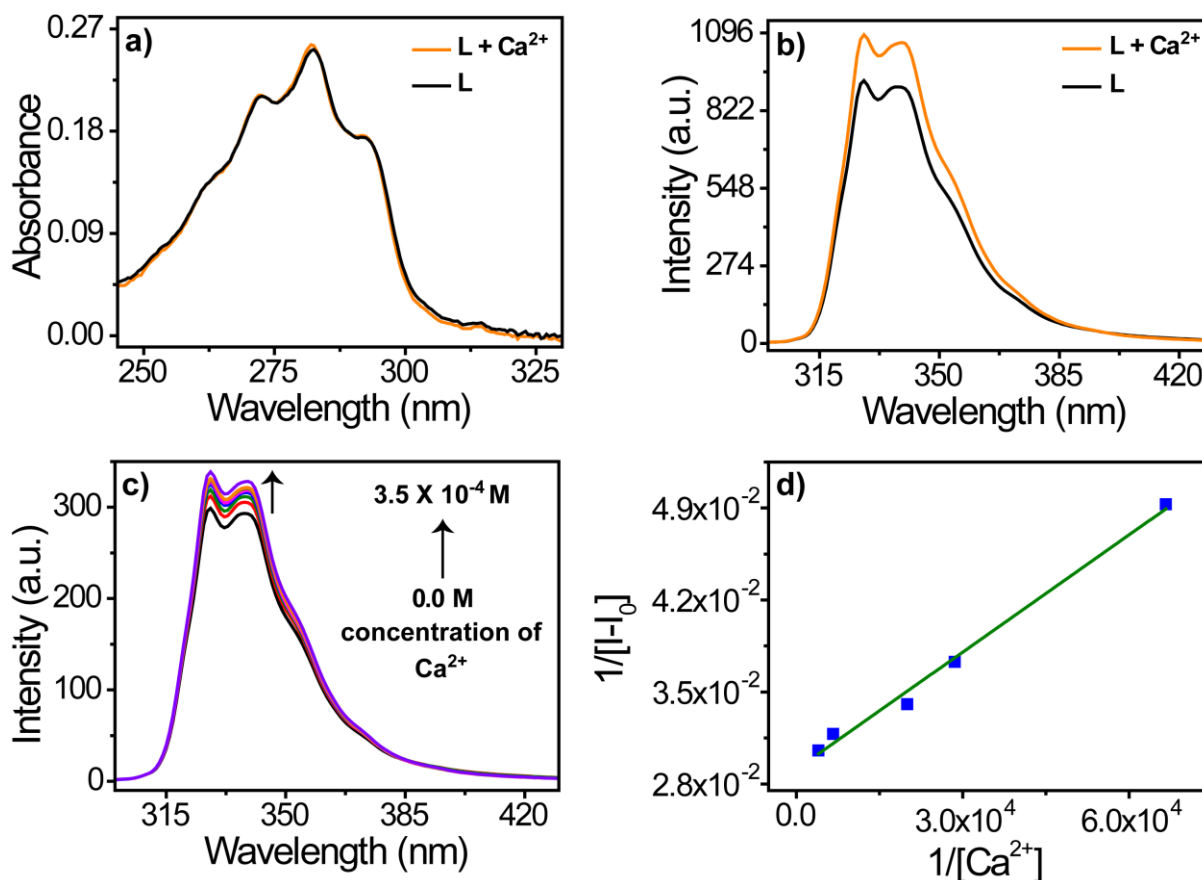


Figure 9. UV-Vis absorption (a) and fluorescence (b) spectra of gelator (L) (1.0×10^{-5} M) in absence (black line) and presence (orange line) of 20 mol equivalent of Ca²⁺ ion; (c) change in fluorescence spectral pattern for (L) (1.0×10^{-5} M) with varying the concentrations of Ca²⁺ (from 0.0– 3.5×10^{-4}); (d) Benesi–Hildebrand (B-H) plot of $1/[I - I_0]$ vs $1/[Ca^{2+}]$. For all studies were performed in pure acetonitrile medium, for fluorescence spectra ($\lambda_{\text{ex}} = 283$ nm).

Presumably, binding to Ca²⁺ helped in attaining a little more rigid structure compared to its metal-free flexible form (Figure 5.5a and 5.5b), and hence the increase in luminescence intensity took place. The binding affinity of (L) towards Ca²⁺, was evaluated based on a systematic fluorescence titration in acetonitrile medium with varying the concentrations of Ca²⁺ (from 0.0 - 3.5×10^{-4} M), while the concentration of (L) was kept constant (1.0×10^{-5} M). With the increase of Ca²⁺ ion concentration, a small but gradual increase of emission intensity of (L) was observed (Figure 5.9c). Using parameters that were obtained from this titration plot (Figure 5.9c), formation constant (K_a) for L•Ca²⁺ was evaluated using Benesi-Hildebrand (B-H) plot (Figure 5.9d), and it was found to be $(9.7 \pm 0.2) \times 10^4 \text{ M}^{-1}$. A good linear fit of the B-H plot for $1/[I - I_0]$ vs $1/[Ca^{2+}]$ also confirmed the 1 : 1 binding stoichiometry.³⁶ Calculated formation constant

value for the formation of $L \cdot Ca^{2+}$ in pure organic solvent confirmed a moderate binding affinity.

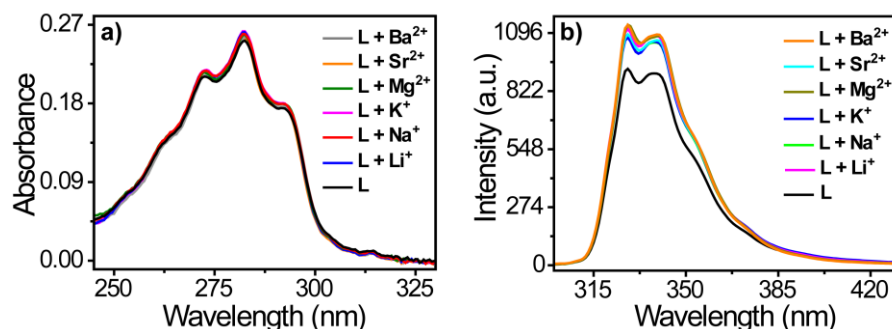
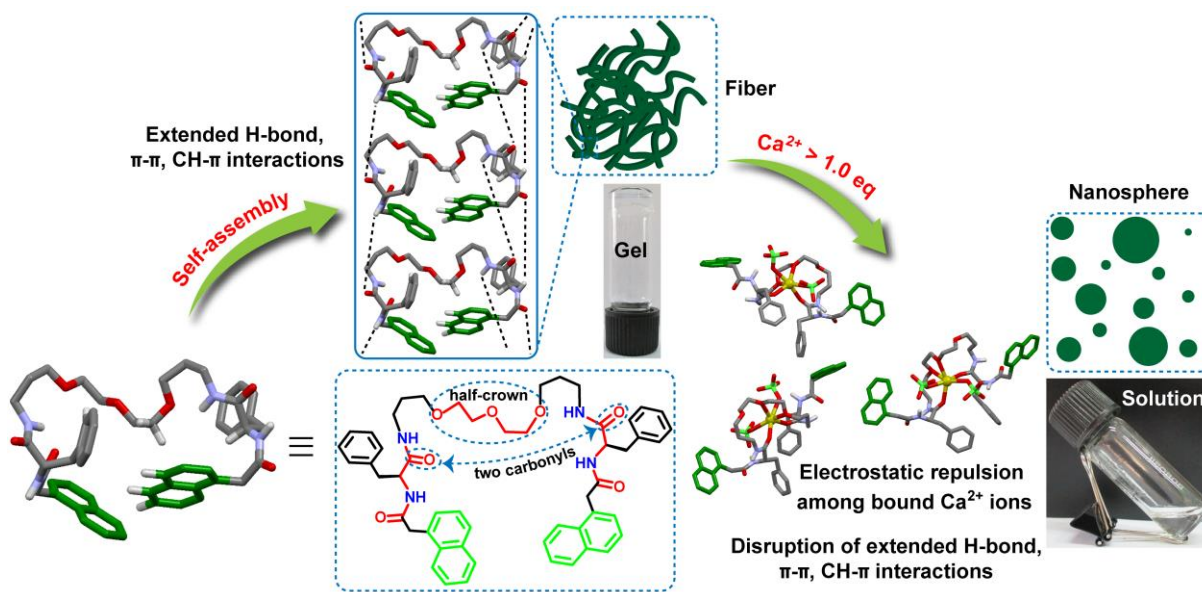


Figure 10. (a) Uv-Vis absorption, (b) fluorescence spectra of gelator (**L**) (1.0×10^{-5} M) in absence and presence of 20 mol equivalent of different alkali and alkaline earth metal ions in acetonitrile medium. For fluorescence spectra ($\lambda_{\text{ex}} = 283$ nm).

We had also recorded UV-Vis and fluorescence spectra of the of (**L**) (1.0×10^{-5} M) in presence of other alkali and alkaline earth metal ions (such as Li⁺, Na⁺, K⁺, Mg²⁺, Sr²⁺ and Ba²⁺) in acetonitrile medium. The results are identical as we observed for the case of the Ca²⁺ ion. No detectable change in absorption spectrum was observed, whereas a little enhancement in emission intensity of the (**L**) was observed when the specified metal ion (Figure 5.10a and 5.10b) was added.

Based on the results of the above discussed experimental facts and theoretical calculations, it is now possible to summarize the impact of Ca²⁺ ion coordination with the "half-crown/two carbonyl" motif of (**L**) on the mechanism of its fiber to nanosphere morphology transformation along with gel-to-sol phase transition. Metal-free gelator (**L**) initially enriched with various noncovalent interactions such as intramolecular H-bonds among the carboxyamides, aromatic H-atoms and the ethereal oxygen atoms (Figure 5.5a). Along with these intramolecular interactions, during the course of self-assembly, the conjunctive (**L**) molecules could build an extended network structure with the help of intermolecular H-bonding interactions among the amide (-NHCO) groups. This resulted into a gel formation with entangled fibrillar morphology (Scheme 5.2). This is evident that H-bonding interactions among the amide (-NHCO) groups play a crucial role in achieving the fibrillar network structure.



Scheme 5.2. Schematic presentation of the mechanism of fiber to nanosphere morphology transformation along with the gel-to-sol transition of (L) upon "half-crown/two carbonyl"– Ca^{2+} coordination.

Now with incorporation of Ca^{2+} ions, (L) is coordinated with the Ca^{2+} using its "half-crown/two carbonyl" binding motif, as a result the strength of the H-bond becomes weak, as the two carbonyl groups are no more available to participate in the intermolecular H-bonds and hence the gel phase of (L) becomes unstable. Further, in favor of Ca^{2+} ion coordination, the molecular orientation of (L) also changes in a manner that the existed intramolecular interactions disappear (Figure 5b); this also contributes to destabilizing the self-assembled gel state of (L). Finally with the addition of excess equivalent of Ca^{2+} ion, the electrostatic repulsion among the bound Ca^{2+} ions comes to the picture, which asserts neighbouring (L) molecules keep away from each other and extinguish the network assemble structure of (L) (Scheme 5.2); as a result complete fibrillar network morphology disassembles into basic spherical structure and gel-to-sol phase transition takes place.

5.4. Conclusions

In conclusion, we have introduced a relatively new kind of metal ion binding motif ("Half-crown/two carbonyl") based LMWG. In response to alkaline earth metal (Ca^{2+}) ion, gelator shows its morphological transformation from fiber to nanosphere with a visual gel-to-sol phase transition. The computational calculation and experimental study have shown that the "Half-crown/two carbonyl"– Ca^{2+} metal ion interaction is the key issue for the response of gelator (L) to Ca^{2+} . Although the

experimental results states the interaction between “Half-crown/two carbonyl” – Ca^{2+} ion is not so strong, but due to the participation of two amide carbonyl oxygen atoms (-NHCO) in metal coordination rather than H-bonding and the originated repulsive electrostatic repulsions force among the bound Ca^{2+} ions were collectively strong enough to disrupt the extended intermolecular H-bonded network structure of (L), and hence resulted to its morphological (assembled entangled fibers to disassembled spheres) as well as gel-to-sol phase transition. In quick summary, we have represented a unique example in which “Half-crown/two carbonyl” – Ca^{2+} interactions play a vital role in mediating a response in soft matter systems, providing fundamental insight into the nature of this interaction and acting as a step on the way to the development of metal-responsive materials.

5.5. References

1. (a) T. Aida, E. W. Meijer and S. I. Stupp, *Science.*, 2012, **335**, 813; (b) X. Zhao, F. Pan, H. Xu, M. Yaseen, H. Shan, C. A. E. Hauser, S. Zhang and J. R. Lu, *Chem. Soc. Rev.*, 2010, **39**, 3480; (c) L. C. Palmer and S. I. Stupp, *Acc. Chem. Res.*, 2008, **41**, 1674; (d) G. M. Whitesides and B. Grzybowski, *Science.*, 2002, **295**, 2418; (e) W. Li, Y. Kim, J. Li and M. Lee, *Soft Matter*, 2014, **10**, 5231; (f) E. Busseron, Y. Ruff, E. Moulin and N. Giuseppone, *Nanoscale*, 2013, **5**, 7098; (g) F. J. M. Hoebe, P. Jonkhøj, E. W. Meijer, A. P. H. J. Schenning, *Chem. Rev.*, 2005, **105**, 1491; (h) A. Wang, W. Shi, J. Huang and Y. Yan, *Soft Matter*, 2016, **12**, 337; (i) A. Maity, A. Dey, M. Gangopadhyay and A. Das, *Nanoscale*, 2018, **10**, 1464; (j) Y. Yan, Y. Lin, Y. Qiao and J. Huang, *Soft Matter*, 2011, **7**, 6385; (k) S. Kushwaha, A. Maity, M. Gangopadhyay, S. Ravindranathan, P. R. Rajamohanam and A. Das, *Langmuir.*, 2017, **33**, 10989; (l) H. Frisch, P. Besenius, *Macromol. Rapid Commun.*, 2015, **36**, 346.
2. (a) P. Terech and R. G. Weiss, *Chem. Rev.*, 1997, **97**, 3133; (b) L. Zhang, X. Wang, T. Wang and M. Liu, *Small.*, 2015, **11**, 1025; (c) S. S. Babu, V. K. Praveen and A. Ajayaghosh, *Chem. Rev.*, 2014, **114**, 1973; (d) L. A. Estroff and A. D. Hamilton, *Chem. Rev.*, 2004, **104**, 1201; (e) M. George and R. G. Weiss, *Acc. Chem. Res.*, 2006, **39**, 489; (f) N. M. Sangeetha and U. Maitra, *Chem. Soc. Rev.*, 2005, **34**, 821; (g) L. E. Buerkle and S. J. Rowan, *Chem. Soc. Rev.*, 2012, **41**, 6089; (h) E. R. Draper and D. J. Adams, *Chem.*, 2017, **3**, 390; (i) B. O. Okesola and D. K. Smith, *Chem. Soc. Rev.*, 2016, **45**, 4226.
3. (a) A. Baral, S. Basak, K. Basu, A. Dehsorkhi, I. W. Hamley and A. Banerjee, *Soft Matter*, 2015, **11**, 4944; (b) Z. Shen, Y. Jiang, T. Wang and M. Liu, *J. Am. Chem. Soc.*, 2015, **137**, 16109; (c) A. Maity, F. Ali, H. Agarwalla, B. Anothumakkool and A. Das, *Chem. Commun.*, 2015, **51**, 2130; (d) P. Xing, P. Li, H. Chen, A. Hao and Y. Zhao, *ACS Nano.*, 2017, **11**, 4206; (e) S. Datta and S. Bhattacharya, *Soft Matter*, 2015, **11**, 1945; (f) S. Ahmed, J. H. Mondal, N. Behera and D. Das, *Langmuir.*, 2013, **29**, 14274; (g) A. Maity, M. Gangopadhyay, A. Basu, S. Aute, S. S. Babu and A. Das, *J. Am. Chem. Soc.*, 2016, **138**, 11113; (h) T. M. Babu and E. Prasad, *Chem. - A Eur. J.*, 2015, **21**, 11972; (i) S. Saha, J. Bachl, T. Kundu, D. Díaz Díaz and R. Banerjee, *Chem. Commun.*, 2014, **50**, 3004; (j) L. Jiang, Y. Yan and J. Huang, *Soft Matter*, 2011, **7**, 10417.
4. (a) H. Maeda, *Chem. - A Eur. J.*, 2008, **14**, 11274; (b) S. Banerjee, R. K. Das and U. Maitra, *J. Mater. Chem.*, 2009, **19**, 6649.
5. (a) Y. Hisamatsu, S. Banerjee, M. B. Avinash, T. Govindaraju and C. Schmuck, *Angew. Chem., Int. Ed.*, 2013, **52**, 12550; (b) J. Nanda, A. Biswas and A. Banerjee, *Soft Matter*, 2013, **9**, 4198.

6. S.-I. Kawano, N. Fujita, S. Shinkai, *J. Am. Chem. Soc.*, 2004, **126**, 8592.
7. C. D. Jones and J. W. Steed, *Chem. Soc. Rev.*, 2016, **45**, 6546.
8. (a) E. Carretti, M. Bonini, L. Dei, B. H. Berrie, L. V. Angelova, P. Baglioni and R. G. Weiss, *Acc. Chem. Res.*, 2010, **43**, 751; (b) A. Dawn, T. Shiraki, S. Haraguchi, S. -I. Tamaru and S. Shinkai, *Chem. Asian J.*, 2011, **6**, 266.
9. (a) C. Wang, Q. Chen, F. Sun, D. Zhang, G. Zhang, Y. Huang, R. Zhao and D. Zhu, *J. Am. Chem. Soc.*, 2010, **132**, 3092; (b) Y. Lin, Y. Qiao, P. Tang, Z. Li and J. Huang, *Soft Matter*, 2011, **7**, 2762.
10. (a) J. Eastoe, M. Sánchez-Dominguez, P. Wyatt and R. K. Heenan, *Chem. Commun.*, 2004, 2608; (b) P. Xue, J. Ding, M. Jin and R. Lu, *J. Mater. Chem. C.*, 2017, **5**, 5299.
11. S. Mondal, P. Chakraborty, P. Bairi, D. P. Chatterjee and A. K. Nandi, *Chem. Commun.*, 2015, **51**, 10680.
12. (a) S. Wang, W. Shen, Y. Feng and H. Tian, *Chem. Commun.*, 2006, 1497; (b) J. W. Chung, S. -J. Yoon, S. -J. Lim, B. -K. An and S. Y. Park, *Angew. Chem., Int. Ed.*, 2009, **48**, 7030.
13. D. Chang, W. Yan, Y. Yang, Q. Wang and L. Zou, *Dyes Pigm.*, 2014, **110**, 2.
14. (a) A. Y. -Y. Tam and V. W. -W. Yam, *Chem. Soc. Rev.*, 2013, **42**, 1540; (b) M. -O. M. Piepenbrock, G. O. Lloyd, N. Clarke and J. W. Steed, *Chem. Rev.*, 2010, **110**, 1960; (c) J. H. Lee, S. Kang, J. Y. Lee and J. H. Jung, *Soft Matter*, 2012, **8**, 6557; (d) K. Lalitha, V. Sridharan, C. U. Maheswari, P. K. Vemula and S. Nagarajan, *Chem. Commun.*, 2017, **53**, 1538; (e) K. Jie, Y. Zhou, B. Shi and Y. Yao, *Chem. Commun.*, 2015, **51**, 8461; (f) S. Banerjee, N. N. Adarsh and P. Dastidar, *Soft Matter*, 2012, **8**, 7623; (g) A. Ghoussoub and J. -M. Lehn, *Chem. Commun.*, 2005, 5763.
15. W. Edwards and D. K. Smith, *Chem. Commun.*, 2012, **48**, 2767.
16. Q. Jin, L. Zhang, X. Zhu, P. Duan and M. Liu, *Chem. - A Eur. J.*, 2012, **18**, 4916.
17. A. A. Sobczuk, S. -I. Tamaru and S. Shinkai, *Chem. Commun.*, 2011, **47**, 3093.
18. A. Gasnier, G. Royal and P. Terech, *Langmuir.*, 2009, **25**, 8751.
19. W. Deng and D. H. Thompson, *Soft Matter*, 2010, **6**, 1884.
20. (a) K. Sawada and Y. Kikuchi, *Bunseki Kagaku.*, 2004, **53**, 1239; (b) B. Tümmler, G. Maass, E. Weber, W. Wehner and F. Vögtle, *J. Am. Chem. Soc.*, 1977, **99**, 4683; (c) C. Xu, W. Liu and W. Qin, *J. Phys. Chem. A.*, 2011, **115**, 4288.
21. (a) G. W. Gokel, *Crown Ethers and Cryptands.*, Royal Society of Chemistry: London, 1991; (b) Y. Suzuki, T. Morozumi and H. Nakamura, *J. Phys. Chem. B.*, 1998, **102**, 7910.
22. (a) J. Kim, T. Morozumi, H. Hiraga and H. Nakamura, *Anal. Sci.*, 2009, **25**, 1319; (b) H. Hiraga, T. Morozumi and H. Nakamura, *Eur. J. Org. Chem.*, 2004, 4680; (c)

- T. Morozumi, T. Anada and H. Nakamura, *J. Phys. Chem. B.*, 2001, **105**, 2923; (d) H. Hiraga, T. Morozumi and H. Nakamura, *Tetrahedron Lett.*, 2002, **43**, 9093; (e) J. Kim, T. Morozumi, N. Kurumatani and H. Nakamura, *Tetrahedron Lett.*, 2008, **49**, 1984; (f) J. Kim, T. Morozumi and H. Nakamura, *Chem Lett.*, 2009, **38**, 994; (g) J. Kim, T. Morozumi, and H. Nakamura, *Org. Lett.*, 2007, **9**, 4419.
23. (a) E. N. W. Howe, M. Bhadbhade and P. Thordarson, *J. Am. Chem. Soc.*, 2014, **136**, 7505; (b) A. Bajaj, P. Kondaiah and S. Bhattacharya, *Bioconjugate Chem.*, 2007, **18**, 1537; (c) S. Bhattacharya and A. Bajaj, *J. Phys. Chem. B.*, 2007, **111**, 2463; (d) S. Bhattacharya and Y. Krishnan-Ghosh, *Mol. Cryst. Liq. Cryst.*, 2002, **381**, 33.
24. (a) A. Reddy, A. Sharma and A. Srivastava, *Chem. - A Eur. J.*, 2012, **18**, 7575; (b) S. D. Bhagat and A. Srivastava, *CrystEngComm.*, 2016, **18**, 4369.
25. D. Perrin, W. L. F. Armarego and D. R. Perrin, *Purification of Laboratory Chemicals*, 2nd Ed., Oxford: Pergamon 1980.
26. H. T. A. Merck, *J. Comput. Chem.*, 1996, **17**, 490.
27. S. Profeta and N.L. Allinger, *J. Am. Chem. Soc.*, 1985, **107**, 1907.
28. T. A. Halgren, *J. Comput. Chem.*, 1996, **17**, 490.
29. *Spartan 08*, Software, Wavefunction Inc: Irvine, CA, USA, 2008.
30. A. D. Becke, *Phys. Rev. A*, 1988, **38**, 3098.
31. C. Lee, W. Yang and R.G. Parr, *Phys. Rev. B.*, 1988, **37**, 785.
32. G. A. Peterson and M. A. Al-Laham, *J. Chem. Phys.*, 1991, **94**, 608.
33. A. V. Marenich, C. J. Cramer and C. J. Truhlar, *J. Phys. Chem. B.*, 2009, **113**, 6378.
34. M. J. Frisch, G. W. Trucks, H. B. Schlegel, G. E. Scuseria, M. A. Robb, J. R. Cheeseman, G. Scalmani, V. Barone, B. Mennucci, G. A. Petersson, et al., *Gaussian 09, Revision B01*, Gaussian, Inc., Wallingford, CT, 2010. Y. Wang, P. Xing, S. Li, M. Ma, M. Yang, Y. Zhang, B. Wang and A. Hao, *Langmuir.*, 2016, **32**, 10705; (b) J. Nanda and A. Banerjee, *Soft Matter*, 2012, **8**, 3380; (c) R. Misra, A. Sharma, A. Shiras and H. N. Gopi, *Langmuir.*, 2017, **33**, 7762.
35. (a) H. Agarwalla, K. Jana, A. Maity, M. K. Kesharwani, B. Ganguly and A. Das, *J. Phys. Chem. A.*, 2014, **118**, 2656; (b) M. Gangopadhyay, A. Maity, A. Dey and A. Das, *J. Org. Chem.*, 2016, **81**, 8977; (c) F. Ali, S. Saha, A. Maity, N. Taye, M. K. Si, E. Suresh, B. Ganguly, S. Chattopadhyay and A. Das, *J. Phys. Chem. B.*, 2015, **119**, 13018; (d) M. Gangopadhyay, A. K. Mandal, A. Maity, S. Ravindranathan, P. R. Rajamohan and A. Das, *J. Org. Chem.*, 2016, **81**, 512.

A. Conclusion of the Thesis

The present dissertation has focused on design and synthesis of series of low molecular weight gelators, utilization of various noncovalent interactions and encompasses the broader area of *Supramolecular Chemistry*. To achieve our objectives, building blocks with strategically chosen functionality as well as chromophoric group are being utilized to favor their self-assembly process with desired photophysical functions and morphological structures. Influence of different stimuli (such as changing the solvent compositions, subtle structural modification or addition of chemical reagents etc.) on these supramolecular architectures and assemblies are being studied with necessary rationalization at the molecular level.

In chapter 2, a gelator derived from poly(aryl ether) dendron based amphiphilic compound showed an interesting tuneable multiple luminescence color property along with white-light emission with the relative change in the water to THF ration in the mixed solvent system. A systematic photophysical study suggests that an ESIPT coupled AIEE process is operational in this system. The gelator shows a bright yellow color luminescence in gel and solid state.

In chapter 3, solvent dependent diverse aggregation behavior of the above referred amphiphilic gelator molecules has been discussed. The amphiphilic gelator shows helical fiber-like morphology in THF. Upon gradual addition of water to into its THF solution the helical morphology of the gelator changes to rodshaped morphology as confirmed by the SEM and TEM study. Results of the microscopic studies, together with various spectroscopic studies indicate the transformation of helical fiber to nanorod through an intermediated scrolled fiber pathway. Role of various noncovalent interactions and media polarity is achieving various structures have been rationalized. Luminescence behavior of the gelator with nanorod structure was exploited for constructing a model light-harvesting system via doping of small quantities of two newly designed BODIPY based acceptor molecules as energy acceptor and the gelators molecules as an antenna chromophore.

In chapter 4, we introduce a new class of small cationic C_3 -symmetric gelator molecule devoid of any conventional gelation functional unit. It forms a thermo reversible gel in MeOH/H₂O (1:1, v/v) medium. Although the gelator is achiral in nature, the morphological investigation of this gelator by SEM study shows the formation of simultaneous form right (*P*) - and left (*M*) - handed chiral helical rope-like structures. To control the helical handedness, a chiral counter anion exchange-assisted approach was successfully introduced here, and thereby we achieve to get the homochiral helical assembly in this system. The homochiral sign was confirmed by

SEM, CD and X-ray single crystal structure. The X-ray structure reveals that an Ion-Pair assisted Hydrogen (IPA-H) bond play the key role to attain the homochiral structure of the chiral counteranion exchanged gelator. Overall, results of this chapter demonstrate a general methodology to control and bias chirality in ionic achiral assemblies and also to stabilize the chiral assembly in (MeOH/H₂O; 1 : 1 v/v) polar media.

In chapter 5, a gelator with an unusual metal binding motif is described. Binding motif could be best described as “*half-crown/two carbonyl*” for Ca²⁺ ion as well as few other alkali and alkaline earth metal ions. A gel to sol transformation was achieved in response to the binding to any of these metal ions. Apart from the gel-to-sol phase transition, the fibrillar morphology of the metal-free gelator also changes to nanosphere with the treatment of excess equivalent (2.0 eq) of the Ca²⁺ ion. Changes in the nature of various noncovalent interactions in metal-free gelator and to its Ca²⁺ complex were proposed based on computational calculation and with various spectroscopic studies. The present study could provide fundamental insight into the nature of unusual “*half-crown/two carbonyl*” – Ca²⁺ interaction and act as a step on the way to the development of metal ion-responsive materials.

B. Possible Direction of Future Work

In the present investigation, we have developed various chromophoric functional groups based low molecular weight supramolecular gelators and show some ways to controlling their optical property and their self-organization structure. One of the ways through which the work can be taken forward is to use the gelation functional moiety from this investigation to design new π -conjugate gelator molecule with exciting luminescence property for fabrication of electroluminescent display devices. The luminescence gelator could also be used for light-harvesting by incorporating suitable acceptor molecule. Another option would be to generate hydrogels from these gelation functional units through suitable chemical modification so that toxic metal ions in water can be detected and extracted. The C₃-symmetric gelator used in chapter 4, has metal coordinating pyridine functional group. One can plan to develop metal coordination polymeric gel using this gelator for study the metal-based redox, optical, electronic and magnetic properties, or for used the metallo gel as a template to synthesize the metal nanoparticles. In literature, various gels have been extensively utilized for the drug and gene delivery, so the designing of drug delivery vehicles based on the described gel systems is also could be one of the suitable ways of taking the research forward.

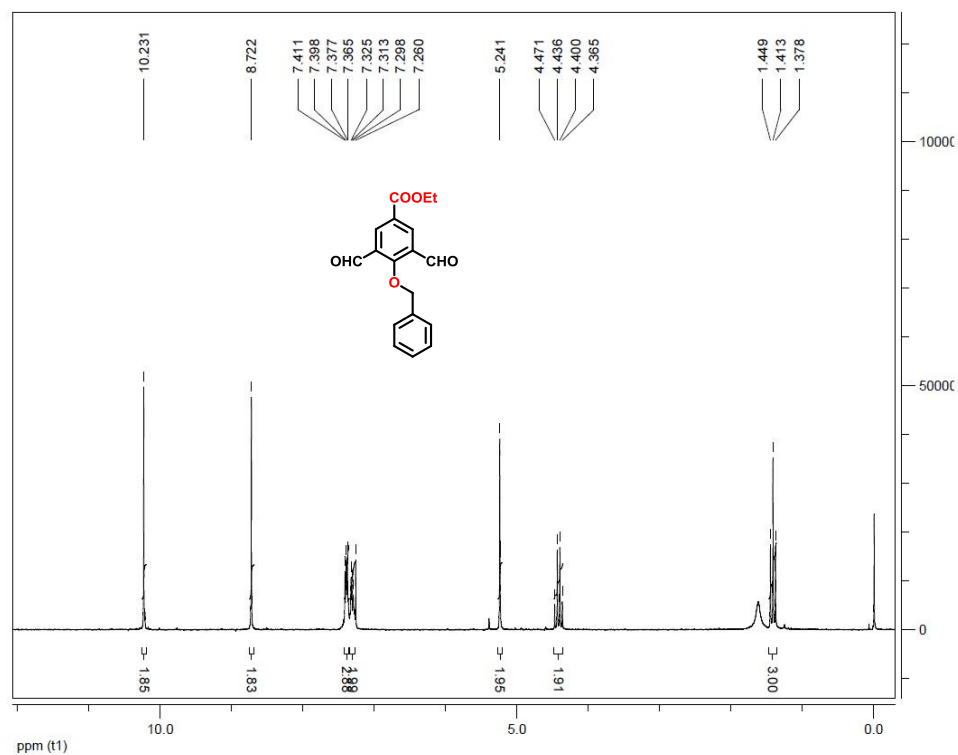


Figure 1. ¹H NMR (200 MHz, 25°C) spectra recorded in CDCl₃.

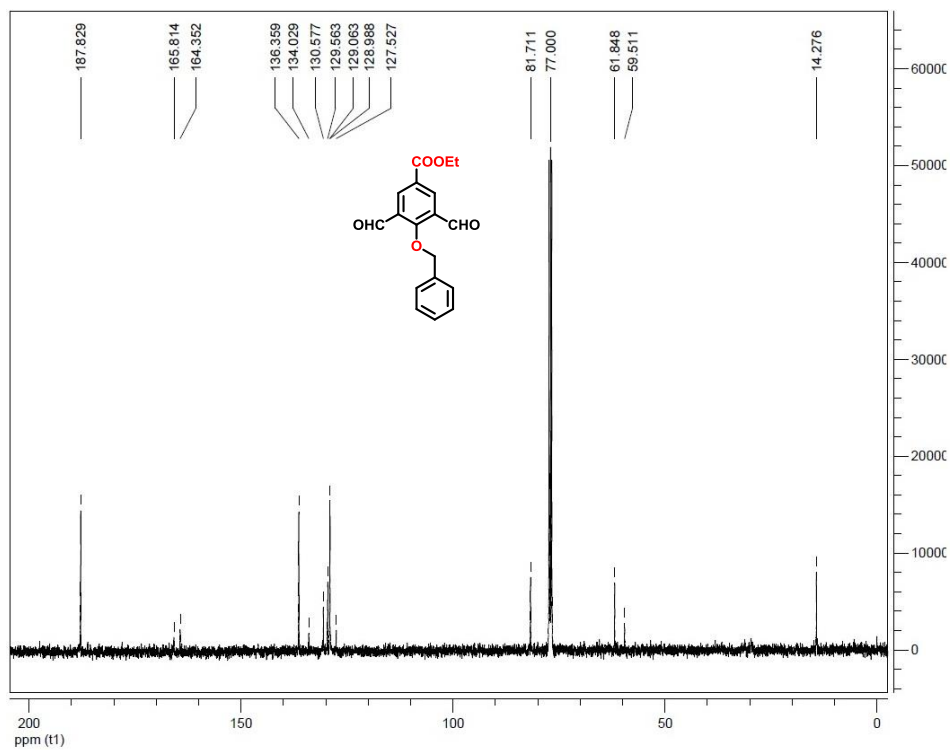


Figure 2. ¹³C NMR (100 MHz, 25°C) spectra recorded in CDCl₃.

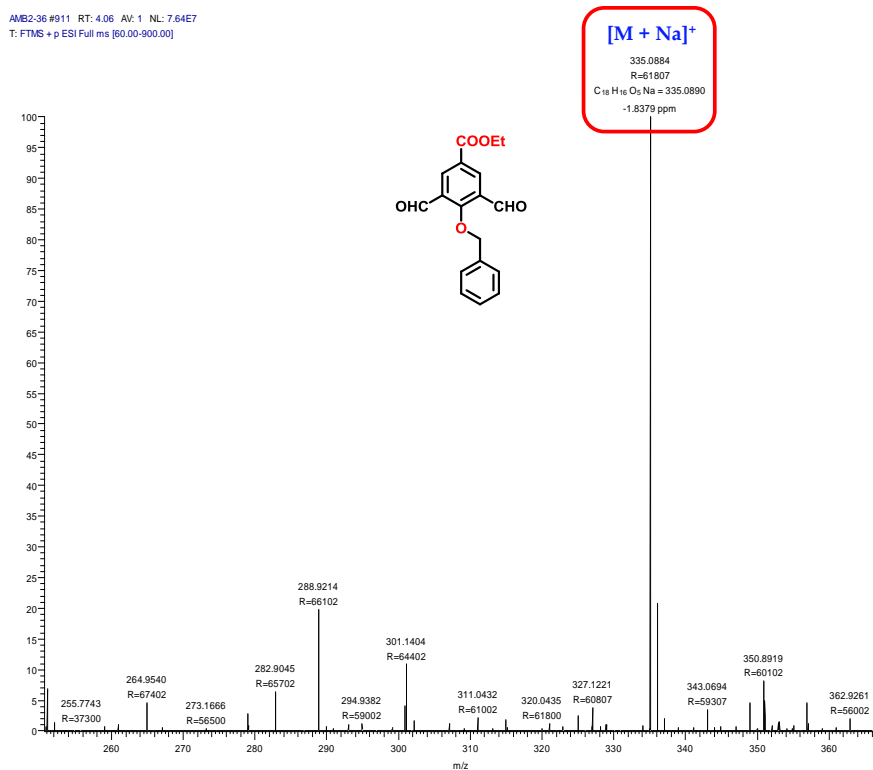


Figure 3. HRMS (ESI) spectra recorded in MeOH.

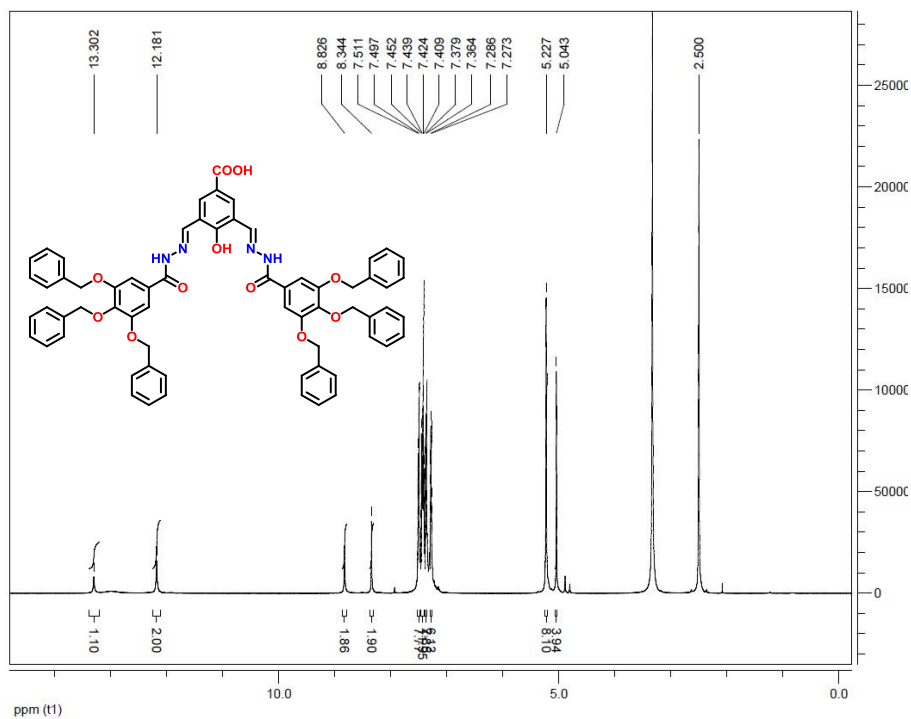


Figure 4. ¹H NMR (500 MHz, 25°C) spectra recorded in DMSO-d₆.

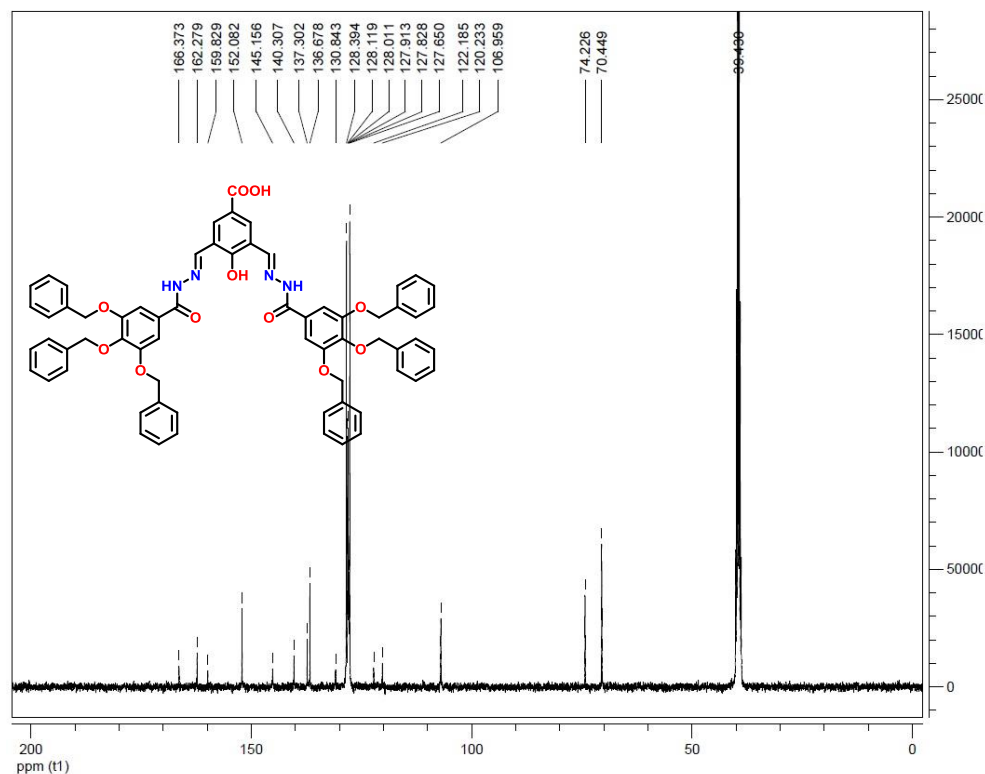


Figure 5. ^{13}C NMR (100 MHz, 25°C) spectra recorded in $\text{DMSO}-d_6$.

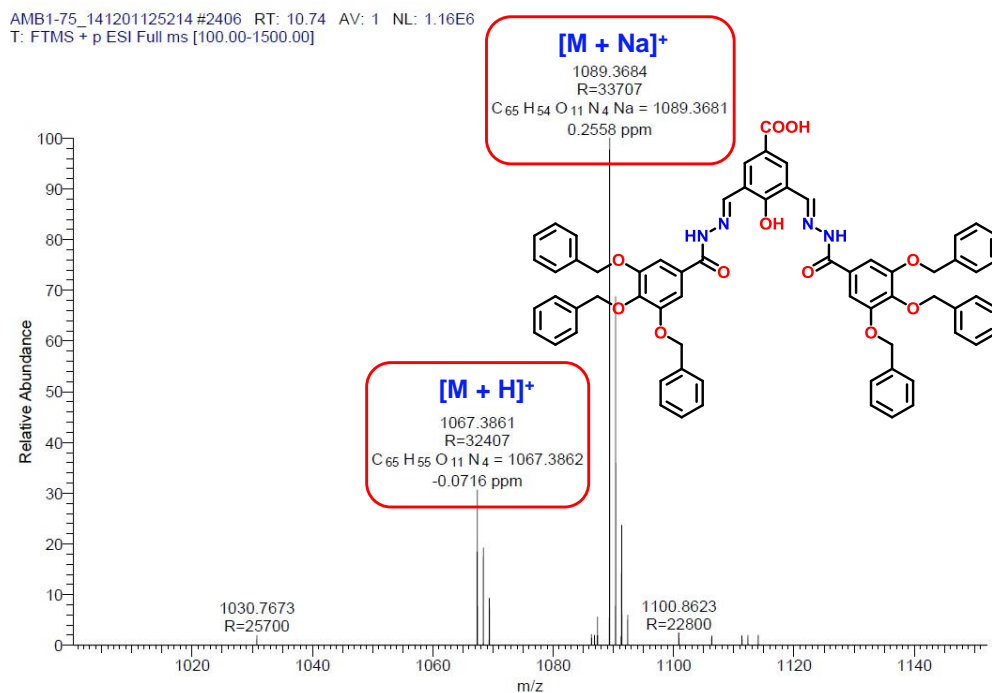


Figure 6. HRMS (ESI) spectra recorded in MeOH.

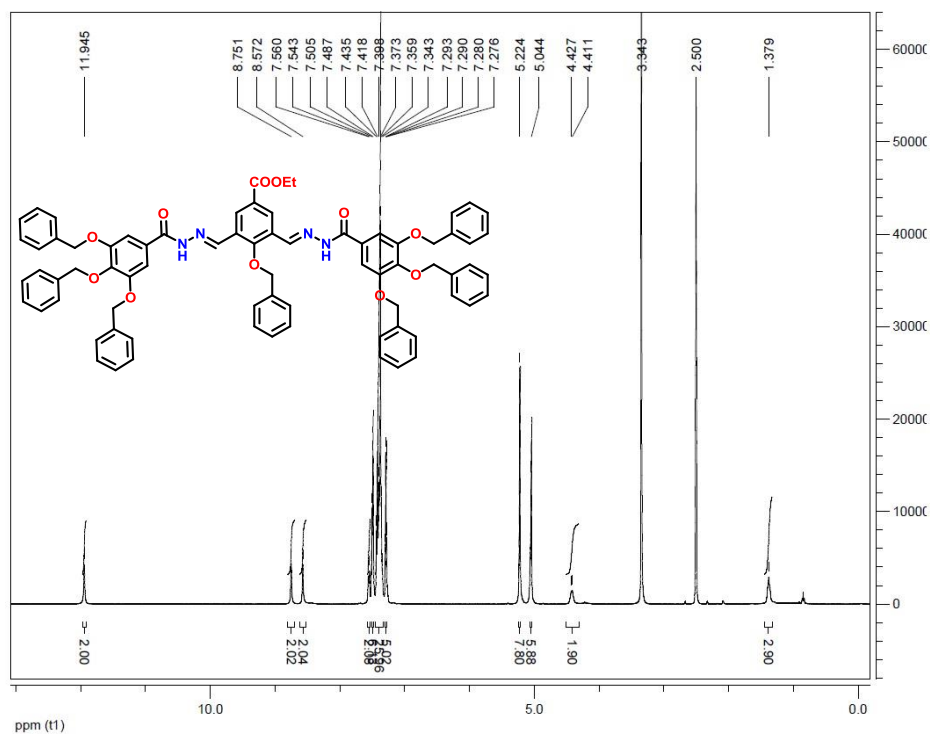


Figure 7. ¹H NMR (400 MHz, 25°C) spectra recorded in DMSO-d₆.

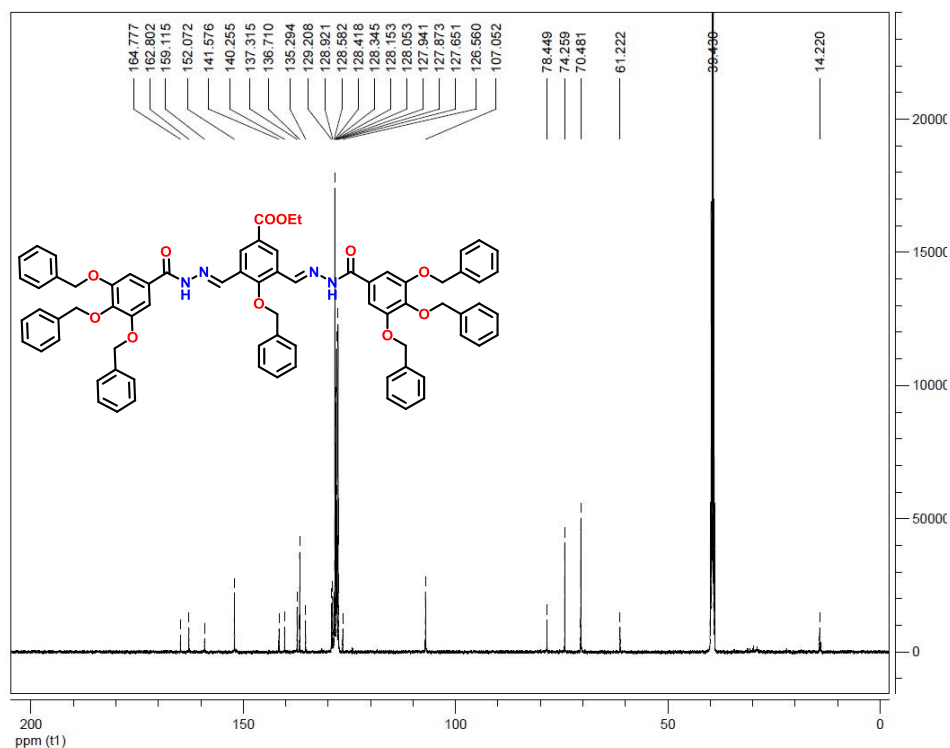


Figure 8. ¹³C NMR (100 MHz, 25°C) spectra recorded in DMSO-d₆.

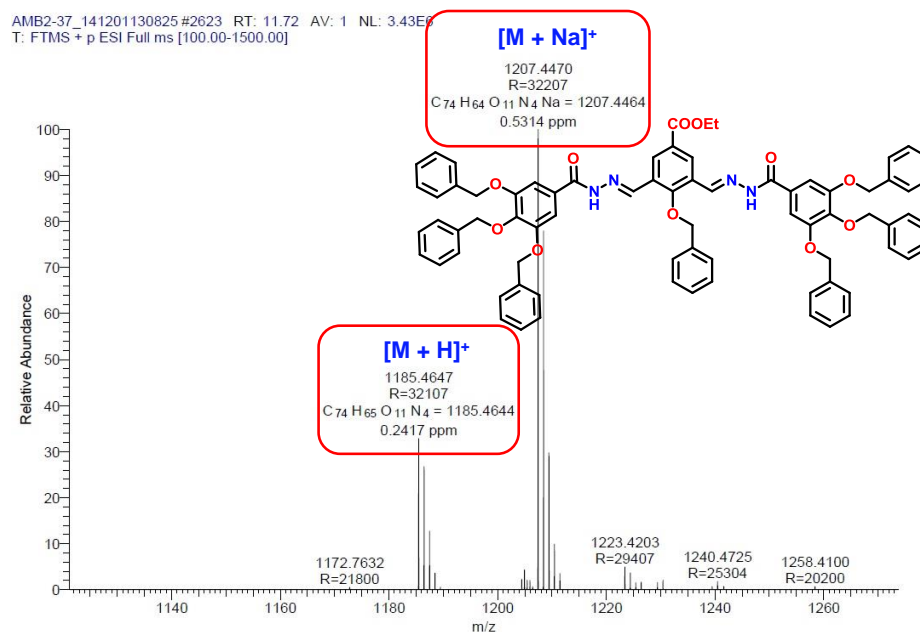


Figure 9. HRMS (ESI) spectra recorded in MeOH.

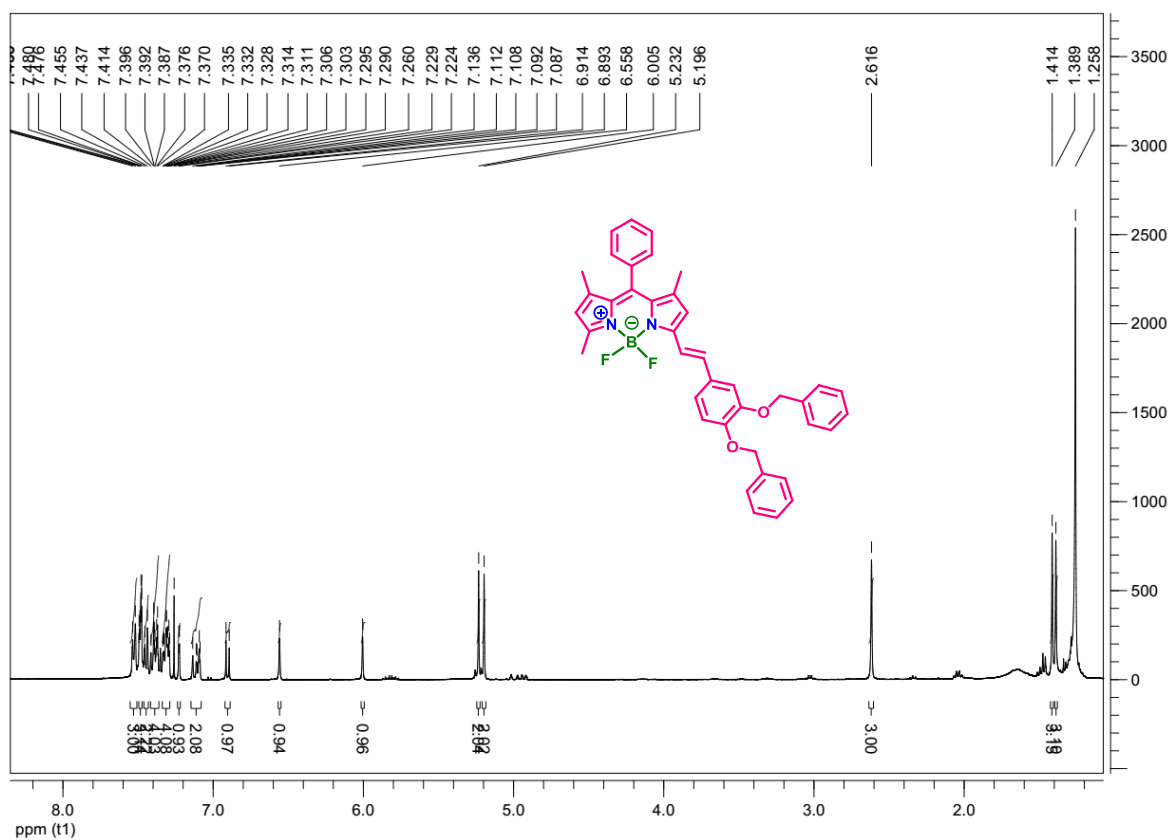


Figure 10. ^1H NMR (400 MHz, 25°C) spectra recorded in CDCl_3 .

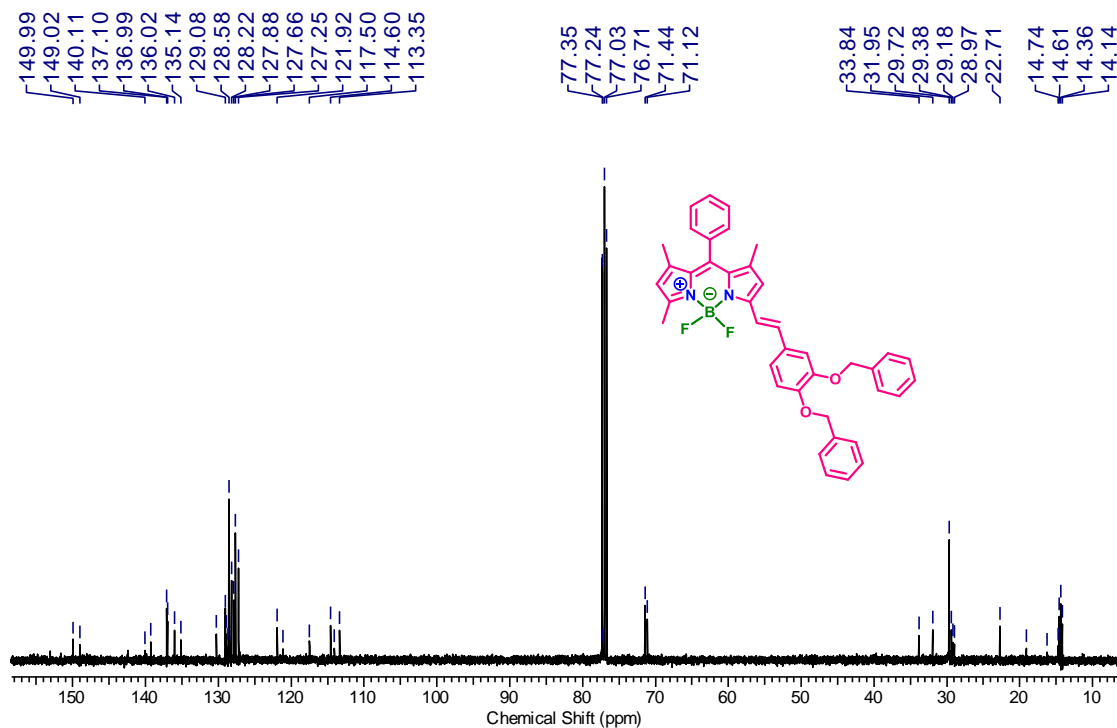


Figure 11. ¹³C NMR (100 MHz, 25°C) spectra recorded in CDCl₃.

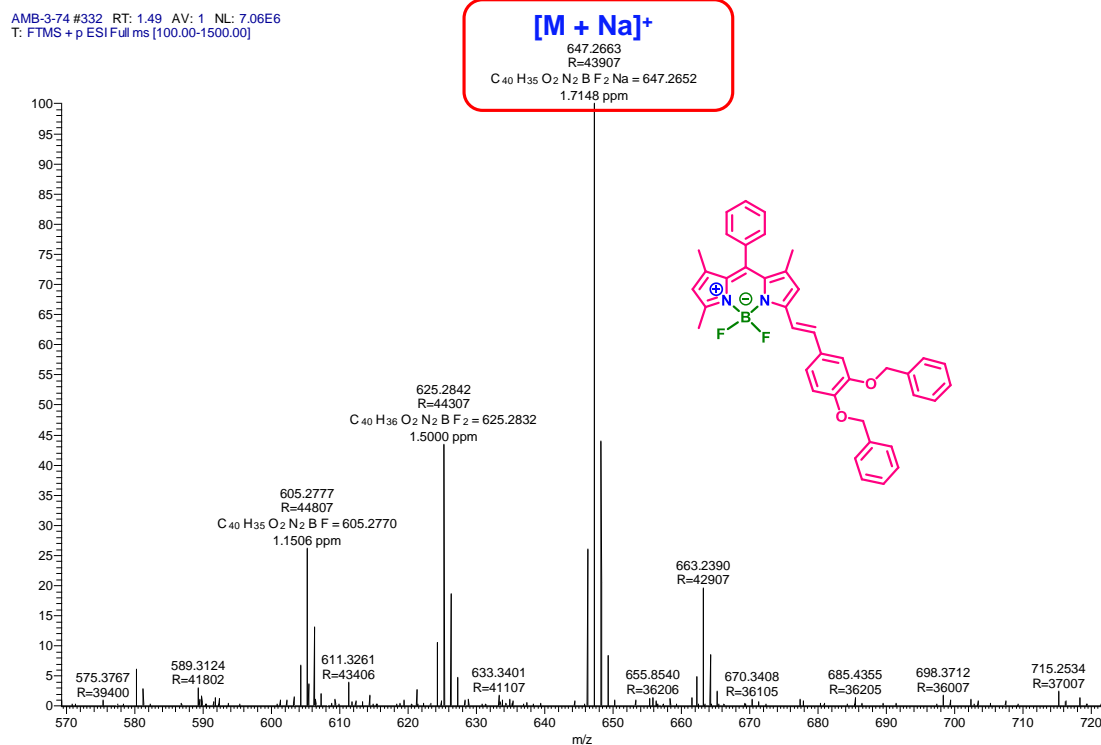


Figure 12. HRMS (ESI) spectra recorded in MeOH.

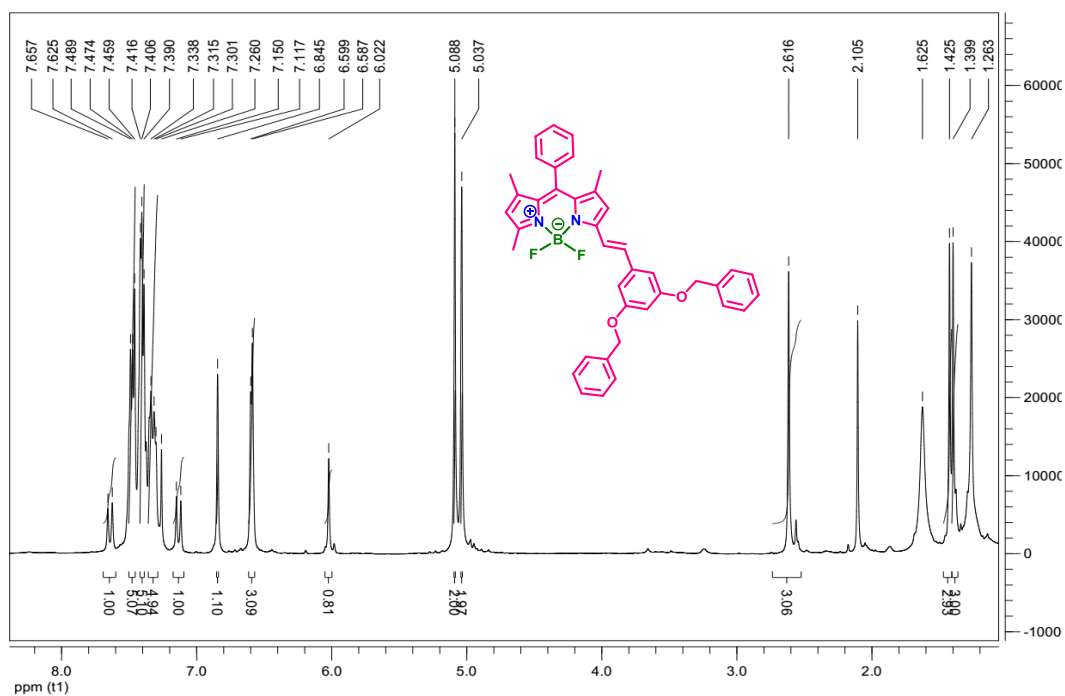


Figure 13. ^1H NMR (500 MHz, 25°C) spectra recorded in CDCl_3 .

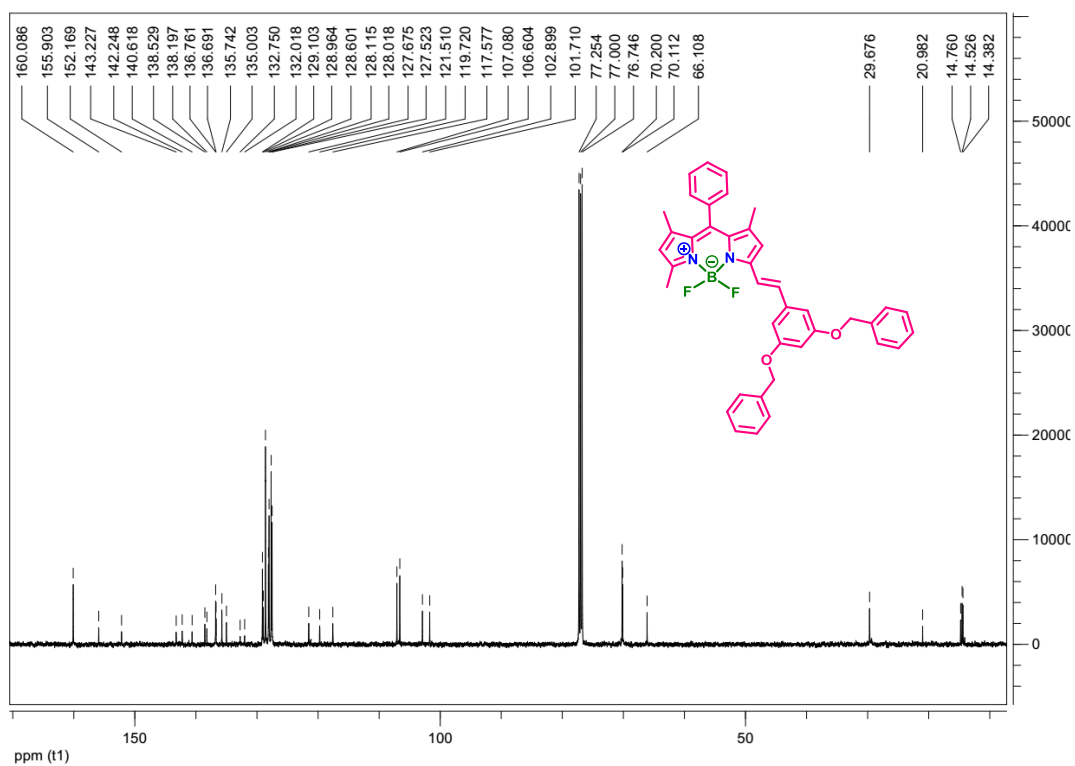


Figure 14. ^{13}C NMR (125 MHz, 25°C) spectra recorded in CDCl_3 .

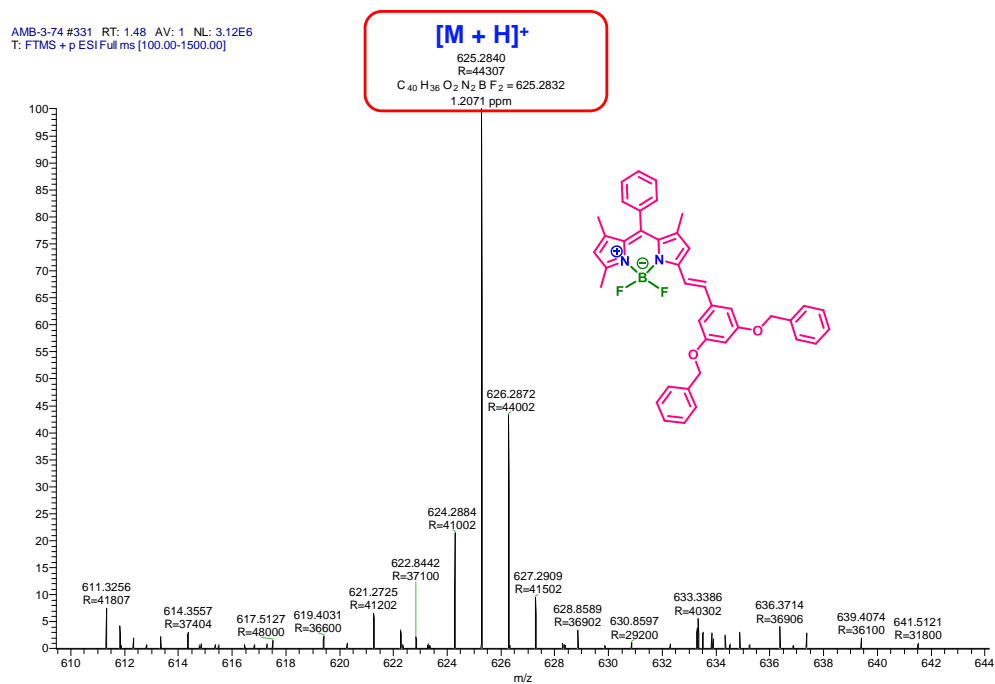


Figure 15. HRMS (ESI) spectra recorded in MeOH.

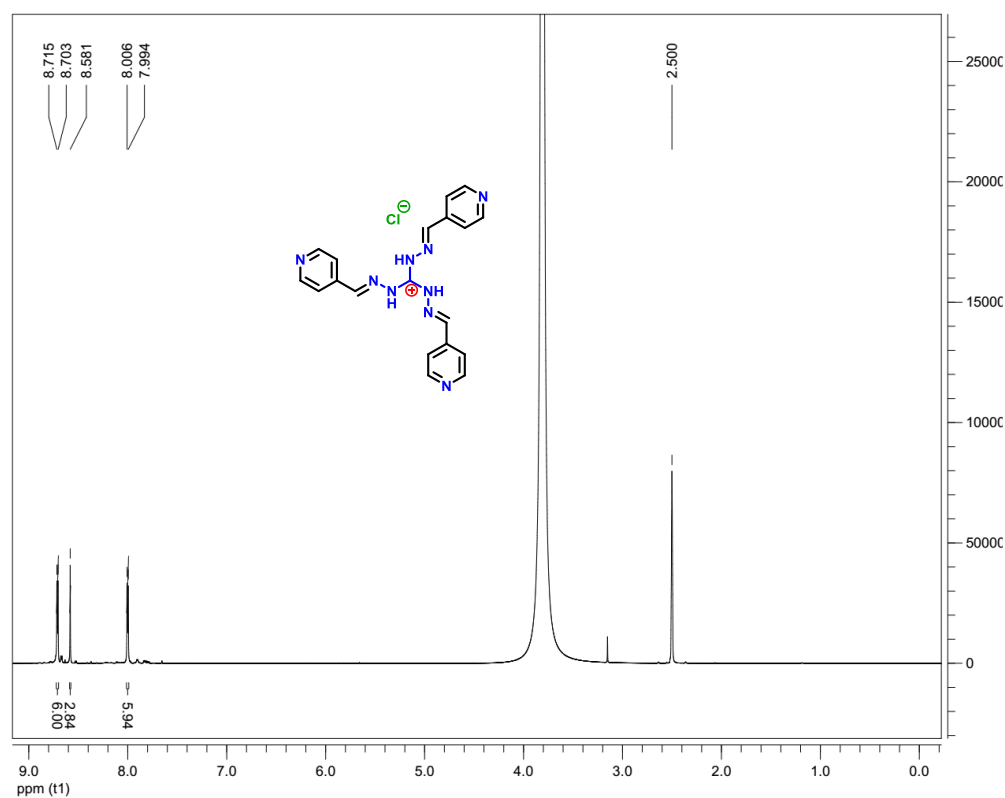
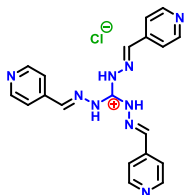
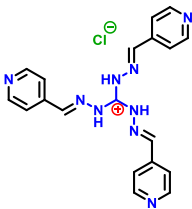


Figure 16. ¹H NMR (500 MHz, 25°C) spectra recorded in DMSO-d₆.



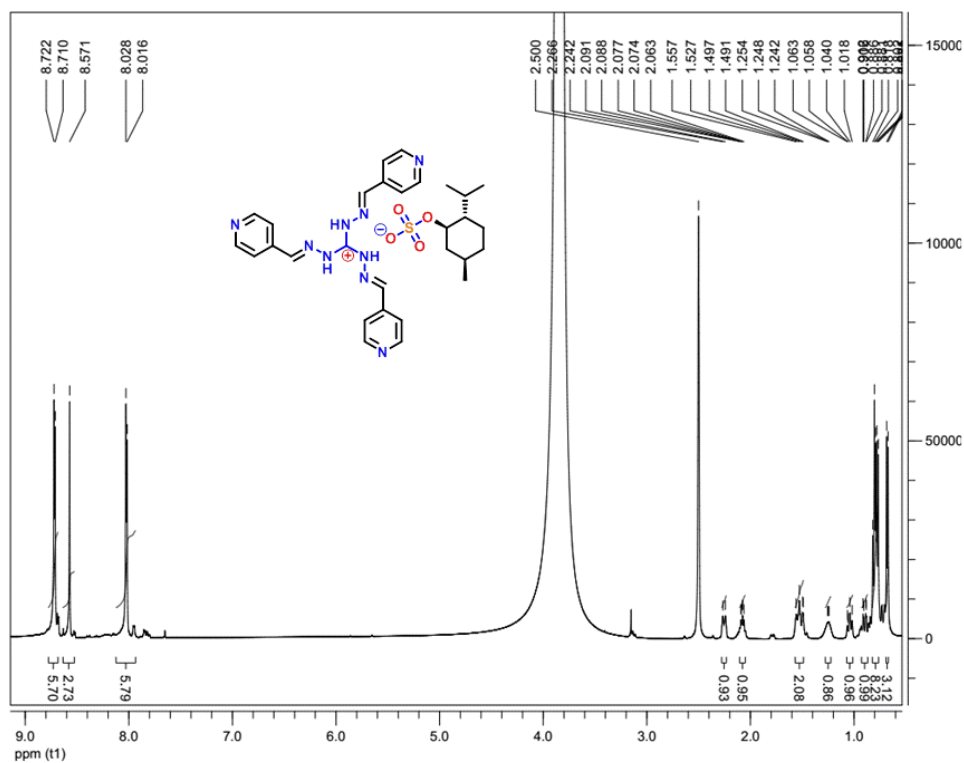


Figure 19. ¹H NMR (500 MHz, 25°C) spectra recorded in DMSO-d₆.

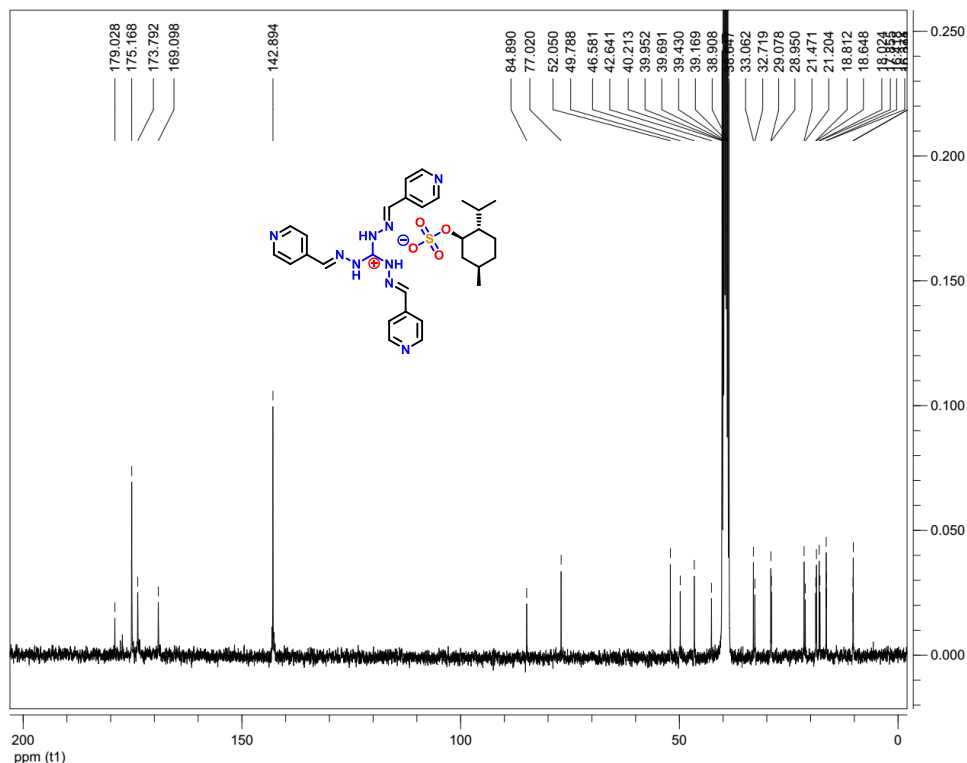


Figure 20. ¹³C NMR (100 MHz, 25°C) spectra recorded in DMSO-d₆.

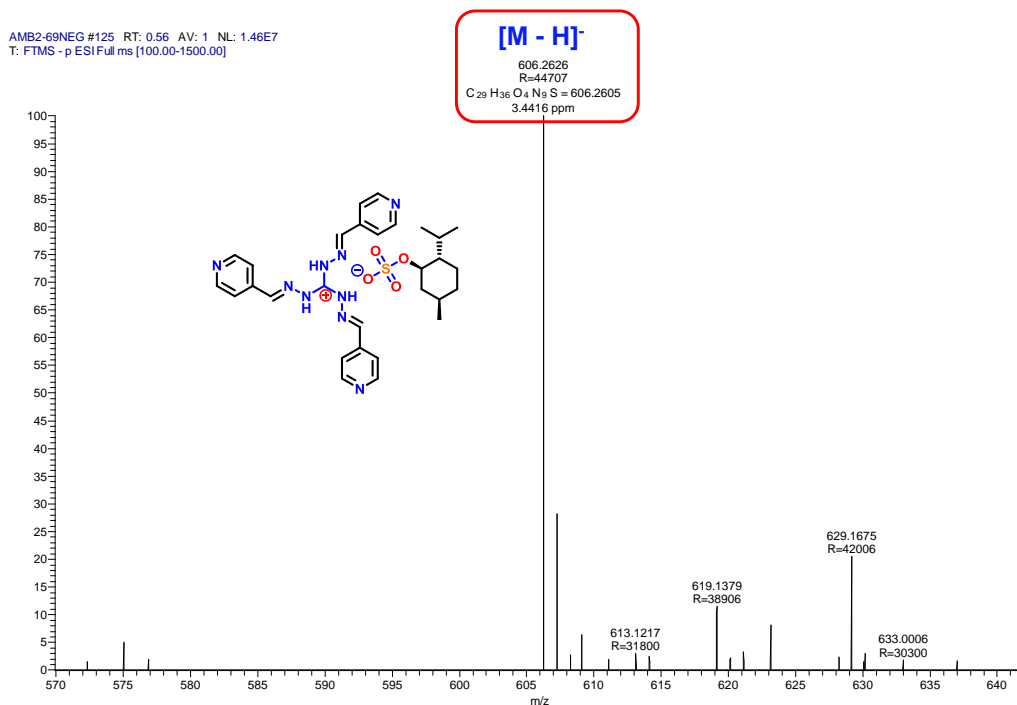


Figure 21. HRMS (ESI) spectra recorded in MeOH.

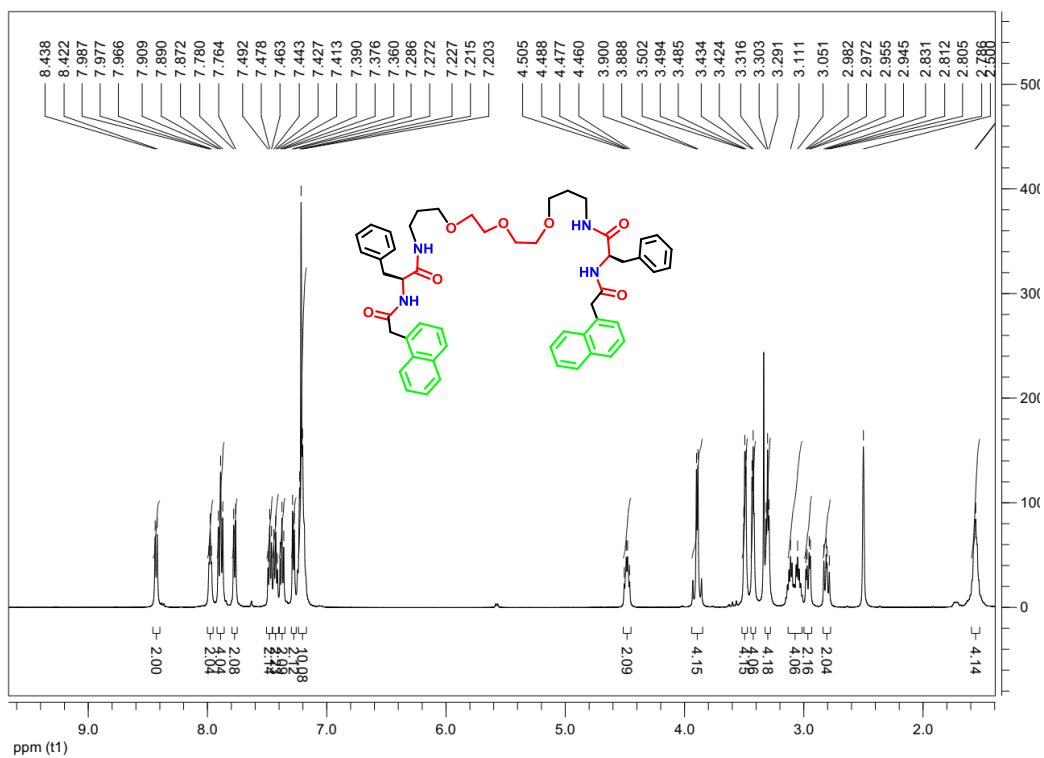


Figure 22. ¹H NMR (500 MHz, 25°C) spectra recorded in DMSO-d₆.

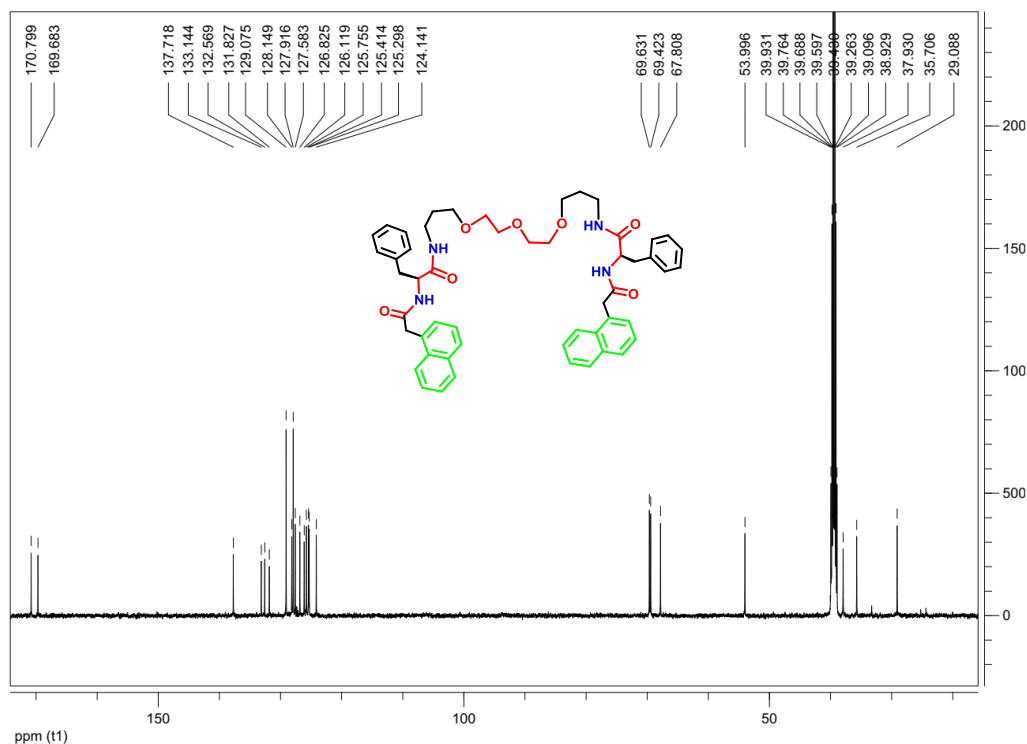


Figure 23. ¹³C NMR (125 MHz, 25°C) spectra recorded in DMSO-d₆.

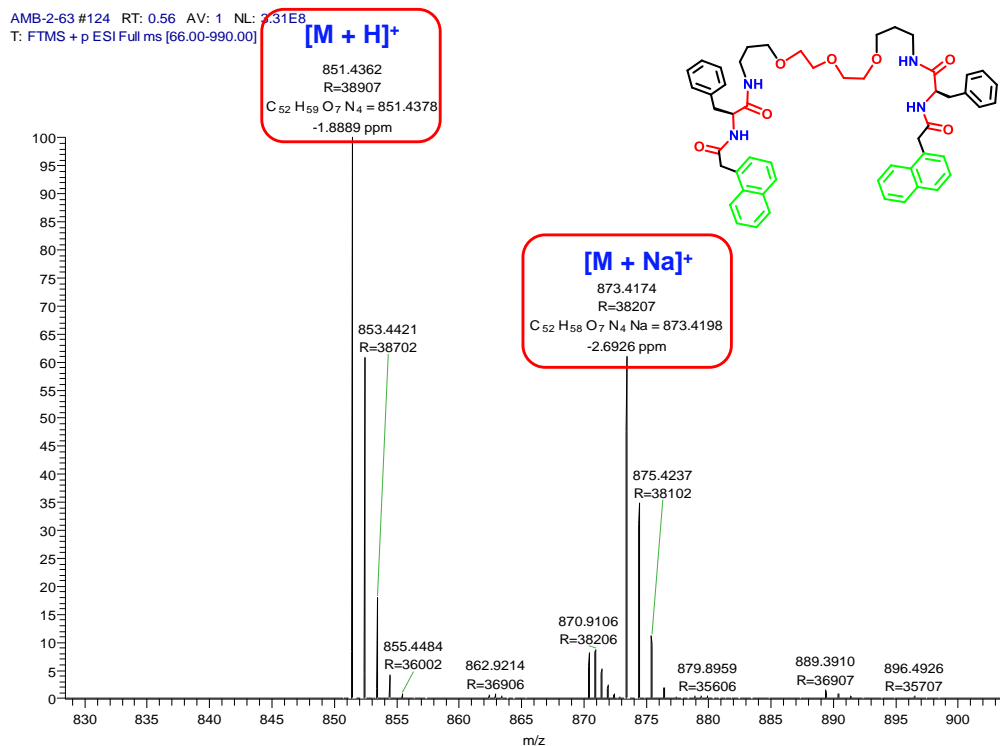


Figure 24. HRMS (ESI) spectra recorded in MeOH.

List of Publications

1. "Tuning of Multiple Luminescence Outputs and White-Light Emission from a Single Gelator Molecule through an ESIPT Coupled AIEE Process".
Arunava Maity,* Firoj Ali, Hridesh Agarwalla, Bihag Anothumakkool, Amitava Das. *Chem. Commun.*, 2015, **51**, 2130 (***corresponding author**).
2. "Water Induced Morphological Transformation of a Poly(aryl ether) dendron Amphiphile: Helical Fibers to Nanorods; as Light-Harvesting Antenna Systems".
Arunava Maity,* Ananta Dey, Monalisa Gangopadhyay, Amitava Das. *Nanoscale.*, 2018, **10**, 1464 (***corresponding author**).
3. "Counteranion Driven Homochiral Assembly of aCationic C₃-Symmetric Gelator through Ion-Pair Assisted Hydrogen Bond".
Arunava Maity,* Monalisa Gangopadhyay, Arghya Basu, Sunil Aute, Sukumaran Santhosh Babu, Amitava Das. *J. Am. Chem. Soc.*, 2016, **138**, 11113 (***corresponding author**).
4. "Fiber to Nanosphere Morphology Transformation and Gel-to-Sol Phase Transition Triggered by an Unusual "Half-Crown/two Carbonyl" - Ca²⁺ Metal Ion Interaction of a Low Molecular Weight Gelator (LMWG)".
Arunava Maity,* Ananta Dey, Mrinal Kanti Si, Bishwajit Ganguly, Amitava Das. To be communicated., (***corresponding author**).
5. "Regioselective Synthesis of a Novel Core-Substituted Azaperylene based Functional Assembly and its Solvent Dependent Archetype Aggregation Behavior".
Arunava Maity,* Ananta Dey, Amitava Das. To be communicated., (***corresponding author**).
6. "Cucurbit[7]uril Induced Formation of FRET Enabled Uni-lamellar Lipid Vesicles".
Shilpi Kushwaha, **Arunava Maity**, Monalisa Gangopadhyay, Sapna Ravindranathan, Pattuparambil R. Rajamohanan, Amitava Das. *Langmuir.*, 2017, **33**, 10989.
7. "A New Class of AIE Luminogens with Mega Stokes Shift, Mechanochromism, and Mechanoluminescence".
C. Arivazhagan, **Arunava Maity**, K. Bakthavachalam, Arijit Jana, Suraj Kumar Panigrahi, Eringathodi Suresh, Amitava Das, Sundargopal Ghosh. *Chem. Eur. J.* 2017, **23**, 7046.
8. "Chiral Discrimination through ¹H NMR and Luminescence Spectroscopy: Dynamic Processes and Solid Strip for Chiral Recognition".
Monalisa Gangopadhyay, **Arunava Maity**, Ananta Dey, Pattuparambil R. Rajamohanan, Sapna Ravindranathan, Amitava Das. *Chem. Eur. J.*, 2017, **23**, 18303.

9. "[2]Pseudorotaxane Formation with FRET Based Luminescence Response: Demonstration of Boolean Operationsthrough Self-Sorting on Solid Surface".
Monalisa Gangopadhyay, **Arunava Maity**, Ananta Dey, Amitava Das. *J. Org. Chem.*, 2016, **81**, 8977.
10. "PVAc/PEDOT: PSS/Graphene-Iron Oxide Nanocomposite (GINC): an Efficient Thermoelectric Material".
Abhijit Dey, **Arunava Maity**, Md Abdul Shafeeuulla Khan, Arun Kanti Sikder, Santanu Chattopadhyay. *RSC Adv.*, 2016, **6**, 22453.
11. "Tuning Emission Responses of a Triphenylamine Derivative in Host-Guest Complexes and an Unusual Dynamic Inclusion Phenomenon".
Monalisa Gangopadhyay, Amal K. Mandal, **Arunava Maity**, Sapna Ravindranathan, Pattuparambil R. Rajamohanan, Amitava Das. *J. Org. Chem.*, 2016, **81**, 512.
12. "Specific Reagent for Cr(III): Imaging Cellular Uptake of Cr(III) in Hct116 Cells and Theoretical Rationalization".
Firoj Ali, Sukdeb Saha, **Arunava Maity**, Nandaraj Taye, Mrinal Kanti Si, Eringathodi Suresh, Bishwajit Ganguly, Samit Chattopadhyay, Amitava Das. *J. Phys. Chem. B.*, 2015, **119**, 13018.
13. "Hydrogen Bonding Interaction between Active Methylene Hydrogen Atoms and an Anion as a Binding Motif for Anion Recognition: Experimental Studies and Theoretical Rationalization".
Hridesh Agarwalla, Kalyanashis Jana, **Arunava Maity**, Manoj K. Kesharwani, Bishwajit Ganguly, Amitava Das. *J. Phys. Chem. A.*, 2014, **118**, 2656.
14. "Highly Emissive Organic Solids with Remarkably Broad Color Tunability based on N,C-Chelate, Four-Coordinate Organoborons".
Aslam C. Shaikh, Dnyanesh S. Ranade, Shridhar Thorat, **Arunava Maity**, Prasad P. Kulkarni, Rajesh G. Gonnade, Parthapratim Munshi, Nitin T. Patil. *Chem. Commun.*, 2015, **51**, 16115.

Selected Presentations

1. Poster presentation in Polymer-Solvent Complexes & Intercalates (POLYSOLVAT-11) held in IACS, Kolkata (January 2016). Poster title: *"Tuning of Multiple Luminescence Outputs and White-Light Emission from a Single Gelator Molecule Through an ESIPT Coupled AIEE Process"*.
2. Oral presentation in Gordon Research Seminar (GRS) on "Self-Assembly & Supramolecular Chemistry", Switzerland, May 2017. Presentation title: *"Counteranion Driven Homochiral Assembly of a Cationic C₃-symmetric Gelator Through Ion-Pair Assisted Hydrogen Bond"*.
3. Poster presentation in Gordon Research Conference (GRC) on "Self-Assembly & Supramolecular Chemistry", Switzerland, May 2017.
4. Oral presentation in National Science Day 2017 at CSIR-NCL Pune, India.